HELBING, H. (2003): No suture in the Sardinian Variscides: A structural, petrological, and geochronological analysis.
--> *Tübinger Geowissenschaftliche Arbeiten, Reihe A* 68, ISSN 0953-4921, 1-190.
--> http://w210.ub.uni-tuebingen.de/dbt/volltexte/2003/918/

No suture in the Sardinian Variscides: A structural, petrological, and geochronological analysis

Heiko Helbing

2003

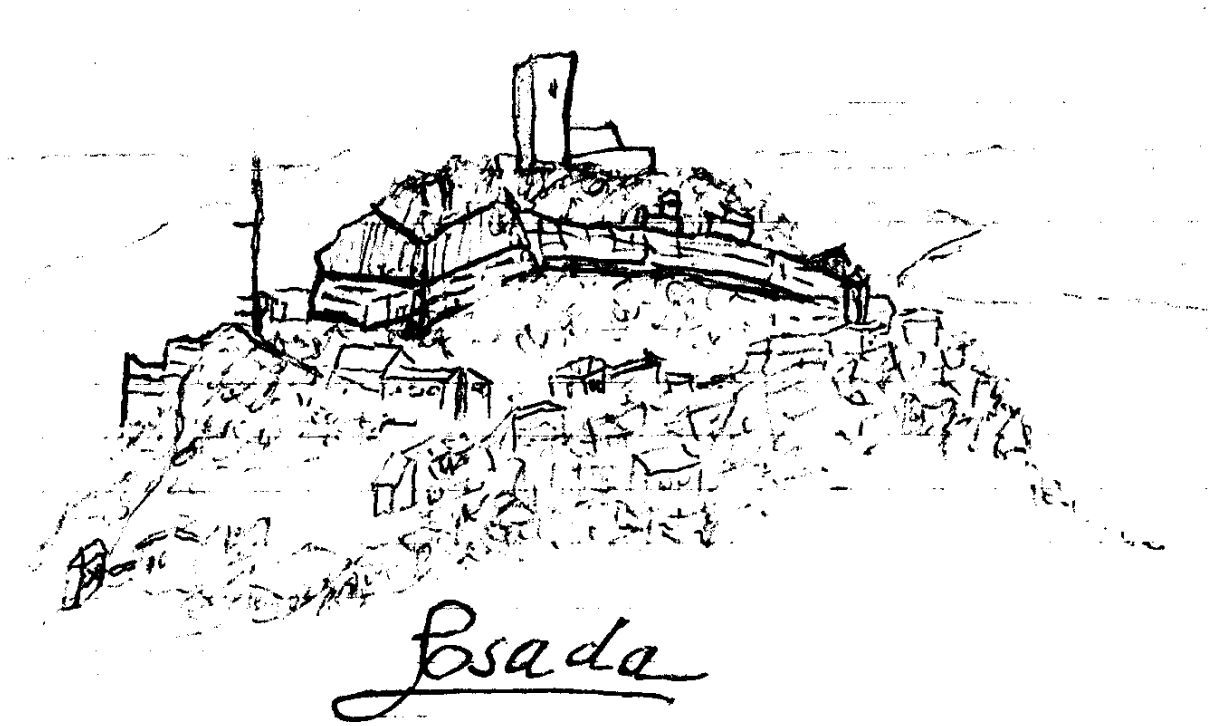

Heiko Helbing (heiko.helbing@uni-tuebingen.de)
Inst. für Geowissenschaften, Univ. Tübingen, Sigwartstr. 10, 72076 Tübingen

Acknowledgements

I thank Prof. Dr. Wolfgang Frisch for inspiring discussions, critical reviews of earlier manuscript versions, and encouraging support.

I'm grateful to Prof. Dr. Paul Bons for helpful discussions and corrections of an earlier manuscript version.

I whish to thank Prof. Dr. Wolfgang Zacher for his interest on my studies and his crucial support to finish them.

Gratefully acknowledged is the effort by Prof. Dr. Jörn Heinrich Kruhl to improve my skills in microscopy and fieldwork.

I gratefully acknowledge the critical review of an older manuscript version by Prof. Dr. Ron Vernon, the introduction to Sardinia's regional geology by Prof. Dr. Giacomo Oggiano, the supply of literature by Prof. Dr. Carlo Alberto Ricci and Prof. Dr. Franco Marco Elter.

I thank Prof. Dr. Gregor Markl, Dr. Wolfgang Siebel, Dr. Massimo Tiepolo, and Dr. Joachim Kuhlemann for the critical review of parts of the manuscript. Urte Haupt and Dr. Birgit Gruner are thanked for their improving comments.

I'm grateful to Dr. István Dunkl, Martin Danišík, and Margret Bayer for expert collaboration.

My special thanks go to my parents and my girlfriend Antonella.

Key words: Sardinia, Sardic, Tyrrhenian, Posada, Asinara, Monte Albo, Variscan, Hercynian, Alpine, pre-Variscan, pre-Hercynian, pre-Alpine, tectonics, structure, fabric, geochronology, metamorphism, suture, palaeogeography, paleogeography, stratigraphy, petrology, texture, Paleozoic, Palaeozoic, Ordovician, Carboniferous, Tertiary, zircon, U-Pb, shear zone, mantled gneiss dome, magmatism, eclogite, porphyroid, orthogneiss, migmatite, unconformity, detachment, transtension

Herausgeber: Institut für Geowissenschaften, Universität Tübingen, Sigwartstrasse 10, D-72076 Tübingen,

Fax: ++49 7071 5059, e-mail: kuhlemann@uni-tuebingen.de

Aktueller Stand erschienener Bände über:

http://www.uni-tuebingen.de/geo/gpi/publikationen/seiten/Info_A.html

Abstract

The NE Sardinian Posada fault was proposed by Cappelli et al. (1992) to mark a Variscan suture, which is refuted by this study of tectonostratigraphy, structure, texture, petrology, and geochronology.

For the sequence that hosts the Posada fault, an Ordovician magmatic belt upon pre-Variscan basement is delineated by the separately occurring metavolcanic and metaplutonic rocks of basic to acidic composition. The extrusive level comprises the Orune schists, which derived from Ordovician volcanic to semipelitic protoliths and Silurian black shales. The intrusive level includes the pelitic Siniscola schists and Brunella gneisses, to which the occurrence of D1 and of pre-D2 metamorphic mineral assemblages is limited. In-situ U-Pb isotopic data obtained by laser-ablation inductively coupled plasma mass spectrometry on zircon yield for the Tanaunella orthogneiss 453 ± 8 Ma (MSWD 0,63), the Lodè orthogneiss 493 ± 10 Ma (MSWD 0,32) and for the Lula porphyroid 485 ± 10 Ma (MSWD 0,67). Besides these lower to middle Ordovician ages, Neoproterozoic ages are inherited from a Pan-African episode.

Decompressional peak metamorphic conditions were achieved during the foreland directed transport of the main Variscan deformational event D2. An up to kilometre-scaled recumbent D3 folding coaxial with the D2 transport direction and the D4 Posada detachment-faulting led to the formation of a mantled gneiss dome. The dominant orogen-parallel trend is related to the Posada shearing. S4 crosscut previous foliations at a low angle and retrogressed the high-grade Brunella gneisses under medium-grade conditions and the medium-grade Siniscola schists under low-grade conditions during early faulting stages. The initial temperature gradient across the fault was overcome with progressing retrogression. The Posada fault rocks evolved from the adjacent wall rocks by retrograde shearing. In response to the tectonic denudation further exhumation was achieved by a large D5 flexure at the flank of the gneiss dome. D4 and D5 are expression of the same exhumation process. The flexure axis is coaxial with the displacement direction in the Posada fault. In the steep limb of this flexure, the Posada fault became a dextral wrench fault and the previously recumbent D3 folds became antiformal synclines and/or synformal anticlines.

In the internal dome, peak metamorphic muscovite dehydration melting at about 760°C and 8 kbar led to the *K-feldspar* + *sillimanite* zone, on which the *muscovite* + *sillimanite* zone was retrogressively superimposed at the Posada fault, so that the metamorphic jump to the medium-grade Siniscola schists is less obvious. The latter expose a Barrovian metamorphic suite continuously developed from chloritoid disappearance to kyanite appearance. The *garnet* + *albite* zone results from the interference of Variscan and pre-Variscan metamorphic mineral assemblages. The *andalusite* + *cordierite* zone in the contact aureole of the Concas granite indicates that the studied sequence was already exhumed to shallow crustal level when the Variscan deformational activity ceased.

Two contrasting tectonostratigraphic domains are juxtaposed in the Sardinian Variscides. The axial and nappe zones correlate with the Variscan domain presently exposed in the Alps, whereas the foreland shows an affinity to the Ibero-Aquitaine domain. The reorientation of the basement structures by Alpine faulting is estimated and set into the wider context of the Tyrrhenian basin opening.

Riassunto

La faglia Posada (NE Sardegna) è stata interpretata da Cappelli et al. (1992) come espressione di una zona di sutura Varisica; tale ipotesi è stata confutata dal presente studio tectonostratigrafico, strutturale, tessiturale, petrologico e geocronologico.

La successione che ospita la faglia Posada è delineata da una cintura magmatica Ordoviciana caratterizzata da distinti livelli di rocce metavulcaniche e metaplutoniche a composizione basica ed acida posta al disopra di un basamento pre-Varisico. Il livello effusivo comprende gli scisti di Orune, derivanti da protoliti vulcanici e semipelitici Ordoviciani e da scisti neri Siluriani. Il livello intrusivo è costituito dagli scisti pelitici di Siniscola e dagli gneisses di Brunella, nei quali sono presenti degli insiemi di minerali metamorfici relativi agli eventi D1 e pre-D2. Dati isotopici in-situ U-Pb ottenuti tramite laser-ablation con spettrometria di massa ICP su zircone hanno indicato una età pari a 453 ± 8 Ma (MSWD 0,63) per l'orthogneiss di Tanaunella, 493 ± 10 Ma (MSWD 0,32) per l'orthogneiss di Lodè e 485 ± 10 Ma (MSWD 0,67) per il porfiroide di Lula. Oltre a queste età Ordoviciano inf.-medio, sono state trovate età Neoproterozoiche ereditate da un episodio Pan-Africano.

Le condizioni del picco metamorfico decompressionale sono state raggiunte durante il principale evento deformativo Varisico D2 avente una direzione di trasporto tettonico verso l'avampaese. Un duomo gneissico estensionale si è formato a seguito di pieghe a scala chilometrica coassiali coricate D3, aventi direzione di trasporto tettonico simile a D2, e della faglia-scollamento Posada D4. L'andamento dominante orogene - parallelo è legato al taglio nella zona di Posada. Durante le prime fasi di sviluppo della faglia la superficie S4 ha tagliato con un basso angolo le precedenti foliazioni, gli gneiss di alto-grado di Brunella sotto condizioni di medio-grado e gli scisti di medio-grado di Siniscola sotto condizioni di basso-grado. Il gradiente di temperatura iniziale lungo la faglia è stato livellato con la progressiva retrogressione. Le rocce della faglia Posada si sono evolute dalle adiacenti rocce incassanti attraverso uno shear retrogrado. Ulteriore esumazione è stata raggiunta in risposta alla denudazione tettonica per mezzo di una grande piega flessurale D5 nel fianco del duomo gneissico. D4 e D5 sono espressione dello stesso processo di esumazione. L'asse della piega flessurale è coassiale con la direzione di spostamento della faglia Posada. Nel fianco più inclinato della piega flessurale, la faglia Posada diventa una faglia trascorrente destra e le pieghe D3 si trasformano da coricate a una successione di anticlinali sinformi e sinclinali antiformi.

Nella parte interna del duomo, la fusione per disidratazione della muscovite durante il picco metamorfico a circa 760°C e 8 kbar ha portato alla formazione della zona a *K-feldspato* + *sillimanite*, sulla quale si è sovraimposta in modo retrogrado la zona a *muscovite* + *sillimanite* nella faglia Posada, e quindi il salto metamorfico al medio-grado degli scisti di Siniscola è meno ovvio. Quest'ultimi litotipi mostrano una suite metamorfica Barroviana continua che si è sviluppata dalla scomparsa del cloritoide fino alla comparsa della cianite. La zona a *granato* + *albite* risulta dall'interferenza di insiemi minerali metamorfici Varisici e pre-Varisici. La zona a *andalusite* + *cordierite* in contatto con l'aureola dei graniti di Concas indica che la successione studiata era già stata esumata fino a livelli crostali poco profondi quando cessò

l'attività deformativa Varisica.

Due domini tectonostratigrafici contrastanti sono giustapposti nella Sardegna Varisica. La zona assiale e quella a falde si correlano con i domini Varisici attualmente esposti nelle Alpi, mentre l'avampaese mostra un'affinità con il dominio Ibero-Aquitano. E' stata stimata la riorientazione delle strutture di basamento provocata da faglie Alpine ed inserita nel contesto più ampio dell'apertura del bacino Tirrenico.

Zusammenfassung

Laut Cappelli et al. (1992) reaktivierte die spätvariszische Posada-Scherzone in Nordostsardinien die Plattensutur, entlang der die Kontinente Armorika und Gondwana im Zuge der variszischen Gebirgsbildung kollidierten. Die vorliegenden Untersuchungen zur Tektonostratigraphie, Strukturgeologie, kristallographischen und metamorphen Gefügeentwicklung sowie zur Geochronologie widerlegen diese Suturtheorie.

Separat vorkommende Metavulkanite and Metaplutonite basischer bis saurer Zusammensetzung charakterisieren die Gesteinsabfolge, in der die Posada-Scherzone eingebettet ist, als magmatischen Gürtel, der im Ordovizium auf einem älteren Grundgebirge entstand. Das effusive Niveau besteht aus den Orune-Schiefern, die sich aus vulkanischen und semipelitischen Ausgangsgesteinen ordovizischen Alters bildeten sowie Einschaltungen silurischer Schwarzschiefer enthalten. Das Nebengestein der Metaplutonite umfasst die pelitisch zusammengesetzten Siniscola-Schiefer und Brunella-Gneise, die dadurch gekennzeichnet sind, dass nur in ihnen die Strukturen des ersten Deformationsereignisses (D1) und das pre-D2-Mineralgefüge entwickelt sind. In-situ Uran-Blei-Isotopenanalysen an Zirkon mittels Laser-beprobender Massenspektrometrie (LA-ICP-MS) deuten für den Tanaunella-Orthogneis auf ein Intrusionsalter von 453 ± 8 Millionen Jahren (MSWD 0,63), für den Lodè-Orthogneis auf ein Intrusionsalter von 493 ± 10 Millionen Jahren (MSWD 0,32) und für den Lula-Porphyroid auf ein Effusionsalter von 485 ± 10 Millionen Jahren (MSWD 0,67) hin. Neben diesen früh- bis mittelordovizischen Altern wurden spätproterozoische Alter in Altkernen gemessen, die der pan-afrikanischen Gebirgsbildung zuzuordnen sind.

Die Spitzentemperaturen der variszischen Regionalmetamorphose stellten sich unter abnehmendem Druck im Verlauf des vorlandgerichteten tektonischen Transports während des Hauptdeformationsereignisses (D2) ein. Bis zu kilometergroße liegende D3-Falten mit Faltenachen, die koaxial zum D2-Transportlinear orientiert sind, und die D4-Abscherung der hangenden Schiefer von den liegenden Gneisen an der abschiebenden Posada-Scherzone führten zur Entstehung eines Domes mit den Brunella-Gneisen im Kern und ummantelt von einer Hülle aus Siniscola- und Orune-Schiefern. Die vorherrschend orogenparallele Streichrichtung ist auf die Reorientierung durch die Posada-Scherung zurückzuführen. Die abschiebenden D4-Scherbänder durchschlagen die ältere Foliation in spitzem Winkel. Dabei werden zunächst in einem frühen Scherstadium die mittel metamorphen Siniscola-Schiefer unter niedrig metamorphen Bedingungen und die hoch metamorphen Brunella-Gneise unter mittel metamorphen Bedingungen retrograd alteriert. Der so zum Ausdruck kommende Temperaturgradient wurde im Verlauf der retrograden Scherung überwunden. Die Mylonite und Kataklasite in der Posada-Scherzone entwickelten sich durch intensive retrograde Scherung aus den angrenzenden Siniscola-Schiefern und Brunella-Gneisen. Durch die tektonische Entfernung der auflastenden Schiefer wurde die Heraushebung der Gneise ausgelöst, sodass die Flanke des aufsteigenden Gneisdomes von einer Flexur gebildet wird. Diese D5-Flexur und die D4-Posada-Scherzone sind Ergebnis des selben Heraushebungsprozesses. Flexurachse und D4-Transportlineare sind koaxial orientiert. Im steilen Schenkel der Flexur fungierte die Posada-Scherzone als rechtsgerichtete

Seitenverschiebung und die zuvor liegenden D3-Falten wurden reorientiert zu Tauchfalten.

Im Inneren des Domes führte Dehydrierungsschmelzen von Muskovit während des Metamorphosehöhepunkts bei etwa 760°C und 8 kbar zur Ausbildung der metamorphen *Kalifeldspat* + *Sillimanit* Mineralzone. Die retrograde Überprägung im Bereich zur angrenzenden Posada-Scherzone ist in der *Muskovit* + *Sillimanit* Zone manifestiert, sodass der Metamorphosesprung über die Posada-Scherzone zu den mittel metamorphen Schiefern auf den ersten Blick nicht so deutlich wird. Die kontinuierliche Folge vom Verschwinden des Chloritoids bis zum Erscheinen des Disthens in den Mineralparagenesen der mittel metamorphen Schiefer reflektiert die mittleren Druck- und Temperaturbedingungen einer progressiven Barrow-Metamorphose. Die Ausbildung einer *Granat* + *Albit* Zone resultiert aus der Überlagerung von variszischer und pre-variszischer Mineralparagenesen. Die *Andalusit* + *Cordierit* Zone in der Kontaktaureole des Concas-Granits zeigt an, dass die untersuchte Gesteinsabfolge bereits auf ein flaches Krustenniveau herausgehoben war, als die variszische Deformation ausklang.

In den sardischen Varisziden sind Teilbereiche zweier tektonostratigraphisch unterschiedlicher Domänen aufgeschlossen. Sowohl die Zentralzone als auch der Falten- und Überschiebungsgürtel, deren Übergang von der Posada-Scherzone gebildet wird, korrelieren beide mit der variszischen Domäne, die sich in den heutigen Alpen befindet. Das Vorland der sardischen Varisziden zeigt hingegen mehr Gemeinsamkeiten mit der Ibero-Aquitaine-Domäne.

Die Reorientierung der Strukturen im variszischen Grundgebirge durch die alpidische Deformation wurde rekonstruiert und in Bezug zur Beckenbildung im Tyrrhenis-Gebiet gesetzt.

Contents:

1 Introduction

Several sutures are proposed to occur in the Variscan belt of Europe (fig. 1.1). Cappelli et al. (1992) suggested that the South Armorica-Massif Central ocean branched into northern Sardinia, forming part of a south Variscan suture zone. The idea of a south Variscan suture zone is controversially discussed. It is generally inferred from structural data (Matte 2001). In contrast, paleobiostratigraphic data rule out a major ocean, closed at a south Variscan suture zone (Robardet 2003). On the other hand, Stampfli (1996) locates the Paleotethys ocean, which was not sutured before Triassic times, at the south Variscan flank of Europe. This study in NE Sardinia was initiated to prove the suture hypothesis by Cappelli et al. (1992).

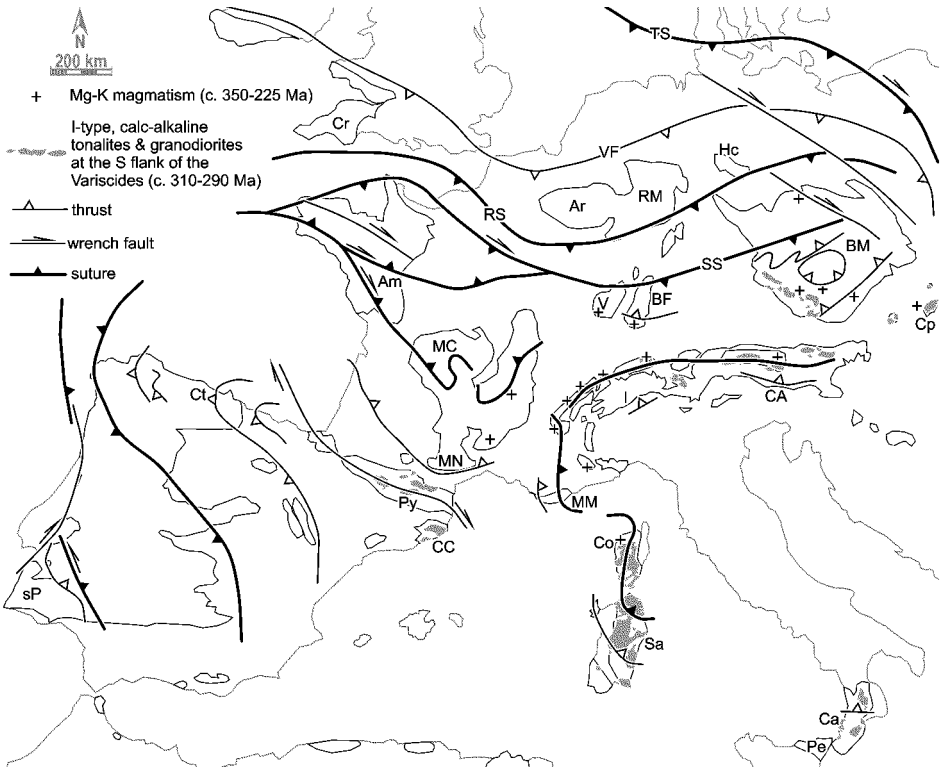

Fig. 1.1: Sketch map of the structural correlation between the Variscan massifs of Europe (Zwart & Dornsiepen 1978, Vai & Cocozza 1986, Matte 1991, von Raumer 1998, Winchester et al. 2002) and the distribution of Mg-K magmatism (Finger et al. 1997, Wenzel et al. 1997, von Raumer 1998) as well as of a distinct group of I-type, calc-alkaline tonalities and granodiorites at the southern flank of the Variscides (Poli et al. 1989, Rottura et al. 1990, Vissers 1992, Cocherie et al. 1994, Finger et al. 1997); **Am**: Armorica, **Ar**: Ardennes, **BF**: Black Forrest, **BM**: Bohemian Massif, **CA**: Carnic Alps, **Ca**: Calabria, **CC**: Catalonian Costal Range, **Co**: Corsica, **Cp**: Carpathians, **Cr**: Cornwall, **Ct**: Cantabria, **Hc**: Hercynian Massif, **I**: Ivrea zone, **MC**: Massif Central, **MM**: Maures Massif, **MN**: Montagne Noire, **Pe**: Peloritan Massif, **Py**: Pyrenees, **RM**: Rhenish Massif, **RS**: Rheic suture, **Sa**: Sardinia, **sP**: south Portuguese zone, **SS**: Saxothuringian suture, **TS**: Thor suture, **V**: Vosges, **VF**: Variscan front.

1.1 Orogenic anatomy of the Sardinian Variscides

At the Posada fault, which is inferred to mark the aforementioned suture, the axial zone of the Sardinian Variscides borders against a fold and thrust belt, which in turn borders against a foreland

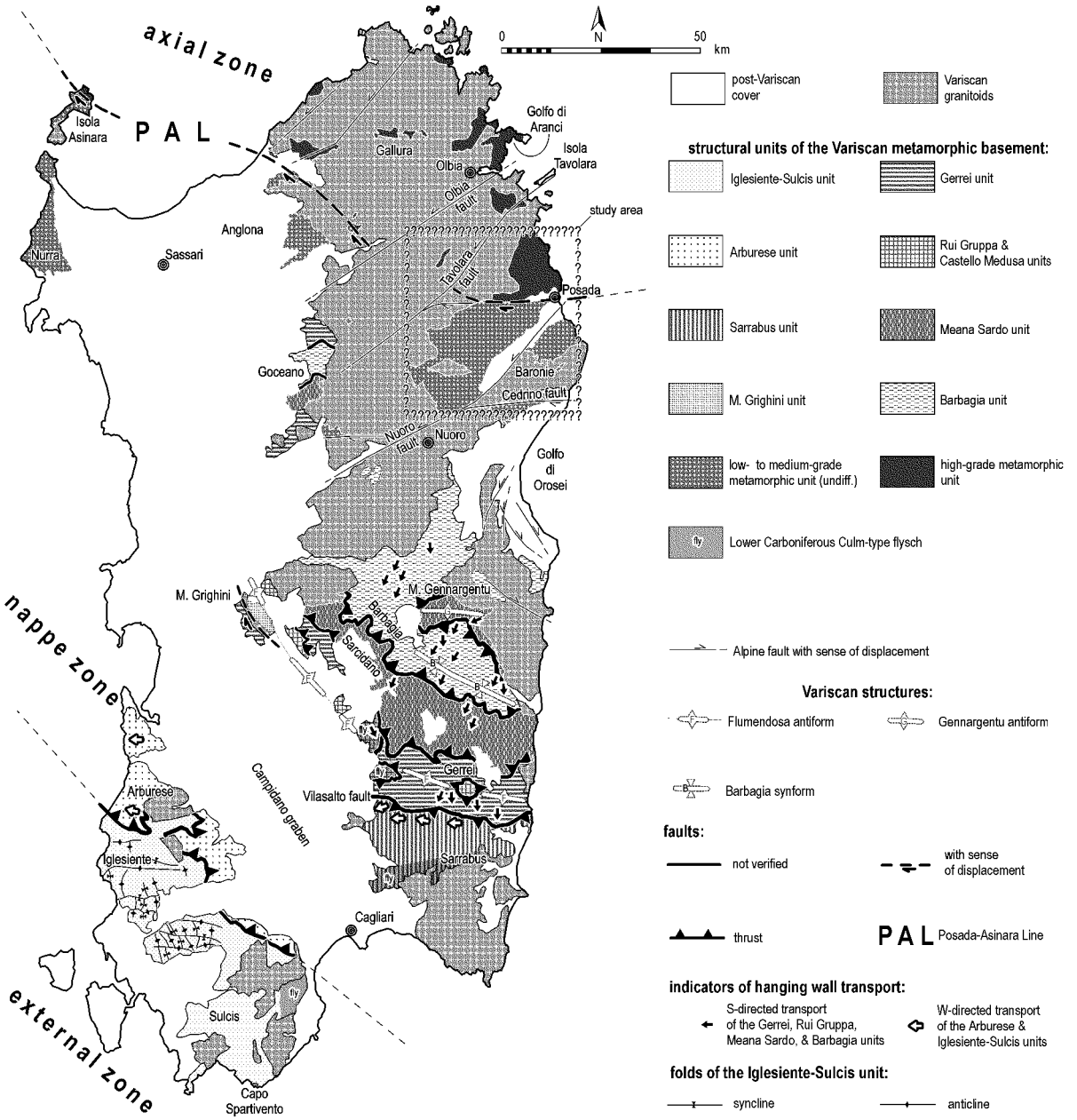

Fig. 1.2: Structural sketch map of the Sardinian Variscides (Zwart & Poll 1964, Arthaud & Sauniac 1981, Barca et al. 1992, Carmignani et al. 1992a & b, Lüneburg & Lebit 1998, Conti et al. 2001).

(fig. 1.2). This zoning is expression of increasing deformation under externally very low- to low-grade and internally high-grade metamorphic conditions (Di Simplicio et al. 1974, Arthaud & Sauniac 1981). The foreland, also named external zone, exposes interfering folds that derive from Variscan and Sardic tectonics (Zwart & Poll 1964, Poll 1966). Here, the Sardic event is further manifested in an angular unconformity (Teichmüller 1931), at which Arenigan shales are overlain by Caradocian conglomerates (Barca et al. 1987).

The fold and thrust belt, also called nappe zone, comprises allochthonous units that are thrust towards the foreland (Conti et al. 2001). Abundant metavolcanics, which are related to an active margin (Memmi et al. 1983, Carmignani et al. 1994), occupy the Ordovician stratigraphic position (Carmignani et al. 1982b), instead of the Sardic unconformity that is not documented here.

The transition to the axial zone is marked by an increased metamorphic field gradient (Franceschelli et al. 1982) and the Posada fault that displays a dextral displacement (Elter et al. 1990).

The granitoids of the Sardinia-Corsica batholith intruded the Paleozoic basement during late stages of the Variscan orogeny (Del Moro et al. 1975). A Tertiary rift system filled with a thick volcano-sedimentary sequence, e.g. the Campidano graben (Cherchi & Montadert 1982), and large faults crosscutting the Paleozoic basement, e.g. the Nuoro fault (Carmignani et al. 1992b), are expression of the Alpine overprint.

Alpine dismembering and shuffling at the southern flank of the Variscan orogenic belt complicate the correlation of the Sardinian Paleozoic section with its surrounding. The Alpine overprint is outlined after the introduction to Sardinian's Paleozoic history.

1.2 Sardinia's Paleozoic history

Sardinia's Paleozoic history comprises a supercontinent cycle that began with the early Paleozoic break-up of the pan-African supercontinent Protogondwana and finished with the late Paleozoic accretion of the Variscan supercontinent Pangea. This plate tectonic reorganisation is characterised by the high-latitude domain Gondwana and the domain of Laurentia, Baltica, and E Avalonia, which drifted clockwise around Gondwana (Dalziel et al. 1994, Dalziel 1997). The pre-Carboniferous fauna of the SW-European part of the Variscan belt, which includes the Sardinian section, belonged to the high-latitude domain of Gondwana (Robardet et al. 1990), while the central European portion (Ardennes, Rhenisch massif, Harz mountains) was part of the low-latitude domain of Laurentia-Baltica. Also, the geochemical signature (Nägler at al. 1995) and the ages of detrital zircons (Vidal et al. 1981, Paquette et al. 1985, Peucat et al. 1986) of the pre-Carboniferous sedimentary record derived from the Gondwanan domain in the SW-European part, while the pre-Carboniferous deposits were supplied from the Laurentia-Baltica domain in the central European portion of the belt (Franke et al. 1978). This pre-Carboniferous contrast indicates a major geographic barrier, which is named the Rheic ocean. As a result of the closure of the Rheic ocean by the final accretion of Pangea during the Variscan orogeny, this contrast was overcome within the overlaying Carboniferous deposits.

Sardinia's Paleozoic history began with the separation from the Gondwanan mainland, according to Strampfli et al. (2002, fig. 1.3A). The external zone of the Sardinian Variscides (fig. 1.2) allows an insight into this early Paleozoic stage. Here, the Cambrian deposits of terrigenous siliciclastics, an overlying carbonate platform (fig. 1.4 a2), and eventually Early Ordovician pelites (fig. 1.4 a1) display the change from a proximal to a distal setting of Sardinia with respect to the Gondwanan shelf (Carmignani et al. 1994).

Ordovician tectonics is manifested in folding and the Sardic unconformity in the external zone (Teichmüller 1931, Zwart & Poll 1964, Poll 1966) as well as in a calc-alkaline magmatism, giving rise to volcanic deposits, generally known as porphyroids, and granitoid intrusions in the internal zones (fig. 1.4b, Memmi et al. 1983).

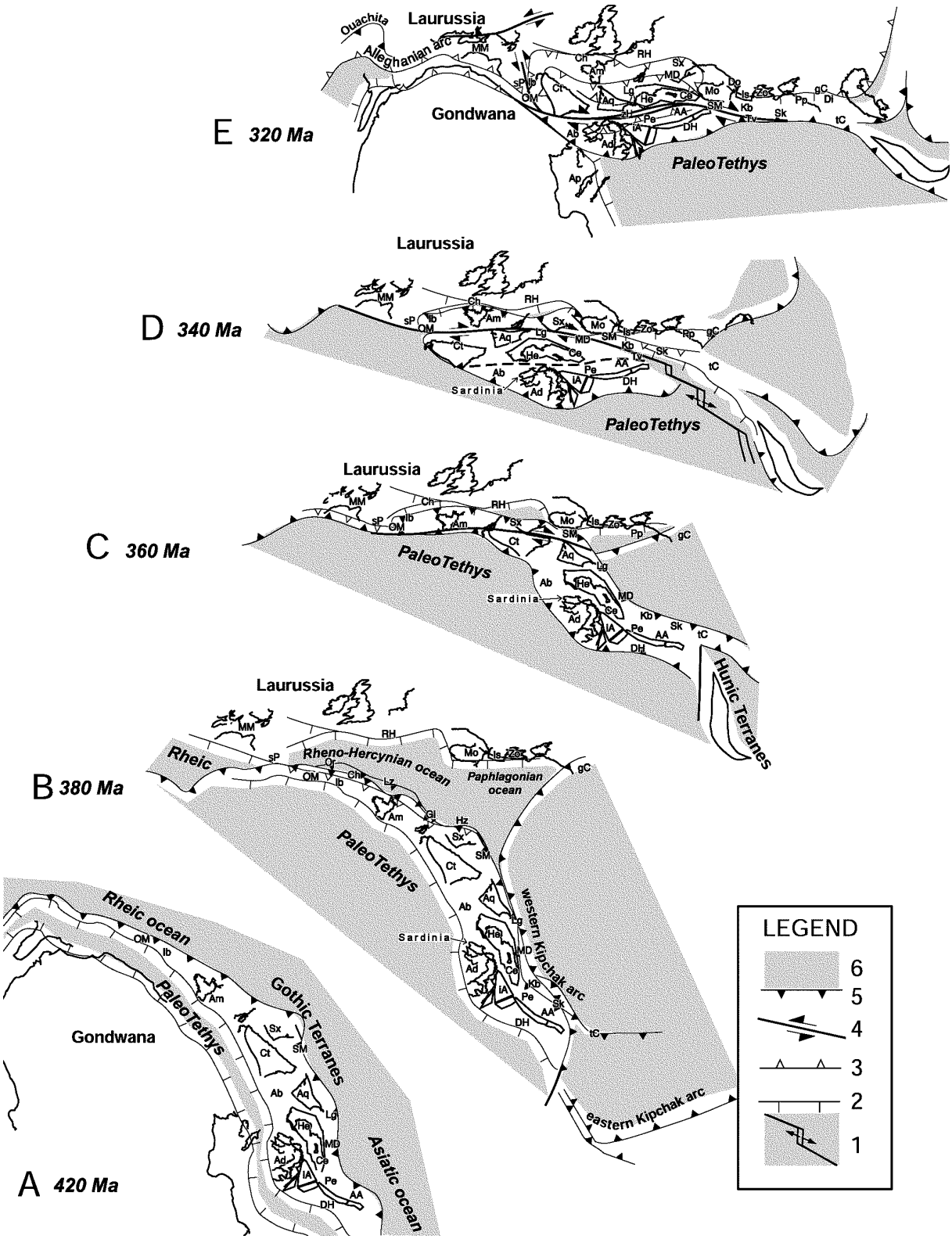

Fig. 1.3: Evolving Paleozoic geography (Stampfli et al. 2002), explanation in the text. **AA:** Austro-Alpine, **Ab:** Alboran (Betics, Rift, Kabylies), **Ad:** Adria (Sardinia-Corsica, southern Alps, Calabria), **Am:** Armorica, **Ap:** Apulia, **Aq:** Aquitaine (Montange Noire), **Ch:** Cornwall, **Ct:** Cantabria (Pyrenees, Catalunia, Balleares), **DH:** Dinarides-Hellenides, **Gi:** Gießen, **He:** Helvetic, **Hz:** Harz mountains, **IA:** intra-Alpine, **Ib:** Iberia, **Is:** Istambul, **MD:** Moldanubian, **Lg:** Ligerian, **MM:** Meseta-Meguma, **Mo:** Moesia, **OM:** Ossa-Morena, **Pe:** Penninic, **RH:** Rhenohercynian, **SM:** Serbo-Macedonian, **sP:** south Portugal, **Sx:** Saxothuringian, **Zo:** Zonguldak. **1:** oceanic spreading centre, **2:** passive continental margin, **3:** thrust fault, **4:** transcurrent fault, **5:** subduction zone, **6:** ocean floor.

Orogenic activity with its climax during the Ordovician (Le Corre 1994) is a widespread phenomenon of the Variscan belt (Montagne Noire: Laurent & Arthaud 1992, Armorican Massif: Ballèvre et al. 1994, Pyrenees: den Brok 1989, eastern Alps: Frisch & Neubauer 1989, Southern Alps: Hunziker & Zingg 1980) and is generally related either to intracontinental rift tectonics, due to associated leptyno-amphibolite bimodal magmatism (Paquette et al. 1989, Pin & Marini 1993), or to active margin tectonics, due to associated eclogites or migmatites (Oberli 1994, von Raumer et al. 2002).

The begin of continental rifting in Sardinia is indicated by the onset of an alkaline to transitional within-plate magmatism documented by Upper Ordovician basic rocks (Ricci & Sabatini 1978, Memmi et al. 1983, Di Pisa et al. 1992). The sedimentation changed from prevailing terrigenous to marine, as the Silurian black shales and pelagic deposits show, into which the basic rocks are emplaced (fig. 1.4c-d). Increasing carbonate sedimentation during the Devonian could be due to drifting towards warmer paleolatitudes (Babin et al. 1980).

Paleozoic terrane accretion progressed in time and space as follows (fig. 1.3). In the north American Appalachians, pre-Variscan terrane accretion gave rise to the Caledonian orogeny proper during Late Silurian and Early Devonian times, and the subsequent Variscan orogeny appears as continuation of the earlier Caledonian accretion (Williams 1985). Towards the central part of the Variscan orogen in Europe, the north Variscan deformational front points out the spatial and temporal separation between the Caledonian and Variscan orogen (Le Gall 1990). The Rheic suturing during Early Carboniferous times is preceded by the Saxothuringian amalgamation of the Armorican terrane assemblage during Late Devonian times (Winchester et al. 2002). In the eastern part of the Variscan orogen - in the regions of the Balkans, Asia Minor, and Persia - major terrane accretion lasted until Early Triassic times and was closely connected to the beginning Alpine cycle (Stampfli 1996). A final collision between the landmasses of Laurentia-Baltica and Gondwana is recorded in the southern Appalachians and W African Mauritanides only, while the European south Variscan flank was still influenced by the active margin regime of the Paleotethys ocean during Late Carboniferous to Permian times (Stampfli 1996). A distinct group of late Variscan, calc-alkaline, I-type granitoids (fig. 1.1), to which also the Sardinia-Corsica batholith belongs (Tommasini et al. 1995), is referred to a magmatism related to the subduction of Paleotethys ocean floor (Finger & Steyrer 1990, Stampfli 1996).

Besides successive convergence and collision, the Variscan belt underwent major dextral displacement (fig. 1.3, Arthaud & Matte 1977, Shelley & Bossière 2000) and may carried out a rotation of more than 100°, according to paleomagnetic data (Edel 2001).

For the Variscan orogeny in Sardinia, an Early Carboniferous collision of two distinct tectonostratigraphic terranes is proposed at the so-called Posada-Asinara Line, involving the overthrust axial zone and the underthrust nappe zone and causing the foreland directed nappe emplacement (fig. 1.4e, Carmignani et al. 1992a, Cappelli et al. 1992).

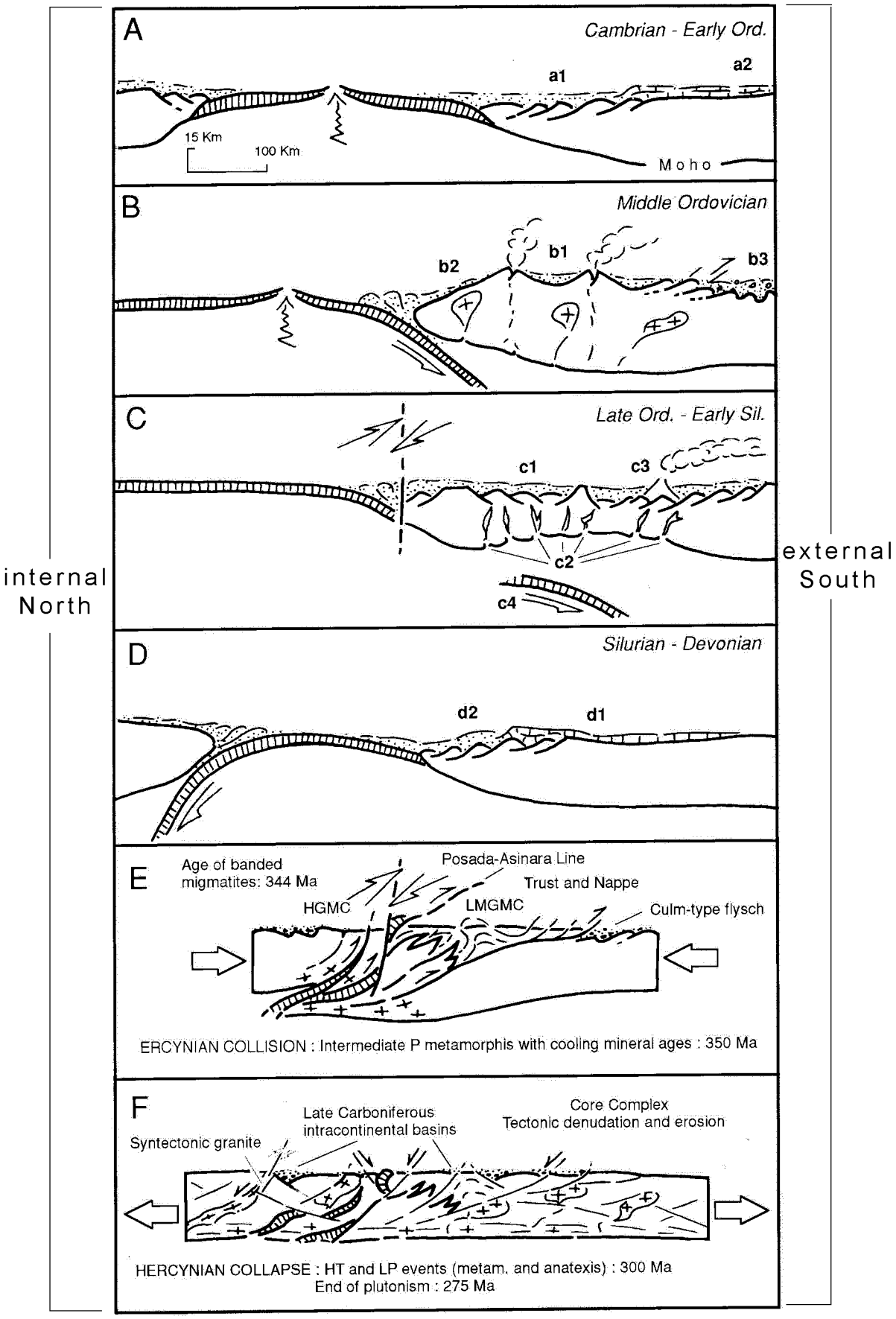

Fig. 1.4: Geodynamic cartoon of Paleozoic Sardinia (fig. 4 in Carmignani et al. 1992a), explanation in text.

First radiometric ages record the Early Carboniferous begin of exhumation (Ferrara et al. 1978, Del Moro et al. 1991). Simultaneous flyschoid deposits in Culm-type facies are the expression of accelerated uplift of the sedimentary source area (fig. 1.2, Barca 1991, Barca et al. 1992). The flyschoid deposits got incorporated into the progressing nappe pile, and the latest deposits cover the nappe front. Thus, the flyschoid deposition in Sardinia is thought to last until Late Carboniferous times. However, its climax is supposed to be of Early Carboniferous age (Barca 1991).

A Late Carboniferous to Permian collapse stage (fig. 1.4f) is characterised by synsedimentary normal faults, controlling deposition in basins attached to the flanks of the ascending Flumendosa antiform (Barca et al. 1995). Anatexis occurred in places and is related to a high-temperature/low-pressure metamorphism and synkinematic granitoid intrusions (Oggiano & Di Pisa 1988).

1.3 Sardinia's post-Variscan history

The post-Variscan history of Sardinia is framed by the Mesozoic break-up of the Pangea supercontinent and by the Tertiary to recent collision and rift tectonics related to the Alpine convergence of the African and the Eurasian continental margins (Channell et al. 1979).

Permo-Triassic volcanics and sediments were unconformably deposited on the Paleozoic basement and progressively transgressed by a Jurassic to Cretaceous carbonate platform, which covered Sardinia entirely during Jurassic times (Cocozza & Jacobacci 1975). During Late Cretaceous to Early Tertiary times, the Iberian plate associated with the Sardinia Corsica block collided to the north and formed the Pyrenean fold and thrust belt in addition to it's Languedoc-Provençal segment to the east (Séranne 1999). Folding and thrusting phenomena in SW Sardinia are correlated with the Pyrenean tectonics (Barca & Costamagna 1997). The simultaneous prevailingly fluvial sedimentation of the molassic Cixerri formation in Sardinia has a basal discordance and derives from Pyrenean uplift and erosion (Barca & Palmerini 1973, Cherchi & Schröder 1976, Cherchi 1979). Also, the collisional nappe emplacement in Alpine Corsica is constrained for this period, spanning from Late Cretaceous to Early Tertiary times (Brunet et al. 1997). The compressional front, which was followed by extensional tectonics behind, migrated from Corsica to the east, causing Late Oligocene nappe emplacement in the Apennines (Carmignani & Kligfield 1990) and opening of the north Tyrrhenian basin (Jolivet et al. 1991).

The fore- and/or hinterland of the Alpine and Pyrenean belt underwent a complex deformation. Major rifting gave rise to intracontinental basins and large sinistral shear zones (Séranne 1999). Concerning this tectonic activity, Séranne (1999, page 17) distinguishes an Late Eocene to Early Oligocene climax at the Rhine and Bergerat grabens on the W European mainland and an Late Oligocene to Early Miocene climax at the Campidano graben in Sardinia. The latter is related to the opening of the Balearic sea. For the same time, Carmignani et al. (1995) suppose still compression in eastern Sardinia, followed by extension not before the Early Miocene.

This outlined evolution from collision accompanied by crustal shortening to extension facilitating the eastward migration of the compressional front is best explained by an arc migration model (fig. 1.5) proposed among others by Scandone (1979), Malinverno & Ryan (1986), Wortel & Spakman (1992). The sink of the old oceanic lithosphere is the driving force for this slab rollback. It is most probably originated from the negative buoyancy of the subducted slab, and may be supported by an eastward asthenospheric flow (Doglioni et al. 1999). The switch from eastward directed subduction in Alpine Corsica to westward subduction in the Apennines during Late Eocene is accommodated most probably by mantle processes (Jolivet et al. 1999) such as convective removal of the thermal boundary layer and slab detachment (Houseman et al. 1981, Fleitout & Froidevaux 1982, Dewey 1988, Platt & England 1994, Wong & Wortel 1997). Sardinia's evolution since Late Oligocene within the hanging wall of the retreating Apenninic-Maghrebidic subduction is best illustrated by the following facts.

- The oceanic crust in the Balearic and Tyrrhenian sea shows progressively younger ages from west to east (Rehault et al. 1984, Feraud 1990).
- The orogenic magmatism bounded on the eastward retreating subduction has also a progressively younger age from west to east, and is concomitant with ongoing rifting in the magmatic arc and sea floor spreading in the back arc basins to the west (Wilson & Bianchini 1999).
- Palaeomagnetic studies on volcanic rocks formed by the eastward retreating magmatic arc in Sardinia show an anticlockwise rotation in the Early Miocene (Vigliotti & Langenheim 1995).

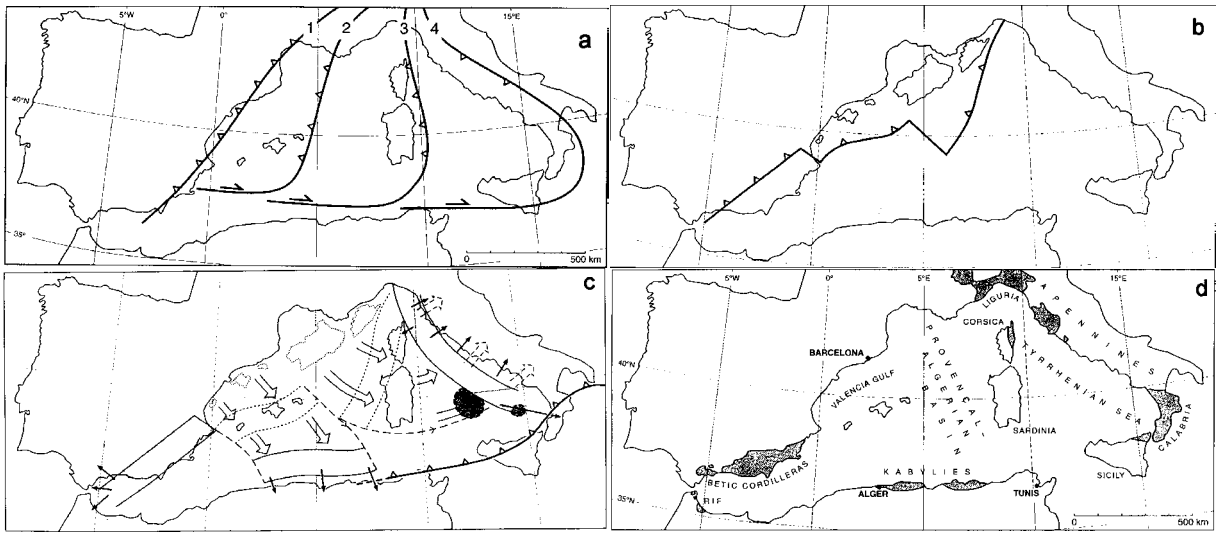

Fig. 1.5: The arc migration model and how it led to the present distribution of the Alpine chain (fig. 1 and 4 in Zeck 1999); **a**: series of slab roll-back phases (Wortel & Spackman 1992), **b**: initial stage of the arc at the Iberian plate margin, **c**: Sardinia reached its present day position during a Miocene stage, while the east migration is still going on east of Sardinia, **d**: present day dispersed position of the Alpine metamorphic core complexes (Coward & Dietrich 1989).

1.4 Purpose and scope of the thesis

The study area, which covers the transitional section between the axial and the nappe zone of the Sardinian Variscides (fig. 1.2), represents the key section for deciphering the evolution of the Sardinian

Variscides and might be of importance for the entire European Variscides as well. The interpretation of this section to be part of a south Variscan suture zone by Cappelli et al. (1992) bases on the following assumptions, which will be taken in particular consideration.

- The axial zone recorded a single retrograde history, while the adjacent nappe zone experienced a Barrovian metamorphism followed by retrogression, suggesting a distinct metamorphic evolution.
- The thrusting of the axial zone over the nappe zone during collision caused a strong retrogression at the base of the overriding axial zone and an inverted metamorphic gradient below.
- The pre-collisional record across the Posada fault reflect the mutually exclusive history typical of exotic terranes.
- The Posada fault rocks derive from an oceanic melange, containing remnants of ocean floor.

Moreover, new data from Sardinia contribute to the terrane analysis at the southern flank of the Variscides that was additionally dismembered and shuffled during the Alpine overprint. Thus, its geological evolution is still poorly constrained, despite the wealth of data and the excellent work so far done.

Tectonostratigraphic investigations (chapter 2) shall give information about the younging direction and discontinuities of the lithologic sequence as well as about the geodynamic setting, in which the sequence formed. Insights about the tectonic evolution shall be achieved by the analysis of the structure (chapter 3) and petrofabrics (chapter 5). The petrofabics are of particular interest for the estimation of basic P-T conditions during the metamorphic overprint. Object of the structural analysis is to obtain data about the nature of the Posada fault, whether extensional, transcurrent or compressional tectonics was involved, to understand the deformation mechanisms and to clarify overprinting relations, which are crucial for the relative timing. The absolute timing will be acquired by radiometric dating of metavolcanics and metagranitoids in the studied sequence (chapter 6). Particularly important for the structural analysis is the consideration of the Alpine reorientation. Another part of the structural analysis comprises the interpretation of kinematic indicators, additionally proven by measurements of the lattice preferred orientation of quartz (chapter 4), in order to infer a tectonic transport direction.

The new results will be discussed in consideration of published data and compared with the paleogeographic surrounding.

2 Tectonostratigraphy

2.1 General remarks

In order to introduce the tectonostratigraphic sequence of the study area, its lithology is briefly described and the concluded geodynamic settings are discussed in as much as they are not subject of the subsequent chapters.

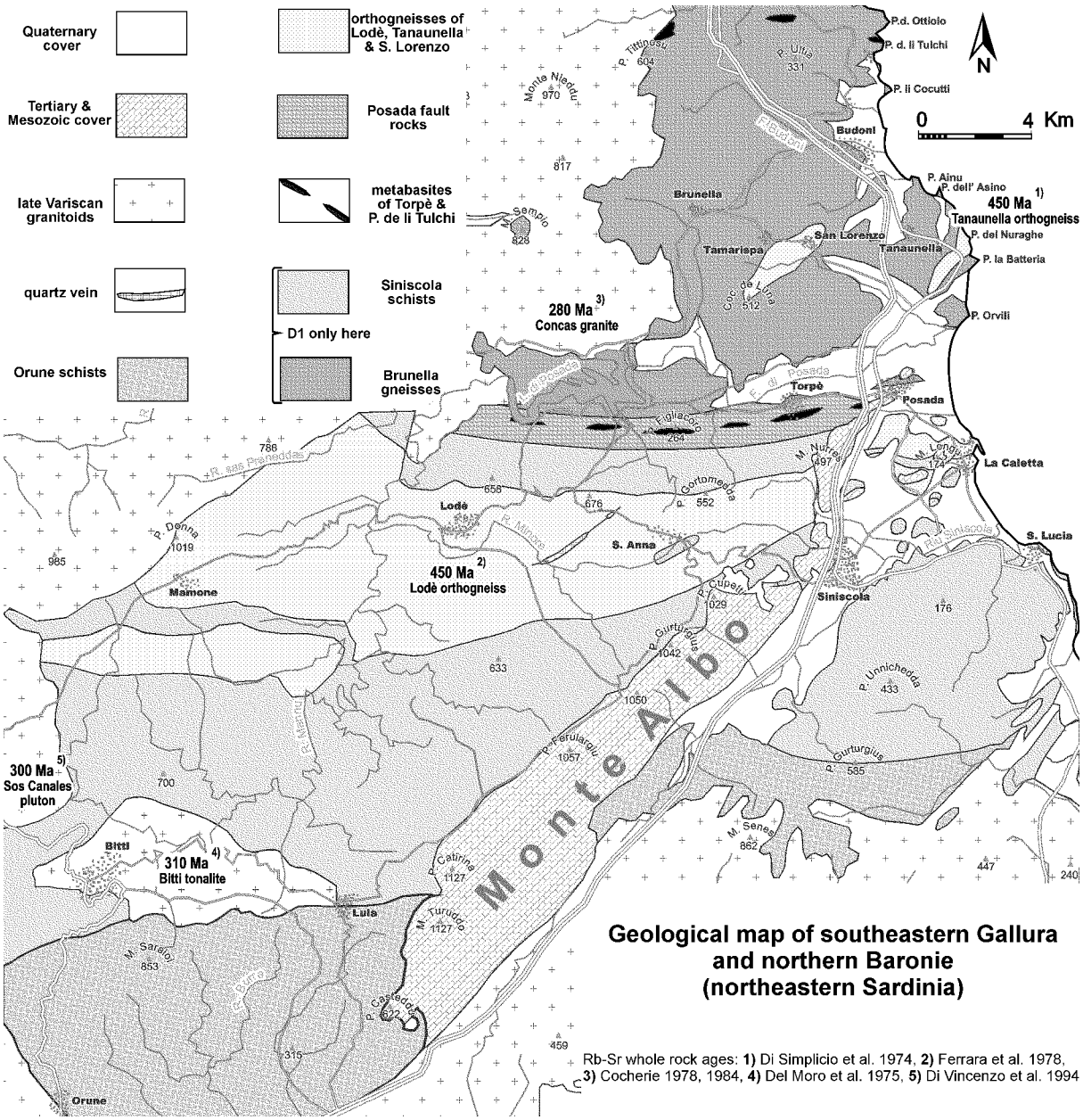

Fig. 2.1: NE Sardinian section of the geological map of Sardinia modified after Carmignani et al. (1996), showing some age relationships within the tectonostratigraphic sequence of the study area.

The lithologies, such as distinguished in the geological map of Sardinia, 1:200000 (Carmignani et al. 1996), are accepted (fig. 2.1), and their names, hereafter used, refer to the rock type localities mentioned in the legend of this map.

2.2 Tectonostratigraphic sequence

The metamorphic part of the Paleozoic basement is constituted from south to north as follows:

- The Orune schists consist of quartz, white mica, biotite, chlorite, albite and accessory calcite. The absence of chloritoid and kyanite/andalusite, refers to the semi-pelitic composition of these low-grade schists (fig. 5.5a). The Orune schists are interlayered by porphyroids and tremolite-actinolite greenschists as well as by graphitic schists.
- The garnet-bearing Siniscola schists contain typical mineral assemblages commonly observed in true metapelites of medium-grade metamorphism (fig. 5.7a), probably because they derived from sediments with a considerable pelitic component (chapter 5). Furthermore, the Siniscola schists contain metabasite and calc-silicate intercalations, and host the Lodè orthogneiss.
- The orthogneisses from Lodè, Tanaunella, and San Lorenzo have a granodioritic, granitic to monzogranitic composition (table 6.1-3).
- The Posada fault rocks comprise mylonites (plate 3.3a-c; plates 5.7e-h, 5.8a-g) and cataclasites (plate 5.9a-b). The fault rocks derive from the adjacent Siniscola schists and Brunella gneisses by retrograde deformation focused in high-strain zones that anastomose around low-strain islands that host for instance the Torpè metabasite (chapter 3 & 5).
- The Brunella gneisses comprise partly migmatic para- and orthogneisses; e.g. orthogneisses from Tanaunella and San Lorenzo; local calc-silicate gneisses, and metabasite intercalations; e.g. the Punta de li Tulchi metabasite (fig. 3.24). The early record of the Punta de li Tulchi metabasite is exotic with respect to the surrounding Brunella gneisses. It contains eclogitic relics that partly survived the subsequent granulite facies (chapter 5).

This sequence of increasing metamorphic grade exposes two major discontinuities, namely the retrograde Posada fault that juxtaposes the medium-grade Siniscola schists against the high-grade Brunella gneisses and the contact between low-grade Orune and medium-grade Siniscola schists. At the latter, porphyroid-interlayered low-Al metapelites border against orthogneiss-hosting high-Al metapelites. The retrograde Posada fault represents a late orogenic feature. On the other hand, the contact between Orune and Siniscola schists might represent a primary discontinuity that coincides with the change from volcanic to plutonic protolith appearance of the acidic to basic meta-igneous rocks, which occur throughout the whole sequence and may distinguish between intrusive and extrusive level.

The metamorphic portion of the Paleozoic basement is crosscut by multiple granitoid intrusions of the Sardinia-Corsica batholith.

Calcareous rocks of mainly Mesozoic and, to a lesser extent, of Tertiary age cover the Paleozoic basement and form the Monte Albo massif. The calcareous matrix of the Tertiary breccias bears clasts of Mesozoic as well as of Paleozoic rocks (fig. 3.13).

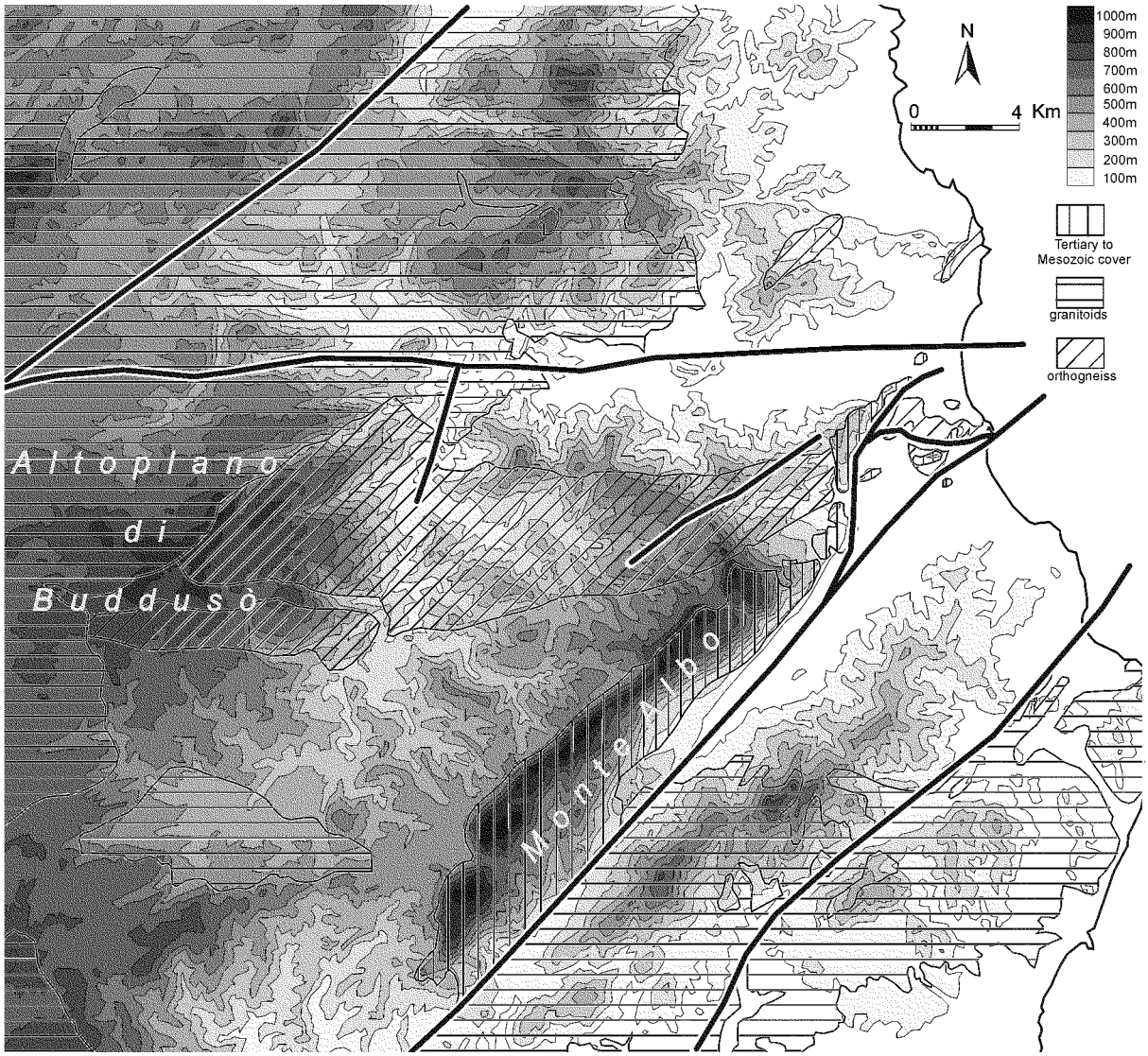

Fig. 2.2: Contoured elevation map with some lithologies and major Alpine faults modified after the geological map of Sardinia (Carmignani et al. 1996), demonstrating the dominant influence of the Alpine structure on the topographic relief. The Monte Albo plateau and the Altoplano di Buddusò probably remain from an uplifted Tertiary peneplain, explanation in text.

The Quaternary sediments are mainly deposited in river valleys and along the coast. The valleys commonly follow large Alpine faults, so that the entire topographic relief appears dominated by the Alpine structure (fig. 2.2). This is supported by the Altoplano di Buddusò, which extends across lithological boundaries, demonstrating the secondary influence of the lithology on the topographic relief. Thus, the erosive resistance of the Paleozoic to Tertiary rocks is mainly weakened by the Alpine faulting. In the centre of the Alpine faults, brittle deformation culminated in the formation of incohesive breccias and gauges (plate 3.3e,,3.4 h). Moreover, that the Altoplano di Buddusò and the Monte Albo plateau probably originate both from a single uplifted peneplain is suggested by the findings of Paleozoic basement-derived pebbles, locally remaining from gravel deposits on top of the Monte Albo plateau. In order to enable the deposition of the basement-derived plateau gravel onto the cover beds, the Mesozoic to Tertiary Monte Albo rocks have to be brought tectonically into a structural low, probably by the Alpine overprint. The subsequent erosion caused the relief inversion.

2.3 Discussion

Such porphyroids, greenschists, and graphitic schists as interlayered in the Orune schists are common in volcano-sedimentary sequences of the external and central nappe zone as well, where they are considered to be derived from acidic to intermediate volcanics of an Ordovician calc-alkaline suite (Memmi et al. 1983) and/or Late Ordovician alkaline basalts (Ricci & Sabatini 1978), closely associated with Silurian graphitic schists (Carmignani et al. 1994). Thus, the volcano-sedimentary protoliths of the Orune schists may correlate lithostratigraphically with these Ordovician to Silurian sequences exposed in central and southern Sardinia.

The porphyroids are generally considered as equivalents to the Ordovician orthogneisses (Memmi et al. 1983), i.e. the orthogneisses of Lodè, Tanaunella and San Lorenzo (fig. 2.1), which would support the inferred intrusive and extrusive levels represented, respectively, by the Brunella gneisses and the Siniscola schists on the one hand and the Orune schists on the other hand.

In analogy to the acidic meta-igneous rocks, the metabasite intercalations of the Brunella gneisses and Siniscola schists might be intrusive equivalents to the greenschist protoliths interlayered in the Orune schists. However, the age of the metabasites has to be considered as undetermined so far, despite an Middle Ordovician protolith age given in an unreviewed abstract (Palmeri et al. 1997 quoted in Cruciani et al. 2002) and a Late Proterozoic Sm-Nd model age (Cappelli et al. 1992).

Furthermore, the metabasites provide a varying and partly ambiguous geochemistry. Some were interpreted to be intra-continental rift-derived (Ricci & Sabatini 1978), but partly reinterpreted to be MORB-derived (Cappelli et al. 1992, Francescelli et al. 1998), whereas other metabasites were interpreted to be supra-subduction-derived (Cruciani et al. 2002).

This variety of the pre-Variscan magmatism is consistent with the idea of a Middle Ordovician magmatic arc, Late Ordovician arc collapse, and Silurian intra-continental rifting (fig. 1.4b-c, Carmignani et al. 1994). On the other hand, the locally closely associated occurrence of acidic and basic meta-igneous rocks might derive from a bimodal magmatism typical of intra-continental rifts, such as proposed for the leptyno-amphibolite association, which is widespread in the Variscides (Paquette et al. 1989, Pin & Martini 1993). The former interpretation implies an active margin stage before the Gondwana supercontinent broke apart (fig. 1.4b). The latter implies that the Gondwana break-off is later followed by an active margin setting during the Variscan accretion of Pangea. Transitional scenarios of these two end member interpretations are possible as well. Crucial for the solution of this classical Variscan dispute might be the structural and metamorphic evolution of the eclogitic Punta de li Tulchi metabasite, which is considered in the following chapters.

The Permo-Carboniferous granitoid intrusions that crosscut the metamorphic sequence (fig. 2.1) belong to a late magmatic stage of the Sardinia-Corsica batholith, which is preceded by an Early Carboniferous magnesian-potassic, calc-alkaline stage mainly restricted to Corsica (Tommasini et al. 1995, Ferré & Leake 2001). The Permo-Carboniferous I-type, calc-alkaline tonalities and granodiorites of the Sardinia-Corsica batholith are part of a distinct belt at the southern flank of the Variscides

(fig. 1.1) that might be related to the subduction of the Paleotethys (fig. 1.3, Stampfli 1996, Finger et al. 1997). Furthermore, the Early Carboniferous intrusions of the internal axial zone in Corsica appear as part of a distinct magnesian-protassic belt that marks the high-grade axial zone of the Saxothuringian and Moldanubian massifs, where it might be related to post-collisional extension and magmatic underplating associated with high-temperature fluid-absent melting (Finger et al. 1997, Wenzel et al. 1997, von Raumer 1998). This magmatic zoning of the Sardinia-Corsica batholith will be taken additionally in consideration for the correlation of the tectono-metamorphic evolution of the Sardinian section with the paleogeographic surroundings (chapter 7).

The Mesozoic calcareous rocks derived from a Middle to Late Jurassic carbonate platform (Massari & Dieni 1983). The Tertiary breccias and conglomerates are generally considered to be of post-Lutetian, probably late Eocene to Oligocene age (Dieni & Massari 1965). Major uplift is inferred for Pliocene times (Hiller 1981). Consequently, the Alpine faulting and the subsequent deposition of basement-derived gravel on top of the Monte Albo plateau should have an age in between.

In contrast, Hiller (1981) refers the remnants of basement-derived plateau gravel on the Mesozoic cover beds to an Early Tertiary deposition. This would imply that the tectonic event, which brought the Mesozoic cover into a structural low, is older than the Tertiary breccias and conglomerates. Furthermore, the Alpine faulting is commonly related to the Alpine collision in Corsica (Alvarez & Cocozza 1974, Carmignani et al. 1995), spanning from late Cretaceous to Early Tertiary times (Brunet et al. 1997).

However, there are no evidences that the Mesozoic calcareous rocks were deformed separately from the Tertiary breccias and conglomerates. The extent of the Alpine faulting and whether it is related to the Alpine collision or the subsequent retreat of the Apenninic-Maghrebidic arc (fig. 1.5) will be considered in chapter 3.

2.4 Conclusion

The following conclusions can be drawn.

- Across the contact between Orune and Siniscola schists, the meta-igneous rocks change from an extrusive to an intrusive protolith appearance.
- The Orune schists are correlated lithostratigraphically with Ordovician to Silurian volcano-sedimentary sequences in the external and central nappe zone of the Sardinian Variscides.
- Basement-derived gravel was deposited on the Mesozoic to Tertiary Monte Albo cover rocks, when the Altoplano di Buddosò and the Monte Albo plateau were part of a Middle Tertiary peneplain.

3 Structure

3.1 Previous work and open questions

Superimposed Sardic and Variscan tectonics form an interference pattern of early and late Paleozoic folds in the external zone of the Sardinian Variscides (fig. 1.2, Poll & Zwart 1964, Poll 1966). On the other hand, pre-Variscan tectonics, such as manifested in the Sardic folding and an angular unconformity in the external zone, is not documented in the nappe and axial zones, although the separate occurrence of Ordovician metavolcanics and metagranitoids in the study area (chapter 2) suggests a possible pre-Variscan cover-basement relationship at the transition between nappe and axial zone.

That the main foliation is formed by S1 in the low-grade external belt and by S2 in the internal higher metamorphic belt is interpreted by Elter et al. (1986) to be result of increasingly transposing deformation towards the internal belt. They propose that large E-W trending folds, such as the Lodè orthogneiss crest (fig. 3.1), arose from a D2 folding phase, superimposed by N-S trending D3 folds. Retrograde mylonites developed during the dextral D4 Posada wrenching and became refolded during D5 (Elter et al. 1990).

According to the suture model of Cappelli et al. (1992), the high-grade axial zone has been thrust southwards over medium- and low-grade nappes during D1. The thrust pile became inverted by the D2 folding (fig. 3.1). However, this model lacks proof (1) that the axial zone is structurally situated above the nappe zone, (2) that different structural histories across the suture preceded the collisional thrusting, and (3) that the amphibolites in the Posada fault identify a Variscan suture zone.

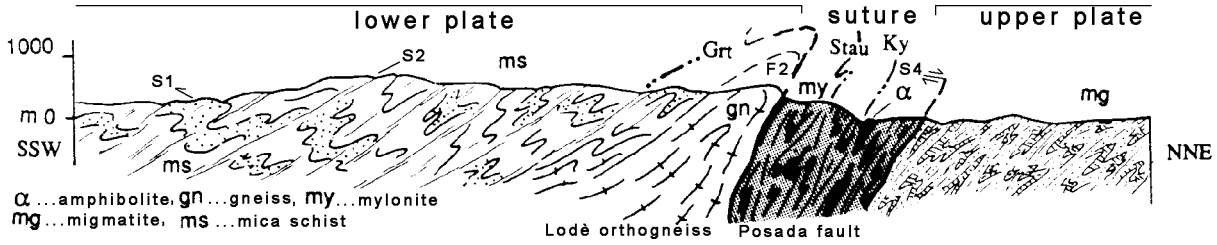

Fig. 3.1: The sketch across the Posada fault proposes collisional suturing and N-S over thrusting during D1 (compiled after Cappelli et al. 1992). The D1 pile of southern plate below, suture zone in between, and northern plate on top is inferred to became inverted after peak metamorphism by D2 back folding with the Lodè orthogneiss forming a F2 crest. It implies a north-dipping F2 enveloping surface and increasingly deeper structural levels to the south. The suture is supposed to be overprinted by D4 dextral wrenching in the Posada fault.

Large NE-SW trending faults in NE Sardinia (fig. 1.2) have been related to the Alpine collision in Corsica (Alvarez & Cocozza 1974, Carmignani et al. 1995). The Tertiary to Mesozoic cover at the SE flank of the Monte Albo became involved in sinistral movements along the Nuoro fault system that constitutes a positive flower structure, according to Carmignani et al. (1992b). Although involvement of the Paleozoic basement in the Alpine faulting was recognised, the impact on the basement structure was not considered.

The structural setting of the Ordovician meta-igneous rocks will be investigated, because it should indicate, whether or not pre-Variscan tectonics were involved in the internal belt as well. Furthermore, the suture model by Cappelli et al. (1992) will be examined critically, and the extent of the Alpine reorientation will be considered. In particular, the study concerns outline and orientation of structural elements, correlation of structural successions by identification of key structures and overprinting as well as crosscutting relations, and kinematic analyses.

3.2 General remarks

The broad structure of the studied sequence is delineated in the structural map (fig. 3.2) and cross sections (fig. 3.3). It is dominated by an orogen-parallel trend and an externally-directed dip, i.e. towards the external orogen. A shallow plunge of stretching lineations and fold axes prevails. Up to kilometre-scaled folds, a steep belt, and Alpine faults control the orientation of the structural elements; i.e. foliations, fold axes, intersection lineations, and stretching lineations. In order to minimise the resulting dispersion and to take into account the changing outline from the external to the internal sequence, the structural elements are presented separately in seven structural zones (fig. 3.2).

The Paleozoic fivefold deformational history, proposed in this study, distinguishes:

- D1 that is restricted to the Siniscola schists and Brunella gneisses,
- D2 that refers to the most pervasive structural generation,
- D3 that refolds mainly the most pervasive structural generation,
- D4 that is related to the Posada faulting,
- and D5 that led to upright folding, steep cleavage and an up to 8 km wide steep belt.

Generations of structural elements are locally not to distinguish, so that they are referred to be composite elements, e.g. S2/4, L2/4, B2/3/5, following the approach of Tobisch & Paterson (1988).

The composite foliation S2/4 in structural zones II to VI can be described as asymmetric extensional crenulation cleavage (ecc, Platt & Vissers 1980), type II S-C mylonitic foliation (Lister & Snoke 1984), normal slip crenulation (Dennis & Secor 1987), and/or shear band cleavage of C'-type (Passchier & Trouw 1996). The latter term is used hereafter. Moreover, S2 in structural zone II can be locally described as C/S fabric (Berthé 1978), type I S-C mylonitic fabric (Lister & Snoke 1984), reverse slip crenulation (Dennis & Secor 1987), and/or shear bands cleavage of C-type (Passchier & Trouw 1996). The latter synonym is used in this study.

The structural presentation is supported by more than 3600 field measurements of orientation, which are stereographically projected on equal area lower hemispheres and tabulated in the appendix. Density plots provide up to 7 contour levels with intervals of 1.0 multiples of random distribution counted by cosinus powered weighting function 128 using DOS execution ARiAne version 2.01 (Adam, 1989). Additionally, the poles to the best fit girdle and weighted average of data cluster are calculated after the eigenvalue method (Woodcock 1977).

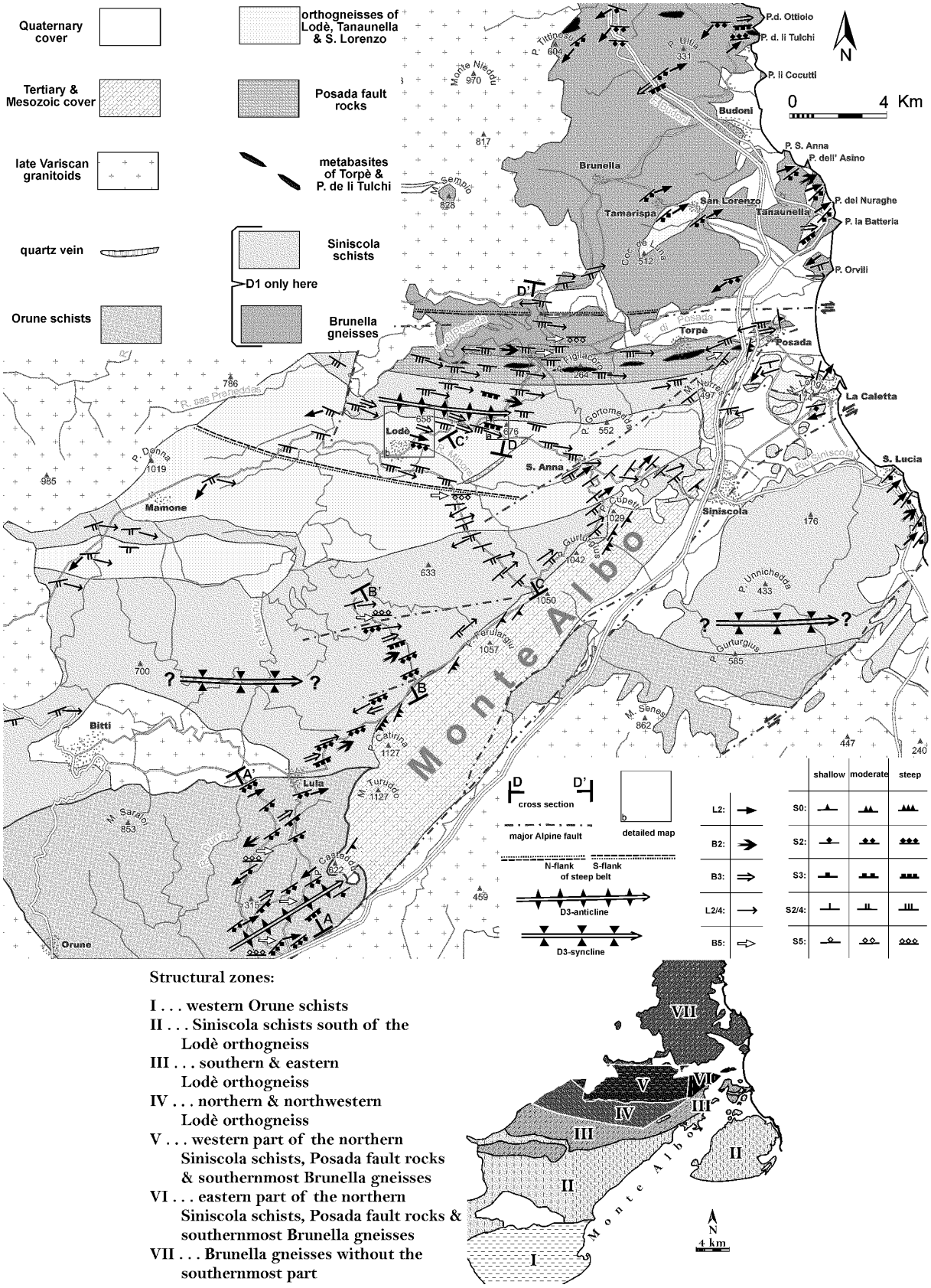

Structural zones:

I . . . western Orune schists
II . . . Siniscola schists south of the Lodè orthogneiss
III . . . southern & eastern Lodè orthogneiss
IV . . . northern & northwestern Lodè orthogneiss
V . . . western part of the northern Siniscola schists, Posada fault rocks & southernmost Brunella gneisses
VI . . . eastern part of the northern Siniscola schists, Posada fault rocks & southernmost Brunella gneisses
VII . . . Brunella gneisses without the southernmost part

Fig. 3.2: Generations of structural elements (B: fold axis and intersection lineation, L: stretching lineation, S: foliation) in geological map and structural zoning of Paleozoic NE Sardinia. Cross sections are shown in fig. 3.3. Detailed maps 'a' and 'b' refer to fig. 3.16 and 3.17 respectively.

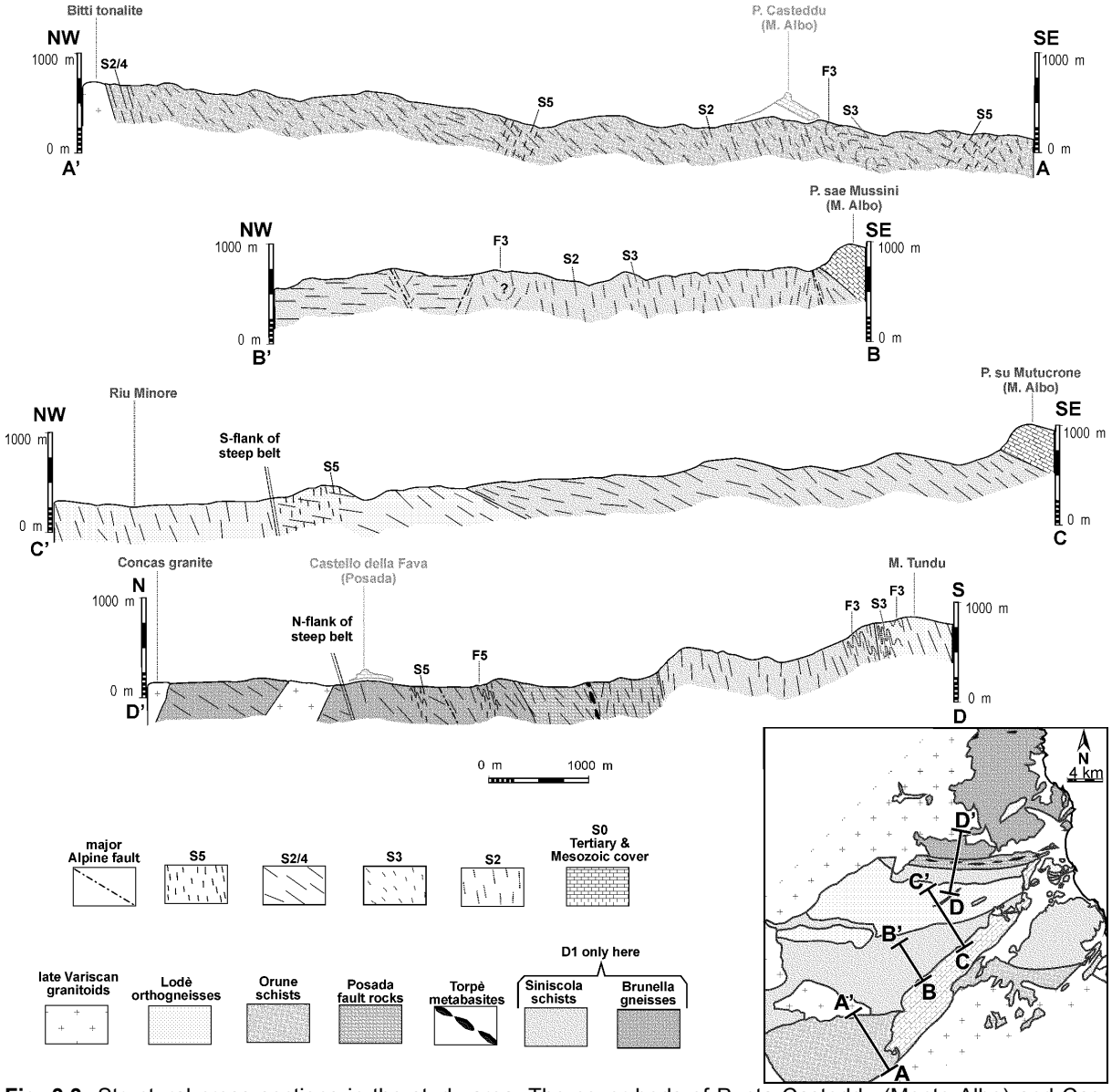

Fig. 3.3: Structural cross sections in the study area. The cover beds of Punta Casteddu (Monte Albo) and Castello della Fava (Posada) are projected on the sections A-A' and D-D' respectively.

3.3 Structural zone I

The structural zone I refers to the western Orune schists (fig. 3.2), which comprise alternating metapsammopelites interlayered with greenschists and graphitic schists as well as porphyric metavolcanics - the so-called porphyroids of Ordovician age (chapter 2 and 6). D2 is directly superimposed on the primary structures. The phenocrysts of the volcanic protolith survived D2 transposition as porphyroclasts (plate 3.1a). The sedimentary bedding S0 is folded into tight to isoclinal D2 folds and transposed by S2 (fig. 3.4). S2 lies in the axial plane of F2 and forms the main foliation. S2 is developed as a continuous cleavage and exhibits a stretching lineation L2 oriented parallel to B2. L2 is defined by aligned quartz grains and fringes in pressure shadows of clasts. It plunges shallowly to the NE (fig. 3.5c).

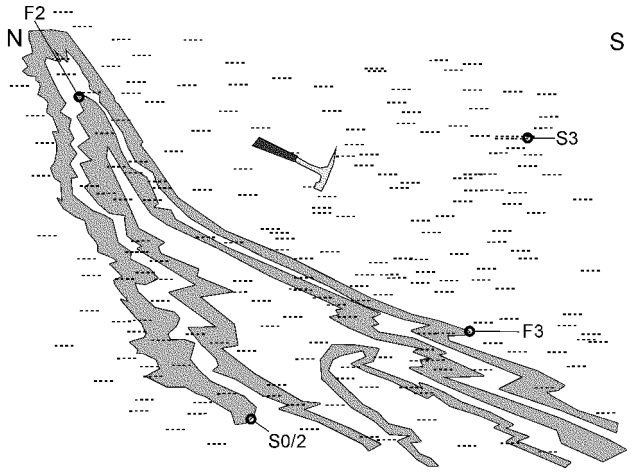

Fig. 3.4: N-S profile of a tight F2 refolded by smaller F3, Orune schists (HH255). The sedimentary bedding S0 has been transposed by S2, forming a composite foliation S0/2. The steeper attitude of F2 in comparison to F3 indicates the apparently inverted limb of a first order kilometre-scaled F3 (fig. 3.3, profile A-A').

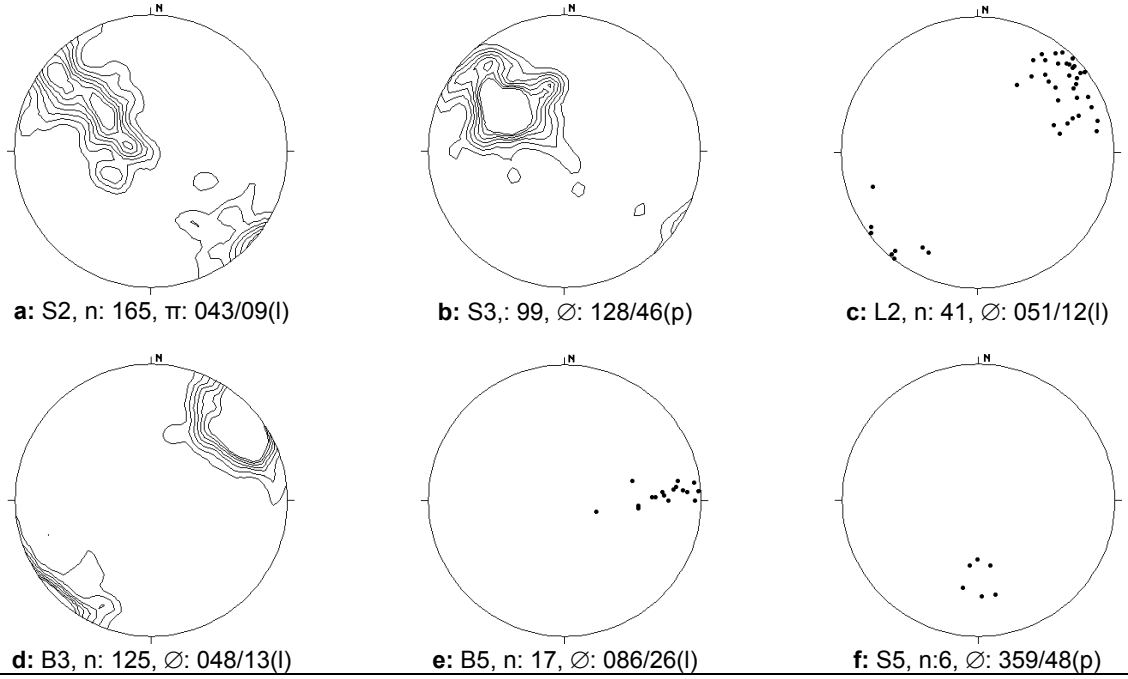

a: S2, n: 165, π: 043/09(l) **b:** S3,: 99, ∅: 128/46(p) **c:** L2, n: 41, ∅: 051/12(l)

d: B3, n: 125, ∅: 048/13(l) **e:** B5, n: 17, ∅: 086/26(l) **f:** S5, n:6, ∅: 359/48(p)

Fig. 3.5: Orientation of structural elements in structural zone I, which refers to the western Orune schists (fig. 3.2), π: pole to the best fit girdle of data cluster, ∅: weighted average of data cluster.

S2 is overprinted by cylindrical D3 folds (fig. 3.5a), which show a tighter interlimb angle in pelitic schists (plate 3.1b) and a more open one in psammitic schists (plate 3.1c). B3 has a shallow plunge to the NE (fig. 3.5d). The coaxial orientation of B2, L2, and B3 contributes locally to a pencil-like lineation. S3 is coplanar with the axial plane of F3 and developed either as a crenulation cleavage in the hinges or as a spaced cleavage in the limbs. It dips moderately to the SE (fig. 3.5b). The steeper dip of S2 with respect to S3 as well as the S- and Z-shapes of monoclinic D3 folds (plate 3.1d) delineate a large inverted limb that crops out over several kilometres south of Lula, but also in the Siniscola schists north of Lula (fig. 3.3, profile A-A' & B-B'). S2/3 turns northwards to a concordant E-W trending contact with the Bitti tonalite, probably due to the decreasing Alpine reorientation with increasing distance to the Nuoro fault (fig. 3.2). S5 is developed as crenulation cleavage without corre-

sponding folds. It only occurs in pelitic schists and cuts S3 at a high angle (fig. 3.5f). The intersection lineation plunges shallowly to the E (fig. 3.5e).

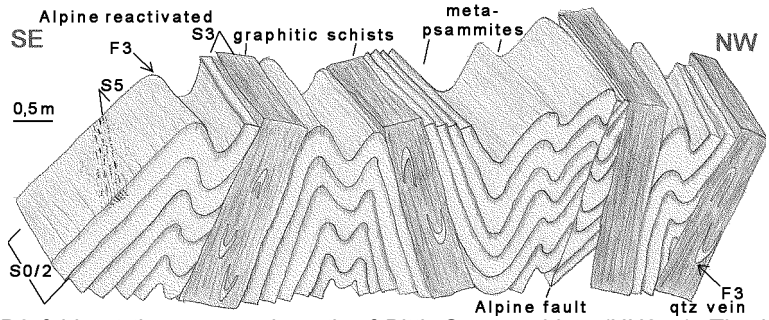

Fig. 3.6: Sketch of D3 folds at the new road south of Bitti, Orune schists (HH245). The incompetent graphitic schists have accommodated Alpine deformation by frictional slip along the D3 cleavage planes, allowing the passive rotation of the competent metapsammites.

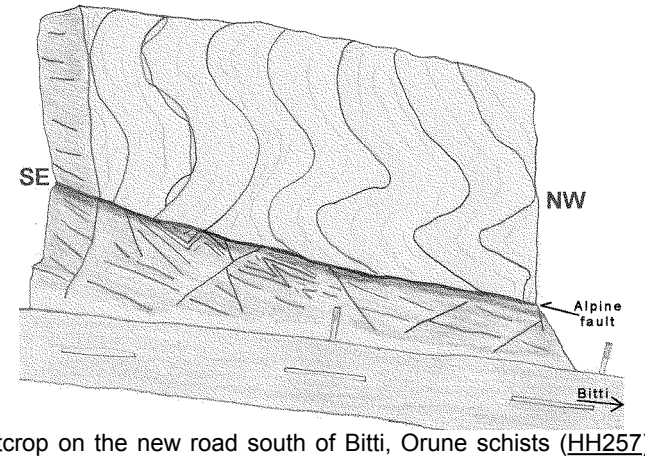

Fig. 3.7: Sketch of an outcrop on the new road south of Bitti, Orune schists (HH257), showing an Alpine fault, along which the hanging wall schists have been reoriented and displaced towards the southeast.

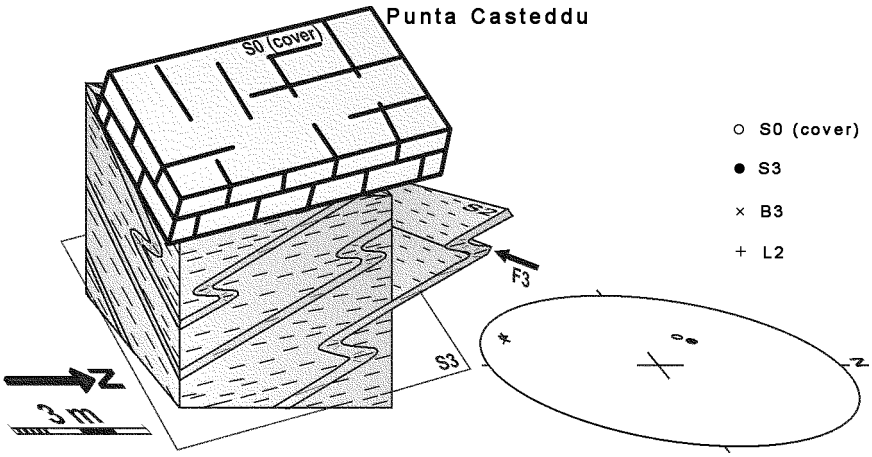

Fig. 3.8: Sketch of the cover-basement contact with pole diagram at P. Casteddu, pointing out the spatial relation between Mesozoic bedding and Paleozoic structures. According to this relation, the D3 folds are pre-Alpine recumbent folds.

Abundant brittle shear zones, which have preferentially reactivated the cleavage planes in pelitic schists (fig. 3.6-7), and the tilted bedding of the post-Variscan cover (plate 3.1e) are expression of the Alpine overprint. S3 and the Mesozoic bedding at the Punta Casteddu cover-basement contact have a similar orientation. Both dip moderately to the SE (fig. 3.8). Undoing the Alpine tilting by rotation

around the NE-SW trend axis until the Mesozoic bedding reaches a horizontal position reveals an originally shallow attitude of S3 and a steep dip to the south of S5 before the Alpine overprint. Thus, F3 is inferred to have originally had a recumbent attitude.

The shallow NE-SW lineation in the basement is only weakly affected by the Alpine tilting due to its coaxial orientation with the tilting axis. The tendency for a great circle distribution of S3 around a NE pole in the pole diagram (fig. 3.5b) is attributed to the varying extent of Alpine tilting, whereas the indicated tendency for a great circle distribution perpendicular to the NE-poled great circle reflects the Alpine rotation of the Variscan E-W trend towards the NE-SW trending Nuoro fault (fig. 3.2).

3.4 Structural zone II

The structural zone II corresponds with the Siniscola schists south of the Lodè orthogneiss (fig. 3.2). The Siniscola schists are composed of alternating pelitic and quartzitic to quartzofeldspathic schists, as well as metabasite and calc-silicate intercalations. They expose S1, which distinguishes them from the D1-absent Orune schists. Primary structures such as cross bedding or synsedimentary folds survived in some quartzofeldspathic layers (fig. 3.9).

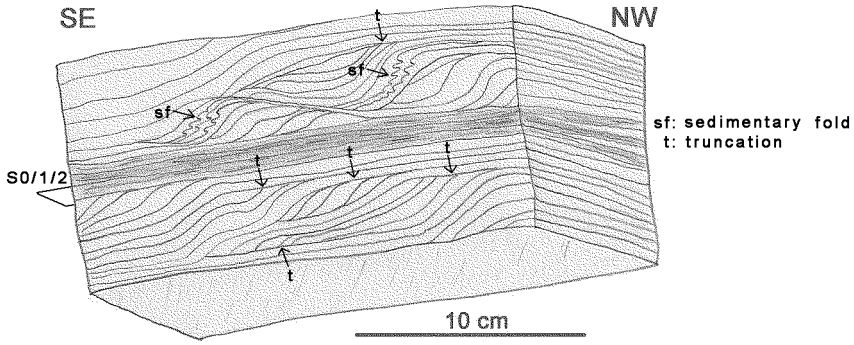

Fig. 3.9: Sketch of cross bedding and synsedimentary folds in a quartzofeldspathic Siniscola schists (HH203). No metamorphic fabric; i.e. cleavage, shear bands, intersection and/or stretching lineations, etc.; is associated with the slumping folds and erosive truncations. This identifies them to be synsedimentary.

S1 transposed the primary compositional layering, is developed as a continuous cleavage in quartzofeldspathic domains, and exhibits coplanar segregation quartz veins in mica domains. It was isoclinally folded around B2 and is transposed by the main foliation S2, which is coplanar with the F2 axial plane (plate 3.1f). The stretching lineation L2 is commonly well developed and oriented coaxial with B2. F3 shows a close interlimb angle and refolds F2 around a common axis with a shallow plunge to ENE (fig. 3.10c). Consistently, the resulting interference displays a hook-shaped fold pattern (plate 3.1g-h). F3 commonly displays an axial planar cleavage S3, which is developed as spaced cleavage in the limbs and as crenulation cleavage in the hinges.

The steeper dip of S2 with respect to S3 and the monoclinic D3 fold morphology, typical of an inverted limb, such as described for the Orune schists near Lula, change to a morphology, typical of a normal limb. Thus, the presence of a first order D3 hinge is suggested (fig. 3.2, 3.3, profile B-B').

During D4, the main foliation S2 was preferentially reactivated by C'-type shear bands in schistose domains. The extensional shear direction during D4 is indicated by the spatial relation between S2 and S4. In order to minimise dispersion, due to subsequent reorientation, the S2 and S4 measurements have been rotated around the common intersection lineation, so that S2 comes into a horizontal orientation (fig. 3.10d). According to the so demonstrated western dip of S4 with respect to S2, a D4 hanging wall transport down towards western directions is inferred.

S4 is weakly developed in the external parts, but becomes generally more pronounced towards the Posada fault. It contributed to tightening and stretching of the previous foliations, and thus focused their common maximum in the stereo plot (fig. 3.10a). Slickensides and/or slickenlines define L4 and are generally coaxial oriented with L2. S5 occurs as an E-W trending crenulation cleavage without corresponding folds, such as in the Orune schists (fig. 3.10e-f).

Reorientation of the one structural element relative to the other in the Paleozoic basement indicates a Variscan overprint, whereas an Alpine overprint is suggested, where all basement structures and the Tertiary to Mesozoic cover are reoriented. Approaching the Alpine Nuoro fault, the general basement trend rotates from E-W into a trend parallel to the NE-SW trending Nuoro fault, so that it describes an arc concave to the south (fig. 3.2). Besides this Alpine reorientation of the trend, the dip of the basement foliation was reoriented, according to the southeastward tilted Mesozoic bedding of the Monte Albo (fig. 3.3).

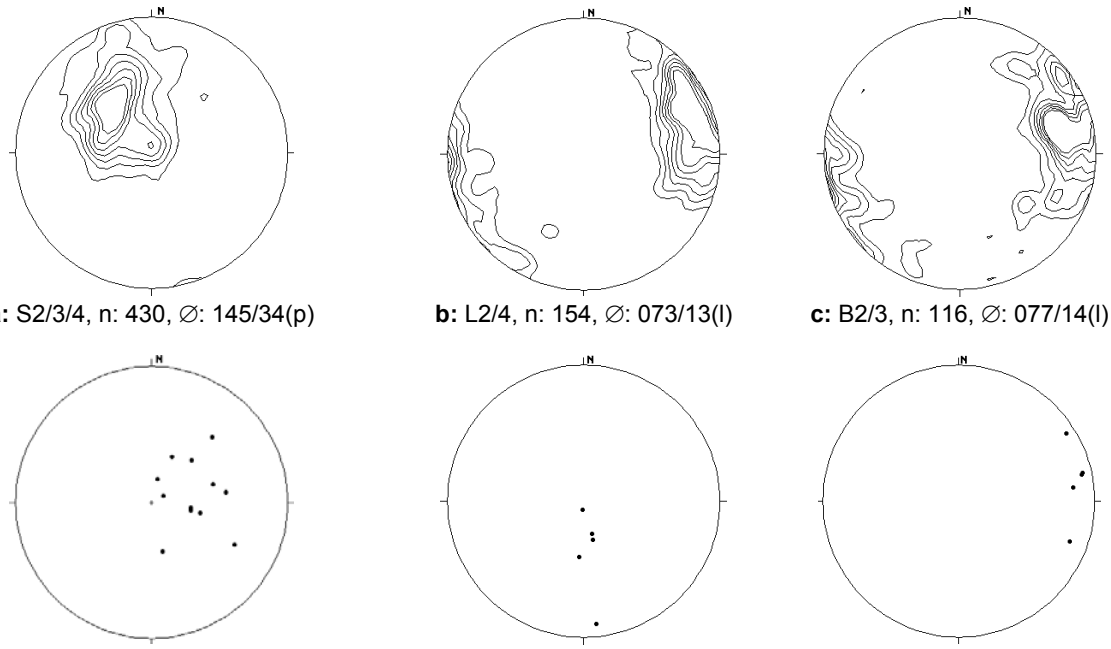

a: S2/3/4, n: 430, ∅: 145/34(p)

b: L2/4, n: 154, ∅: 073/13(l)

c: B2/3, n: 116, ∅: 077/14(l)

d: dots: rotated S4, n: 12, ∅: 258/26(p); cross: S2 rotated in horizontal orientation

e: S5, n: 5

f: B5, n: 5

Fig. 3.10: Orientation of structural elements in structural zone II, which refers to the Siniscola schists south of the Lodè orthogneiss (fig. 3.2), ∅: weighted average of data cluster.

The Alpine reorientation becomes evident in the pole diagrams, where the foliation cluster shows tendencies towards two perpendicular girdle distributions around NE and SE poles due to the Alpine change of dip and trend respectively (fig. 3.10a). Furthermore, the fold axes and the stretching linea-

tions display a girdle distribution consistent with a rotation from a pre-Alpine E-W trend to an Alpine NE-SW trend (fig. 3.10b-c).

3.5 Structural zone III

The structural zone III comprises the southern and eastern Lodè orthogneiss (fig. 3.2), which is shallowly foliated and thus distinguished from its steeply-foliated northern and northwestern parts. Furthermore, the absence of D1 structures is different from the adjacent Siniscola schists of structural zone II.

Thus, D2 is directly superimposed on the primary plutonic fabric. Parallel to the shallowly SE-dipping main foliation S2 (fig. 3.11a), there are aligned elongated aggregates of quartz, biotite enclaves, feldspar phenocrysts as well as white mica. They define, by their long axes, the stretching lineation L2, plunging gently to SW (fig. 3.11b). Asymmetric σ clasts developed from K-feldspar phenocrysts in places of more intense D2 simple shear, constituting C-type shear bands.

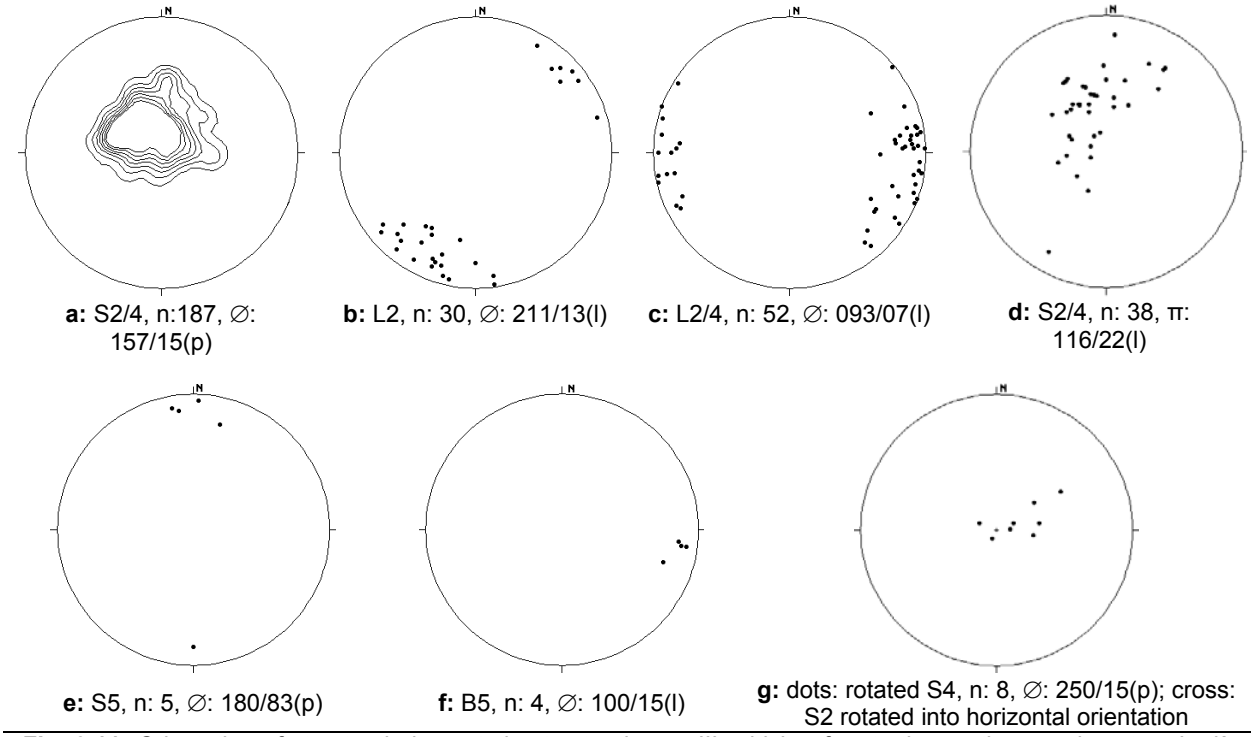

Fig. 3.11: Orientation of structural elements in structural zone III, which refers to the southern and eastern Lodè orthogneiss (fig. 3.2), π: pole to the best fit girdle of data cluster, ∅: weighted average of data cluster.

On the other hand, S2 was reactivated by S4, forming C'-type shear bands. S2 and D4 shear band crenulation have been rotated around the common intersection lineation, so that S2 becomes horizontal, in order to demonstrate the western dip of S4 with respect to S2 (fig. 3.11g). According to this spatial relation, which is the same as in structural zone II (fig. 3.10d), the D4 hanging wall transport down towards western directions is reconfirmed.

Particularly evident in this structural zone IV is that L2 was rotated dextrally during D4, so that a composite lineation L2/4 was formed, which plunges shallowly to the E (fig. 3.11b-c).

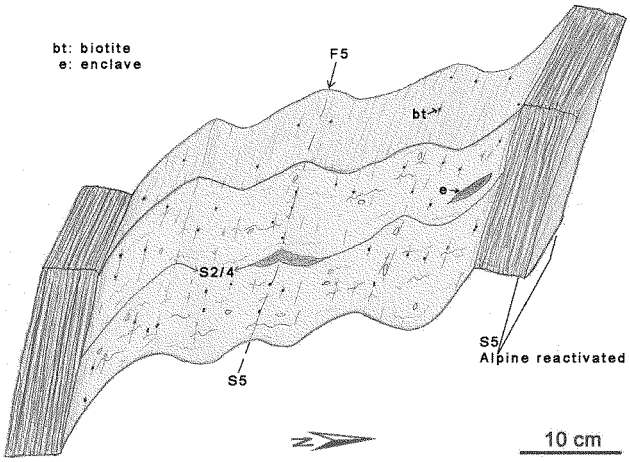

Fig. 3.12: Sketch of D5 buckle folds at the southern flank of the steep belt (fig. 3.2), Lodè orthogneiss (HH227). Biotite enclaves are aligned in S2/4 and became refolded in the F5 hinges. Biotite porphyroblasts preferentially formed along S5. Biotite-rich domains parallel to S5 became reactivated by Alpine frictional slip.

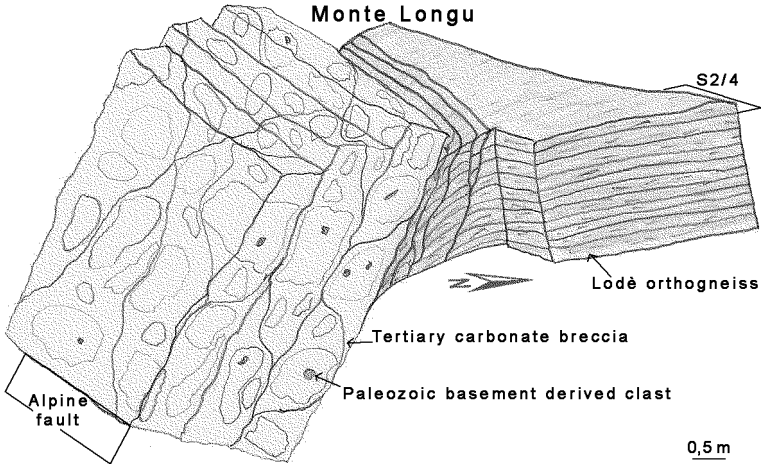

Fig. 3.13: Sketch of a 20 m long section along the road to the water station of La Caletta at the SE slope of Monte Longu (HH239). The network of SE-dipping brittle faults juxtaposed Alpine-reworked Tertiary breccia against subhorizontal Lodè orthogneiss. The Tertiary breccia contains fragments of Siniscola schists and Lodè orthogneiss, and shows carbonate neomineralisation along fault planes and in cavities.

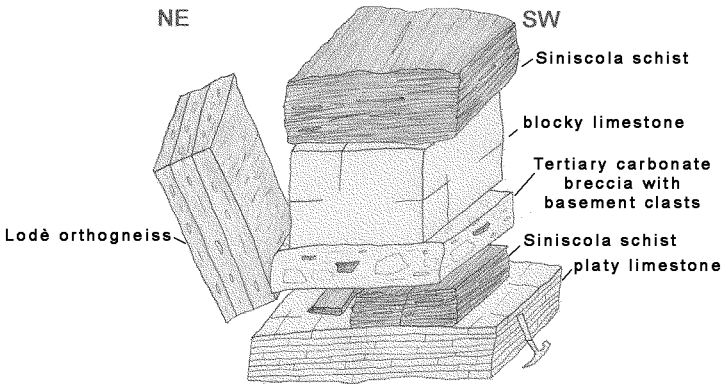

Fig. 3.14: Sketch of an Alpine tectonic sequence cropping out at the crest of Monte Longu, La Caletta (HH240).

F5 appears in the central Lodè orthogneiss at the transition to the steeply-foliated part of structural zone V, and increases within half a kilometre from centimetre to decimetre half wavelength before the dip of S2/4 changes abruptly from shallow to steep. The upright E-W trending D5 buckle folds have a

steeply south-dipping axial plane and deform S2/4 (fig. 3.11d-f). The F5 axial plane is marked by aligned biotite porphyroblasts (fig. 3.12).

Along the Alpine Santa Anna fault, the Lodè orthogneiss and intercalated Siniscola schists dip shallowly to moderately southeastwards and rest discordantly upon the steeply-foliated Lodè orthogneiss of structural zone IV (fig. 3.2). This is referred to a sinistral displacement of tectonic slices at the SE flank of the Lodè orthogneiss in relation to Alpine movements along the Nuoro fault system. This Alpine movement is additionally manifested in the curved structural trend, describing an arc concave to the south (fig. 3.2).

The spatially varying extent of the Alpine overprint becomes evident at Monte Longu (fig. 3.2). At its northern slope, the horizontal S2/4 layering of the Lodè orthogneiss is concordantly overlain by horizontal beds of Tertiary carbonates (plate 3.2e). At its southern slope, the horizontal S2/4 layering of the orthogneiss is crosscut by southeast-dipping Alpine faults, which juxtaposed the orthogneiss against Tertiary carbonate breccias with incorporated clasts of Lodè orthogneiss as well as of Siniscola schists (fig. 3.13-14).

3.6 Structural zone IV

Structural zone IV comprises the northern and northwestern Lodè orthogneiss (fig. 3.2). It shows the same D2/4 structures as the southern and southeastern Lodè orthogneiss of structural zone III, but steepened around a rotation axis coaxial with L2/4. Consequently, the down to the west symmetry, indicated by the D2/4 structures in structural zone III (fig. 3.11g), is changed into a dextral strike-slip symmetry. This dextral fabric displays the WNW-ESE trending S2, which is crosscut at a low angle along a steep intersection lineation by S4, that trend more toward NW-SE than S2 (fig. 3.15a, e).

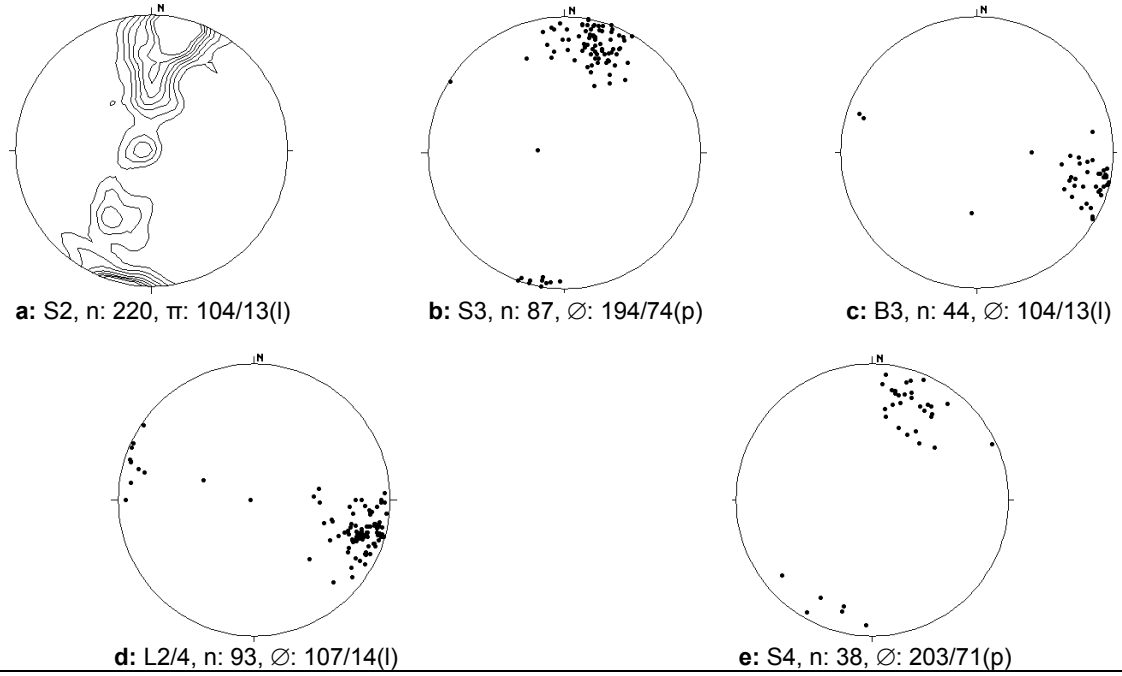

a: S2, n: 220, π: 104/13(l) **b:** S3, n: 87, ∅: 194/74(p) **c:** B3, n: 44, ∅: 104/13(l)

d: L2/4, n: 93, ∅: 107/14(l) **e:** S4, n: 38, ∅: 203/71(p)

Fig. 3.15: Stereo plots from structural zone IV, which refers to the northern and northwestern Lodè orthogneiss (fig. 3.2), π: pole to the best fit girdle of data cluster, ∅: weighted average of data cluster.

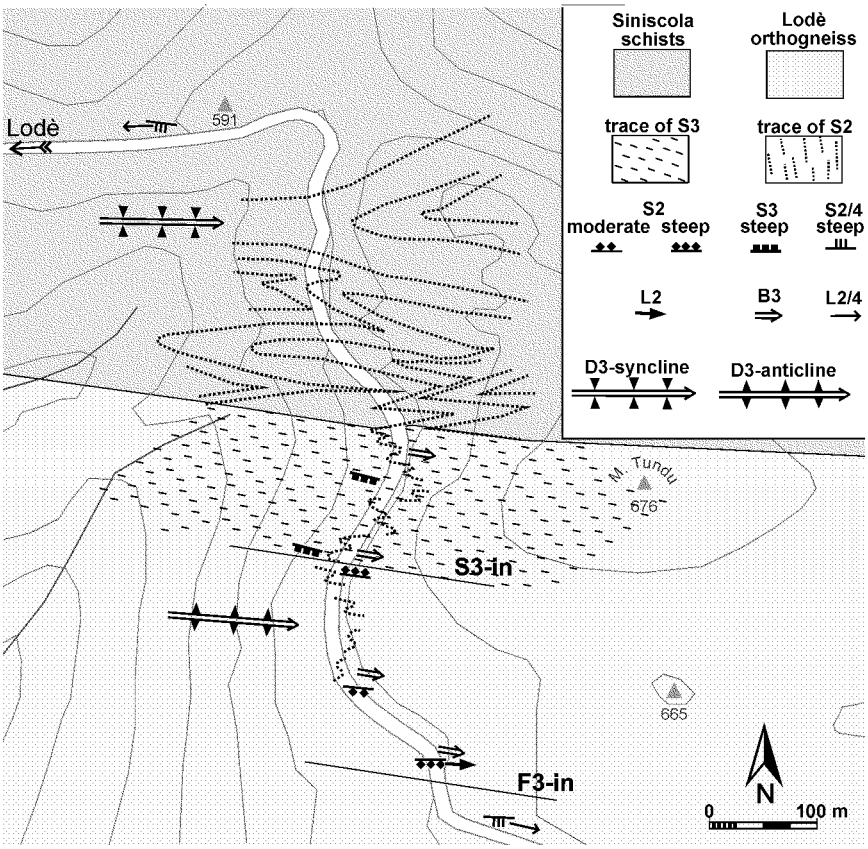

Fig. 3.16: Detailed map 'a' indicated in fig. 3.2. F3 traced by S2 is redrawn from aerial photographs in the Siniscola schists and obtained from road outcrop in the Lodè orthogneiss. The size of the lower order F3 is tentative in the Lodè orthogneiss due to the scarcity of folded markers.

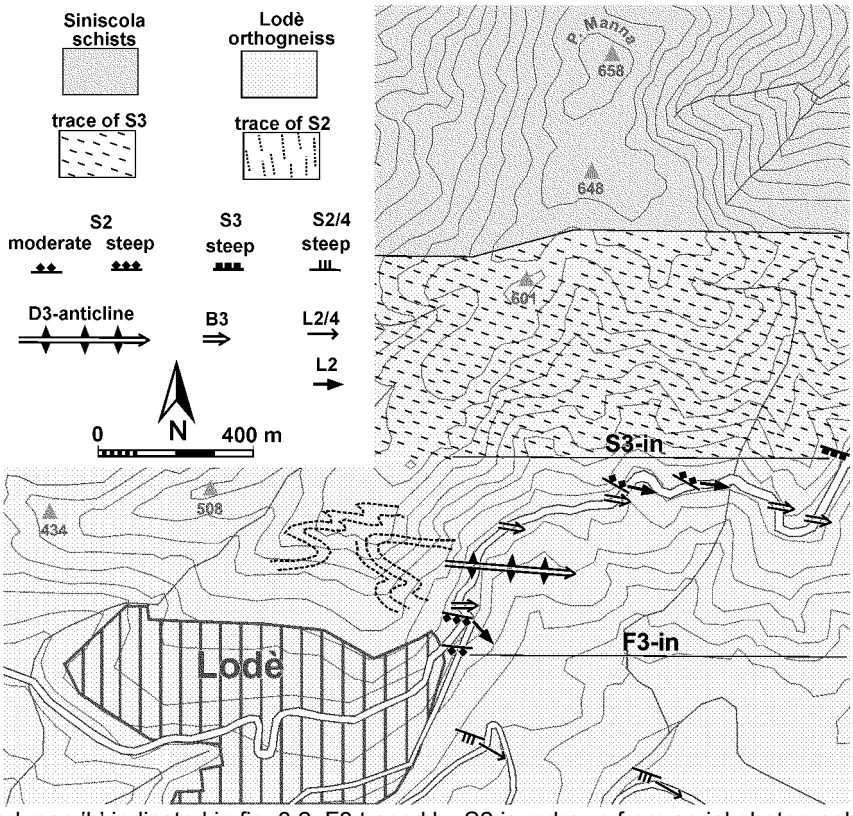

Fig. 3.17: Detailed map 'b' indicated in fig. 3.2. F3 traced by S2 is redrawn from aerial photographs.

D3 folds appear at the northern margin of the Lodè orthogneiss. Accordingly, S2 is displayed as a great circle girdle in the pole diagram (fig. 3.15a). The axial planar cleavage S3 dips steeply to the SSW (fig. 3.15b), and the F3 axis is coaxial with L2/4 (fig. 3.15c, d). Attenuation of the limb that makes a small angle with the axial plane (plate 3.2b), and dark seams along S3 in the axial plane (plate 3.2c) suggest pressure solution as the deformation mechanism.

The D3 folds are exposed in aerial photographs (scale 1: 10 000, Compagnia Generale Ripresearee di Ferretti Geom. Licinio di Parma, 1977) taken of the western slope of Monte Tundu and the area north of Lodè (fig. 3.16, 3.17). Here, the half wavelength of F3 reaches hectometre scale, and the enveloping surface of F3 is approximately horizontal. F3 tightens towards the northern margin of the orthogneiss over a distance of half a kilometre from open and concentric to close and similar-like folds, which have developed an axial planar cleavage as a consequence of increasing strain.

S2 has transposed the schist-orthogneiss contact (fig. 3.16). Consequently, the incoming F3 in the northern Lodè orthogneiss probably marks the beginning curvature of S2 into a first order F3 hinge that extends into the Siniscola schists.

3.7 Structural zone V

The western parts of the Siniscola schists north of the Lodè orthogneiss, of the Posada fault rocks, and of the southernmost Brunella gneisses are combined into structural zone V (fig. 3.2). It is distinguished from structural zone VI in the east by the differing Alpine reorientation. The Alpine overprint is manifested in the abundant occurrence of incohesive breccias (plate 3.3e).

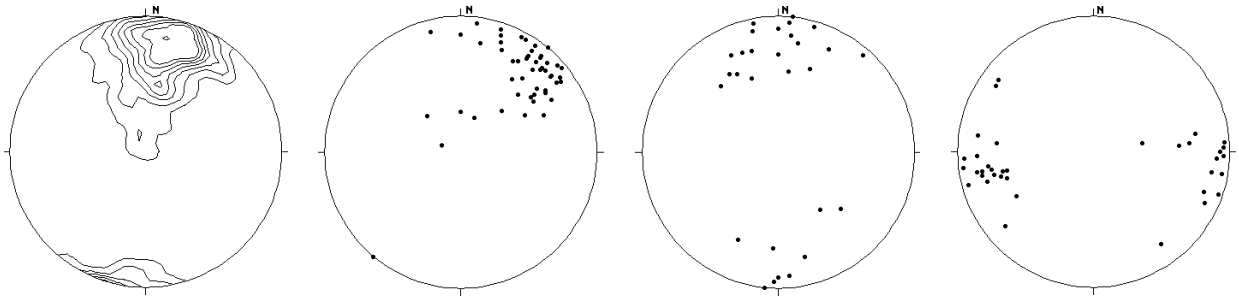

a: S2/3/4, n: 378, π: 278/01(l), ∅: 188/66(p)

b: S4, n: 49, ∅: 219/70(p)

c: S5, n: 28, ∅: 177/79(p)

d: B5, n: 37, ∅: 268/05(l)

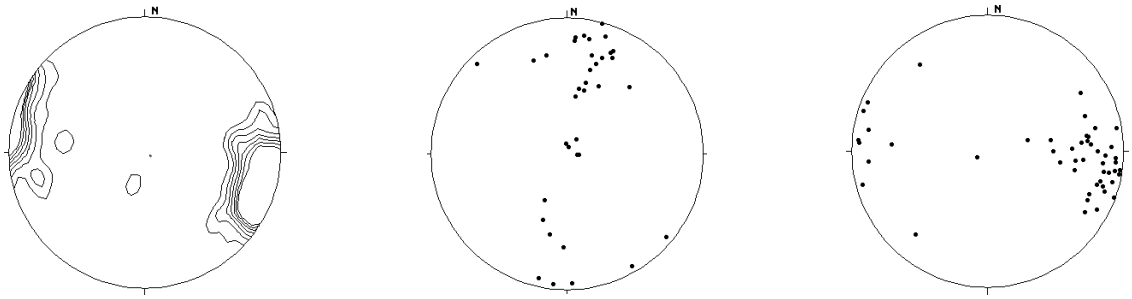

e: L2/4, n: 126, ∅: 104/08(l)

f: S2, n: 34, π: 278/05(l)

g: B2/3, n: 51, ∅:096/15(l)

Fig. 3.18: Stereo plots with structural elements of structural zone V, which refers to the western parts of northern Siniscola schists, Posada fault rocks, and southernmost Brunella gneisses (fig. 3.2), π: pole to the best fit girdle of data cluster, ∅: weighted average of data cluster.

The D4 shearing overprinted Siniscola schists and Brunella gneisses increasingly to the centre of the Posada fault, forming a network of high-strain zones that anastomose around low-strain islands and show a gradual transition between high- and low-strain rocks. Thus, the finite foliation is constituted to a varying extent by S2 and S4. Therefore, the main fabric in the Posada fault rocks is referred to be a composite fabric, e.g. S2/4, L2/4.

The composite S2/4 in the Siniscola schists can be described as C'-type shear bands crenulation cleavage such as aforementioned for the external Siniscola schists south of the Lodè orthogneiss in structural zone II.

D3 folding up to hectometre scale is documented in the Siniscola schists north of the Lodè orthogneiss (fig. 3.16). The interfering D2 and D3 folds display a hook-shaped pattern, indicating a coaxial orientation of the F2 and F3 axes. The dextral D4 reorientation has affected the previous structures to a varying extent, which is reflected by the Z-shaped girdle distribution of S2 in fig. 3.18 f. With increasing D4 strain towards the centre of the Posada fault the shallow S2 in the fold hinges become increasingly sheared (plate 3.2h) though the shearing is less intense than in the steep fold limbs.

The more competent layers of the Torpè metabasite intercalated in less competent gneiss became asymmetrically boudinaged during the Posada faulting. This expresses an increased ductility in comparison to the shear band-crenulated Siniscola schists, suggesting higher temperatures during the early D4 stages in the Brunella gneisses (plate 3.2g).

Quartzofeldspathic veins have intruded the D1 fabric of the Brunella gneisses and are interpreted as leucosomes (plate 3.2f). Progressive deformation and transposition, particularly during D4, led to the formation of banded gneisses with quartzofeldspathic and biotite-rich layers (fig. 3.19). Locally, late shear bands are associated with S2/4 in the Brunella gneisses. Aligned sillimanite porphyroblast aggregates commonly mark the stretching lineation L2/4 (plate 3.3c).

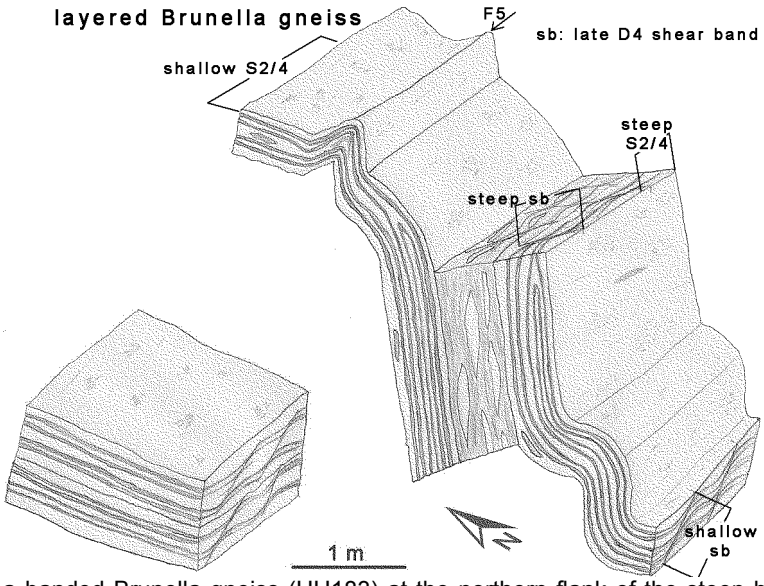

Fig. 3.19: Sketch of a banded Brunella gneiss (HH183) at the northern flank of the steep belt (fig. 3.2). The D5 flexures accommodate the apparent change of displacement indicated by the D4 shear bands from dextral in steeply dipping layers to top to the west in shallowly dipping layers.

Pre-D4 structures became erased in the fine-grained, well-foliated mylonites of the Posada fault. The mylonites that derived from Brunella gneiss commonly have a darker colour than the mylonites that derived from the Siniscola schists, because the latter inherited more white mica, which is manifested in a more pronounced shear band crenulation as well (plate 3.3 a, b).

The orientation of the structural elements can be summarised as follows. Foliation and fold axial planes generally dip steeply to the SSW (fig. 3.18a, b, c). Fold axes and stretching lineation are coaxial and plunge shallowly to the ESE (fig. 3.18d, e, g). The trend of the pre-D4 structures became dextrally displaced, reconfirming the dextral strike-slip kinematics of the D4 shear bands, which is also displayed by their spatial relation to the pre-D4 foliations (fig. 3.18a, b).

However, the steeply dipping foliation with the dextral shear band symmetry changes to a shallowly dipping foliation with a top down to the west symmetry in the north at the transition to structural zone VII (fig. 3.2). This change is partly accommodated by decametre sized flexures associated with D5 folds (fig. 3.19). F5 is commonly developed as upright buckle folds with a crenulation cleavage in the hinges dipping steeply to the south and a horizontal E-W trending axis (fig. 3.18c, d). It is superimposed on S2/3/4, as displayed by the girdle distribution (fig. 3.18a).

3.8 Structural zone VI

Structural zone VI comprises the Siniscola schists north of the Lodè orthogneiss, the Posada fault rocks and the southernmost Brunella gneisses in trending prolongation of structural zone V to the east. Therefore, the same structures occur and their relative orientation remains the same as in structural zone V. However, the structures are displaced as a whole due to Alpine reorientation, so that an ENE-WSW trend is displayed by the steeply southwards dipping foliations and the shallowly plunging stretching lineation, which is fairly coaxial oriented with the fold axes, (fig. 3.20a, b, c).

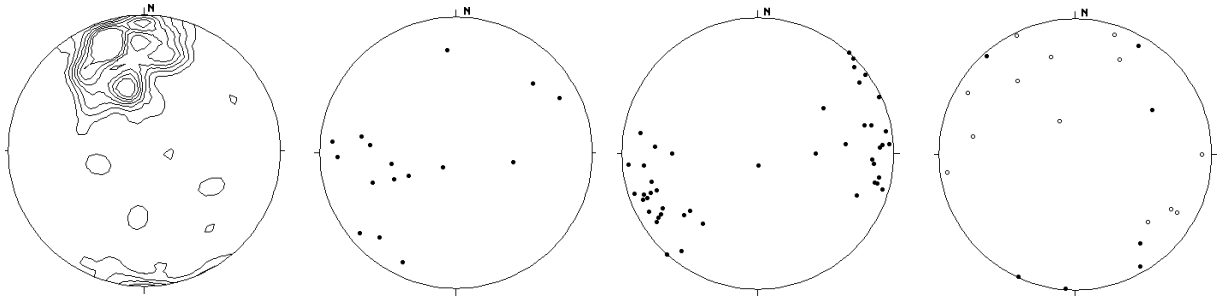

a: S2/3/4, n: 105, π: 085/15(l), ∅: 167/64(p)

b: B2/3/5, n: 16, ∅: 249/29(l)

c: L2/4, n: 44, ∅: 253/03(l)

d: basalt dikes, n: 20, ∅: 145/86(p), dots: in steep belt, circles: outside steep belt

Fig. 3.20: Stereo plots from structural zone VI, which refers to the eastern parts of northern Siniscola schists, Posada fault rocks, and southernmost Brunella gneisses. The basalt dikes occur in and outside the steep belt (fig. 3.2), π: pole to the best fit girdle of data cluster, ∅: weighted average of data cluster.

Ductile D4 shearing stretched the Torpè metabasites, which contain numerous quartzofeldspathic layers and patches, so that they display a characteristic dark-bright banding (fig. 3.21).

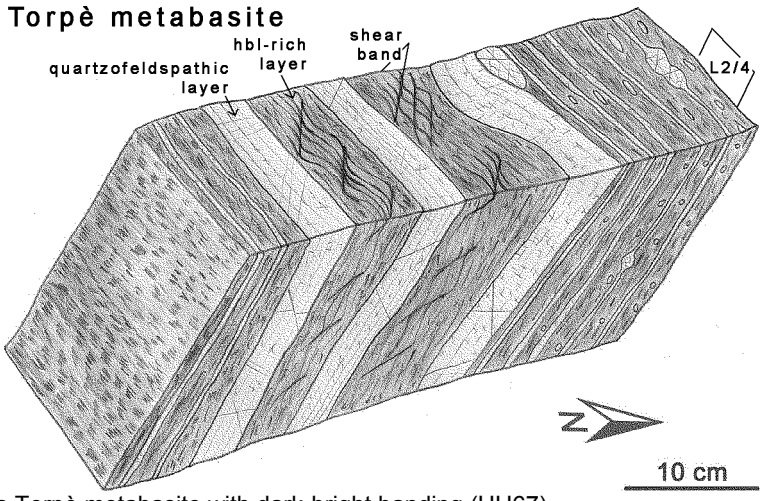

Fig. 3.21: Sketch of a Torpè metabasite with dark-bright banding (HH67).

To the southeast, the steeply-foliated western part of this structural zone is discordantly overlain by a sliver of shallowly to moderately southeast-dipping basement and Mesozoic beds at Monte Nurres (fig. 3.2, plate 3.3d). Thus, the aforementioned Santa Anna fault probably accommodated the emplacement of the Monte Nurres sliver and might be related to the sinistral rotation in the basement below from an E-W to a NE-SW trend.

The Monte Nurres sliver wedges out to the NE, according to the structural state of the Mesozoic limestone at Posada, which rests subhorizontally on the steeply foliated E-W trending basement (fig. 3.22). The cover-basement contact at Posada confirms the original steep attitude of the basement foliation in this area, which is outlined as steep belt in fig. 3.2. This is also suggested by basalt dikes (fig. 3.20d) that intruded the basement during Permo-Triassic times (Traversa & Vaccaro 1992). Their similar range of orientation in and outside the steep belt favours a steepening of the dip due to Variscan rather than Alpine tectonics.

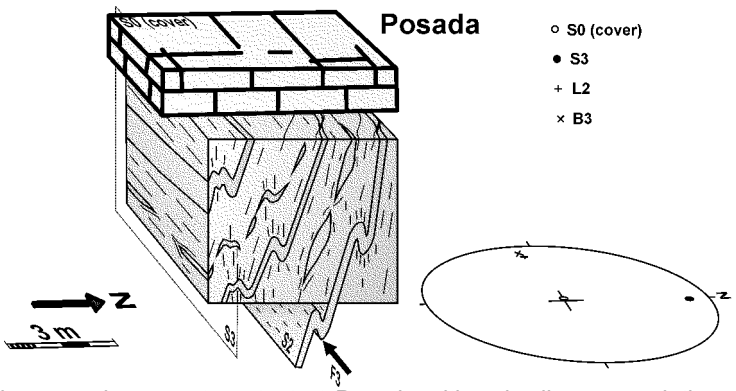

Fig. 3.22: Sketch of the cover-basement contact at Posada with pole diagram, pointing out the spatial relation between Mesozoic bedding and Paleozoic basement structures. According to this relation, the steepening of dip in the steep belt (fig. 3.2) is related to late Variscan rather than Alpine tectonics.

3.9 Structural zone VII

Structural zone VII refers to the Brunella gneisses without their southernmost part. It comprises partly migmatic ortho- and paragneisses, locally intercalated by calc-silicate gneisses and metabasites.

In places, S1 is preserved as continuous cleavage, transposing the primary compositional layering. Quartzofeldspathic veins crosscut S1 and/or contribute to a stromatic layering coplanar with S2 (plate 3.4a). The quartzofeldspathic veins and layers are bordered by biotite selvages and biotite gneiss, representing leucosome and melanosome respectively. The dominant D2 foliation dips mainly to the SE (fig. 3.23a) and is commonly deformed by isoclinal folds, which have curved axes in places (plate 3.3f, fig. 3.23c). Locally, sheath folds are developed (plate 3.3g-h). Elongate sillimanite-containing nodules define L2 in some paragneisses (plate 3.4c). L2 prevailingly trends NE-SW and has a mainly shallow plunge (fig. 3.23b).

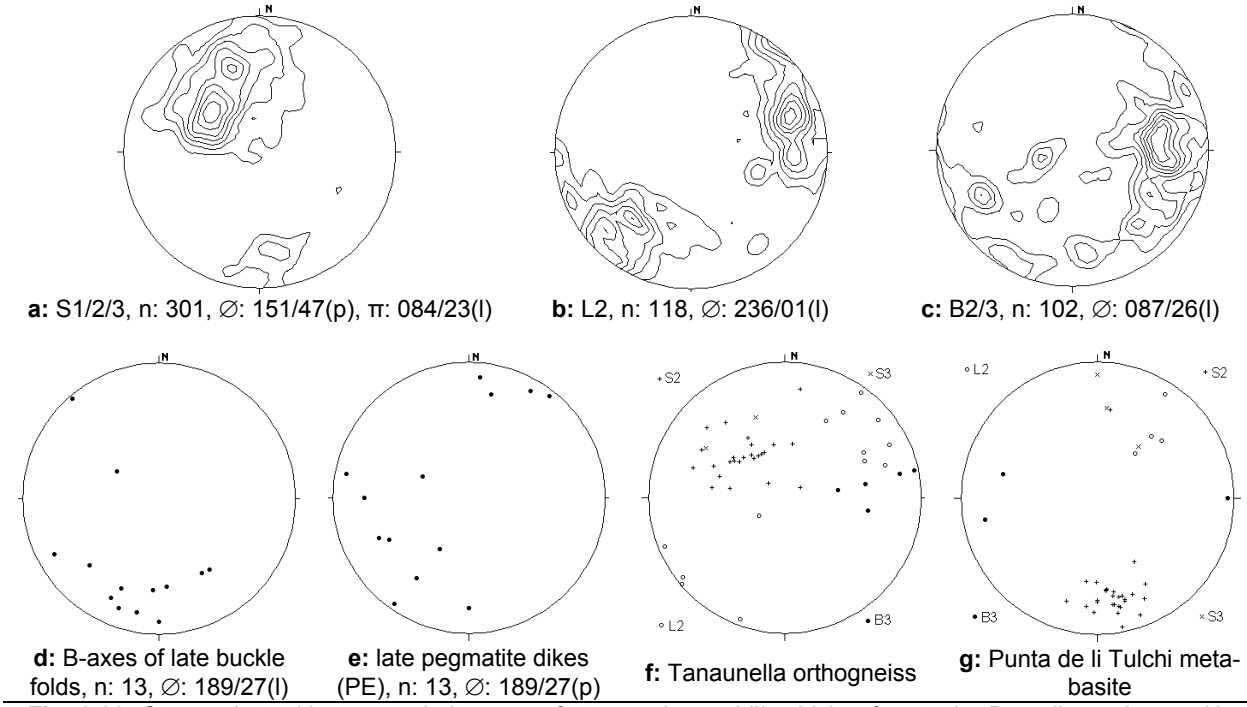

a: S1/2/3, n: 301, ∅: 151/47(p), π: 084/23(l)
b: L2, n: 118, ∅: 236/01(l)
c: B2/3, n: 102, ∅: 087/26(l)
d: B-axes of late buckle folds, n: 13, ∅: 189/27(l)
e: late pegmatite dikes (PE), n: 13, ∅: 189/27(p)
f: Tanaunella orthogneiss
g: Punta de li Tulchi metabasite

Fig. 3.23: Stereo plots with structural elements of structural zone VII, which refers to the Brunella gneisses without the southernmost part (fig. 3.2), π: pole to the best fit girdle of data cluster, ∅: weighted average of data cluster.

The style of D3 folding varies considerably, from similar to buckle folds (plate 3.4f-g). B3 is commonly coaxial with L2 and B2 (fig. 3.23b-c). Thus, hook-shaped fold interference patterns are common.

Late folds overprint previous structures mainly in buckle-like style. Their fold axes plunge gently to the south (fig. 3.23d). Late shear bands, commonly with normal sense of slip, developed in places. The indicated movement is mainly top towards the south.

The orthogneisses of San Lorenzo and Tanaunella form elongated outcrops enveloped by the main D2 layering of the surrounding gneisses and are aligned parallel to the NE-SW stretching lineation L2 (fig. 3.2, fig. 3.23f). The D2 structures of these orthogneisses are superimposed on the magmatic protolith fabric. The continuous D2 foliation is mainly marked by aligned biotite. S2 dips to the SE (fig. 3.23f). S3 is developed as crenulation cleavage in places, showing an intersection lineation coaxial with L2 (fig. 3.23f), and thus contributes to a pencil-like lineation locally. The fairly equigranular

quartz and feldspar of the orthogneisses from San Lorenzo and Tanaunella counterpoint the feldspar augen developed in other orthogneisses, e.g. at Porto di Ottiolo (plate 3.4b).

The metabasite at Punta de li Tulchi is part of an E-W trending array of metabasite bodies intercalated within migmatic ortho- and paragneisses (fig. 3.2). The compositional layering is pronounced by garnet-rich layers and transposed by the main foliation S2. The exposed porphyroblast aggregates of coronitic garnet derive from retrogression of a preceding high-pressure mineral assemblage (plate 3.4d-e). The shallowly NE-plunging stretching lineation L2 (fig. 3.23g) is defined by the aligned porphyroblast aggregates and by slickensides and/or slickenlines. Locally, a D3 crenulation cleavage is developed (fig. 3.24, fig. 3.23g). The late shear bands of normal displacement with respect to the main foliation are consistent with the top to the south shear bands in the surrounding gneisses, taking an overturned attitude of the metabasite layering into account. Accordingly, the Punta de li Tulchi metabasite appears to be reoriented by late Variscan and/or Alpine tectonics.

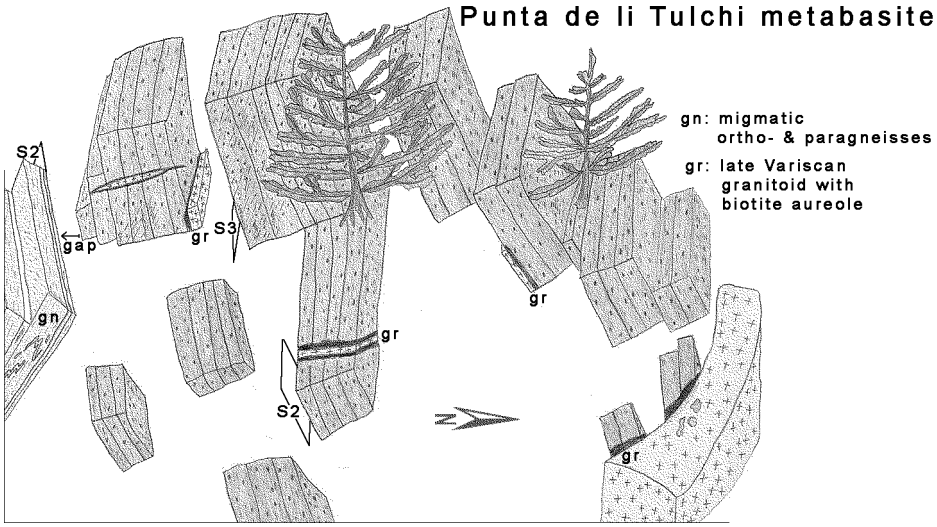

Fig. 3.24: Retrogressed eclogite in the approx. 25 m long coastal outcrop at Punta de li Tulchi (HH115). The contact to the migmatic gneisses is obscured by an exposal gap.

Alpine brittle deformational structures are abundant (plate 3.4h, 3.5a). However, considerations about the Alpine reorientation are limited due to the long distance to the Mesozoic cover rocks (plate 3.5b).

3.10 Deformational succession

1) A continuous cleavage and segregation quartz veins coplanar with S1 remain from D1. The D1 structures occur within the Siniscola schists and Brunella gneisses, which represent the internal part of the studied sequence with respect to the orogenic anatomy, but are absent in the Ordovician porphyroid interlayered Orune schists of the external part as well as in the Ordovician orthogneisses of the internal part.

2) D2 gave rise to the most pervasive structures from the low-grade Orune schists to the high-grade Brunella gneisses. The dominant foliation lies in the axial plane of the tight to isoclinal intrafolial D2 folds and exposes a stretching lineation L2, which is coaxial with the shallowly plunging F2 axis. L2 developed originally in orthogonal orientation with respect to the orogenic trend.

3) Two hinges of kilometre-sized first order D3 anticlines have been identified south of Lula and north of Lodè, and one first order syncline has been inferred to exist in between. F3 and F2 display a hook-shaped interference pattern. Consequently, they are coaxially oriented.

4) The retrograde D4 non-coaxial shearing is focused in the mylonitic to cataclastic Posada fault rocks, along which medium-grade Siniscola schists are juxtaposed against the high-grade Brunella gneisses. S4 is commonly developed as a C'-type shear band crenulation cleavage, crosscutting and/or reactivating the previous foliations at low angles, so that they became thinned and stretched. The shear bands formed under low-grade conditions in the Siniscola schists from the early D4 stages on, whereas they might be superimposed on the D2/4 layering of the Brunella gneisses not before the D4 retrogression had progressed from medium- to low-grade conditions. Previous lineations became rotated dextrally from orthogonal into parallel orientation with respect to the orogenic trend. The symmetry of the D4 structures displays a lateral hangingwall transport downwards to western directions.

5) A large D5 flexure parallel to the orogenic trend accommodated uplift of the axial zone relative to the external vicinity. Previously shallow-dipping foliations became rotated around an axis coaxial with the D4 stretching lineation in the steeply south-dipping to upright limb of this flexure, in which the Posada fault rocks crop out as well. Crenulation cleavages and/or buckle folds of the same attitude like the large flexure developed inside the steep limb and in the external vicinity.

6) Brittle Alpine faulting involves tilting downwards to the southeast and a sinistral displacement component parallel to the tilting axis, which resulted in the sinistral shift of the basement trend from the Variscan E-W trend towards the NE-SW trend of the Nuoro fault. According to its dominance, the Nuoro fault operated as a master fault, while the complementary dextral reactivation of the Posada fault rocks maintained the Variscan attitude in the steep belt.

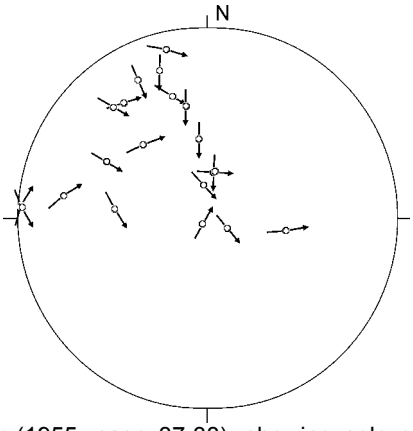

Fig. 3.25: Lineation after Hoeppener (1955, page 37-38), showing pole of the plane, lineation and movement direction of hangingwall in Alpine faults measured at various places throughout the study area.

Numerous minor faults and the spatially varying extent of Alpine tilting indicate a complex and widespread deformational pattern that has affected the entire Paleozoic basement. Shear sense indicators, such as slickenfibers, drag folds or Riedel shears, show displacement directions varying

from northeast to south (fig. 3.25), confirming a complex pattern of the Alpine overprint. The extent of the Alpine reorientation on the basement is estimated by the spatial relation between Paleozoic structures and Tertiary to Mesozoic bedding at the post-Variscan cover-basement contact along the Monte Albo massif, such as summarised in fig. 3.26. Accordingly, the F3 axial planar cleavage as well as the composite D2/4 cleavage outside the steep belt show a similar dip like the cover bedding. Thus, they had a shallowly inclined pre-Alpine orientation outside the steep belt, whereas the dip in the steep belt was not modified by the Alpine overprint.

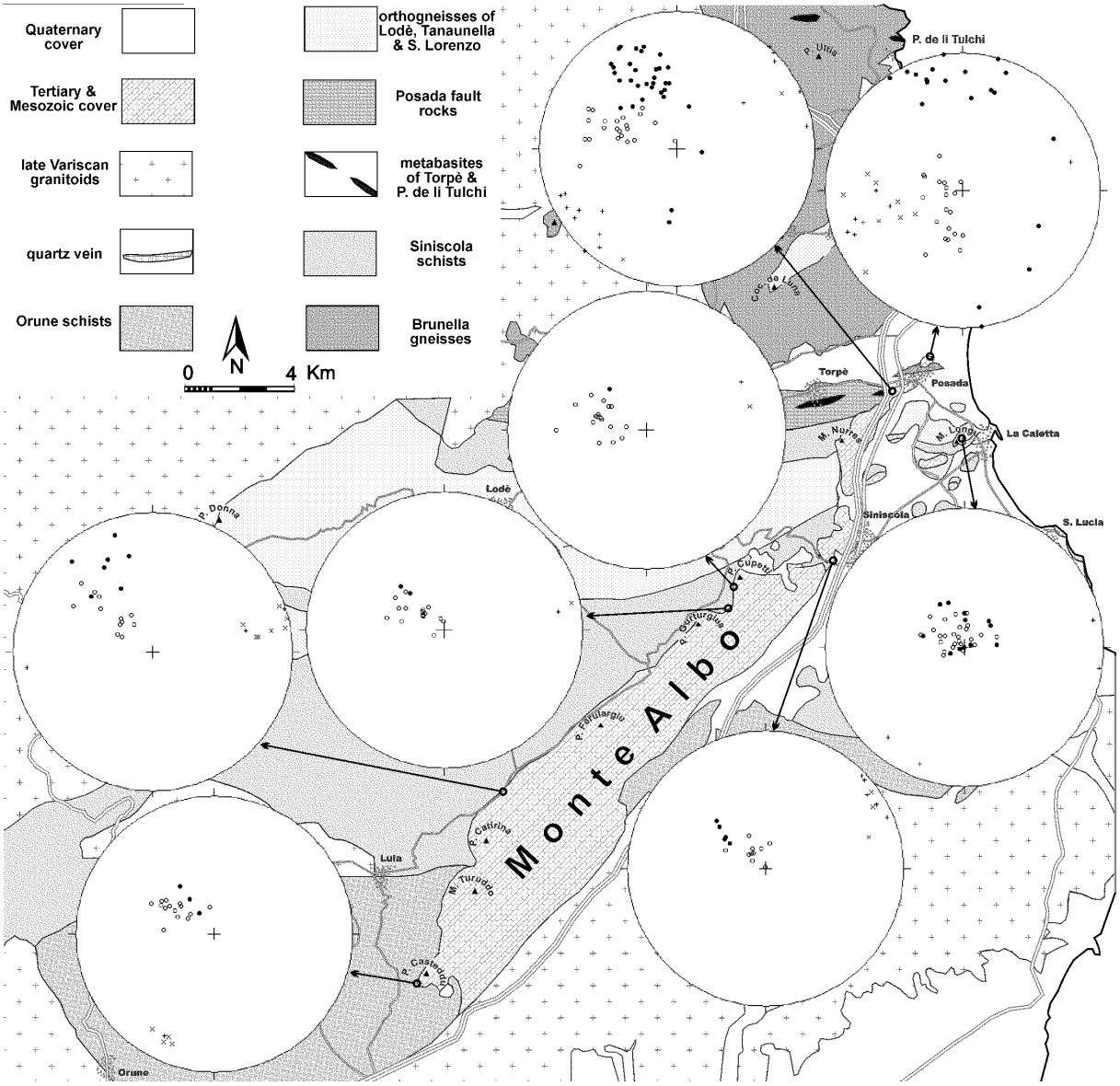

Fig. 3.26: Pole diagrams from the cover-basement contact showing spatial relation between cover bedding and basement structures. Circles: cover bedding, dots: basement foliation (P. Casteddu: S3; M. Longu: S2/4; Posada: S2/3/4/5; the others: S2/3/4), asterisks: basement fold axes (P. Casteddu: B3; Posada: B2/3/5; the others: B2/3), cross: basement stretching lineations (P. Casteddu: L2; the others: L2/4).

3.11 Discussion

Based on the structural data, the Alpine reorientation of the basement structures and their pre-Alpine orientation can be estimated. Following the cover-basement contact along Monte Albo from southwest

to northeast leads from the structurally higher Orune schists across the underlying Siniscola schists to the structurally deeper Lodè orthogneiss (fig 3.2-3). Taking this and the measured low-angle orientation between cover beds and basement layers into account (fig. 3.26), an originally shallowly southwards dipping attitude is inferred for the basement layering outside the steep belt (fig. 3.27a).

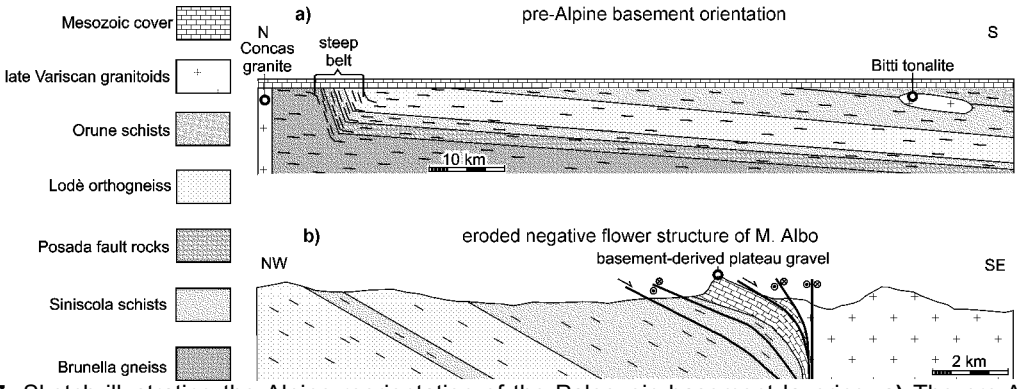

Fig. 3.27: Sketch illustrating the Alpine reorientation of the Paleozoic basement layering. **a)** The pre-Alpine orientation of the basement layering is inferred to be shallowly dipping to southern directions with respect to present coordinates. **b)** The negative Monte Albo flower structure evolved from dextral strike-slip and normal displacement along the Nuoro fault. The resulting structural low of the Monte Albo is confirmed by the occurrence of basement-derived pebbles ('Augensteine') on top of the Monte Albo plateau, remaining from Tertiary gravel deposits.

The interpretation by Carmignani et al. (1992b) of the Nuoro fault and the Monte Albo massif to its northwest is accepted in as much as the Monte Albo probably constitutes a flower structure. In contrast to the proposed compressive component of the Monte Albo flower structure (Carmignani et al. 1992b), the Tertiary to Mesozoic cover of Monte Albo should be situated in a structural low; otherwise it would not have survived the subsequent erosion. Indeed, its situation in a structural low is confirmed by the remaining basement-derived gravel, occurring on top of the Monte Albo plateau. Contrary to Carmignani et al. (1992b), the Monte Albo massif and the Nuoro fault system should constitute a negative rather than a positive flower structure therefore (fig. 3.27b). Also, the movement directions ranging from south to northeast (fig. 3.25) would fit a negative better than a positive flower structure. A positive flower structure would require movements in opposite directions instead.

Based on their interpretation, Carmignani et al. (1995) proposed Oligocene compression in NE Sardinia, related to the Alpine collision in Corsica. However, this is incompatible with the contemporaneous post-collisional extension in Corsica (Jolivet et al. 1990, 1991, 1994, Daniel & Jolivet 1996) and in the north Tyrrhenian basin (Mauffret & Contrucci 1999) as well as with the contemporaneous extensional setting that led to the Sardic rift system (Cherchi & Montadert 1982). Thus, the negative flower structure of Monte Albo fits the regional setting better.

Furthermore, a model for back arc kinematics is deduced by referring related structures of the region to the retreat of the Apenninic-Maghrebidic arc (fig. 3.28, 3.29). There are a couple of theoretical models about the kinematics in the Apenninic-Maghrebidic back arc, proposing lithospheric boudinage due to eastward mantle flow (Gueguen et al. 1997, Doglioni et al. 1999), or opening of mega-

continental tension gashes (Gelabert et al. 2002). However, the model proposed hereafter might be less speculative, because it relies on the interpretation of structures, which are proven to exist.

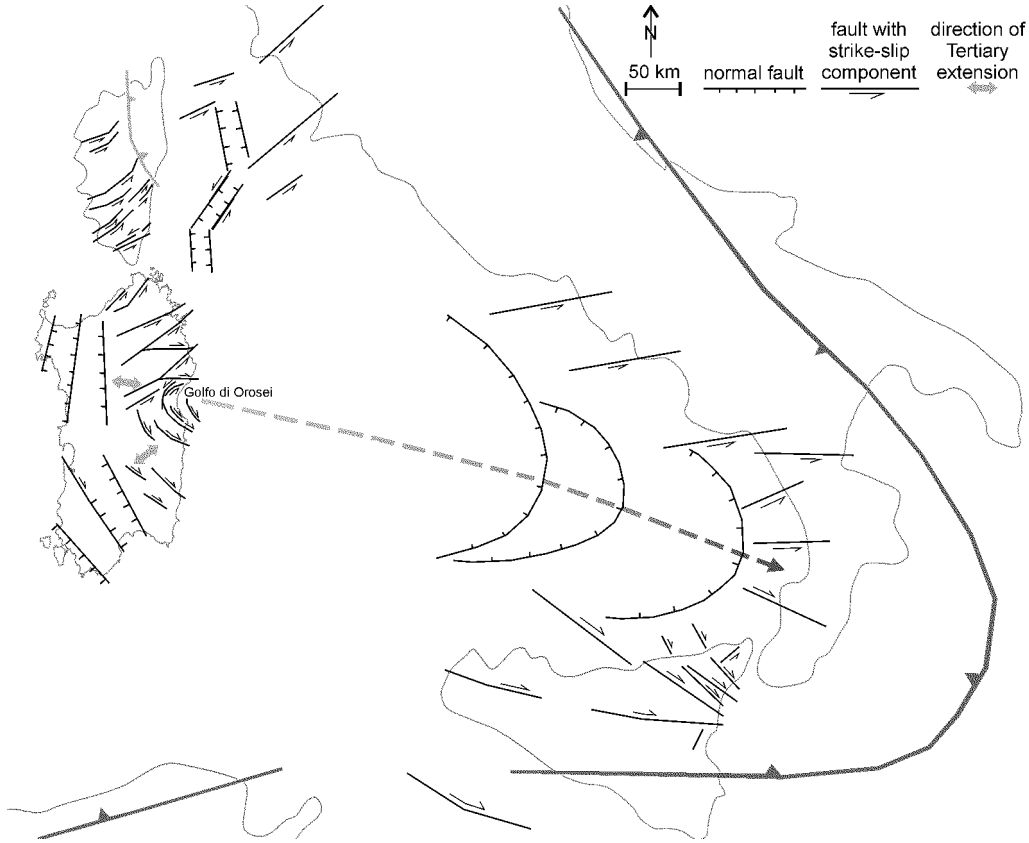

Fig. 3.28: Fault pattern at the Tyrrhenian basin in relation to the retreating Apenninic-Maghrebidic arc.

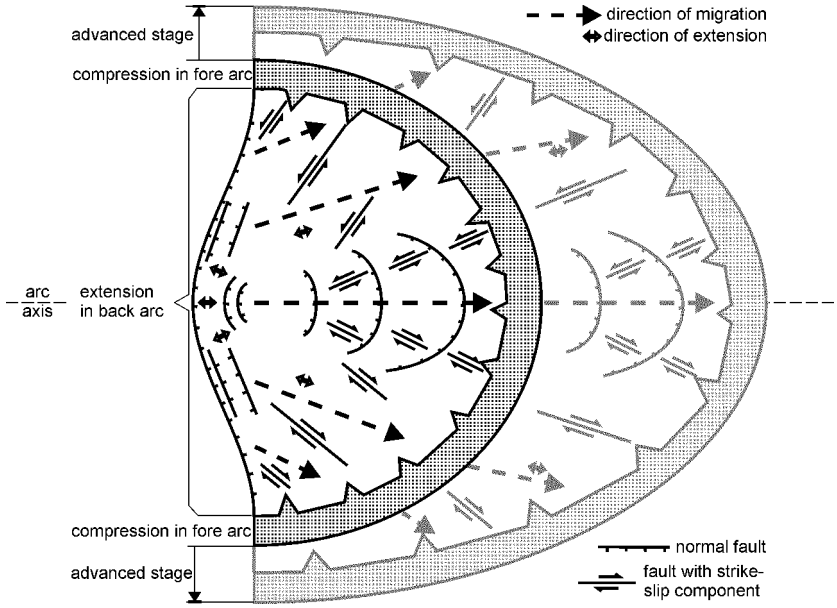

Fig. 3.29: Schema of a migrating arc, illustrating the varying strain in the back arc due to the laterally decreasing slab pull. It displays circular faults on the arc axis and transtensive radial faults with complementary displacement in the opposing halves.

Accordingly, further structural lows are marked by several more occurrences of Mesozoic to Tertiary cover coupled with Alpine faults in NE Sardinia; e.g. the Tavolara massif at the Tavolara fault, the Golfo di Aranci massif at the Olbia fault, the Tutavista massif at the Cetrino fault, etc.. Also, major

sinistral NE-SW trending faults, such as the Nuoro fault, occur in Corsica (Carmignani et al. 1995) and the north Tyrrhenian basin (Mauffret & Contrucci 1999). The E-W extension indicated by the conjugate sinistral NE-SW and dextral E-W trending faults in NE Sardinia is consistent with the N-S trending northern branch of the Sardic rift (fig.3.28). The circular faults at the Golfo di Orosei ('Kesselbrüche', Teichmüller 1931) indicate a change of strain orientation along strike from E-W to NE-SW extension that agrees with the NW-SE trending southern branch of the Sardic rift, i.e. the Campidano graben, and the dextral faults in southern Sardinia. Furthermore, sinistral faults in Calabria, circular faults in the southeast Tyrrhenian sea and dextral faults in the Peloritan mountains (Lentini et al. 1995, Van Dijk et al. 2000) fit into the Sardinian pattern. Consequently, circular faults probably developed in response to radial extension at the arc axis, whereas transtensive faults occur with complementary displacement in the opposing halves (fig. 3.29). The transtensive faults presumably accommodated in addition to tangential rifts the differential extension and rotation due to the laterally decreasing slab pull.

The presence of a pre-Variscan cover-basement relationship is suggested by the distinct occurrence of the Ordovician metavolcanics and metagranitoids, i.e. orthogneisses of Lodè and Tanaunella and porphyroids in the Orune schists (chapter 2 and 6). Moreover, it is confirmed by the distinct occurrence of S1, which is restricted to the metagranitoid-hosting Siniscola schists and Brunella gneisses. Consequently, pre-Variscan tectonics was involved in the internal Sardinian Variscides as well, although such an unconformity as the Sardic unconformity in the external zone is not developed.

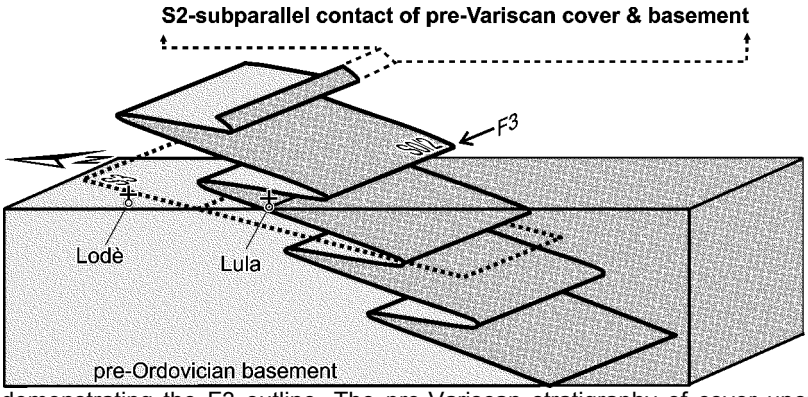

Fig. 3.30: Sketch demonstrating the F3 outline. The pre-Variscan stratigraphy of cover upon basement is still preserved, according to the pre-D3 Barrovian metamorphism, progressing from the external to the internal Siniscola schists (chapter 5). Consequently, a southern vergence of the D3 folds (after the concept of Bell 1981) and a southern dip of the enveloping F3 surface can be deduced. The reverse F3 attitude results from post-D3 reorientation of the originally recumbent F3 attitude by Alpine tilting and D5 flexuring. The latter is not shown.

The pre-Variscan cover-basement contact, which is represented by the contact between the Orune and Siniscola schists, is used to reconstruct the F3 outline due to the lack of other mapped marker horizons. Moreover, that the external parts overlaid the internal parts after D2 is supported by the pre-D3 Barrovian metamorphism, progressing from the external to the internal Siniscola schists (chapter 5). Thus, the pre-Variscan stratigraphic order of cover upon basement is still preserved. Furthermore, it is

reasonable to assume a fairly S2-subparallel orientation of the contact, because the turbiditic protolith character common in the Orune schists implies a low angle between cover bedding and basement surface due to the low relief-distal sediment relation. This contact probably became tectonically further aligned by the D2 transposition. Consequently, a southern dip for the enveloping surface and a southern vergence for the D3 folds are inferred, according to their presently prevailing E-W trending orientation (3.30). Moreover, a reverse attitude is deduced for the D3 folds, taking into account their post-D3 reorientation due to D5 flexuring and Alpine tilting. The reverse F3 attitude implies that the limbs that appear as normal limbs in the outcrop are actually inverted limbs and the limbs that appear as inverted limbs in the outcrop are actually normal limbs.

The externally-directed dip of the F3 enveloping surface indicates that the internal sequence was overlain by the external sequence after D2. Therefore, the model by Cappelli et al. (1992, fig. 3.1) that the internal part was thrust over the external part followed by structural inversion due to subsequent back folding is refuted. Moreover, it shows that the Lodè orthogneiss is situated in the inverted limb of a reverse first order D3 fold. Only at its contact to the internal Siniscola schists, the hinge curvature of a first order synformal anticline is exposed, which extends into the adjacent Siniscola schists. Consequently, a situation of the Lodè orthogneiss in the core of a large anticline, such as proposed by Cappelli et al. (1992, fig. 3.1), is ruled out. Also, it is demonstrated that the mylonites in the Posada fault derived from the adjacent Siniscola schists and Brunella gneisses. Thus, the idea that the Posada fault was superimposed on a Variscan suture zone is untenable.

The D5 flexuring caused a differential uplift between the axial zone and its external vicinity. The lower limit of this D5 exhumation should correspond to the eight kilometre width of the steep belt due to reasons of flexure geometry. This exhumation might be related to the tectonic denudation by the lateral D4 hangingwall transport along the Posada fault. According to this interpretation, the Posada fault is a lateral detachment fault bounding an uplifting gneiss dome below and a schistose mantle above, which is confirmed by:

- the low-angle crosscutting relation with the axial planar cleavage of the recumbent D3 folds,
- the extensional D4 morphology with respect to the overprinted structures,
- the retrograde evolution in the Posada fault,
- the decreasing peak metamorphism from foot- to hangingwall,
- the presence of high-pressure rocks in the footwall,
- the occurrence of the stratigraphic younger rocks in the hanging wall
- the overall externally-directed dip, i.e. towards external parts of the orogen.

Consequently, that segment of the Posada fault, which is exposed in the steep belt, represents a stair-stepping segment of a detachment fault. An overlap of D4 and D5 is reasonable, because tectonic denudation and uplift are probably components of a continuous exhumation process. Thus, the late normal displacement of the detachment fault was associated with strike-slip displacement at the flank of

the uplifting gneiss dome. Consequently, the primary tectonic process behind the strike-slip movement in the steep segment is normal faulting. Therefore, the Posada fault is better described as detachment fault, instead of wrench fault.

this study	external nappe zone Conti et al. (2001)	Barbagia Carosi et al. (1992)	Nurra Franceschelli et al. (1990)	Monte Grighini Musumeci (1992)	Anglona Oggiano & Di Pisa (1992)
D1			D1 ≥ bt zone	D1 lower plate	S1 inclusion trails
D2	Gerrei phase Meana phase	D1	D1 ≤ chl zone D2 ≥ bt zone	D1 upper plate D2 lower plate	D2
D3		D2 folds	D2 ≤ chl zone D3 ≥ bt zone	F3 lower plate	D3 crenulation
D4	Sarrabus phase	extensional S2	shear deformation Elter et al. (1986)	C-S mylonites lower plate	S-C fabric
D5	Flumendosa phase			detachment	

Fig. 3.31: Structural correlation with other areas in the Sardinian Variscides, explanation in text.

For a better understanding of the Variscan structural evolution and in order to prove the significance of the deformational succession established in this study, a correlation with other areas in Sardinia is proposed. Considered are studies from the external nappe zone (Conti et al. 2001), the Monte Grighini core complex (Musumeci 1992), as well as from the Barbagia (Carosi et al. 1992), Nurra (Elter et al. 1986, Franceschelli et al. 1990), and Anglona (Oggiano & Di Pisa 1992) regions (fig. 3.31).

1) D1 is only common in the internal units of the belt, e.g. in the lower plate of the Monte Grighini core complex and in the biotite and subsequent higher metamorphic zones of the Nurra. D1 is also described in inclusion trails of some porphyroblasts from Anglona. In the Nurra, the abrupt incoming of biotite is accompanied by the sudden appearance of an additional deformation phase as well as by a jump of the celadonite content in muscovite (Carmignani et al. 1982a, Simpson 1998). This could be explained by the coincidence with the pre-Variscan cover-basement contact, in analogy to this study (chapter 5).
2) D2 is referred to the most dominant foliation in all studies. In the external nappe zone and upper plate of the Monte Grighini core complex, the overturned to recumbent D2 folds have axes parallel to the orogenic trend, but perpendicular to the D2 stretching lineation, whereas in the Barbagia, Nurra, and lower plate of the Monte Gringhini core complex, the axes of intrafolial D2 folds and the D2 stretching lineations are coaxially oriented at high angle to the orogenic trend. Thus, the D2 transport was generally southwards directed.
3) F3 is coaxial with F2 in the Barbagia, Nurra, and lower plate of the Monte Grighini core complex. The metamorphic peak commonly has a syn-/post-D2 to pre-D3 timing.
4) A hangingwall transport to the west is documented in the external nappe zone. Dextral shear band crenulations are common in the lower plate of the Monte Grighini core complex as well as in Anglona. In the Barbagia, non-coaxial D4 extension is indicated by a subhorizontal shear foliation

with a stretching lineation perpendicular to the previous lineations. Consequently, D4 is generally associated with a lateral transport parallel to the orogenic trend.

5) During D5, the large Flumendosa antiform, to which also the Monte Grighini core complex belongs, was exhumed. It extends parallel to the orogenic trend. The upper plate of the Monte Grighini core complex became detached from the lower plate during the exhumation of the Flumendosa antiform.

Accordingly, the structural evolution of the Sardinian Variscides shows three principal characteristics:

- An early frontal transport to the south and a late lateral transport to the west are recorded.
- With respect to the convergence direction, the fold axes have a high-angle orientation in the external belt, but a low-angle orientation in the internal belt.
- The structures of the lateral transport display an extensional morphology with respect to the overprinted structures in the internal belt.

Associated frontal and lateral transport is a common phenomenon in orogenic belts and is addressed to oblique plate convergence by Harland (1971), leading to the interference of transcurrent and compressive regimes. Spatial and/or temporal partitioning might result in distinct domains of compression and transcurrence or in a successive timing of compression and transcurrence. Consequently, the frontal compression and lateral transcurrence in the Variscan belt of Sardinia could be referred to such a transpressive regime. However, the lateral hangingwall transport is difficult to explained with this concept.

Alternatively, crustal thickening followed by extensional collapse is another concept to explain frontal and lateral transport in orogens (Dewey 1988). Early convergence and shortening might result in thrusting parallel to the plate slip vector. According to the normal or decreased thickness of post-orogenic lithosphere, such as documented for the Variscides, delamination (Bird 1979) or convective removal (Houseman 1981) of the lithospheric mantle might cause isostatic uplift of the thickened crust, so that the increasing body forces drive crustal thinning to overcome elevation contrasts. Examples from the Alps, Andes, and Tibetan plateau (Molnar & Tapponnier 1975, Dewey 1988, Selverstone 1988) show that the extensional mass transfer operates laterally easier than frontally.

Indeed, the extensional geometry of the lateral hangingwall transport in the internal parts of the Sardinian Variscides as well as the low-pressure/high-temperature metamorphism recorded in Anglona and the lower plate of the Monte Grighini core complex are well explained with extensional collapse of the previously thickened crust.

On the other hand, the lateral hangingwall transport recorded in the external nappe zone lacks any indications of extension. Instead, the change from frontal to lateral transport is recorded simply as changing thrust direction. This suggests that the lateral transport might be additionally driven by superimposed boundary forces that might be caused by orogenic processes centred in the paleogeographic surroundings of Sardinia.

3.12 Conclusion

The following conclusions can be drawn.

- D1 precedes Ordovician magmatism. In addition to the separate occurrence of Ordovician metagranitoids and metavolcanics, the restricted occurrence of the D1 structures outlines a pre-Variscan cover-basement relationship.
- The main deformational event D2 caused a hangingwall transport orthogonal to the orogenic trend and might be related to suturing somewhere in the internal Variscides.
- The kilo- to millimetre-sized D3 folds of returned attitude are coaxial with the D2 stretching lineations and F2 axes. The enveloping F3 surface has a externally-directed dip. Consequently, the internal sequence is structurally overlain by the external sequence. Thus, F3 can not be invoked for a structural inversion of the overall dip by back folding as suggested by Cappelli et al. (1992).
- The contact between Lodè orthogneiss and internal Siniscola schists is covered by a hinge area of a large synformal D3 anticline, which trends parallel to the contact and comprises Lodè orthogneiss as well as Siniscola schists. Thus, the Lodè orthogneiss does not form the core of a large anticline as generally assumed so far (Elter et al. 1986, Cappelli et al. 1992).
- D4 led to the development of the shallowly dipping, retrograde Posada fault, which detached the medium-grade schists from the high-grade gneisses below. C'-type shear bands formed in the hangingwall schists from the early D4 stages on, whereas they are late features in the footwall gneisses, where the retrogression probably reached low-grade metamorphic conditions during a later stage than in the hangingwall. The shear bands indicate a down to the west hangingwall transport, parallel to the orogenic trend.
- The kilometre-sized D5 flexure that has a subhorizontal axis parallel to the orogenic trend accommodated the exhumation of the axial zone probably in response to the tectonic denudation during the Posada faulting. The segment of the Posada fault that crops out in the steep limb of the flexure represents a stair-stepping segment, steepened due to the uplifting gneiss dome. The normal displacement was transformed into a strike-slip displacement at the flank of the gneiss dome. Thus, D5 is considered as advanced stage of the D4 Posada normal faulting. The Posada fault is therefore better described as detachment fault than as wrench fault.
- The Posada fault rocks evolved from the wallrocks. Thus, the idea by Cappelli et al. (1994) that the Posada fault were superimposed on an oceanic melange, marking a Variscan suture, is ruled out.
- Estimates of the Alpine reorientation reveal a shallowly southwards inclined pre-Mesozoic attitude of the basement layering outside the steep belt.
- The Alpine deformation is referred to the Tertiary opening of the Tyrrhenian basin in the transtensive regime of the eastward retreating Apenninic-Maghrebidic back arc, rather than to the collision between the Adriatic and Iberic plates and a resulting transpressive regime as postulated by Carmignani et al. (1995).

DESCRIPTION OF PHOTOS IN PLATE 3.1

a: Section from a porphyroid layer in the Orune schists, structural zone I (HH142). Feldspar phenocrysts are aligned in S2. They derived from the volcanic protolith of the porphyroids, which are characteristic for the Ordovician sequence in Sardinia (Memmi et al. 1983, Carmignani et al. 1982b). The slight crenulation formed during D3.

b: Detailed section from a semipelitic layer in the Orune schists, structural zone I (HH1), showing a S2 parallel quartz vein folded during D3.

c: D3 fold in psammitic layers is marginally overprinted by brittle Alpine faulting in the Orune schists, structural zone I (HH141).

d: D3 folding of the S2 transposed sedimentary bedding in the Orune schists, structural zone I (HH255). The long short relation of the F3 limbs indicates that this section is from an inverted limb of a large D3 fold, which crops out over several kilometres near Lula (fig. 3.2-3).

e: View to the NE at Punta Casteddu. The bedding of the Mesozoic limestone dips to the SE and witnesses Alpine reorientation, which has also affected the underlying the Orune schists, structural zone I.

f: Quartz veins in S1 isoclinally folded and transposed by the main foliation S2 in the external Siniscola schists, structural zone II (HH154).

g: S1 parallel quartz veins mark a hook-shaped fold interference pattern caused by the D3 refolding of F2 around a common axis in the external Siniscola schists, structural zone II (HH154).

h: Hook-shaped fold interference pattern composed of a close F3 refolding an isoclinal F2 around a common axis in the external Sinscola schists, structural zone II (HH187).

PLATE 3.1

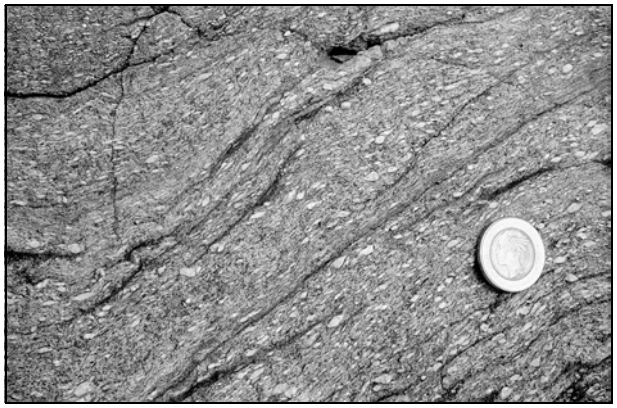

a

b

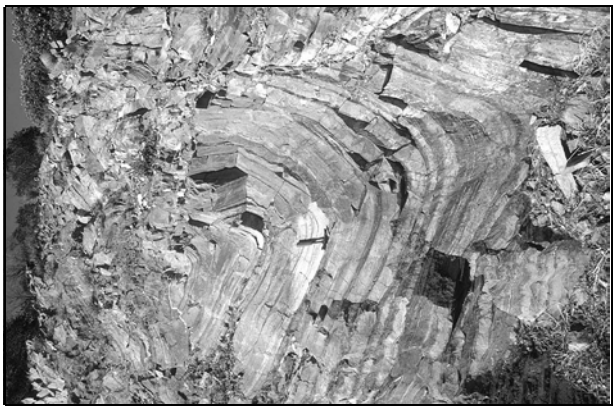

c

d

e

f

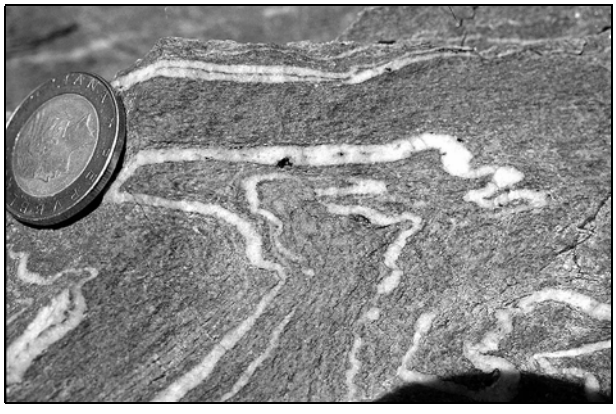

g

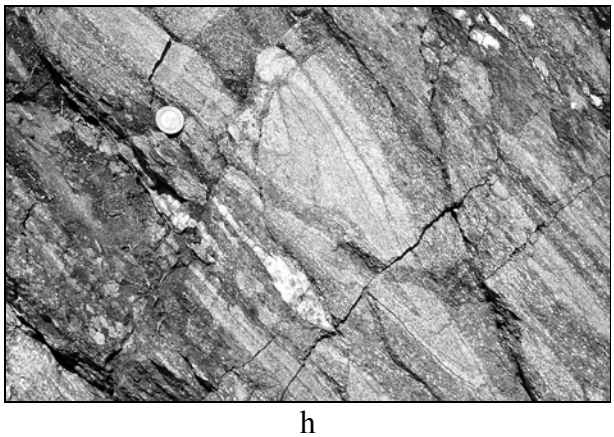

h

DESCRIPTION OF PHOTOS IN PLATE 3.2

a: View to the SW along Monte Albo from Cantoniera Guzzurra. The SE-dipping Jurassic cover limestone of the Monte Albo massif constitutes an Alpine flower structure. The spatial relation between cover bedding and basement structures reveals the extent of Alpine reorientation, due to the formation of the flower structure, on the external Siniscola schists, structural zone II.

b: Aplite dikes folded during D3 in the Lodè orthogneiss, structural zone IV (HH212). The limbs at low-angle orientation to the fold axial plane are attenuated in comparison to the limbs at a high-angle orientation, which suggests pressure solution as deformation mechanism.

c: Detailed section of a D3 fold with axial planar cleavage in the Lodè orthogneiss, structural zone IV (HH213). Aplites and biotite enclaves were stretched out in S2, so that they form a S2 parallel layering in places, which was folded and crenulated during D3. The axial planar cleavage is traced by dark seams in the bright aplite layer. Dark particles probably remained in the cleavage planes, due to their low solubility.

d: The shear band crenulation cleavage developed during D4 in the Lodè orthogneiss, structural zone IV (HH226). The asymmetry implies a dextral displacement. The feldspar augen derived from D2.

e: Subhorizontal Tertiary limestone beds resting conformably on the Variscan foliation S2/4 in the Lodè orthogneiss at the north-eastern slope of Monte Longu near La Caletta, structural zone III (HH51). Compare with the sketch.

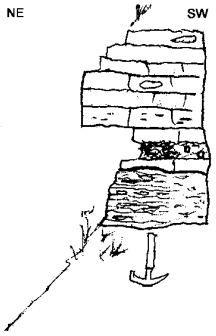

f: Quartzofeldspathic veins, probably of leucosome-derived origin, intruded the S1 parallel layering and became folded subsequently in Brunella gneiss, structural zone V (HH29).

g: Dark metabasite layers and bright quartzo-feldspathic veins are S2/4 aligned in a Brunella gneiss, structural zone V (HH309). The competent metabasite layers became boudinaged during D4, in contrast to the less competent gneiss and quartzofeldspathic veins.

h: Vertical view on horizontal S2 transposed layers in a Brunella gneiss, structural zone V (HH304). The E-W trending D3 crenulation was overprinted by dextral shear bands during D4. Compare with the sketch.

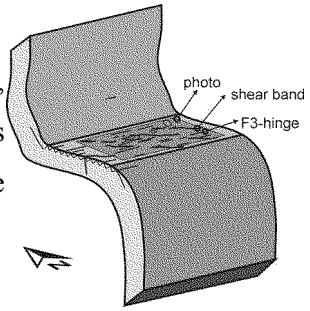

PLATE 3.2

a

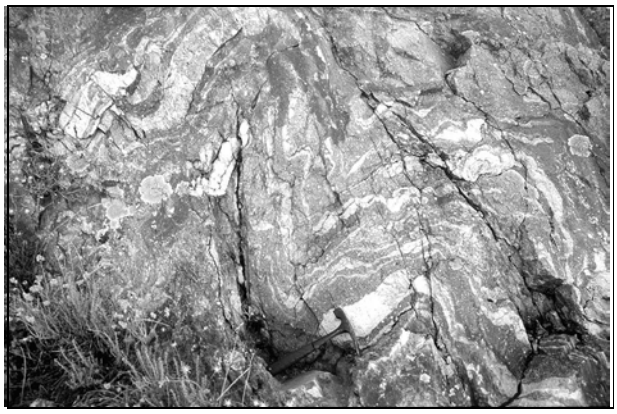

b

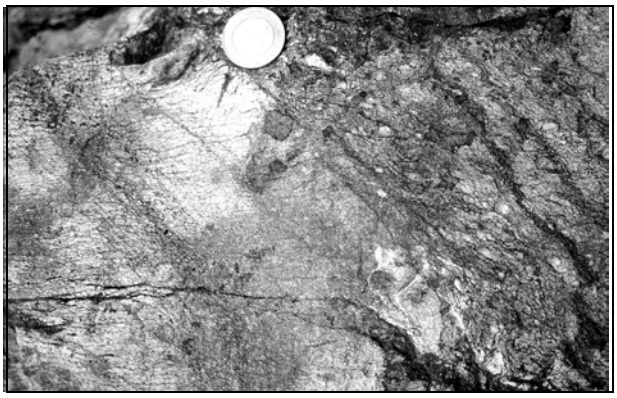

c

d

e

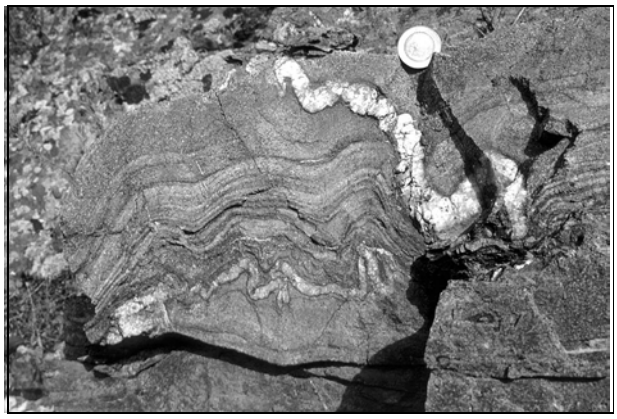

f

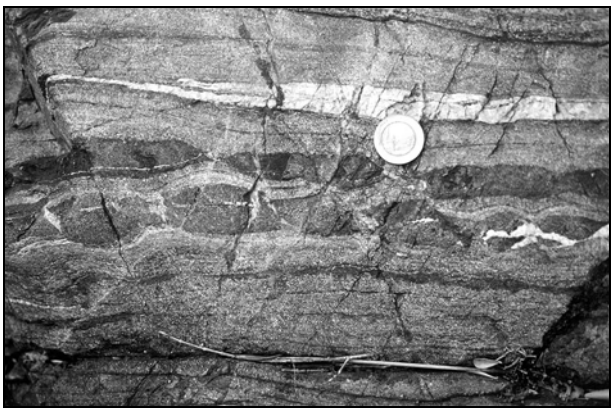

g

h

DESCRIPTION OF PHOTOS IN PLATE 3.3

a: Close-up of a fine-grained, dull-looking mylonite that derived from the Siniscola schist, structural zone V (HH91). Previous structures have been destroyed by the D4 mylonitisation. Recognisable is the D4 shear band crenulation with a dextral sense of movement in the photo.

b: Fine-grained, well foliated, monotonous-looking mylonite that derived from the Brunella gneisses, structural zone V (HH82). Internal structures of the precursor, such as compositional layering, porphyroblasts, crenulation etc. have been erased by the D4 mylonitisation.

c: View on a mylonitic foliation plane with a survivor clast of a fibrous sillimanite aggregate, structural zone V (HH70). The long axis of the clast defines the stretching direction L4, which is additionally traced by a slight crenulation.

d: View to the NE at Monte Nurres from Punta Cupetti. The Monte Nurres represents an allochthonous slice that has been placed on the steep belt by Alpine movements along the Santa Anna fault (fig. 3.2).

e: A tectonic breccia formed by Alpine reactivation of the Posada fault, structural zone V (HH82). The rock fragments are emplaced in an incohesive matrix.

f: Isoclinal D2 folds with axes of varying orientations, due to the curvature of the axes, in a stromatic Brunella gneiss, structural zone VII (HH40).

g: The eye shaped structure consists of concentric layers, so that it is probably a D2 sheath fold in a migmatic Brunella gneiss, structural zone VII (HH40).

h: The tub in the bright quartzofeldspathic layer indicated by the coin is probably part of a D2 sheath fold in a migmatic Brunella gneiss, structural zone VII (HH40).

PLATE 3.3

a

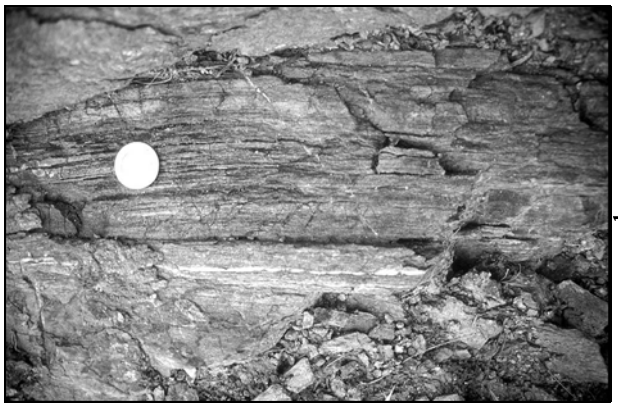

b

c

d

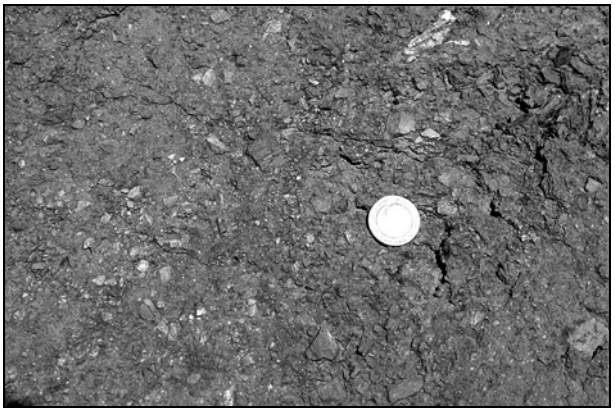

e

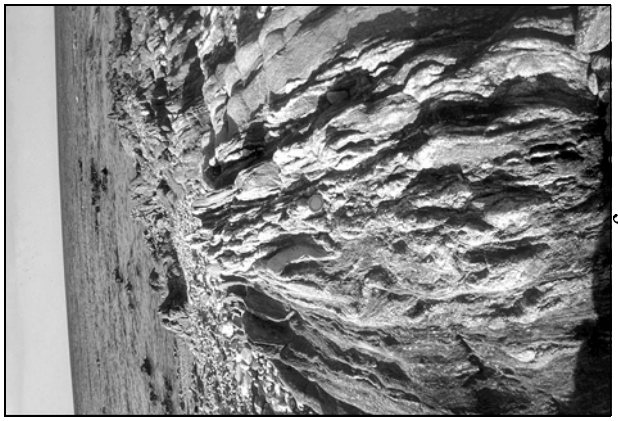

f

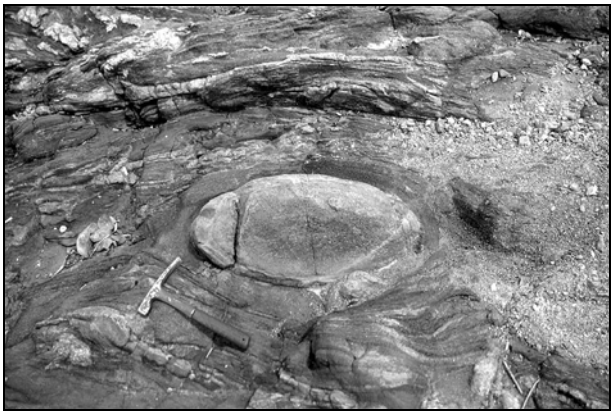

g

h

DESCRIPTION OF PHOTOS IN PLATE 3.4

a: D2 transposed contact between the bright leucosome and the dark melanosome in a migmatitic Brunella gneiss, structural zone VII (HH111).

b: The orthogneiss in the Brunella gneisses, structural zone VII (HH117), that has been sheared during D2. Some relict phenocrysts remain as clasts.

c: Brunella gneiss with sillimanite-containing nodules that became stretched and aligned during D2, structural zone VII (HH108).

d: Coronitic garnets in a garnet-rich layer from the Punta de li Tulchi metabasite that is intercalated in the Brunella gneisses, structural zone VII (HH115), and contains eclogitic relics, according to Miller at al. (1976).

e: Close-up of an euhedral garnet porphyroblast, which has developed a corona, from the Punta de li Tulchi metabasite that is intercalated in the Brunella gneisses, structural zone VII (HH115). Compare with the photo of a coronitic garnet in thin section (plate 5.9h).

f: Quartzofeldspatic veins, which are probably leucosome-derived, mark a hook-shaped fold interference pattern in a the Brunella gneiss, structural zone VII (HH108).

g: Leucosome-derived quartzofeldspathic layers are lain out in a fold interference pattern formed by a isoclinal fold and open folds of varying style in Brunella gneiss, structural zone VII (HH114).

h: An Alpine fault transecting the S2 parallel layering in a Brunella gneiss, structural zone VII (HH125). The fault gouge is partly foliated.

PLATE 3.4

a

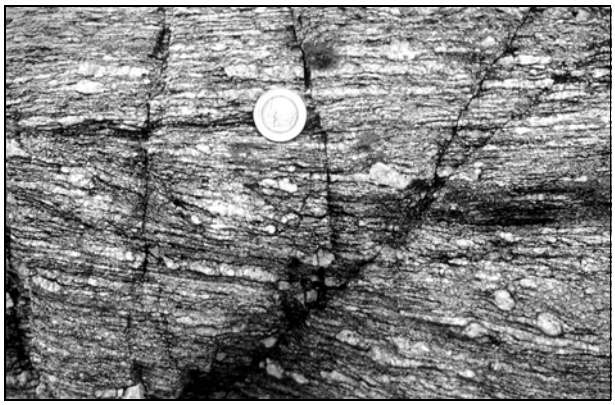

b

c

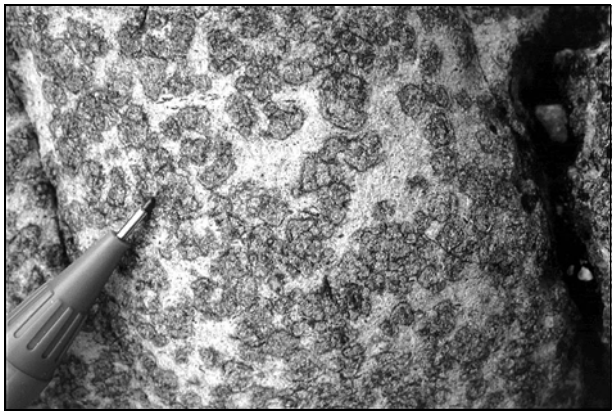

d

e

f

g

h

PLATE 3.5

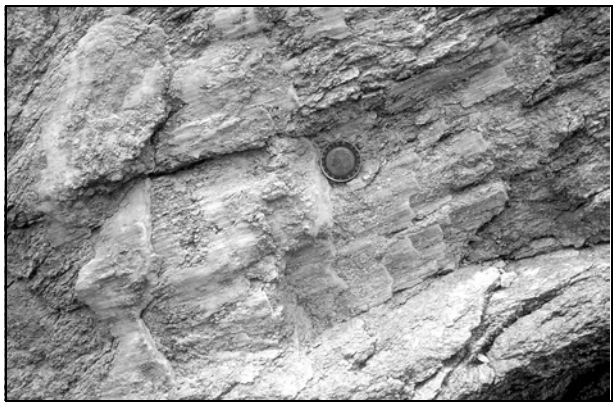

a: Slickenfibers on an Alpine fault plane in a Brunella gneiss, structural zone VI (HH125). The hangingwall on this fault plane moved to the NE (to the right in the photo).

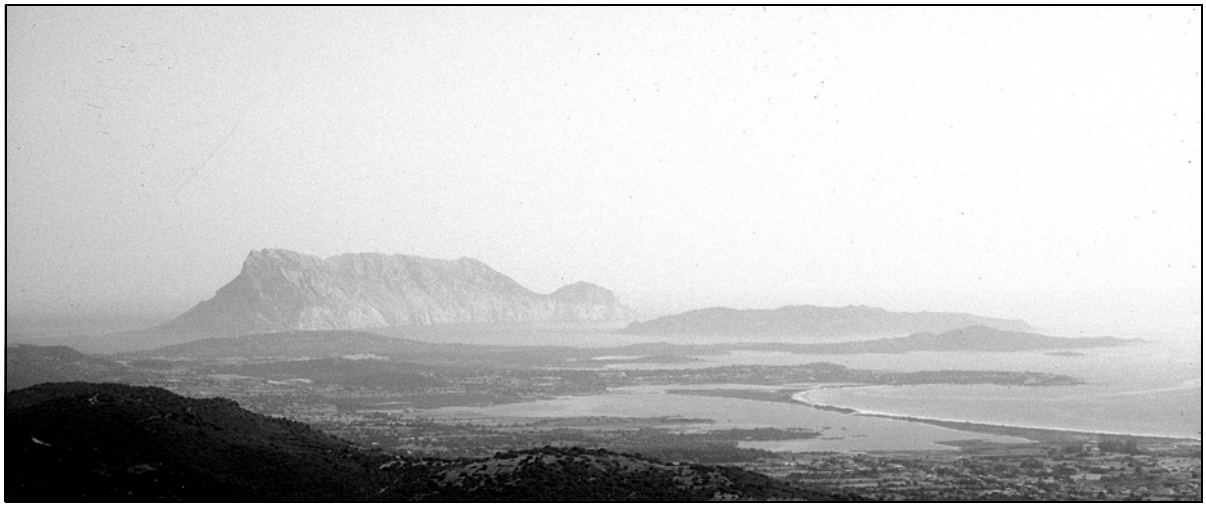

b: Isola Tavolara, view from Punta Tittinosu to the NE. The beds of the Mesozoic limestone on the island dip to the SE, as consequence of sinistral transtensive faulting along the Alpine Tavolara fault (fig. 1.2).

4 Lattice-preferred orientation of quartz

4.1 General remarks

The kinematic indicators for the tectonic transport direction during the main deformational event D2 became modified or obscured by the subsequent deformational overprints. Therefore, it needs to be proven, whether coalescent extinction recognised in thin section or asymmetric lattice-preferred orientation (LPO) of quartz detected through the gypsum test plate correspond with the orientation of the main foliation and stretching lineation in the polyphase-deformed rocks.

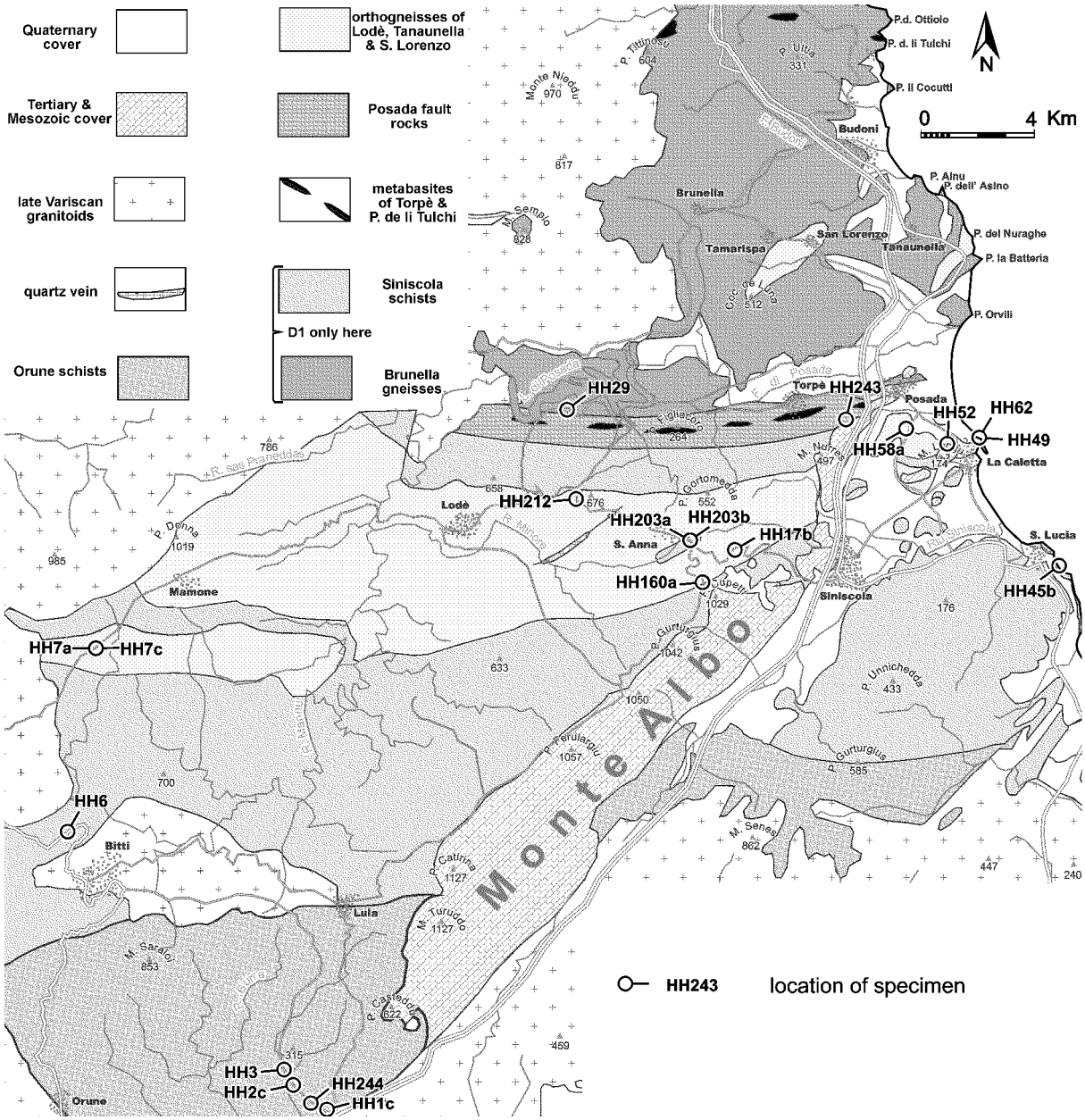

Fig. 4.1: The locations of specimens collected for determination of quartz lattice-preferred orientation.

Moreover, the LPO patterns of quartz indicate whether:

- crystal-plastic deformation was important
- the deformation was coaxial or non-coaxial (Schmid & Casey 1986)

- constrictional, flattening, or plane strain was involved (Lister & Hobbs 1980)
- the deformation involved higher strain rates (Tullis et al. 1973, Marjoribanks 1976, Jessell 1988) and temperatures (Wilson 1975, Bouchez 1977, Lister & Dornsiepen 1982, Law 1990).

So, the deformational events are further characterised, which helps to correlate deformational successions. For these reasons, 19 LPO's of quartz were obtained from various places in the study area (fig. 4.1).

As pointed out in chapter 3, five generations of structures can be distinguished. They are preserved to a varying extent, due to the discontinuous nature of deformation. Therefore, it can be expected that the measured LPO patterns of quartz inherited considerable strain increments of preceding deformation, but also that they became overprinted and changed by subsequent deformation. Therefore, the quartz LPO patterns are commonly diffuse and heterogeneous, rather than well defined small or great circle girdle distributions. In many cases, the universal stage measurements allowed the correlation of diffuse distribution and complicating heterogeneity of the LPO patterns with older relict or newer incipient fabrics in thin section.

For the axes of the finite strain, it is assumed that the stretching lineation refers to the lengthening axis X, the shortening axis Z is normal to the foliation, and the intermediate axis Y is perpendicular to the X- and Z-axes.

The skeleton outline of the LPO pattern commonly shows an opening angle about the Z-axis of strain, which increases at lower strain rates and higher temperatures (Tullis et al. 1973, Marjoribanks 1976, Jessell 1988, Kruhl 1998). This angle will be given for those LPO patterns that allow its estimation.

The stereographic density plots of the quartz c-axes are based on the following parameters: equal area projection on lower hemisphere; counted by cosinus powered weighting function 128 using the DOS program ARiAne v. 2.01 (Adam 1989); up to 7 contour levels with intervals of 1.0 multiples of random distribution; lowest shades contour equal 1.0 multiples of random distribution.

4.2 Orune schists

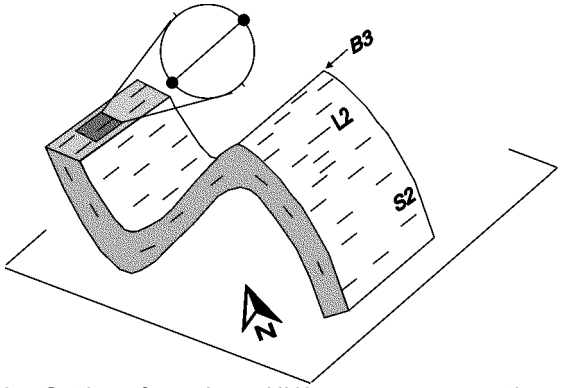

Fig. 4.2a: Setting of specimen HH244 on an apparently normal F3 limb, which is actually an inverted limb, according to the reversed F3 attitude (fig. 3.30).

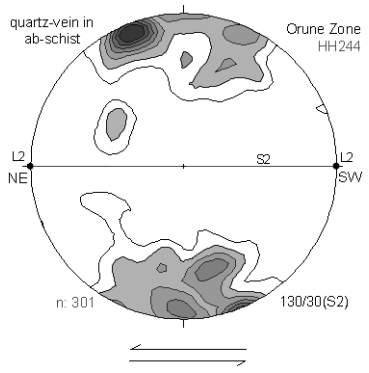

Fig. 4.2b: LPO pattern of specimen HH244.

The D2 structures are superimposed on the primary structures of the Orune schists and form the dominant fabric, which was mainly deformed by the D3 folding. Therefore, strain increments of D2 and D3 should contribute to the four measured LPO patterns.

The LPO pattern of specimen **HH244** is from a S2-parallel segregation quartz vein in an albite schist from a normal F3 limb (fig. 4.2a). It shows a strong single maximum surrounded by a less contoured cluster that indicates a small circle distribution around the Z-axis of strain (fig. 4.2b). The vein quartz is distinctly coarser grained than the quartz in the schistose host rock. Two generations of quartz grains can be distinguished in the vein. The old large grains refer mainly to the strong single maximum, whereas the less contoured part of a cluster reflects mainly the young small grains, which gradually merge with the subgrains at the margin of the old large grains. The sutured grain boundaries and the abundant subgrains in thin section are related to the recrystallisation of the young small quartz grains probably during the D3 folding. Therefore, the indicated small circle girdle distribution of the less contoured part of the cluster around the Z-axis of strain may evolved during coaxial D3 flattening. The old large quartz grains generate the stretching lineation L2 visible in the specimen, and thus, correspond with D2. Also, the asymmetry of the maximum is confirmed by the gypsum plate under the microscope. It suggests a D2 movement of top to the northeast.

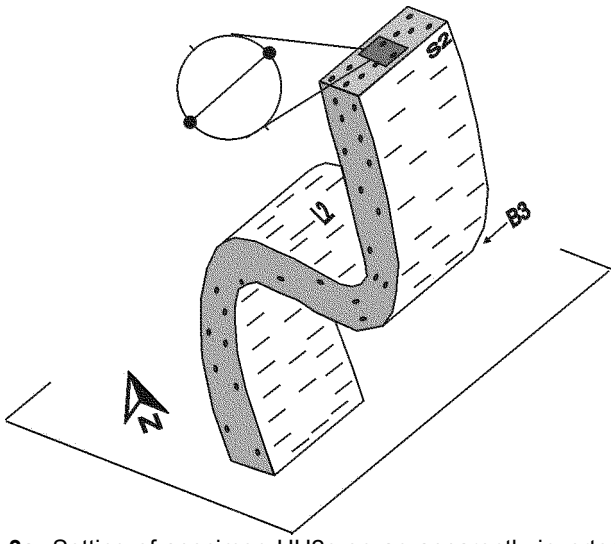

Fig. 4.3a: Setting of specimen HH2c on an apparently inverted F3 limb, which is actually a normal limb, according to the reversed F3 attitude.

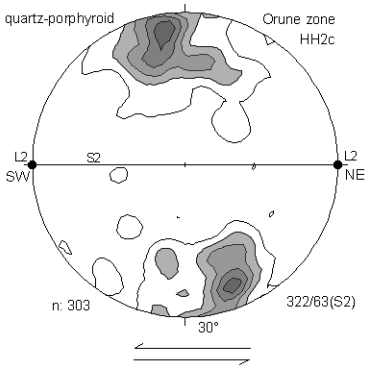

Fig. 4.3b: LPO pattern of specimen HH2c.

The LPO pattern of specimen **HH2c** originates from a porphyroid layer rich in quartz phenocryst in an overturned F3 limb (fig. 4.3a). Two asymmetric maxima in a cluster around the Z-axis of strain may indicate a relict inclined girdle (fig. 4.3b). The quartz in the phenocryst aggregates is coarser grained and corresponds to the maxima, whereas the quartz in the surrounding matrix is finer grained and corresponds mainly to the low-density part of the LPO pattern. The grains in the quartz phenocryst aggregates are fairly equidimensional and have bulged grain boundaries (plate 5.1d), few small inclusions mainly of white mica and some subgrain boundaries parallel to the optical axis. The low content of quartz in the matrix of about 25 % causes a high percentage of quartz grains pinned at the grain

boundaries of other minerals, e.g. white mica and albite. The relict quartz phenocrysts form with their long axis the stretching lineation L2. Therefore, they refer to the D2 increment, which is displayed in the LPO pattern by the main maximum. The asymmetry of the quartz LPO pattern is confirmed by the gypsum test plate. It suggests a hangingwall transport to the southwest, which is apparently opposite to HH244, but consistent with the different setting of both specimens an a normal and an inverted F3 limb respectively.

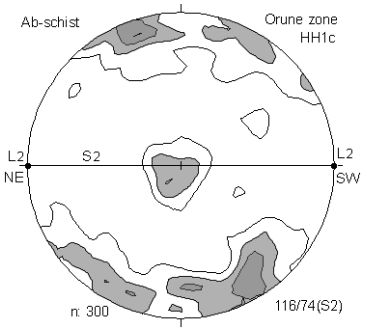

Fig. 4.4: LPO pattern of specimen HH1c.

The pattern of quartz c-axes of specimen **HH1c** is from an albite schist with a well developed D2 cleavage. The c-axes are orientated fairly perpendicularly to the X-Y plane, forming a cluster close to the Z-axis of strain. Additionally, an isolated cluster occurs at the Y-axis of strain (fig. 4.4). The majority of the measured quartz grains relates to the small girdle distribution around the Z-axis of strain, whereas a few larger grains with an upright orientation of the c-axis under the microscope refer to the isolated cluster at the Y-axis of strain. The abundant phyllosilicates and the critically low content of quartz of about 25 % led to pinned grain boundaries. Therefore, plastic deformation of quartz seems rather inefficient and growth by solution and precipitation probably controlled the lattice orientation of quartz to a considerably larger extent. For this reason, the pattern of quartz c-axes is inconsistent with the commonly observed LPO patterns formed by plastic deformation of quartz.

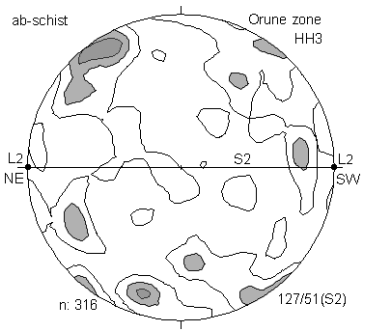

Fig. 4.5: LPO pattern of specimen HH3.

The quartz c-axis pattern of specimen **HH3** is taken from an albite schist with a D3 crenulation that cuts S2 at a small angle. The pattern is poorly contoured and has a weakly preferred to random orientation (fig. 4.5). Although bulged grain boundaries and abundant subgrains indicate plastic deformation, the high number of grain boundaries controlled by phyllosilicates appears as a considerable obstacle for an unhampered plastic deformation of quartz. Additionally, the D3 crenulation caused a weakening of the LPO. Thus, the interference of relict and new strain increments, in addition to the

limiting effect of the phyllosilicate content on the plastic deformation of quartz, influenced the origin of the rather randomly oriented pattern.

The results obtained from the 4 measured quartz LPO in the Orune schists can be summarised as follows. Crystal-plastic deformation of quartz is important in the quartz domains, such as segregation quartz veins (HH244) or relict quartz phenocrysts (HH2c), whereas mechanical rotation and growth seem to be the dominant deformation processes in the mica- and/or albite-rich domains (HH3, HH1c). The quartz grains in the D2 fabric are generally coarser grained than in the D3 fabric, probably because they were exposed longer to the prograde metamorphism. The D3 quartz contributes apparently to a small circle girdle-like distribution around the Z-axis of strain, which indicates coaxial flattening, probably superimposed during D3 folding. The strong maxima refer to the larger D2 quartz grains that remained after the D3 folding. The asymmetry of the maxima is considered as a relic of an inclined girdle and suggests non-coaxial D2 shearing along the stretching lineation L2. The indicated D2 shear sense is opposite in the inverted (HH2c) and normal (HH224) F3 limbs.

4.3 Siniscola schists

In addition to D2 and D3 also D1 and D4 structures are developed in the Siniscola schists, and thus, are expected to be represented as increments in the four measured LPO patterns.

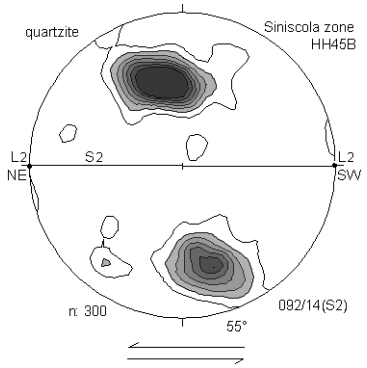

Fig. 4.6: LPO pattern of specimen HH45b.

The LPO pattern of specimen **HH45b** is from a pure quartzite. Two very strong maxima, which might be interpreted as a relict type I crossed-girdle, show an asymmetry with respect to S2 and to the pattern itself (fig. 4.6). Evidence of plastic deformation of quartz in thin section includes sutured grain boundaries and abundant subgrains, which merge into new grains. Quartz inclusions in garnet porphyroclasts (plate 5.2g) do not show a LPO. Obviously, they have not been affected by the D2 overprint. It is possible that increments of the earlier D1 fabric or the later D3 overprint have prevented the formation of a clear type I crossed-girdle LPO pattern. However, the LPO pattern corresponds with the main lineation L2 and its asymmetry suggests a movement of top to the northeast.

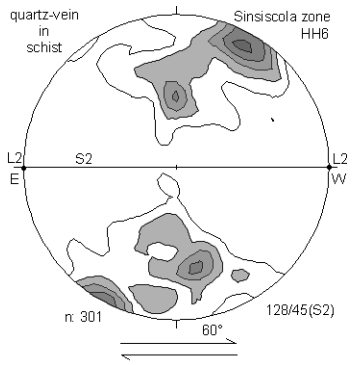

Fig. 4.7: LPO pattern of specimen HH6.

The quartz LPO pattern of specimen **HH6** is from a segregation quartz vein, which is aligned in S2 of a plagioclase poikiloblast containing garnet schist. The distribution of c-axes indicates a diffuse type I crossed-girdle marked by an asymmetric main maximum around the Z-axis of strain (fig. 4.7). The vein quartz is distinctly coarser grained than the quartz in the schistose wall rock of the vein. Large grains can be correlated mainly with the main maximum, and the less contoured areas with small grains that merge gradually into the marginal subgrains of the old large grains. Therefore, the plastic quartz deformation observable in the microscope seems to be related to the transformation of the old D2 fabric into a newer fabric, and thus, is responsible for the weakening of the type I crossed-girdle. The younger quartz fabric might be related to the D3 folding. D4 shear bands have affected the schistose walls, but not the segregation quartz vein. The asymmetry of the LPO pattern suggests a top to the west movement, which can also be revealed by the gypsum plate, but does not really need to be in contrast to the northeast movement direction of other samples, due to a possible reorientation during D3 folding.

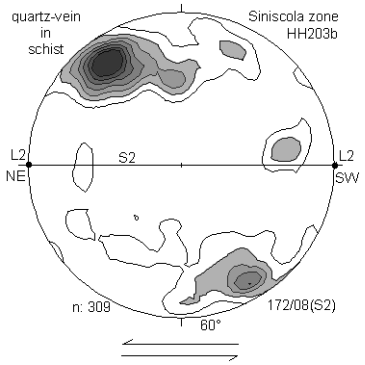

Fig. 4.8: LPO pattern of specimen HH203b.

The LPO pattern of specimen **HH203b** is from a segregation quartz vein aligned in S2 of a fine grained quartzofeldspathic schist. It shows a strong maximum in a small circle distribution around the Z-axis of strain (fig. 4.8). The vein quartz is distinctly coarser grained than the quartz in the schistose wallrock. Two generations of quartz grains can be recognised in the vein. The old large grains refer mainly to the maximum, whereas the less contoured part of the LPO pattern refers to the young small grains that merge into the marginal subgrains of the old large grains. The grain boundaries are sutured. The observed plastic deformation of quartz belongs probably to the rearrangement of the old D2 fabric during the formation of the D3 folds, which are abundantly developed in the quartzofeldspathic schist.

Consequently, the diffuse small-girdle distribution would be caused by coaxial flattening during D3. The asymmetry of the maximum with respect to S2 and to the whole LPO pattern, which can be confirmed by the gypsum test plate as well, is inferred to be a relic of a top to the northeast transport during D2.

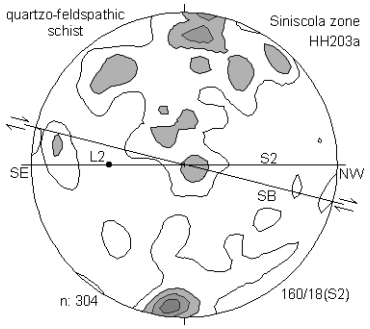

Fig. 4.9: LPO pattern of specimen HH203a.

The quartz c-axis pattern of specimen **HH203a** is taken from a quartzitic S2-parallel layer in a fine-grained quartzofeldspathic schist, which is overprinted by D4 shear bands. A poorly contoured great circle girdle and some maxima at the Z-axis of strain describe a weak preferred orientation (fig. 4.9). The quartz grains in the layering parallel to S2 vary in size and have a prevailing equidimensional shape, probably due to some heat input during prograde metamorphism. Shear bands overprint the equilibrated D2 fabric during D4. The very small quartz grains in the shear bands grade into more larger grains towards the microlithons between the shear bands. Kinked and ruptured white mica occurs preferentially in the shear bands and indicates a considerable accumulation of deformation by sliding on its basal cleavage planes. The inclination of the girdle and its weak contours are probably expressions of the rotation of the older fabric during D4 shearing. The asymmetry of the shear bands indicates a D4 movement top to the northwest.

The obtained results from the 4 measured quartz LPO in the Sinsicola schists can be summarised as follows. The remaining D2 quartz fabric is coarser-grained and produces asymmetric maxima, probably derived from an inclined girdle and/or type I crossed-girdle. It is overprinted by the D3 recrystallisation of smaller grains, which have a tendency to a small circle girdle distribution in the LPO patterns, and thus refer to a coaxial flattening strain. The D2 asymmetry suggests a hangingwall transport to northeastern directions in the normal F3 limb and to southwestern directions in the inverted F3 limb. This characterisation of the D2 and D3 fabrics of quartz in the Siniscola schists is identical with that of the Orune schists, and thus supports the established deformational succession across the contact between the Orune and Siniscola schists, which coincides with the pre-Variscan cover-basement contact. The contribution of the D1 increment to the LPO pattern appears to be small and difficult to estimate. D4 is spatially restricted to discrete shear bands, which occur prevailingly in schistose domains and are marked by kinked mica, sheared along its basal plane. Dominant grain boundary sliding and the spatial discontinuity causes a generally weak and diffuse D4 increment in the quartz LPO pattern.

4.4 Lodè orthogneiss

The D2 structures are superimposed on the magmatic fabric of the plutonic protolith and make up the main fabric, which was overprinted by D3 folding and D4 shear bands. Consequently, varying increments of these deformational events are expected in the 9 measured LPO patterns.

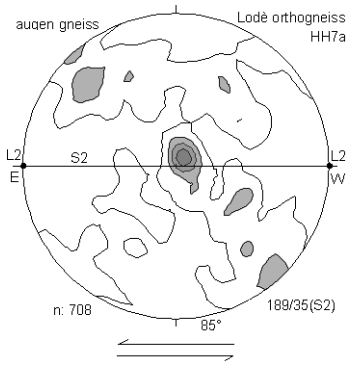

Fig. 4.10: LPO pattern of specimen HH7a.

The quartz LPO of specimen **HH7a** is from an augen gneiss. A single maximum around the Y-axis of strain is elongated within the more pronounced arm of a type I crossed-girdle (fig. 4.10). The quartz occurs in bands and commonly forms large fairly equidimensional grains. Subgrains and bulged grain boundaries are present. Smaller and larger grains have been distinguished during measurement. The smaller grains seem to be related to a later fabric reactivation. The c-axes of the large grains cluster around the maximum and in the more pronounced arm of the asymmetric crossed-girdle, whereas the orientation of the small grains is more diffuse and weakens the LPO pattern. Properties of the D2 quartz, which indicate a certain amount of coarsening and equilibration, were probably achieved during the prograde metamorphism. The asymmetry of the crossed-girdle is a consequence of non-coaxial strain. It suggests a hangingwall transport to the east.

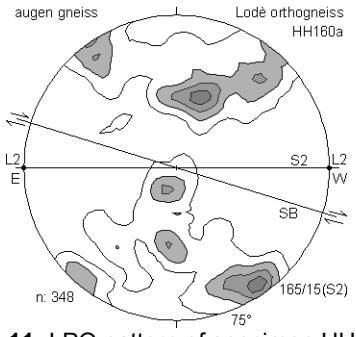

Fig. 4.11: LPO pattern of specimen HH160a.

The LPO pattern of specimen **HH160a** is from an augen gneiss. It has the distribution of an internally asymmetric type I crossed-girdle (fig. 4.11). The quartz occurs in bands that flow around the K-feldspar phenocrysts. The type I crossed-girdle is inclined with respect to S2, which probably happened during the D4 formation of some shear bands. Undoing the D4 inclination reveals the original orientation with respect to S2, the external and internal asymmetry becoming consistent and suggesting a hanging wall transport to the E during D2.

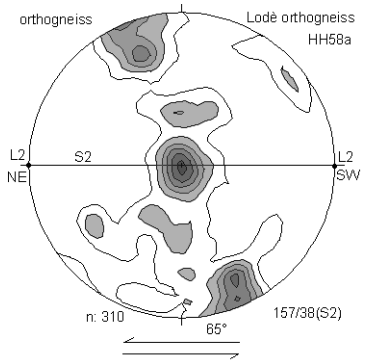

Fig. 4.12: LPO pattern of specimen HH58a.

The quartz LPO of specimen **HH58a** is from an orthogneiss in a zone of enhanced D2 shearing. Highly contoured maxima and one main maximum around the Y-axis of strain outline an asymmetric type I crossed-girdle (fig. 4.12). Quartz and feldspar are distributed in separated domains in thin section. The quartz has a varying grain size, and shows subgrains and sutured grain boundaries. The increased temperature and strain are probably the reason for the clear and highly contoured LPO pattern. The asymmetry of the LPO pattern indicates a D2 movement of top to the northeast.

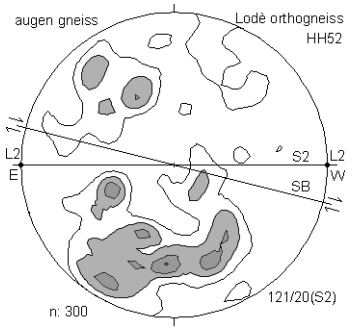

Fig. 4.13: LPO pattern of specimen HH52.

The c-axis pattern of quartz in specimen **HH52** is from an augen gneiss. The contours of the c-axis distribution give a diffuse pattern (fig. 4.13). In the microscope, the quartz occurs in polymineralic domains, together with white mica and fragments and recrystallised grains derived from the K-feldspar phenocrysts. This could have hampered an undisturbed plastic deformation of quartz. Moreover, D4 shear bands have weakly overprinted S2 and so weakened the D2-derived LPO further.

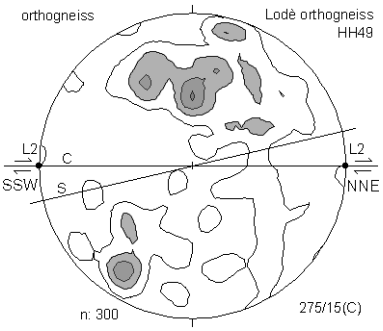

Fig. 4.14: LPO pattern of specimen HH49.

The c-axis pattern of quartz in specimen **HH49** has been taken from an orthogneiss, on which a weak C/S fabric was superimposed during D2. The weakly contoured pattern might be identified as a diffuse type I crossed-girdle with some maxima around the Z-axis of strain (fig. 4.14). Abundant subgrains

and bulged grain boundaries are expressions of the plastic quartz deformation in thin section. Ruptured fragments and recrystallised grains are derived from K-feldspar phenocrysts and probably formed together with mica obstacles during the deformation of the quartz fabric. The shear geometry of the C/S fabric suggests a top to the north-northeast movement during D2.

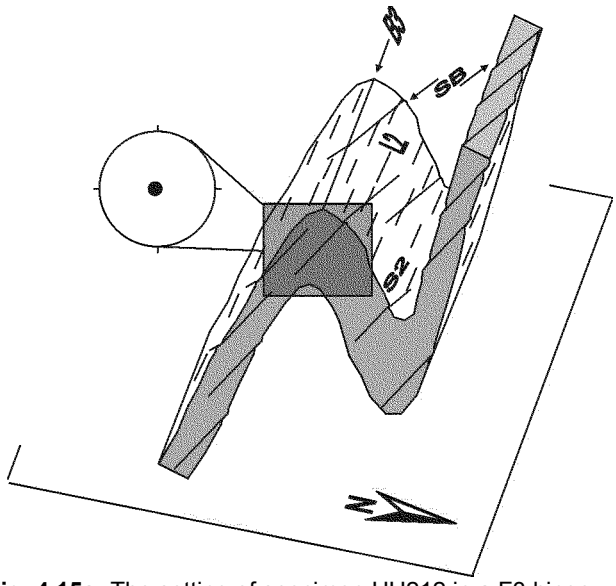

Fig. 4.15a: The setting of specimen HH212 in a F3 hinge.

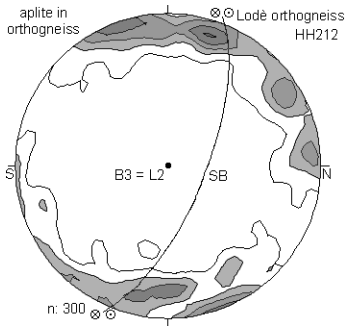

Fig. 4.15b: LPO pattern of specimen HH212.

The quartz c-axis pattern of specimen **HH212** is from a micro-F3 hinge of an aplite layer in an orthogneiss (fig. 4.15a). The LPO pattern forms a great circle girdle around the parallel L2 and B3 (fig. 4.15b). Although subgrains and sutured grain boundaries indicate plastic deformation of the quartz fabric, neither a new D3 foliation nor a pronounced D3 quartz fabric are developed. The older D2 quartz fabric appears to have been unchanged by the D3 folding. Shear bands transected the hinge during D4 and are marked by thin traces of kinked, ruptured and in parts finely recrystallised white mica and fine-grained quartz. The quartz c-axes related to the shear bands changed the whole LPO pattern only weakly. The great circle girdle represents mainly the quartz fabric of D2, which was rotated around its X-axis of strain during the D3 folding. The D2 fabric underwent reorientation during D3 folding without major crystal-plastic deformation of quartz, which is consistent with the field observations suggesting pressure solution as deformation mechanism (plate 3.2b-c).

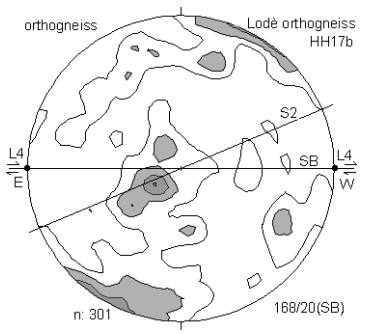

Fig. 4.16: LPO pattern of specimen HH17b.

The quartz LPO pattern of specimen **HH17b** is taken from an orthogneiss, whose D2 foliation is overprinted by D4 shear bands. It shows a diffuse great circle girdle with an asymmetric maximum around

the Z-axis of strain (fig. 4.16). The shear bands and the microlithons in between form two distinct structural domains in thin section. The quartz is coarser-grained in the microlithons and is part of the D2 fabric. The quartz c-axes from the microlithons cluster generally in areas away from the asymmetric maximum around the Z-axis of strain. Towards the shear bands, S2 curves more and more towards a parallel orientation to the shear bands, and the quartz grains become finer-grained. The quartz c-axes from this transition between S2 and the shear bands form traces in the LPO pattern that lead to the asymmetric maximum around the Z-axis of strain. The plastic deformation of quartz is strongest in the shear bands, as the smaller grain size and abundant subgrains show. The quartz grains are aligned in an oblique foliation within the shear bands, and thus show a shape preferred orientation (SPO). The asymmetric maximum around the Z-axis of strain is chiefly made up of c-axes that are mainly parallel to the elongation of the quartz grains in the oblique foliation of the shear bands. In addition to the asymmetry of the quartz LPO, the shear sense is deduced from the transposition geometry of the shear bands and from the quartz SPO of the oblique foliation within the shear bands. All this suggests a top to the west movement during D4.

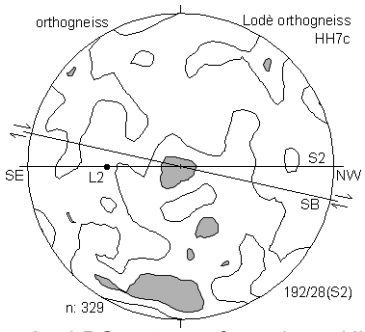

Fig. 4.17: LPO pattern of specimen HH7c.

The pole diagram of quartz c-axes in specimen **HH7c** is from a quartz- and white mica-rich orthogneiss, which has been overprinted by D4 shear bands. The distribution of the quartz c-axes is weakly contoured and has a diffuse pattern (fig. 4.17). Shear bands cross S2 and are marked by thin traces of kinked and ruptured white mica, and of very fine-grained quartz. S2 is mainly marked by porphyroblastic white mica and curves towards the shear bands in an orientation more parallel to the shear bands. The quartz in S2 is coarser grained. The ruptured and kinked white mica appears to have accumulated a lot of deformation by grain boundary sliding along its basal plane, and so a more intense homogeneous plastic deformation of quartz was probably prevented. The quartz c-axes of the large and the small grains have been measured separately and although they are differently distributed, do both not show clear LPO patterns. This spatial and temporal heterogeneity in addition to considerable grain boundary sliding accommodated by mica probably did not allow the formation of a more clearly developed LPO pattern.

The LPO pattern of specimen **HH62b** is from a quartz- and white mica-rich orthogneiss, which has been overprinted by two progressive generations of shear bands during D4. The c-axis distribution is weakly contoured and forms a diffuse pattern (fig. 4.18). The white mica is kinked and ruptured along the two generations of shear bands, and so appears to have accumulated a lot of deformation by grain

boundary sliding along its basal plane. S2 and the two shear band generations caused a temporal and spatial heterogeneity of the quartz fabrics. This heterogeneity and considerable grain boundary sliding accommodated by white mica are reasons for the weakly contoured and diffuse LPO pattern.

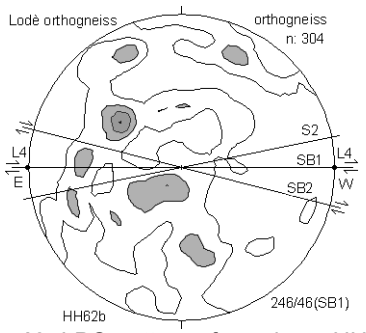

Fig. 4.18: LPO pattern of specimen HH62b.

The obtained results of the 8 measured quartz LPO patterns from the Lodè orthogneiss are summarised as follows. The asymmetric type I crossed-girdles of the well preserved D2 quartz fabrics (HH7a, HH160a, HH 58a) justify the assumption that the asymmetric D2 maxima from the Orune and Siniscola zones are relics of such type I crossed-girdles as well. Moreover, the constant directions of the hangingwall transport to the east and northeast support the idea that the entire Lodè orthogneiss is situated in a normal limb of a large D3 fold. The minor importance of crystal-plastic deformation of quartz during D3 folding is consistent with the field indications of pressure solution as a major deformational mechanism. D4 shear bands commonly occur in mica domains as discrete zones of concentrated deformation. They are generally marked by mica that is deformed by grain boundary sliding. The minor importance of crystal-plastic deformation of quartz and the spatial heterogeneity cause weak and defuse LPO patterns. However, if discrete D4 shear zones in quartz-rich domains are considered on their own, very strong asymmetric LPO and SPO patterns of quartz are common (HH17b).

4.5 Posada fault rocks

D4 is most intense in the Posada fault rocks and led to the formation of mylonites and cataclasites.

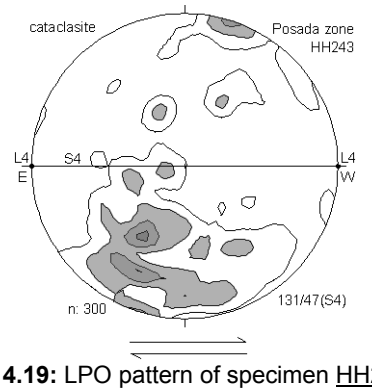

Fig. 4.19: LPO pattern of specimen HH243.

The quartz c-axes of specimen **HH243** are from fragments of a quartz mylonite in the matrix of a cataclasite (plate 5.9a). They have been measured to find out, if the shear sense in the fragments, which appear to have been only slightly rotated, is consistent with the kinematic indicators in the cataclastic matrix, and thus, the cataclasite may reflect an advanced deformation state of the mylonite. The dif-

fuse LPO pattern has few contours and its skeletal outline is mainly defined by the three maxima, indicating an inclined great circle girdle (fig. 4. 19). The fragments consist of ribbon quartz that contains many fine subgrains. New recrystallised quartz is fine-grained and has its optical axis statistically parallel to the elongation of the grains. It commonly forms an oblique foliation or merges into secondary ribbons. Thus, the quartz in each mylonitic fragment shows a strong SPO in addition to a strong LPO. The LPO of the whole section has been weakened during cataclasis. Nevertheless, the old asymmetric LPO of the mylonite remained as a relic and suggests, like the kinematic indicators in the cataclastic matrix, a D4 hangingwall transport to the west.

4.6 Brunella gneisses

The D2 fabric is commonly dominant and superimposed on the D1 fabric under high-grade metamorphic conditions. It became deformed by the D3 folding and overprinted by the D4 fabric in the southern Brunella gneisses.

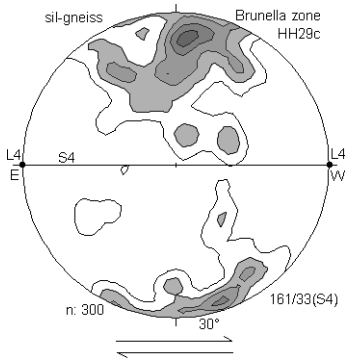

Fig. 4.20: LPO pattern of specimen HH29c.

The LPO pattern of specimen **HH29c** is from a southern Brunella gneiss that contains sillimanite. It shows well contoured maxima around the Z-axis of strain (fig. 4.20). The LPO pattern corresponds mainly to a D4 increment. The quartz grains of the D4 fabric replaced older large grains related to a D2 fabric. The quartz becomes finer grained, and retrograde white mica gets more strongly bent and/or sheared towards D4 shear bands, which are extended parallel to the previous layering. The asymmetry of the LPO pattern indicates a non-coaxial shear component, which suggests a top to the west transport during D4. Some subgrain boundaries normal to the c-axis of quartz were inherited from the high-grade fabric. They are relics of a chess board pattern (plate 5.9g), which is quite common in the Brunella gneisses. Also, the fibrous sillimanite derived from this relict high-grade fabric, and has been aligned in the layering. Coarse-grained quartz has partly overgrown fibrous sillimanite.

4.7 Discussion

The deformational heterogeneity complicated the LPO patterns of quartz. Despite this complication, the universal stage method allowed the correlation of the geometric properties of the LPO patterns with the corresponding fabrics in thin section. Therefore, a general characterisation of the considered generations of crystal-plastically deformed quartz fabrics can be given.

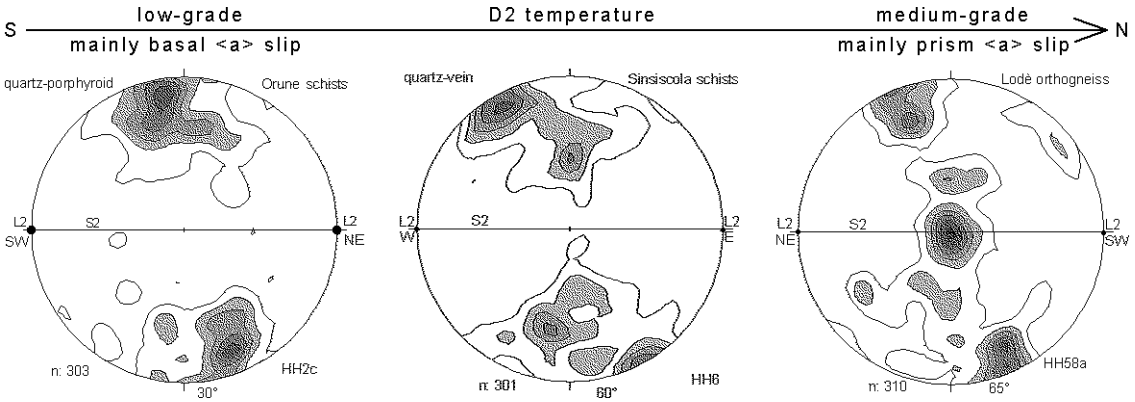

Fig. 4.21: The change from mainly basal <a> slip, indicated by the maxima around the Z-axis of strain in the south, to prevailing prism <a> slip, indicated by the maximum around the Y-axis of strain in the north, reflects northwards increasing D2 temperatures (Wilson 1975, Bouchez 1977, Lister & Dornsiepen 1982, Law 1990).

Within the deformational succession, the D2 fabric (HH2c, HH45b, HH6, HH7a, HH160a, HH58a) is the most penetrative and continuous. Moreover, it displays the strongest LPO. Asymmetric type I crossed-girdles reflect non-coaxial plane strain during D2. The change from mainly basal <a> slip, indicated by the maxima around the Z-axis of strain in the south, to prevailing prism <a> slip, indicated by the maxima around the Y-axis of strain in the north, is expression of the northwards increasing D2 temperatures (fig. 4.21). In thin section, D2 quartz exhibits evidence of coarsening and equilibration during prograde metamorphism, such as a fairly equidimensional grain shape and inclusion of mica and/or sillimanite. The prograde metamorphism has strengthened the D2 quartz fabric and thus its LPO. The D2 maxima of the pole diagram persist during subsequent overprinting.

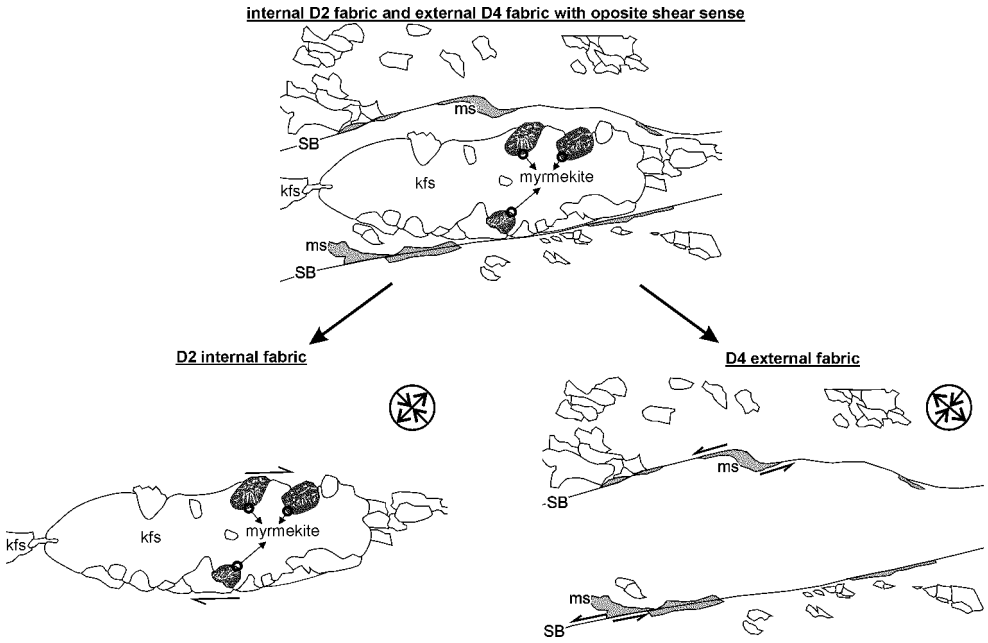

Fig. 4.22: From thin section redrawn sketch, Lodè orthogneiss (HH14). The D2 internal fabric, preserved in the K-feldspar (kfs) porphyroclast, and the D4 external fabric, represented by the shear bands (SB) with white mica (ms) fish, display an opposite shear sense. The opposite shear sense of these internal and external fabrics is a common phenomenon in the Lodè orthogneiss, which is reflected by some quartz LPO pattern as well (HH160a, fig. 4.11).

The D3 fabric (HH244, HH203b, HH212) is less penetrative and continuous, and so, the LPO patterns are weaker in comparison to the D2 fabric. According to the small circle girdle distributions, coaxial flattening strain was involved during D3 folding. D3 quartz is finer grained than the D2 quartz and is commonly arranged around the older D2 grains, displaying a core-mantle structure.

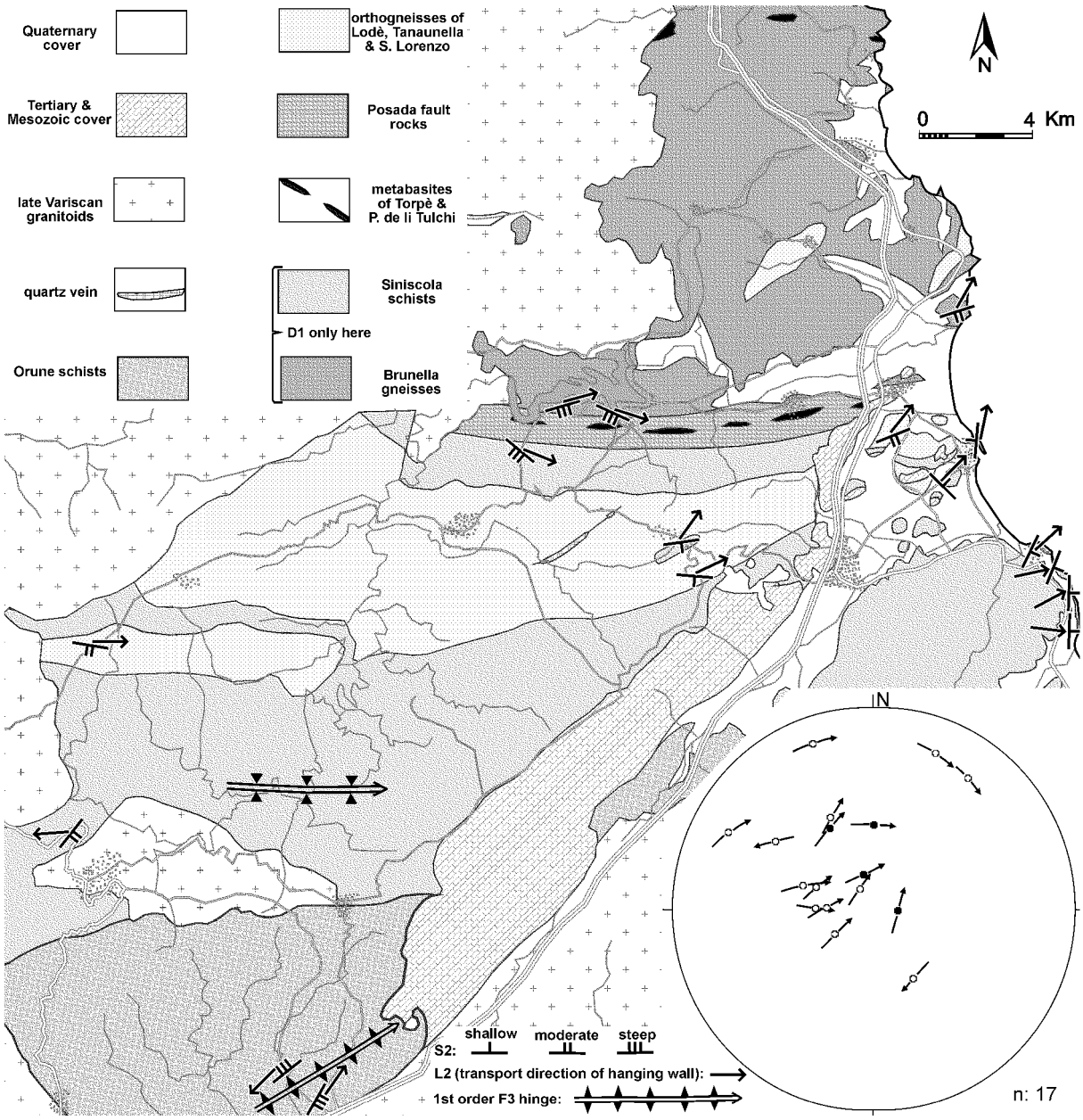

Fig. 4.23: First order D3 fold hinges and S2 with corresponding stretching lineation L2, indicating the direction of the D2 hangingwall transport. In the stereographic projection, the Hoeppener lineation (Hoeppener 1955, page 37-38) with filled circles refer to data from the Lodè orthogneiss. The direction of the hangingwall D2 transport depends probably on the setting of the samples in the normal or inverted F3 limb.

The D4 fabric (HH17b, HH243, HH29c) is more clearly limited to discrete zones than the D2 and D3 fabrics. The inclined great circle girdles with asymmetric maxima around the Z-axis of strain, reflect non-coaxial plane strain. The asymmetry of the LPO pattern is consistent with the abundant shear sense indicators, and confirms a tectonic transport to the west in shallow attitude and a dextral strike-slip displacement in steep attitude. The maxima around the Z-axis of strain in the LPO patterns indi-

cate dominant basal <a> slip as the easiest slip system, which is typical of low-grade metamorphism, and thus confirms the inferred metamorphic conditions during D4 (chapter 5). The D4 quartz recrystallised dynamically to very small, elongated grains commonly arranged in an oblique foliation, or it is developed as ribbon quartz that contains abundant subgrains.

The crystal-plastic deformation of quartz was in competition with other mechanisms, such as growth processes and mechanical rotation (Shelley 1993). Crystal-plastic deformation was less important in those D2 fabrics that contain less than 30 vol. % of quartz (HH1c, HH3). Growth processes, such as precipitation and solution, appear to have been dominant during the formation of the D3 fabrics (HH212). Slip on the basal cleavage of micas and accompanying growth processes dominated over plastic deformation in many D4 fabrics (HH203a, HH7c, HH62b). This explains the weakly contoured and diffuse LPO patterns different to typical LPO patterns exclusively formed by plastic deformation of quartz.

In general, the asymmetric LPO patterns of the D2 fabrics confirm the shear sense detected by the gypsum test plate and prove the proper identification of the stretching lineation L2. In addition to the asymmetric quartz LPO, other shear sense indicators (fig.4.22, chapter 3 & 5), e.g. C/S fabrics, shear bands and asymmetric clasts, have also been used to establish a consistent kinematic evolution. The indicated hangingwall transport for the main Variscan deformational event D2 is approximately either northeast or southwest. It is probably controlled by the setting of the sample in a normal or inverted F3 limb (fig. 4.2a, 4.3a fig. 4.23).

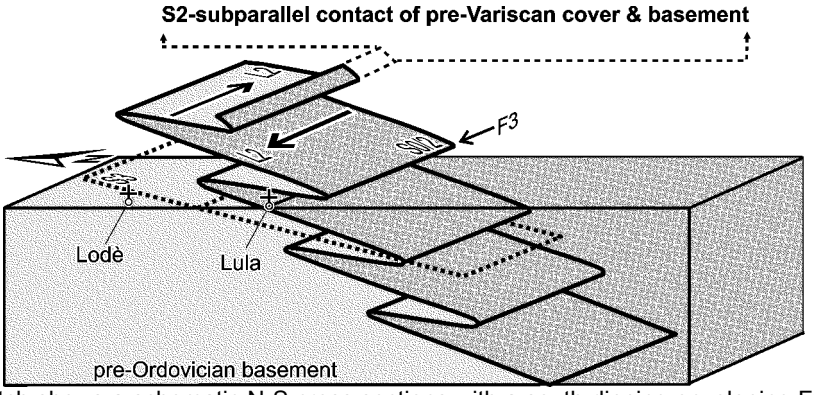

Fig. 4.24: The sketch shows a schematic N-S cross sections with a south dipping enveloping F3 surface, such as reconstructed in chapter 3 (fig. 3.30). Furthermore, the apparently opposite D2 transport directions, due to the different setting of the D2 shear sense indicators on opposing F3 limbs, is illustrated.

As reconstructed in the previous chapter, the dip of the enveloping F3 surface ranges from southern to eastern directions. Furthermore, the originally recumbent D3 folds became reoriented into a returned attitude with varying inclination due to the D5 flexuring and the Alpine tilting. Based on the control of the transport direction by the setting in the F3 limbs, such as shown in fig. 4.24, a D2 hangingwall transport is inferred that ranges from southern to western directions. The NNE-SSW trending stretching lineation L2 in the southern Lodè orthogneiss of structural zone III is considered as fewest reoriented by subsequent deformations (fig. 3.11b). Thus, it probably shows still the D2 transport direction. Consequently, the tectonic transport of the main deformational event D2 can be constrained towards

southern directions, which is in agreement with the southern transport inferred for the nappe zone of the Sardinian Variscides (Conti et al. 2001).

4.8 Conclusion

The following conclusions can be drawn.

- The characteristics of the D2-, D3-, and D4-derived LPO's of quartz are identified across the studied sequence and ensure the correctness of the deformational succession established in this study.
- The asymmetric D4-derived LPO patterns prove the western directions of the hangingwall transport in shallowly dipping parts and the dextral strike-slip displacement in steeply dipping parts during D4.
- Internally increasing D2 temperatures, with respect to the orogenic anatomy, are supported by the D2-derived LPO patterns of quartz.
- A D2 transport apparently in opposite directions is probably related to the different setting of the shear sense indicators on opposing F3 limbs.
- Taking subsequent reorientations into account, the D2 shear sense indicators suggest a hangingwall transport towards southern directions, which is confirmed by the asymmetry of the corresponding quartz LPO.

5 Metamorphic reaction fabrics

5.1 Previous work and open questions

The metamorphism increases successively from zeolite facies in the external zone of the Sardinian Variscides (fig. 1.2) to amphibolite facies in the axial zone (Di Simplicio et al. 1974). Furthermore, a zoning of metamorphic index minerals, ranging from chlorite to sillimanite + K-feldspar, was established on the internal succession and interpreted as continuously increasing Barrovian metamorphism (fig. 5.1a, Franceschelli et al. 1982).

In contrast to the interpretation of a continuously increasing metamorphism, isolated relics of eclogite facies in the Punta de li Tulchi metabasites (fig. 5.4, Miller et al. 1976, Franceschelli et al. 1998) and of granulite facies in the Monti gui Nieddu metabasite near Olbia (Ghezzo et al. 1979, Cruciani et al. 2002) occur intercalated within the axial zone, and migmatic gneisses are juxtaposed abruptly against staurolite schists along the retrograde Posada fault (fig. 5.4, Elter et al. 1990, Ricci 1992).

Moreover, the Posada fault has been interpreted to be superimposed on a Variscan suture zone (Cappelli et al. 1992). According to this interpretation, the Torpè metabasites, which are intercalated in the Posada fault (fig. 5.4), are considered as remnants of an oceanic melange that became involved in thrusting of the migmatic gneisses over the staurolite schists. This model of collisional suturing proposes an entirely retrograde record in the migmatic gneisses distinct from an inverted Barrovian metamorphism in the schists below the overthrust as well as the presence of high-pressure relics in the Posada fault.

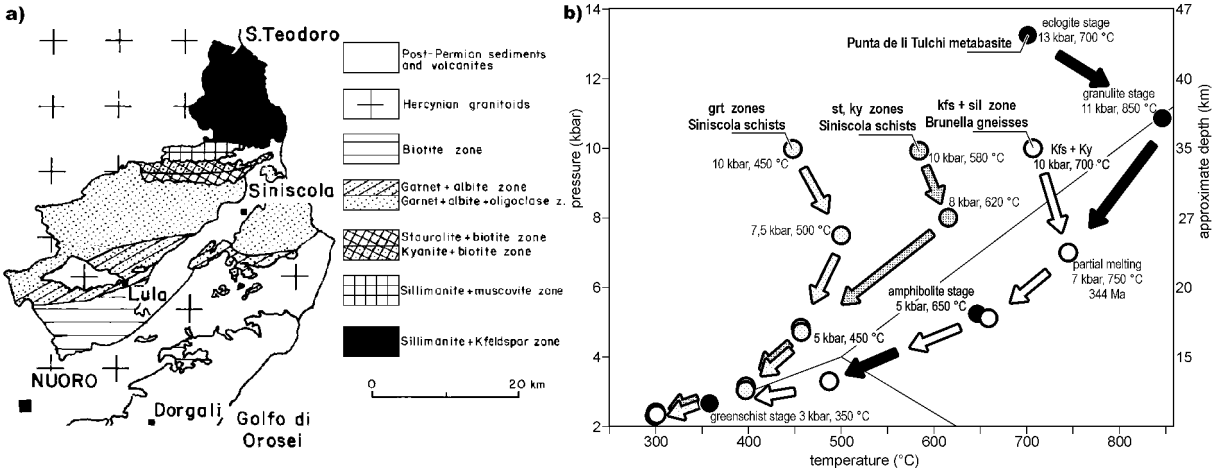

Figure 5.1: The NE-Sardinian study area with: **a)** zoning of metamorphic index minerals (Franceschelli et al. 1982) and **b)** P-T-t paths (compiled after Franceschelli et al. 1989 & 1998, Ricci 1992).

Geothermobarometric data and estimated P-T paths suggest that the thermal peak conditions were achieved in the overlying low- to medium-grade schists in a deeper crustal level than in the underlying high-grade gneisses (fig. 5.1b, 5.2). The decreasing pressure with increasing temperature toward deeper structural level is inferred to result from a thermal peak postponed to an exhumation stage more advanced in the high-grade gneisses than in the medium- to low-grade schists, according to

Franceschelli et al. (1989). Alternatively, these data might reflect a contemporaneous thermal peak, but in spatially separated areas with distinct geothermal gradients, later juxtaposed along the Posada fault. Or instead, the barometric data of the high-grade gneisses might display a retrograde stage rather than the thermal peak, because most of them might be based on retrograde muscovite (fig. 5.2).

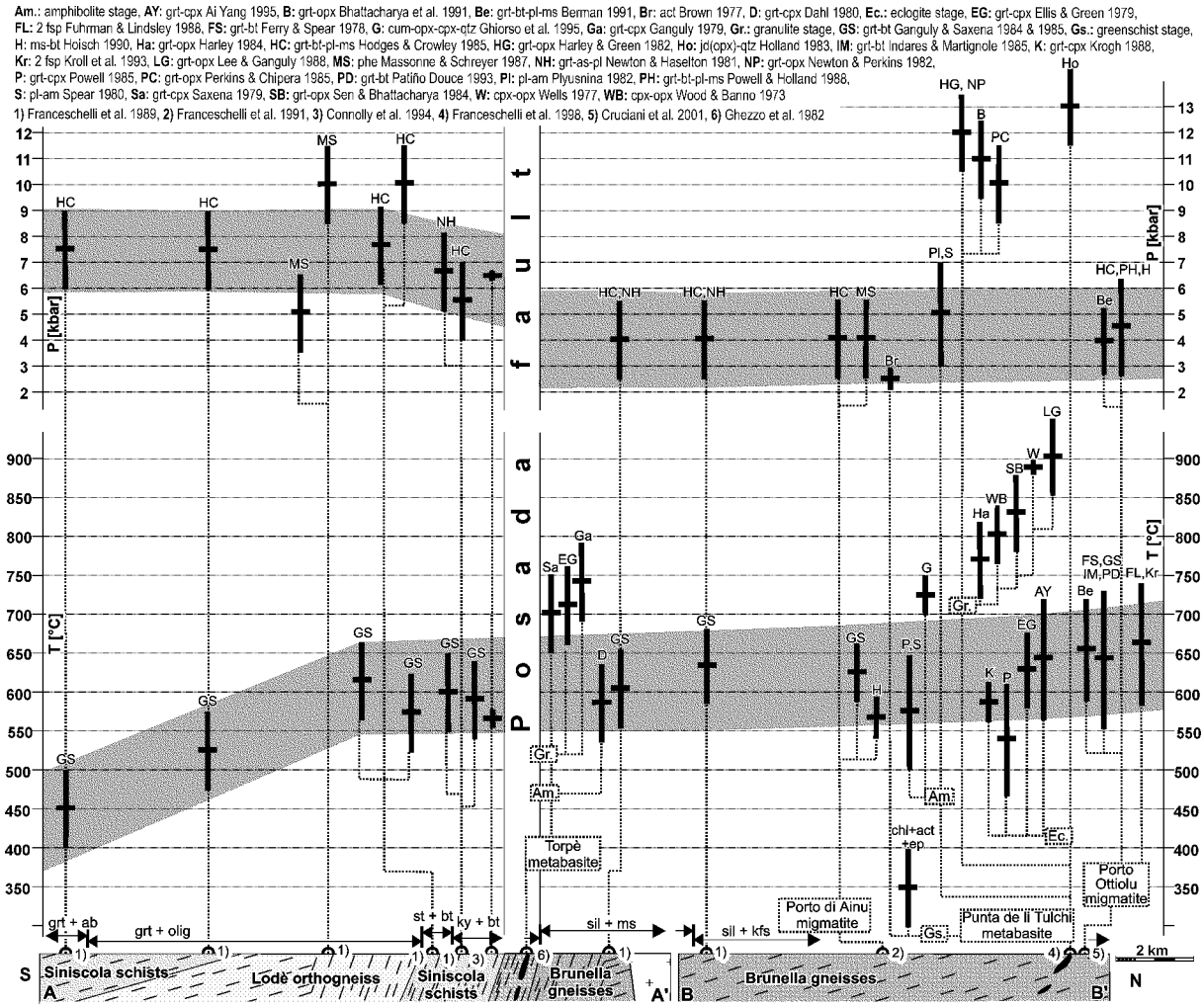

Figure 5.2: Geothermobarometry of Paleozoic NE Sardinia plotted in sketched S-N profile (approx. situation in fig. 5.4) with zoning of metamorphic index minerals (fig. 5.1a, Franceschelli et al. 1982). Mean P-T estimates for the peak of regional metamorphism are underlain in grey.

The timing of the porphyroblast growth changes from post-D1/pre-D2 in the low-grade succession to syn- to post-D2 in the medium- to high-grade succession (Elter et al. 1986), and is inferred to express the postponed thermal peak towards higher metamorphic grades (Franceschelli et al. 1989).

However, this supposed diachrony is contrary to the usual case, namely that the thermal peak in the less buried external parts is later than in the more buried internal parts (Thompson & England 1984). On the other hand, thermal doming related to late Variscan extension and/or magmatism is a well documented phenomenon in many places of the Variscides (von Raumer 1998 and references therein), and could result in a longer lasting porphyroblast growth.

Geochronological data provide cooling ages exclusively in a late Paleozoic range (fig. 6.1), so that a single Variscan metamorphism is generally envisaged (Franceschelli et al. 1989 & 1998, Ricci 1992).

However, pre-Variscan metamorphic ages might have been missed, because no data are obtained on metamorphic minerals with higher blocking temperatures, e.g. monazite or garnet. Furthermore, the structural (chapter 3) investigations document a D1 fabric probably within an older basement that is intruded by Ordovician granitoids (fig. 5.4) and externally overlain by a cover, which contains interlayered acidic volcanic rocks of Ordovician age. Therefore, the supposed diachronous porphyroblast growth might be an expression of a miscorrelated structural succession across the pre-Variscan cover-basement contact.

Pre-Variscan metamorphism related to an Ordovician orogenic event is well documented in the paleogeographically neighbouring Paleozoic basement presently exposed in the Alps (fig. 1.2, Oberli 1994, Romer & Franz 1998, von Raumer 1998, Handy 1999). Therefore, potential metamorphic relics related to the basement fabric D1 or contact aureoles of the Ordovician protolith intrusions around the orthogneisses of Lodè and Tanaunella (fig. 5.4) will be critically examined. Moreover, the mineral zoning of Franceschelli et al. (1982) will be further specified. In order to correlate the timing between metamorphism and deformation from the external low-grade to the internal high-grade sequence, overprinting, crosscutting, and overgrowing relations, as well as marker fabrics will be identified. The geothermobarometric assemblages will be revised to find out, whether they are retrograde, prograde, or coeval with the thermal peak. Additionally to the P-T sensitive mineral assemblages, the interpretation of deformation mechanisms in quartz, feldspar and white mica will supply further P-T constraints. Based on the resolved tectono-metamorphic evolution, the suture model by Cappelli et al. (1992) will be critically reviewed. Alternatively, a mantled gneiss dome model will be adapted to explain the increased metamorphic gradient and the structurally induced, abrupt contrasts of metamorphism across the Posada fault.

5.2 General remarks

This chapter relies on the examination of approx. 450 thin sections made from specimens sampled throughout the study area (fig. 5.3). Mineral assemblages assumed to represent equilibrium are illustrated qualitatively in AFM or ACF diagrams in conjunction with simplified petrogenetic grids. Mineral abbreviations are from Kretz (1983). Furthermore, the following abbreviation are used: olig for oligoclase, P- and Q-domains for phyllosilicate-rich and quartzitic to quartzofeldspathic domains.

The microfabrics refer to the large structures and the fivefold deformational history established by field work (chapter 3). The following microtectonic presentation starts in the Orune schists (fig. 5.4) that represent the Variscan cover in the most external part of the studied sequence, continues through the Siniscola schists underneath that belong to the pre-Ordovician basement, considers the Ordovician Lodè orthogneiss that is hosted in the Siniscola schists, crosses the Posada fault to arrive finally in the pre-Ordovician basement-derived Brunella gneisses, which form the deepest part of the studied sequence and constitute the axial zone.

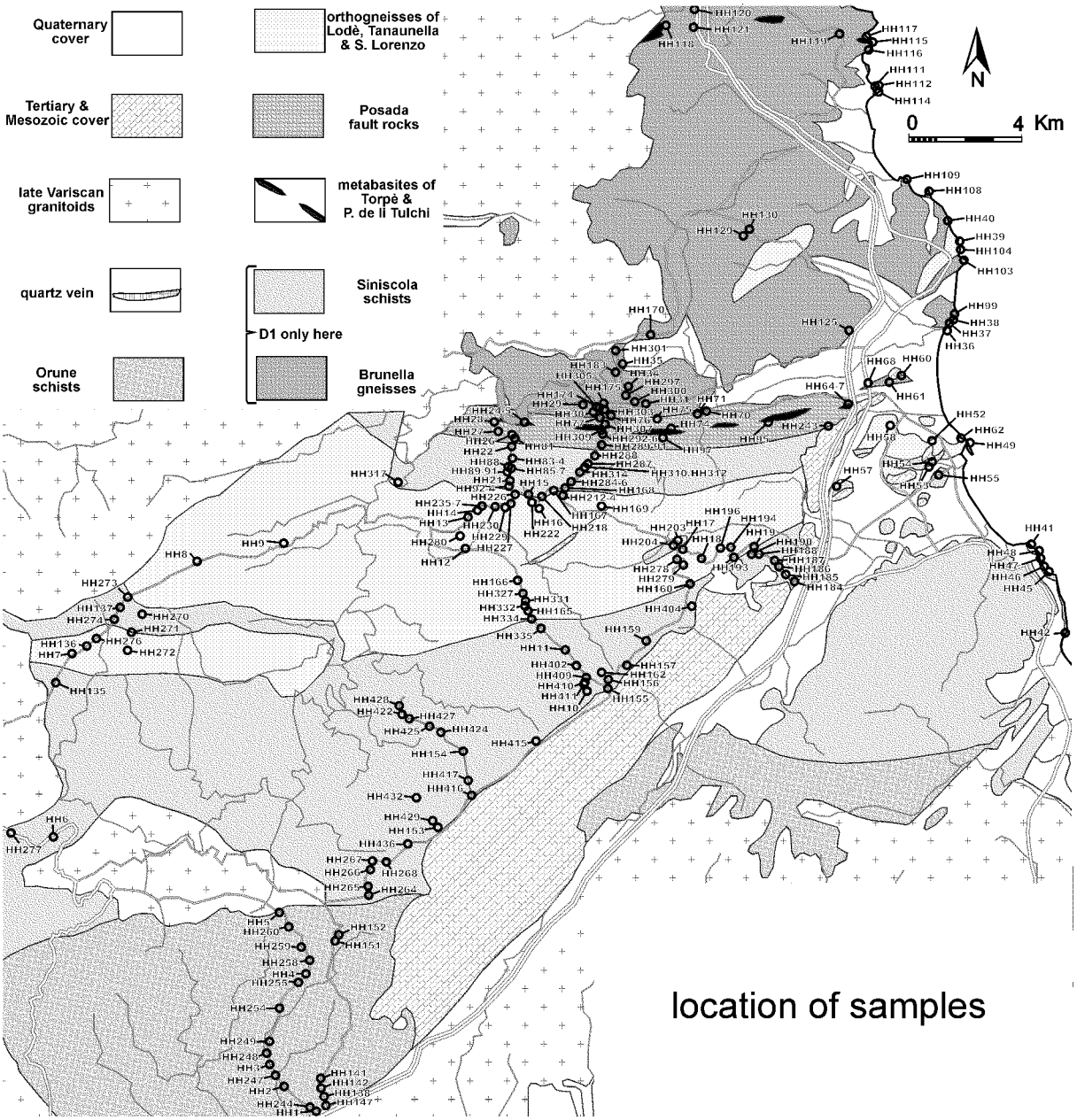

Figure 5.3: Location of samples plotted in geological sketch map of the NE Sardinian study area. The rock-forming minerals of each thin section are listed in the appendix.

5.3 Orune schists

The uppermost external position of the Orune schists in the studied sequence finds expression in the best preserved primary fabrics. The bedding of alternating metapsammopelites with locally interlayered porphyroids, few greenschists, and graphitic schists is transposed by the continuous D2 cleavage, which is developed as the main foliation.

Despite D2 transposition in the metapsammopelites, the alternating P- and Q-domains, which arose from the D2 accompanying metamorphic conversion of the pelitic and psammitic domains in the bedding of the sedimentary precursors, preserved in places a gradual transition from Q- to P-domains and an abrupt transition vice versa from P- to Q-domains that reflect the fining upwards in each bed (plate 5.1a).

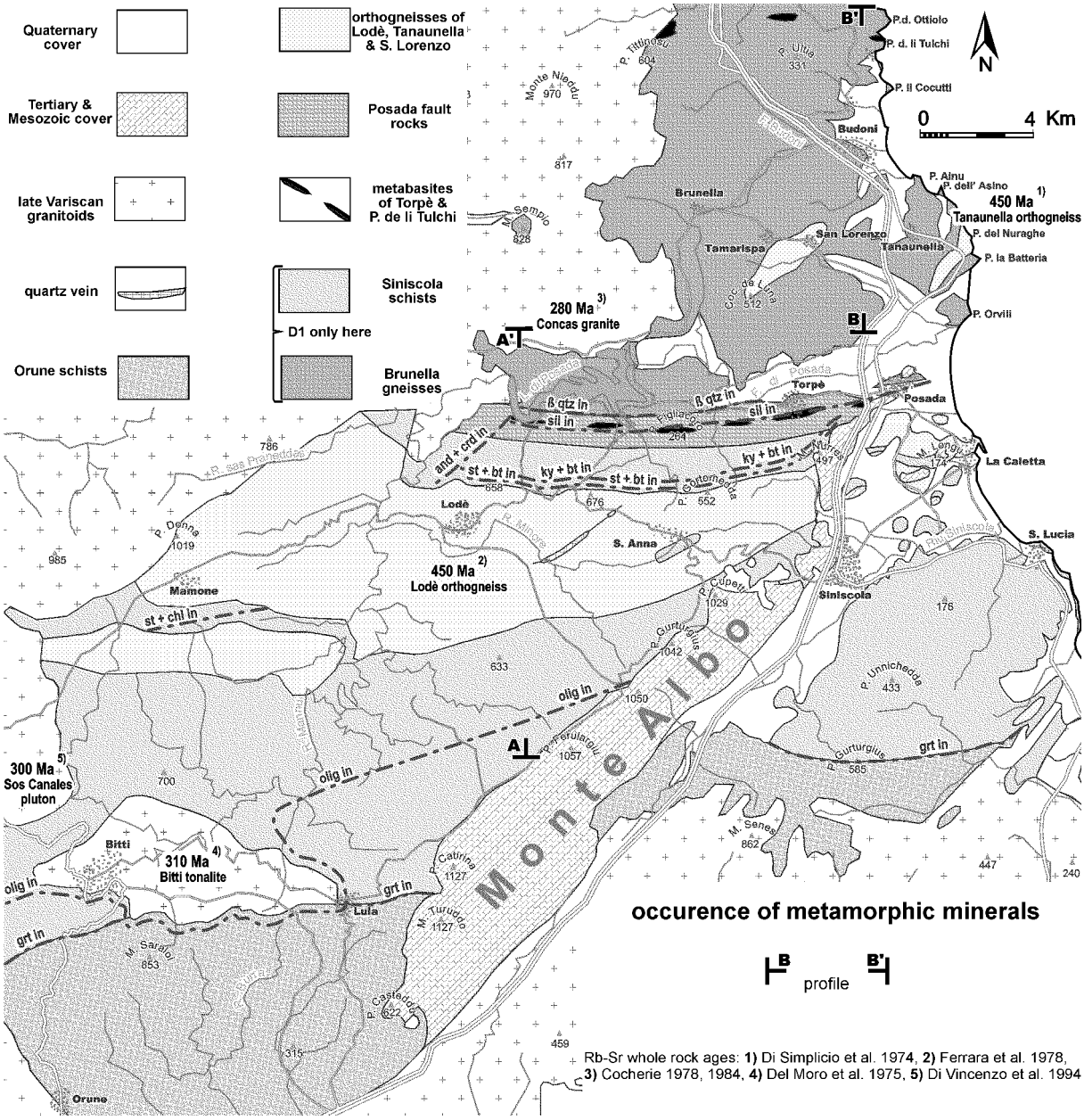

Figure 5.4: Occurrence of metamorphic minerals plotted in geological sketch map of NE Sardinia that shows additionally some Rb-Sr whole rock ages (profile in fig. 5.2).

The P-domains contain mainly white mica, biotite, some chlorite and in places a considerable amount of graphite. Also, S2-parallel quartz veins occur preferentially in the P-domains. The phyllosilicates are generally aligned with their basal cleavage plane coplanar with S2. Some calcite in the Q-domains is locally common.

In the porphyroids, relict feldspar phenocrysts remained from the volcanic precursor. They are commonly fractured, and their ruptured fragments are aligned parallel to S2 (plate 5.1c). Recrystallised fringes of quartz occur in the D2 pressure shadows of the feldspar phenocrysts. S2 in the fine-grained matrix is deflected around the feldspar phenocrysts. It is defined by the alignment of albite, quartz, white mica, chlorite, clinozoisite and epidote. Recrystallised phenocrysts of quartz are also abundant

(plate 5.1d). In contrast to the feldspar phenocrysts, they were less rigid, and thus show a weaker deflection of S2. The former quartz phenocrysts are commonly stretched out to bands.

According to the recrystallised quartz and fractured feldspar, the D2 temperatures overstepped the temperature of incipient quartz recrystallisation, but not of incipient feldspar recrystallisation, which are circa 290 °C and 500 °C respectively (Voll 1976).

The greenschist layers are commonly composed by tremolite/actinolite schists that probably represent basic metatuffs. The very fine tremolite/actinolite needles are aligned parallel to S2. The mineral assemblage *quartz* + *tremolite/actinolite* + *epidote* + *chlorite* + *green biotite* is characteristic for greenschist facies metabasites and confirms the greenschist facies conditions indicated by the D2 quartz/feldspar rheology and by the mineral assemblage *quartz* + *biotite* + *chlorite* + *albite* + *muscovite* in the metapsammopelite layers, which reflects a composition typical of low-Al metapelites (fig. 5.5).

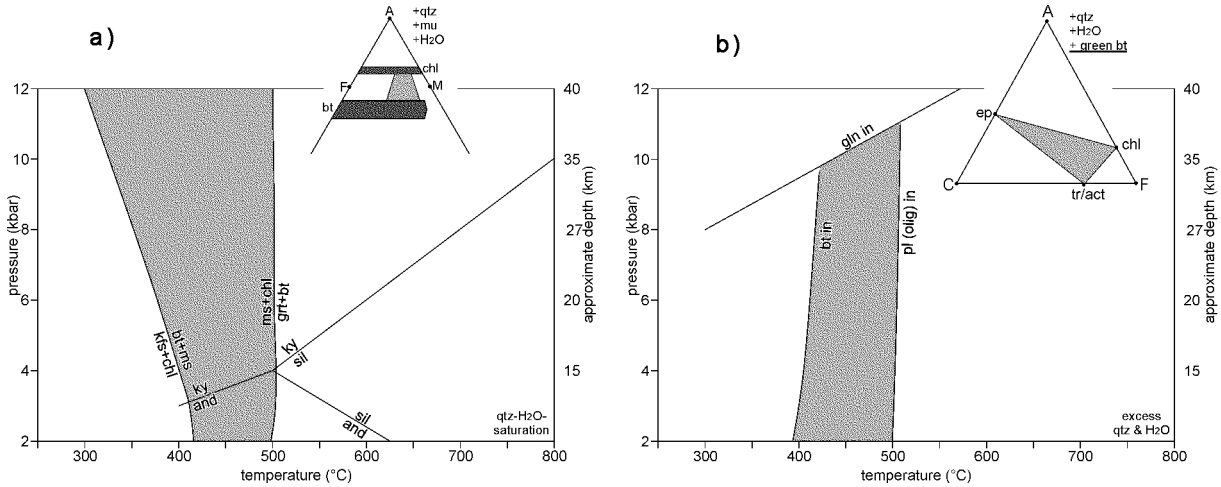

Fig. 5.5: P-T fields and mineral assemblages in: **a)** low-Al metapelites; bt-in and grt-in reaction curves after Bucher & Frey (1994), stability fields of as-polymorphs after Holdaway (1971); and **b)** metabasites; bt-in, olig-in, and gln-in reaction curves after Bucher & Frey (1994); both interlayered in the Orune schists.

Small euhedral garnet grew in epidote- and clinozoisite-rich porphyroid layers (plate 5.2e). However, it does not conflict necessarily with the estimated greenschist facies conditions, because a calcium-rich composition, which is suggested by the coexisting minerals, would lower the temperatures for the garnet-in reactions (Spear 1993).

The S2-parallel layers and quartz veins underwent folding and overprinting by the crenulation cleavage S3 in the F3 hinges (plate 5.1f-g). White mica is bent (plate 5.1h) or kinked, but is also neo- and recrystallised in the D3 crenulation (plate 5.2a), according to its diagnostic arrangement in polygonal arcs (Shelley 1993). So, the D3 temperatures have been around 450 °C, because the incipient recrystallisation of muscovite is referred to this temperature (Kruhl 1993).

S3 is commonly deflected around porphyroblasts that overgrew S2. Consequently, the porphyroblasts mainly grew during the post-D2/pre-D3 time span. Chlorite porphyroblasts are common, especially in the P-domains (plate 5.2a). However, plagioclase forms by far the most abundant porphyroblasts

(plates 5.1b, h, 5.2b, c). They constitute an excellent marker fabric due to their widespread occurrence also in the Siniscola schists. In the Orune schists, plagioclase porphyroblasts commonly have an albitic composition. Some S2 inclusion trails are weakly folded, which indicates that the growth of the plagioclase porphyroblasts continued in places until early D3 (plate 5.2c).

The plagioclase porphyroblasts can be clearly distinguished from the phenocrysts of the porphyroids, because they contain S2 inclusion trails that are commonly still in continuity with the external S2 (plate 5.1e), and they are commonly not fractured and do not show quartz fringes. The feldspar phenocrysts, though albitic in composition too, have generally a saussuritised core with random inclusions of epidote, clinozoisite and some white mica (plate. 5.1e).

The poikilitic plagioclase porphyroblasts mainly enclosed S2-aligned quartz grains and, to minor extent, other S2-defining minerals, i.e. clinozoisite, epidote, titanite, zircon and graphite. The porphyroblasts grew at the expense of white mica and quartz preferably in the Q-domains and, to a minor extent, in the P-domains as well (plate 5.1a-b, 5.2b). Isothermal decompression in sodium-bearing metapelites commonly induces albite expansion at the expense of coexisting white mica, so that sodium and quartz are consumed and potassium and hydrogen ions released (Jamieson & O'Beirne-Ryan 1991):

$KAl_2[AlSi_3O_{10}(OH)_2] + 3Na^+ + 6SiO_2 \rightarrow 3NaAlSi_3O_8 + K^+ + 2H^+$.

Sodium components other than the plagioclase porphyroblasts are missing. The white mica has been identified to be muscovite (Franceschelli et al. 1982). Therefore, the sodium was probably provided either by a sodium component, which became completely consumed, such as for instance detrital alkali feldspar, or by a fluid phase, suggesting sodium metasomatism.

A D5 crenulation (plate 5.2d) is locally developed in schistose layers, displaying bent and kinked mica. According to the lack of general retrogression and the missing recrystallisation of muscovite, the D5 temperatures are still in the greenschist facies range, but dropped below the temperature of incipient recrystallisation of muscovite, which sets on at about 450 °C (Kruhl 1993).

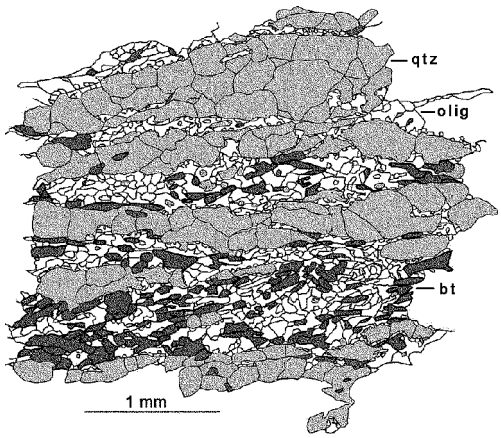

Fig. 5.6: From thin section redrawn sketch of an Orune schist-derived biotite gneiss in the contact aureole of the Bitti tonalite (HH5). It reflects contact metamorphism by the finely recrystallised oligoclase, coarsely annealed quartz, and neocrystallised biotite.

Towards the contact of the Bitti tonalite (fig.5.4) the plagioclase porphyroblasts changed from albite to a composition beyond the peristerite gap and recrystallised marginal to fine grains due to the thermal effect in the contact aureole. Moreover, abundant biotite neocrystallised at the expense of chlorite and quartz annealed to coarser grains (fig. 5.6).

5.4 Siniscola schists

The Siniscola schists consist of garnet-bearing metapsammopelites with local calc-silicate intercalations, contain some metabasites and host the Lodè orthogneiss. They are characterised by the appearance of the older basement fabric of D1 and northwards increasing metamorphism as well as shearing related to the Posada fault.

In the following, the zoning of metamorphic index minerals (fig. 5.1) by Franceschelli et al. (1982) is further specified based on mineral assemblages of high-Al metapelites, which indicate metamorphic conditions that are additionally proven on mineral assemblages of adjacent metabasites; then the timing of the assemblages relative to the structural evolution is constrained.

- The presence of the mineral assemblage *quartz* + *muscovite* + *garnet* + *chlorite* + *chloritoid* indicates that the southern Siniscola schists have undergone the garnet-in reaction (fig. 5.4) at metamorphic conditions of the lower amphibolite facies (mineral assemblage I. in fig. 5.7a).
- The oligoclase appearance within the garnet zone in response to the increasing regional metamorphism has to be distinguished from the extended oligoclase occurrence in the contact aureole of the Bitti tonalite (fig. 5.4).
- A small metabasite body near Siniscola (fig. 5.4, HH185 in 5.3) contains the mineral assemblage *quartz* + *oligoclase* + *epidote* + *hornblende* + *chlorite* + *brown biotite* (mineral assemblage I. in fig. 5.7b), which is diagnostic for the greenschist/amphibolite facies transition and supports the temperature estimate for the adjacent metapelites.
- In the Siniscola schists south of Mamone (fig. 5.4), the mineral assemblage *quartz* + *muscovite* + *staurolite* + *garnet* + *chlorite* suggests that the discontinuous chloritoid-out reaction operated (mineral assemblage II. in fig. 5.7a).
- The appearance of the mineral assemblage *quartz* + *muscovite* + *staurolite* + *biotite* + *chlorite* (mineral assemblage III. in fig. 5.7a) and/or *quartz* + *muscovite* + *staurolite* + *biotite* + *garnet* point to a further increase of temperature towards the northern Siniscola schists (fig. 5.4).
- Eventually, the mineral assemblage *quartz* + *muscovite* + *staurolite* + *biotite* + *kyanite* (mineral assemblage IV. in fig. 5.7a) indicates metamorphic conditions of the middle amphibolite facies in the northernmost Siniscola schists (fig. 5.4).
- The mineral assemblage *quartz* + *hornblende* + *garnet* + *plagioclase* + *brown biotite* (mineral assemblage II. in fig. 5.7b) in metabasite layers intercalated in the northernmost Siniscola schists

(HH93, HH168, HH314 in fig. 5.3) confirms the metamorphic conditions of the middle amphibolite facies recorded in the adjacent metapelites.

- The mineral assemblage *quartz* + *muscovite* + *andalusite* + *cordierite* (plates 5.6h, 5.7a) replaced the assemblages of kyanite and staurolite in the contact aureole of the Concas granite (fig. 5.4), which intruded after the Variscan deformational activity ceased. The randomly oriented minerals of contact metamorphism constrain the depth of intrusion to about 7 kilometres (mineral assemblage V. in fig. 5.7a).

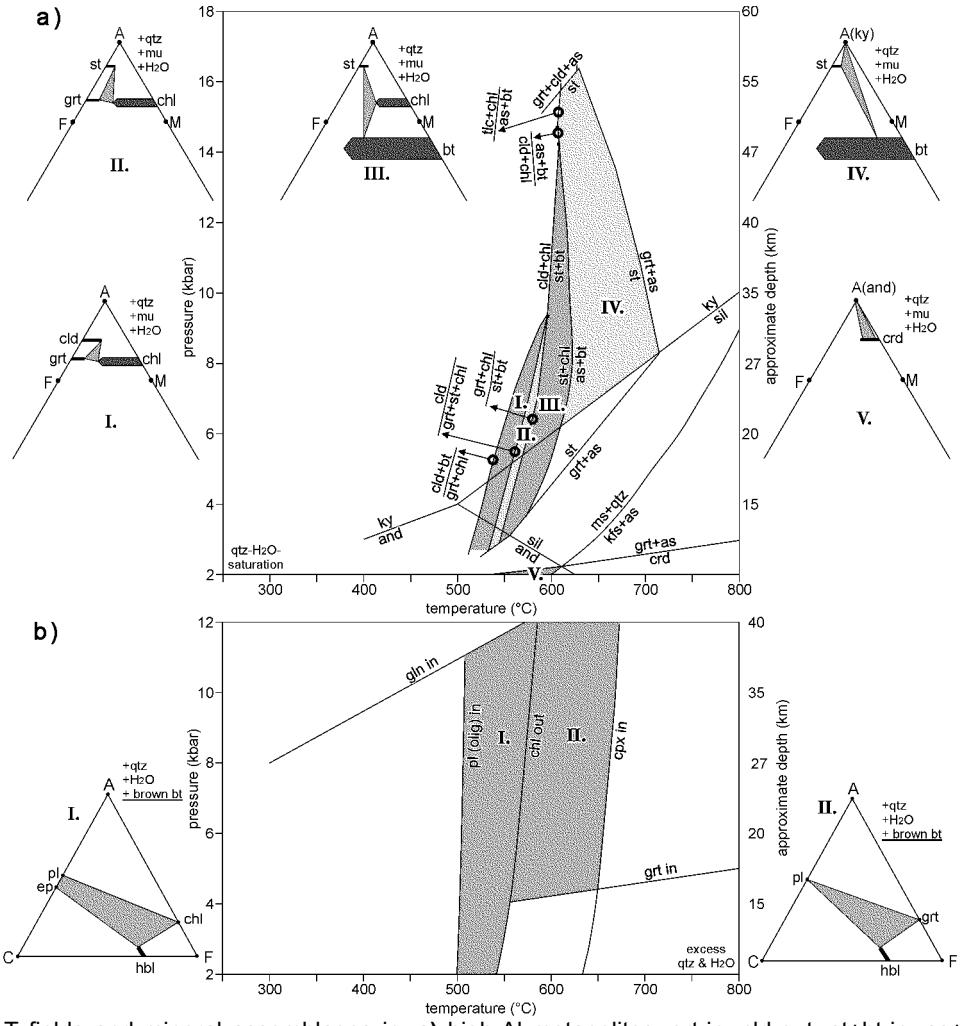

Fig. 5.7: P-T fields and mineral assemblages in: **a)** high-Al metapelites; grt-in, cld-out, st+bt-in, as+bt-in, st-out reaction curves after Spear & Cheney (1989), crd-in, ms-out reaction curves after Bucher & Frey (1994), stability fields of as-polymorphs after Holdaway (1971), location of mineral assemblages **I.**, **II.**, **III.**, **IV.** & **V.** in fig. 5.4; and **b)** metabasites; pl (olig)-in, chl-out, grt-in, cpx-in, gln-in reaction curves after Spear (1993), Bucher & Frey (1994), mineral assemblage **I.**: sample HH185 intercalated in grt+olig schists, mineral assemblage **II.**: samples HH93, HH168 & HH314 intercalated in st+bt & ky+bt schists, location of samples in fig. 5.3; all intercalated in the Siniscola schists.

The older basement fabric of D1 is best preserved in the southern Siniscola schists. Here, S1 survived in the F2 hinges (plate 5.3a) and is developed as continuous cleavage that transposed the alternating P- and Q-domains. Aligned in D2 microfolds, chloritoid and poikiloblastic garnet, which overgrew S1 so that it is preserved as inclusion trails, are truncated by and deflect the external S2 (fig. 5.10b, plates

5.2f-g & 5.3b). According to this morphology, the growth of chloritoid and garnet took place in a post-D1/pre-D2 time span.

On the other hand, poikilobastic plagioclase is aligned in D3 microfolds (plate 5.5e) and overgrew D2 fabrics, such as micro-F2 hinges (plate 5.3c), so that it has S2-aligned inclusion trails truncated by the deflected external foliation S3 (plate 5.2h, 5.3d, 5.4a-b). This plagioclase morphology, which implies the plagioclase growth occurred after D2 and before D3, is common throughout the whole sequence of the Siniscola schists and correlates straightforward with the Orune schists. Furthermore, the mode of the plagioclase expansion at the expense of S2-aligned phyllosilicates is the same as described for the Orune schists. Consequently, the oligoclase-in front reflects a later metamorphic stage than the garnet-in front (fig. 5.4).

In contrast to the south, garnet overgrew S2 (plates 5.4c, 5.5h), so that it generally shows a similar morphology like plagioclase (plate 5.5h) and the other porphyroblasts of staurolite (plate 5.4c, 5.6a) and kyanite in the northern Siniscola schists. In places, the cores of zoned staurolite and particularly garnet preserve earlier cleavage stages, which were already transposed during the rim growth and/or the formation of the external D2 fabric (plate 5.6b-d). Accordingly, the garnet growth in the northern Siniscola schists lasted longer than in the southern Siniscola schists.

Moreover, numerous small and sub- to euhedral garnets (plate 5.5h) nucleated during the post-D2 stage of metamorphism and are overgrown by porphyroblasts in places (plate 5.4a-b). They commonly appear synchronously with the oligoclase-in front further to the south. Here, the oligoclase forms discontinuous seams along the grain boundaries of the poikiloblastic albite (plate 5.3e) or fringes in the pressure shadows of the albite porphyroblasts (plate 5.3d).

The oligoclase zone is characterised by locally occurring oligoclase intergrown with vermicular rods of quartz, composing prograde myrmekite, which has replaced albite (plate 5.3e-h, 5.5 f-g). According to Ashworth (1986), the replacement of albite by prograde myrmekite is described by the following reaction equation:

$(1+x)NaAlSi_3O_8 + xCa^{2+} \rightarrow Na_{1-x}Ca_xAl_{1+x}Si_{3-x}O_8 + 4xSiO_2 + 2xNa^+$.

The intergrowth is generally initiated at the grain boundaries between plagioclase and quartz and proceeds by lobes of quartz projecting into the plagioclase. Rising temperatures led to an increasingly higher anorthite component in plagioclase, so that the released volume of quartz increases too, which is demonstrated by the coarsening of the vermicular quartz rods from 5 µm to 25 µm from south to north of the Lodè orthogneiss (plate 5.3e-h, 5.5 f-g).

5.5 Lodè orthogneiss

The Lodè orthogneiss has a granitic to granodioritic composition. The D2 fabric is superimposed on the plutonic fabric. K-feldspar augen are common remnants of the magmatic fabric. The magmatic phenocrysts commonly survived deformation in a core, which is mantled by smaller grains of recrystallised feldspar and/or marginally invaded by myrmekites (plate 5.4h). Progressing deformation led to

the dragging out of the recrystallising feldspar grains into S2-aligned tails and bands (plate 5.4f), and/or the myrmekites recrystallised to feldspar and quartz grains (plate 5.4g). Grain boundary migration recrystallisation allows coarsening of quartz, whereas prevailing subgrain rotation recrystallisation in feldspar forbids major coarsening. This distinct recrystallisation behaviour of quartz and feldspar is typical of the metamorphic conditions at the greenschist/amphibolite facies transition (Tullis & Yund 1985, Simpson & Wintsch 1989) and finds expression in the generally coarser-grained quartz and smaller-grained feldspar domains aligned in S2. At the southeastern flank of the Lodè orthogneiss, the feldspar deformation appears coevally ductile and brittle (plate 5.4e) probably due to increased strain rates and/or slightly lower temperatures than in the rest of the orthogneiss. However, recrystallised feldspar occurs in the D2 fabrics throughout the Lodè orthogneiss. Thus, the temperature of incipient feldspar recrystallisation, which is at about 500 °C (Voll 1976), was overstepped during D2. Consequently, the estimated temperature range of the Lodè orthogneiss is in agreement with the metamorphic record in the adjacent Siniscola schists.

D3-folding affected the northern Lodè orthogneiss. Here, it is associated with the development of a spaced cleavage. In addition, D5 buckle folds occur in the central part of the Lodè orthogneiss (plate 5.5d). Their formation is accompanied and/or followed by a biotite blastesis. Much of biotite has been subsequently altered to chlorite.

5.6 Posada fault rocks

The Posada shearing overprinted the aforementioned Lodè orthogneiss and Siniscola schists beyond the oligoclase-in front (fig. 5.4) increasingly stronger towards the Posada fault, so that the increased metamorphic field gradient partly appears as consequence of the increasing non-coaxial D4 strain. The D4 foliation is commonly developed as C'-type shear band crenulation cleavage that preferentially occurs in the P-domains of the Siniscola schists (plate 5.4d). Here, it caused bending, kinking, and rupturing of mica by slip on the basal mica cleavage planes generally in association with fine-grained recrystallisation of quartz (plate 5.6g). D4-accompaning processes are commonly chloritisation, sericitisation, and/or saussuritisation of biotite, garnet, staurolite, kyanite, and/or oligoclase correspondingly. Also in the Lodè orthogneiss, chloritisation of biotite, saussuritisation and/or sericitisation of feldspar are connected with D4. Here, feldspar is partly replaced by muscovite (plate 5.5b), irrespectively of the feldspar composition, leading to an enrichment of muscovite in the D4 shear zones (plate 5.5a), where it forms abundant mica fishes (plate 5.5c). The D4-induced alteration of the feldspars to muscovite indicates the involvement of a hydrous fluid and is described by the following reactions (Barnes 1997):

$3KAlSi_3O_8 + 2H^+ \rightarrow KAl_2[AlSi_3O_{10}(OH)_2] + 2K^+ + 6SiO_2$,

$3CaAl_2Si_2O_8 + 2K^+ + 4H^+ \rightarrow 2KAl_2[AlSi_3O_{10}(OH)_2] + 3Ca^{2+}$,

$3NaAlSi_3O_8 + K^+ + 2H^+ \rightarrow KAl_2[AlSi_3O_{10}(OH)_2] + 3Na^+ + 6SiO_2$.

With increasing strain towards the Posada fault, S4 is not restricted to the P-domains of the Siniscola schists anymore, but transposes more and more the entire rock fabric, which results in bending, fracturing, and disrupting of the plagioclase, garnet, staurolite, and kyanite porphyroblasts (plate 5.6e-f). Eventually, the retrograde comminution caused the disappearance of the staurolite, kyanite, and garnet porphyroblasts in the Posada fault rocks, i.e. mylonites and cataclasites (plate 5.7e, 5.9a).

According to the brittle behaviour of feldspar and white mica as well as the ductile behaviour of quartz, which indicate that the temperatures allowed the recrystallisation of quartz (above 290 °C, Voll 1976), but not the incipient recrystallisation of feldspar (at 500 °C, Voll 1976) nor of white mica (at 450 °C, Kruhl 1993), in addition to the D4-accomaning alterations, the Posada shearing overprinted, in terms of the orogenic anatomy, the external wall rocks under retrograde conditions of greenschist facies.

Feldspar is the only major porphyroblastic constituent in the Siniscola schists, which survived retrogression and brittle deformation in the Posada fault rocks. Its repeated fracturing and shearing caused boudinaged arrays of smaller feldspar lozenges (plate 5.7h). The feldspar clasts are commonly wrapped by mica (plate 5.8a). Mica grew at the expense of the feldspar clasts (plate 5.8b). Oligoclase clasts are marginally retrogressed, so that they may show an albitic rim (plate 5.8c). Mica accommodated to a large extent the deformation prevailingly by slip on its basal cleavage planes (plate 5.8d). If the feldspar lozenges flowed in a matrix of quartz or mica, which accommodated the deformation, the strain partitioning kept them undeformed (plate 5.8g).

Locally occurring phyllonites that consist of white mica, chlorite, and quartz appear as the final stage of ongoing deformation and associated retrogression (plate 5.8e). The Posada fault rocks generally show an increasing content of inherited feldspar towards the Brunella gneisses. The survivor feldspar clasts comprise around 50 vol. % in the fault rocks that derived from the Brunella gneisses (plate 5.8f). This exceeds the feldspar proportion of about 25 vol. % in the fault rocks that derived from the Siniscola schists.

Crystal-plastic deformation in quartz-rich domains is in rheological contrast to the prevailingly brittle deformation in feldspar-rich domains (plates 5.7e, 5.8f-g). If the matrix of quartz and mica could not accommodate deformation, feldspar clasts show entirely brittle deformation and rock fragments indicate brittle failure of the whole rock (plates 5.8h, 5.9a).

According to these fabrics, fracturing of feldspar, basal cleavage sliding of white mica, and recrystallisation of quartz accompanied by diffusional mass transfer in a hydrous fluid are the most important mechanisms of the retrograde deformation in the Posada fault rocks. They allowed a ductile flow despite the brittle behaviour of feldspar and mica. Deformation was focused in several generations of repeatedly transposed anastomosing networks that form the mylonitic foliation.

In contrast to the brittle behaviour of feldspar in the external wall rocks and in the Posada fault rocks, feldspar recrystallisation (plate 5.10.h), in places associated with conjugate fracture sets that divide

larger feldspar grains to smaller lozenges (plate 5.7g), is documented for the early stages of the Posada shearing in the internal wall rocks, represented by the Brunella gneisses. This change from earlier ductile to later brittle behaviour of feldspar indicates cooling during the Posada shearing. Also, the Torpè metabasites, which are low-strain domains in the Posada fault, recorded recrystallisation of feldspar (plate 5.7c) before their fabric locked, presumably because of the increasing rigidity due to the temperature drop below the temperature of incipient feldspar recrystallisation. The recrystallisation of feldspar indicates temperatures of above 500 °C (Voll 1976) during the initial Posada shearing in the Brunella gneisses, where it is superimposed on a high-grade fabric. Fibrous sillimanite survived deformation in central parts of the Posada fault (fig. 5.4), which further supports the interpretation that the Posada shearing in the Brunella gneisses initially operated in the stability field of sillimanite.

Taking into account the initial difference between the bimodal rheology of the external wall rocks, given by the brittle feldspar and ductile quartz in the Siniscola schists, and the ductile rheology of the internal wall rocks, given by the Brunella gneisses, the Posada fault formed at the brittle-ductile crustal transition, which can be expected in depths of 8-15 km (Stewart et al. 2000).

The mylonites of the Posada zone have been folded during D5 (plate 5.9b). Late annealing of quartz-fabrics, indicated by its equigranular polygonal grain shape, and neocrystallisation of fine-grained biotite is common close to the Concas granite and is attributed to the thermal contact effect of the granite intrusion.

5.7 Brunella gneisses

The Brunella gneisses comprise mainly para- and orthogneisses, locally calc-silicate gneisses, and host the metabasites of Punta de li Tulchi (fig. 5.4). Also, the metabasites and orthogneisses, which are presently intercalated in the Posada fault rocks near Torpè, are inferred to have been located in the Brunella gneisses before they became involved in the Posada faulting. The Brunella gneisses underwent partial melting, according to the widely occurring migmatic fabrics.

Leucosome veins that cross cut S1 discordantly (plate 5.9d) indicate that the partial melting followed after a first deformation event. Furthermore, centimetre-sized nodules probably represent an early pre-migmatic porphyroblast growth. However, their unusual nodule mineralogy of sillimanite + quartz + muscovite probably represents rather pseudomorph replacement than the original porphyroblast mineralogy.

The presence of lobately intergrown plagioclase and quartz is a conspicuous feature (plate 5.10d) that is generally understood to be characteristic of diffusion creep under high-grade metamorphic conditions (Gower & Simpson 1992). In places, quartz grains have perpendicularly oriented subgrain boundaries coplanar with the basal and prism crystal planes, so that they display a chess board pattern (plate 5.9g), which points out the elevated temperatures of the high-quartz stability field (Kruhl 1996). These elevated temperatures are consistent with the high-grade conditions suggested by the muscovite-absent mineral assemblage of *quartz* + *K-feldspar* + *sillimanite* + *granat* + *biotite* (fig. 5.9) and with

the partial melting indicated by the locally developed migmatic fabric. Furthermore, stromatic migmatites show leucosome with biotite selvages (plate 5.9c). Thus, biotite was a stable component during partial melting, owing to its abundance and to the scarcity of garnet and the absence of cordierite, which would have been formed at the breakdown of biotite. Moreover, the locally occurring garnet is not related to the leucosome. Taking the absence of muscovite into account, muscovite dehydration-melting might have operated after the following reaction (Patiño Douce & Harris 1998):

22ms + 7pl + 8qtz → 25melt + 5kfs + 5sil + 2bt.

On the one hand, only the lower P-T limit of the partial melting is given by the high-quartz stability as well as by the absence of cordierite (fig. 5.9), because the high-Ti content of biotite, which is implied by its reddish brown colour, shifts the onset of the biotite dehydration-melting towards higher temperatures (Dooley & Patiño Douce 1996) and the chess board subgrain patterns of quartz might be acquired under post-migmatic conditions. On the other hand, the lack of kyanite constrains the muscovite dehydration-melting to the stability field of the associated sillimanite, so that an upper P-T limit of 8 kbars and 750 °C would be realistic, in particular with respect to a decompressional P-T path as considered afterwards.

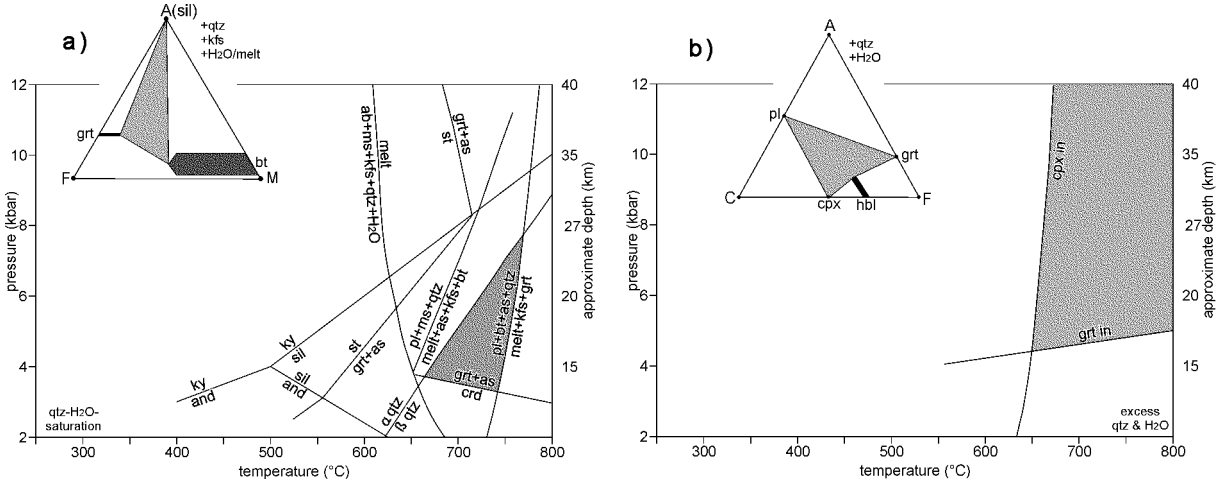

Fig. 5.9: P-T fields and mineral assemblages in: **a)** migmatic Brunella gneisses; granite wet solidus after Huang & Wyllie (1981), stability fields of as-polymorphs after Holdaway (1971), ms-dehydration-melting after Patiño Douce & Harris (1998), bt-dehydration-melting after Le Breton & Thompson (1988), crd-in after Weisbrod (1973), boundary of low-high qtz after Gross & Van Heege (1973); and **b)** metabasites from Torpè and P. Orvili (fig. 5.4); grt-in, cpx-in reaction curves after Spear (1993), Bucher & Frey (1994).

From one point of view, the complex structure of the migmatites reflects a high ductility typical of partially molten rocks, whereas the associated deformational fabrics are typical of a post-migmatic, solid-state overprint. Thus, S2 is generally developed as continuous cleavage that transposes the compositional layering and forms the main foliation. In places, fibrous sillimanite shows a post-migmatic morphology. It is commonly aligned in fold hinges or parallel to the D2 stretching lineation, forming porphyroblast aggregates (plate 5.9e-f), or it has locally overgrown the post-migmatic foliation in radiating aggregates. In places, fibrous sillimanite substitutes feldspar, biotite, and muscovite by base-leaching reactions common in hydrous fluid-induced alteration (Vernon 1979):

ab → sil: $2NaAlSi_3O_8 + 2H^+ \rightarrow Al_2SiO_5 + 2Na^+ + H_2O + 5SiO_2$

an → sil: $CaAl2Si_2O_8 + 2H^+ \rightarrow Al_2SiO_5 + Ca^{2+} + H_2O + SiO_2$

kfs → sil: $2KAlSi_3O_8 + 2H^+ \rightarrow Al_2SiO_5 + 2K^+ + H_2O + 5SiO_2$

bt → sil: $2K(Mg,Fe)_3AlSi_3O_{10}(OH)_2 + 14H^+ \rightarrow Al_2SiO_5 + 2K^+ + 6(Mg,Fe)^{2+} + 9H_2O + 5SiO_2$

ms → sil: $2KAl_3Si_3O_{10}(OH)_2 + 2H^+ \rightarrow 3Al_2SiO_5 + 2K^+ + 3H_2O + 3SiO_2$

Progressing folding and shearing is associated with myrmekitic intergrowth of plagioclase and vermicular quartz at the expense of K-feldspar (plate 5.10b). In places, symplectic intergrowth of muscovite and vermicular quartz replaces not only K-feldspar, which has been reported to be a common reaction fabric by Phillips et al. (1972), but also plagioclase (plate 5.10e). Thus, the fabric of symplectic intergrown muscovite and quartz is described by the same reaction equations as the aforementioned muscovitisation of feldspar in the Lodè orthogneiss.

Towards the Posada fault, more and more muscovite appears and the deformational fabrics can be correlated eventually with the aforementioned early D4 stages of the Posada faulting. The replacement of feldspar by mica commonly progresses from grain boundaries, because they acted probably as pathways for the supply of hydrous fluid (plate 5.10f-g).

The D2 to early D4 development is accompanied by the recrystallisation of feldspar. So, temperatures were above the incipient feldspar recrystallisation temperature of about 500 °C (Voll 1976). Furthermore, the metamorphic conditions from D2 to early D4 are restricted to the stability field of the associated sillimanite.

In contrast, feldspar and partly quartz show a rigid response on the D5 shear bands developed mainly along mica domains, where the mica accommodated deformation by sliding on its basal cleavage (plate 5.11a). D5 microfolds (plate 5.11b) in the Concas granite aureole display preferred orientation of neocrystallised biotite coplanar with the F5 axial plane.

In general, the record of the Brunella gneisses can be summarised as follows: an early metamorphic fabric without P-T memory that became subjected to an episode restricted to the sillimanite stability field, comprising partial melting and subsequent retrograde deformation under amphibolite facies conditions, and a final greenschist facies overprint. The P-T record of the early metamorphic fabric appears erased by the partial melting.

However, the metabasites intercalated in the Brunella gneisses partly preserved relics of an early metamorphic fabric. Thus, the Punta de li Tulchi metabasite contains elongated coronitic garnet porphyroblasts aligned in a matrix of symplectically intergrown pyroxene, albite, hornblende, and rutile. The coronae around garnets have inner zones of symplectic plagioclase, pyroxene and hornblende and outer zones of hornblende (plate 5.9h). This symplectic, coronitic fabric derived from retrogression of an early eclogitic fabric (fig. 5.1b, 5.2). It indicates a disequilibrium state, which was probably maintained due to a shortage of intergranular hydrous fluid, allowing only limited mass transfer, and/or rapidly changing metamorphic conditions (Passchier & Trouw 1996).

In some layers, the coronitic garnet and symplectic pyroxene are replaced by an amphibolite facies assemblage of hornblende and plagioclase, which is deformed by a crenulation cleavage (plate 5.10a). Plagioclase-rich nodules commonly mark the sites of the previous garnet aggregates, so that they mimic the older fabric.

The Torpè metabasites contain abundant quartzofeldspathic layers (plate 5.7b) and preserved the biotite-absent mineral assemblage of *quartz* + *clinopyroxene* + *hornblende* + *plagioclase* + *garnet* in places, which indicates metamorphic conditions of the upper amphibolite facies (fig. 5.11). Garnet is marginally invaded by corona-like arranged plagioclase, resembling a kelyphitic structure (plate 5.11c), so that a preceding granulite facies precursor similar to the coronitic fabric of the Punta de li Tulchi metabasite might be suggested.

Besides this early retrogression, clinopyroxene was later retrogressively replaced by plagioclase, hornblende and clinozoisite in places, which were subjected to the initial Posada faulting. The resulting intensively overprinted matrix consists of recrystallised feldspar and quartz and hosts porphyroblastic hornblende lozenges (plate 5.7b-c). The hornblende accumulated deformation by sliding along its cleavage planes, so that shear bands formed (plate 5.11d). Early D4 temperatures above the temperature of incipient feldspar recrystallisation, are additionally confirmed by the intensively recrystallised K-feldspar (plate 5.7d) in the orthogneisses that occur intercalated in the Posada fault adjacent to the Torpè metabasites.

A metabasite at P. Orvili contains a mineral assemblage of *quartz* + *plagioclase* + *hornblende* + *garnet* + *clinopyroxene*, which confirms the upper amphibolite facies conditions recorded in the Torpè metabasite (fig. 5.9b), but in contrast to the Torpè metabasite, brown biotite occurs and the garnet is common as small sub- to euhedral grains without corona-like replacement (plate 5.10c).

Accordingly, the Brunella gneisses lost, presumably during decompression induced partial melting, their early P-T record, which was probably more pressure-pronounced, taking the early record of the intercalated metabasites into account.

5.8 Discussion

The mineral zoning by Franceschelli et al. (1982, fig. 5.1) has been further refined in this study. The P-T conditions inferred from metapelitic mineral assemblages have been additionally proven on associated metabasite occurrences. It has been shown that the Siniscola schists provide a continuous Barrovian suite from the replacement of chloritoid by staurolite to the appearance of kyanite. Moreover, the superimposed low-pressure/high-temperature assemblage of andalusite and cordierite (fig. 5.10) in the contact aureole of the late Variscan Concas granite points to the shallow levels, to which the studied sequence was already exhumed, when the Variscan deformational activity ceased.

The extent and progressive nature of the *sillimanite* + *muscovite* zone, such as proposed by Franceschelli et al. (1982), has to be revised as follows. First, the redefined sillimanite appearance in the central Posada fault marks the incoming Brunella gneisses-derived fault rocks (fig. 5.1a & 5.4).

Second, the muscovite is retrogressively superimposed on the high-quartz/muscovite-absent assemblage. Therefore, this mineral zone is retrograde rather than the result of a progressively increasing metamorphism.

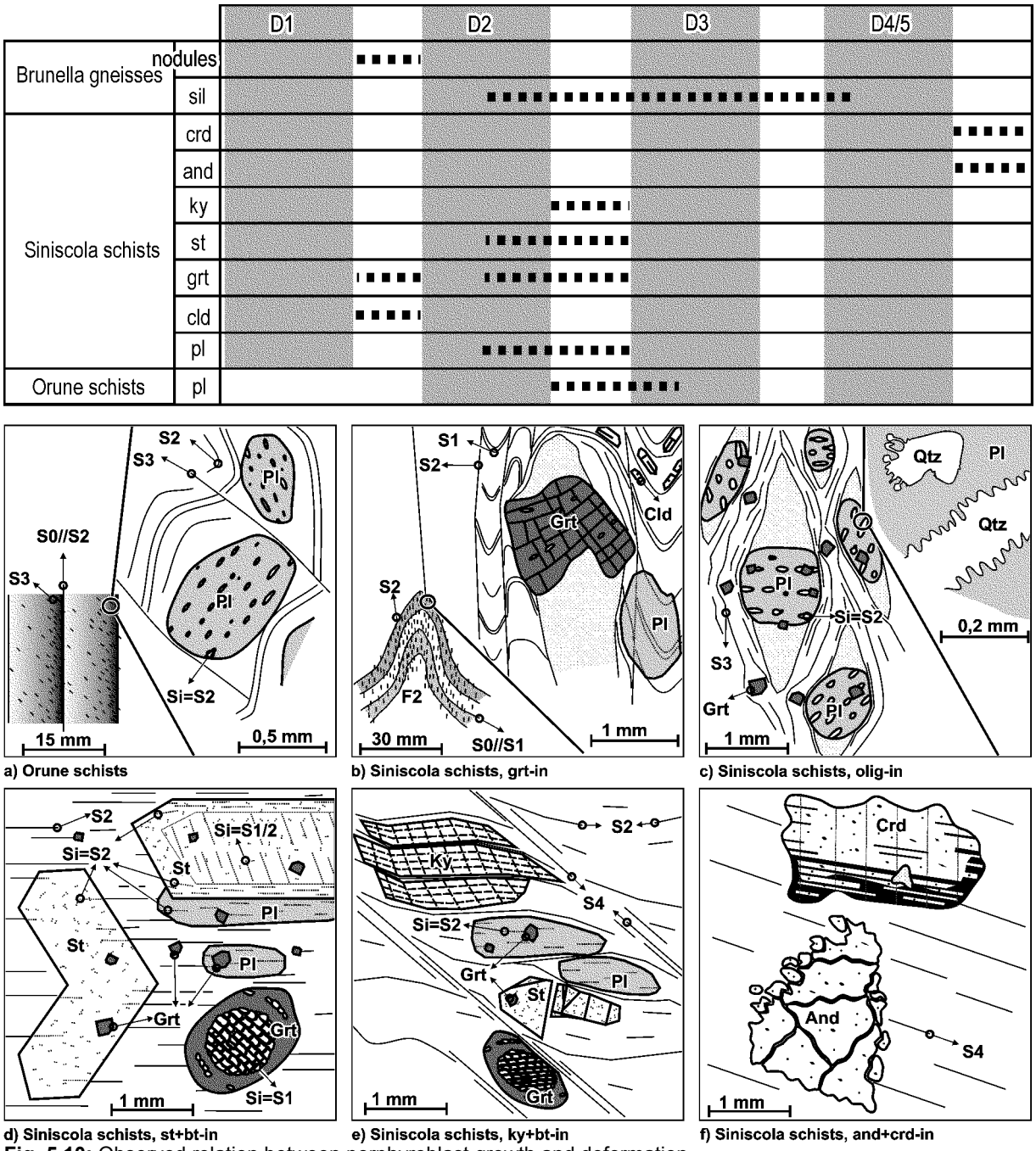

Fig. 5.10: Observed relation between porphyroblast growth and deformation.

A major plagioclase porphyroblast growth has been identified and related to decompression stages of the Variscan prograde and thermal-peak metamorphism. The prograde myrmekites (fig. 5.10c) that accompanied the decompressional plagioclase growth show that the studied sequence was simultaneously subjected to decompression and heating. The plagioclase porphyroblasts have a characteristic morphology of syn- to post-D2/pre-D3 in the Siniscola schists and post-D2/pre- to syn-D3 in the Orune schists (table in fig. 5.10). This delay of growth in the Orune schists might be related to a postponed arrival of heat due to their external position above the Siniscola schists. The plagioclase porphy-

roblasts are widespread in the Orune and Siniscola schists, so that they provide an excellent marker fabric for the correlation between porphyroblast growth and deformation across the pre-Variscan cover-basement contact.

The plagioclase marker fabric helps to understand better the origin of the *garnet + albite* and *garnet + oligoclase* zones established by Franceschelli et al. (1982, fig. 5.1a). Franceschelli et al. (1982b) addressed the unusual order of the garnet and oligoclase appearance to a specific assemblage of calcium-bearing components and CO_2-content of the fluid phase, neglecting the diachronous growth of plagioclase and two garnet generations, as shown in the following.

It has been documented in this study that the post-D1/pre-D2 garnet-chloritoid assemblage precedes the syn-D2/pre-D3 plagioclase marker fabric in the external Siniscola schists. Contrary, the garnet and plagioclase porphyroblasts display both a common syn-D2/pre-D3 morphology in the internal Siniscola schists, because the pre-D2 chloritoid assemblage is replaced by a syn- to post-D2 staurolite assemblage towards the internal Siniscola schists. Furthermore, the garnet growth apparently lasted until post-D2 stages, according to inclusion trails of S1 in the core and of S2 in the rim. A second inclusion-free, small- and sub- to euhedral garnet generation overgrew S2 and became locally incorporated in the contemporaneously growing plagioclase and staurolite porphyroblasts. It commonly coincides with the first appearance of oligoclase. Thus, the pre-D2 garnet and the syn-D2/pre-D3 plagioclase timing shows that the oligoclase-in front developed later than the garnet-in front. Consequently, their spatially independent first appearance is expression of their distinct age. Furthermore, the coincidence of the second garnet generation with the first appearance of oligoclase is consistent with the usually observed coeval appearance of garnet and oligoclase (Bucher & Frey 1994). Therefore, a specific component composition as reason for the unusual order of the garnet and oligoclase appearance, such as invoked by Franceschelli et al. (1982b), is excluded. The relative timing of the garnet and plagioclase growth suggests that the *garnet + albite* and *garnet + oligoclase* zones derive from the interference of the post-D1/pre-D2 and syn-D2/pre-D3 metamorphic stages (fig. 5.11).

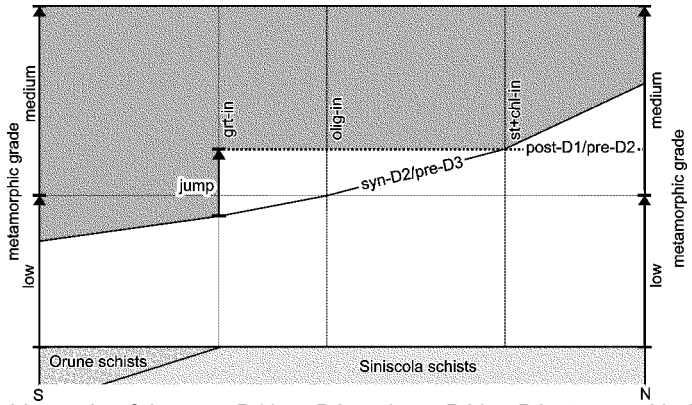

Fig. 5.11: The metamorphic grade of the post-D1/pre-D2 and syn-D2/preD3 stages with the grt-in jump at the pre-Variscan cover-basement contact.

The geothermobarometic data from the garnet zones (Franceschelli et al. 1989) deviate from the P-T conditions implied by the mineral assemblage in the garnet zones (fig. 5.12, **A**: geothermobarometric

data from the garnet zones). This discrepancy between mineral assemblage and geothermobarometry is clarified in fig. 5.11. Accordingly, the post-D1/pre-D2 mineral assemblage, which displays medium-grade metamorphic conditions, was geothermobarometrically not measured, but its syn-D2/pre-D3 re-equilibration under low-grade metamorphic conditions.

The low-Al mineral assemblage of the Orune schists and the high-Al mineral assemblages of the Siniscola schists indicate a compositional discontinuity that coincides with the pre-Variscan cover-basement contact. Moreover, the coincidence of the chloritoid assemblage with the occurrence of the D1 fabric as well as the coincidence of the garnet-in front with the pre-Variscan cover-basement contact suggest a pre-Variscan age of the pre-D2 chloritoid and garnet porphyroblasts. However, whether the pre-D2 porphyroblasts are related to a pre-Variscan basement event or to the Variscan orogeny can be resolved with certainty by radiometric dating of the garnets in the external Siniscola schists only.

Muscovite dehydration-melting has been considered for the Brunella gneisses. The general lack of kyanite restricts the partial melting to the stability field of the associated sillimanite. An early high-pressure stage is assumed for the Brunella gneisses, although high-pressure relics are only preserved in the intercalated Punta de li Tulchi metabasites, but became presumably erased due to the subsequent partial melting in the Brunella gneisses. Missing cordierite on the one hand and the former occurrence of high-quartz on the other hand constrain the decompression path to pass the high-quartz stability field, but to bypass the cordierite stability field (fig. 5.12).

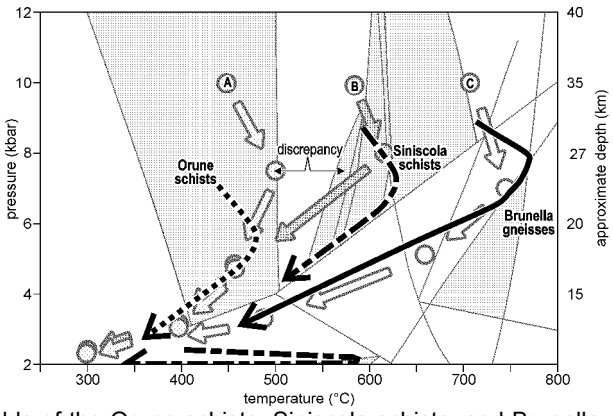

Fig. 5.12: P-T paths and fields of the Orune schists, Siniscola schists, and Brunella gneisses estimated from the mineral assemblages presented in this study. Additionally shown are the P-T paths of the A) garnet, B) staurolite, kyanite, and C) K-feldspar + sillimanite zones (fig. 5.1b, Franceschelli et al. 1989, Ricci 1992), which manly rely on geothermobarometric data (fig. 5.2). Also indicated is the discrepancy between mineral assemblage and geothermobarometry for the garnet zones.

The partial melting in the Brunella gneisses is inferred to be expression of the same metamorphic event as the syn-D2/pre-D3 porphyroblast growth in the Siniscola schists, because both are superimposed on a D1 fabric and on post-D1/pre-D2 porphyroblasts and/or nodules, both are associated with the main deformational event D2, and both are considered to be decompression-related. This conclusion is in agreement with the similar ages obtained on the Brunella migmatites (344 ± 7 Ma, Rb-Sr whole rock, Ferrara et al. 1978) and on S2-aligned muscovite from staurolite-kyanite schists (350 ± 16 & 336 ± 8 Ma, Rb-Sr, Del Moro et al. 1991).

Post-migmatic deformation locally culminated in the formation of layered gneisses and was increasingly associated with retrogression, forming myrmekites, fibrous sillimanite, and muscovite. This retrograde conversion of the migmatic fabric was probably recorded by the phengite and GASP geobarometers applied on the Brunella gneisses (fig. 5.2, Franceschelli et al. 1989, 1991, 1998), because they might rely on the retrograde muscovite, plagioclase, and sillimanite. Consequently, the contrasting barometric data across the Posada fault (fig. 5.2) might actually display the retrogressed footwall and the peak-metamorphic hanging wall.

The post-migmatic deformation under amphibolite facies conditions in the Brunella gneisses is correlated with the recumbent D3-folding documented in the Orune and Siniscola schists as well as in the northern Lodè orthogneiss and grades progressively in the D4-shearing centred in the Posada fault.

In the opposing wall rocks of the Posada fault, non-coaxial deformation initially operated under distinct metamorphic conditions. The external wall rocks, represented by the Siniscola schists, experienced retrograde deformation under low-grade conditions distinct from the overprinted medium-grade fabric. On the other hand, the internal wall rocks, constituted by the Brunella gneisses, underwent retrograde deformation as well, but in continuation of the previous medium-grade conditions, as indicated by the recrystallisation of feldspar and the persistence of sillimanite. The resulting rheological contrast between the internal wall rocks, where quartz, feldspar, and mica responded crystal-plastically, and the external wall rocks, where only quartz reacted crystal-plastically, was overcome during progressing retrogression and deformation, so that a semi-ductile rheology prevailed throughout the Posada fault. This semi-ductile rheology allowed a ductile flow by strain partitioning, despite the rigid behaviour of feldspar and mica. The strain accumulation by basal cleavage slip of mica, dynamic recrystallisation and/or pressure solution of quartz is further enhanced by the retrograde phyllonitisation of feldspar.

According to this rheological constraints, the Posada fault was initiated at the brittle-ductile crustal transition and probably accumulated the exhumation-induced cooling of the axial zone, represented by the Brunella gneisses, from medium-grade down into low-grade metamorphic conditions (fig. 5.13). Furthermore, the initially contrasting rheological behaviour during D4 shows that the Brunella gneisses cooled down later than the Siniscola schists. This is in agreement with the cooling history displayed by the ^{40}Ar-^{39}Ar isotopic system of muscovite (Carosi et al. 2002), which has a blocking temperature of circa 400 °C and yields ~340-310 Ma in the garnet zone, ~320-305 Ma in the staurolite zone and ~315-300 Ma in the sillimanite + K-feldspar zone (zoning after Franceschelli et al. 1982, fig. 5.1).

The increased geothermal gradient recorded in the Brunella gneisses outlines a thermal dome. Preceding magmatic arc and/or rift setting could have contributed to initially elevated temperatures in the lower crust (Thompson et al. 2001). The sharp contrast to the Barrovian geothermal gradient recorded in the Siniscola schists above (fig. 5.2) might be also caused by the lateral displacement along the Posada fault and the limited dimension of the thermal dome. Indeed, schists that contain corresponding

low-pressure/high-temperature assemblages of sillimanite, andalusite, and cordierite occur in the hangingwall of the Posada fault in the Anglona area at a distance of about 40 kilometres from the study area in transport direction (Oggiano & Di Pisa 1992). Thus, spatially separated areas with distinct geothermal gradient, later juxtaposed by the D5 strike-slip displacement along the Posada fault, might have contributed additionally to the contrasting barometric record across the Posada fault (fig. 5.2).

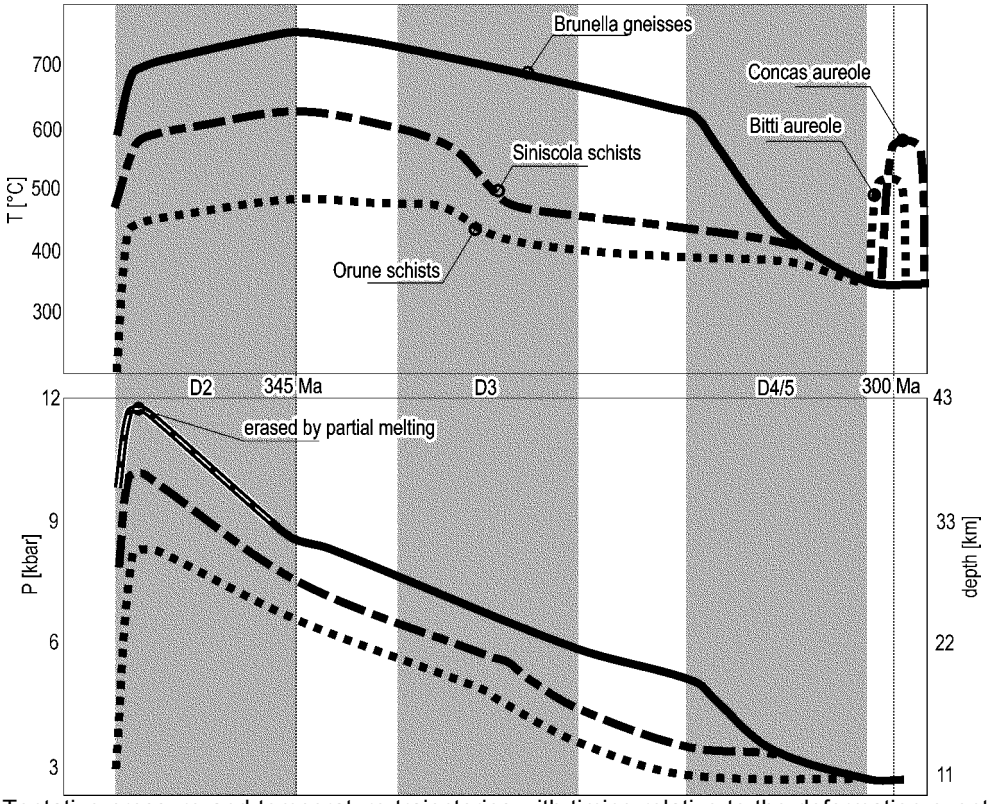

Fig. 5.13: Tentative pressure and temperature trajectories with timing relative to the deformation events and with respect to the dated migmatisation and granitoid intrusions.

From the results presented in this study the metamorphic evolution can be inferred (fig. 5.13). Accordingly, the thermally elevated Brunella gneisses ascended from deeper crustal levels, where the Punta de li Tulchi metabasite with its eclogitic relics became intercalated, to moderate crustal levels, where partial melting took place due to decompression and culminating heat supply. Post-migmatic cooling and continuing ascent are partly accommodated by tectonic denudation recorded in the overburden. Recumbent D3-folding in the Orune and Siniscola schists as well as Lodè orthogneiss is expression of the beginning vertical thinning. Subsequent normal D4-faulting led to the final ascent of the Brunella gneisses and their juxtaposition against the Siniscola schists in shallow crustal levels, sealed by the shallow emplacement of the late Variscan Concas granite. Consequently, the axial zone of the Sardinian Variscides, which is represented in the studied sequence by the Brunella gneisses, is inferred to be an extensional gneiss dome.

The great similarities concerning the deformational and metamorphic succession in the opposing wall rocks of the Posada fault as well as the reasonable explanation of differences across the Posada fault

presented in this study provide strong evidences against the interpretation of the Posada fault to be a reactivated suture zone as proposed by Cappelli et al. (1992).

According to this model of collisional suturing, the initially hot base of the overriding Brunella gneisses should become retrogressed, whereas the initially cold top of the overridden Siniscola schists heated up due to the contact effect, so that an inverted metamorphic gradient developed. However, an inverted metamorphic gradient in the Siniscola schists simultaneous to a retrogression zone in the Brunella gneisses is contradictory and incompatible to the metamorphic record documented in this study, and is therefore ruled out. Furthermore, it has been shown that the Posada fault rocks evolved from the adjacent Brunella gneisses and Siniscola schists by intense shearing and retrogression. Metabasites are common throughout the whole studied sequence and are therefore not particularly characteristic for the Posada fault. Eclogitic relics occur only 10 km north of the Posada fault in the Punta de li Tulchi metabasites. Consequently, characteristic lithologies comparable with ophiolites or high-pressure rocks are missing in the Posada fault. Taking these characteristics of the Posada fault rocks into account, the idea of Cappelli et al. (1992) that the Posada fault rocks derived from an oceanic melange must be refused.

5.9 Conclusion

The following conclusions can be drawn:

- The metamorphic succession from the external nappe to the internal axial zone of the Variscides in NE Sardinia results from a polymetamorphic evolution.
- In addition to the separate occurrences of Ordovician metaplutonics and metavolcanics, the restricted occurrence of the D1 fabric and the post-D1/pre-D2 porphyroblasts, as well as the presence of a compositional discontinuity, which coincides with the pre-Variscan cover-basement contact, outline a pre-Ordovician basement in the more internal part of the studied sequence.
- Decompression-induced growth of plagioclase porphyroblasts marks the Variscan peak metamorphism across the pre-Variscan cover-basement contact.
- The Variscan peak metamorphism in the axial zone is manifested by decompression-induced muscovite dehydration-melting in middle crustal levels.
- Partial melting and porphyroblastic plagioclase growth are syn- to post-kinematic with respect to the main deformation event D2 and pre-kinematic with respect to the subsequent D3-folding in the pre-Ordovician basement. In more external parts of the studied sequence above the pre-Variscan cover-basement contact, the growth of plagioclase porphyroblasts is shifted to a post-D2/syn-D3 timing.
- High-quartz stability conditions were reached during and/or soon after partial melting in the axial zone.

- The exhumation of the axial zone from middle to shallow crustal levels is accompanied by post-migmatic solid state deformation and retrograde alteration under sillimanite stability conditions, and accommodated by the recumbent D3-folding and normal D4-faulting in the overburden.
- Normal D4-faulting subsequently transformed into strike-slip D5-faulting juxtaposed the axial zone against the nappe zone in shallow crustal levels, sealed by the shallow emplacement of the late Variscan granitoids.
- During the retrograde D4/5 Posada faulting, an initial gradient from amphibolite facies conditions in the axial zone-derived wall rocks to greenschist facies conditions in the nappe zone-derived wall rocks was overcome.
- From the internal axial to the external nappe zone, Paleozoic NE Sardinia provides a radial section of a Variscan dome with a normal fault-bounded core of high-grade gneisses enveloped by a schistose mantle of decreasing metamorphism from medium- to low-grade.
- The NE Sardinian mantled gneiss dome emerged from crustal extension after crustal shortening during the Variscan orogeny.
- No evidences have been found that the Posada fault was superimposed on a Variscan suture zone as proposed by Cappelli et al. (1992). A possible origin of the eclogitic relics in the axial zone from an early Paleozoic suture zone needs to be investigated in future studies.

DESCRIPTION OF PHOTOS IN PLATE 5.1

a: Preserved sedimentary bedding, Orune schists (HH141). The younging direction (towards the right) is indicated by a sharp base and fining upwards from psammitic to pelitic deposition. The psammitic and pelitic domains have been converted to albite- and mica-rich domains. S2 has transposed the bedding and is crenulated by S3. Long side of photo 3 cm.

b: Detailed section of photo 'a' shows the contact between two beds, Orune schists (HH141). The albite overgrew the more quartzitic base of the bed and preserved S2 as inclusions. The mica domain (left side) represents the top of the bed below. It contained less quartz, and therefore it was probably a less suitable place for the albite blastesis, which consumes in addition to mica also quartz (chapter 5.3). Long side of photo 1 mm.

c: Relict feldspar and quartz phenocrysts of the volcanic protolith preserved in a porphyroid layer, Orune schists (HH2c). The feldspar phenocrysts have been commonly fragmented, and quartz fringes have grown in the D2 pressure shadows. The quartz phenocrysts have been prevailingly stretched out to bands aligned in S2. Long side of photo 3 cm.

d: Close-up of a recrystallised quartz aggregate surrounded by a fine grained matrix in a porphyroid layer, Orune schists (HH2b). The quartz aggregates probably derived from a quartz phenocryst. Dynamic recrystallisation with a annealing component caused the transformation into the recrystallised quartz aggregate. Long side of photo 3 mm.

e: Close-up of a feldspar phenocryst surrounded by a fine-grained matrix in a porphyroid layer, Orune schists (HH2b). The core was saussuritisised during compositional conversion to albite, and contains inclusions of epidote, clinozoisite and white mica, whereas the rim is fairly inclusion-free and tended to overgrow the matrix. Long side of photo 1 mm.

f: F3 hinge in Orune schists (HH2). The S2-transposed bedding and S2-parallel quartz veins have been folded and crenulated during D3-folding. Long side of photo 3 cm.

g: D3 microfolds deform S2-parallel bedding, Orune schists (HH249). Long side of photo 3 cm.

h: Poikilitic albite porphyroblast in mica-rich domain, Orune schists (HH138a). The inclusions that trace the overgrown S2 are not affected by the D3 microfolding, because the rigid porphyroblast, which acted as obstacle during folding, protected the internal S2 from deformation. Long side of photo 0,5 mm.

PLATE 5.1

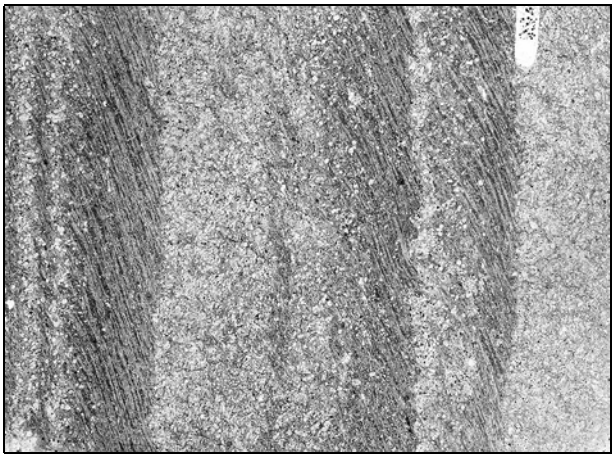

a

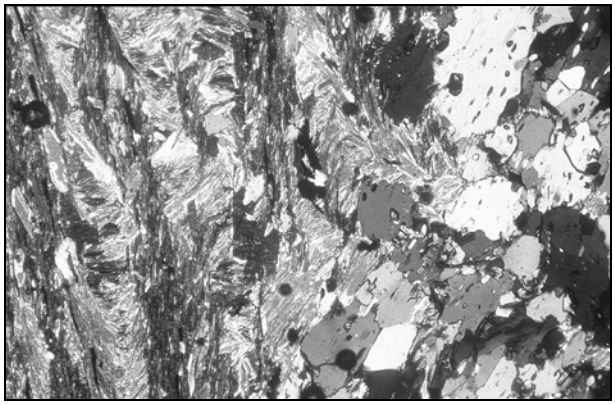

b

c

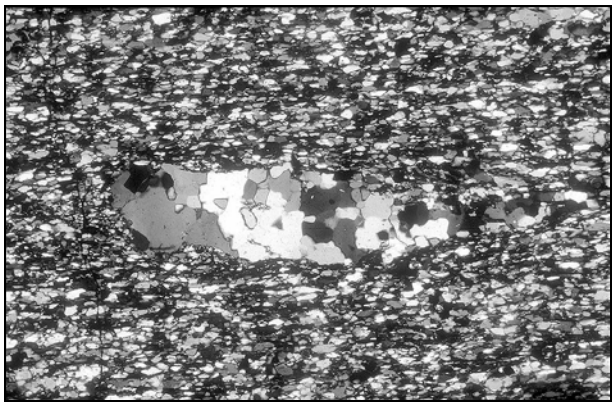

d

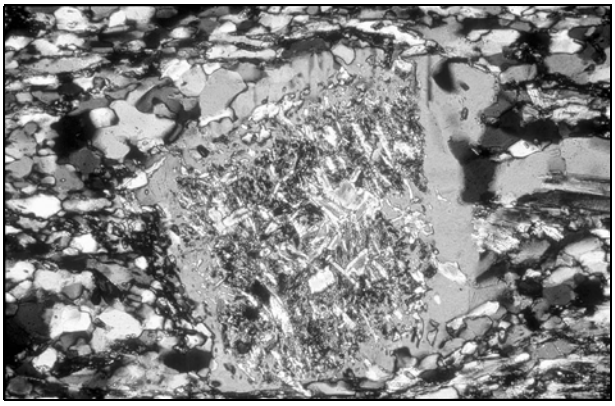

e

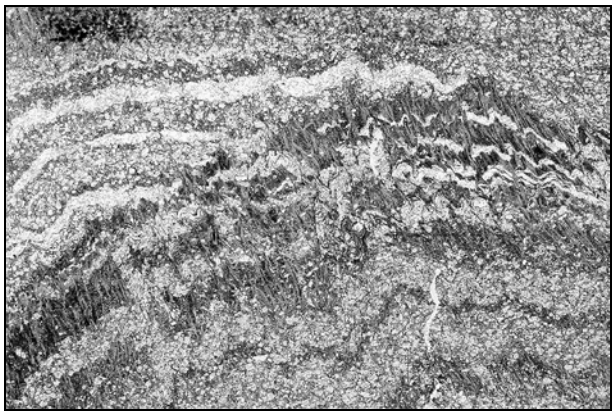

f

g

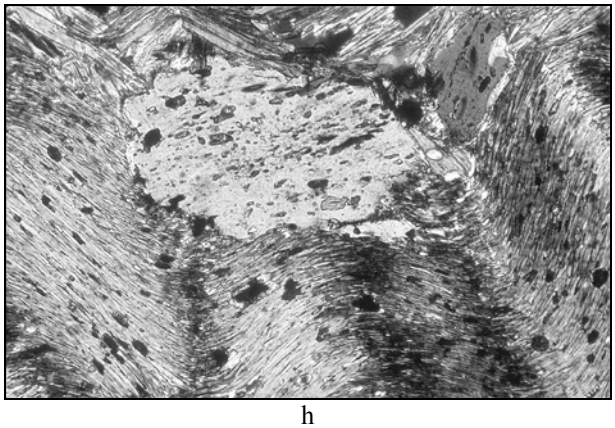

h

DESCRIPTION OF PHOTOS IN PLATE 5.2

a: Chlorite porphyroblasts in mica-rich domain, Orune schists (HH2). White mica is bent and kinked, but also newly arranged in the D3 crenulation by recrystallisation, so that it forms polygonal arcs. Long side of photo 1 mm.

b: Replacement of S2-parallel mica by albite porphyroblast, Orune schists (HH2). Long side of photo 0,5 mm.

c: Poikilitic albite porphyroblasts in D3 spaced cleavage, Orune schists (HH138b). The folded inclusion trails of S2 in the albite porphyroblasts indicate that the blastesis continued in places until early D3 stages. Long side of photo 1 mm.

d: D5 microfold in tremolite/actinolite schist, Orune schists (HH4). The folded composite S2/3 is defined by the alignment of fine-grained tremolite and/or actinolite. Long side of photo 0,5 mm.

e: Small euhedral garnet composite S2/3 in an epidote- and clinozoisite-rich porphyroid layer in the biotite zone of regional metamorphism, Orune schists (HH2b). The garnet occurrence does not necessarily be in conflict with the biotite zone, because a high component of grossular could have lowered the temperature for garnet-in reactions. Long side of photo 0,5 mm.

f: Chloritoid (long-prismatic crystals) and poikilitic garnet porphyroblasts overgrew the D1 fabric before they were folded together with S1-parallel white mica and chlorite in D2 microfolds, Siniscola schists (HH425). The inclusions in the garnet porphyroblasts trace the overgrown S1. The mineral assemblage of chloritoid, garnet and chlorite derived from a overprint of lower amphibolite facies in the external Siniscola schists. Retrogression after formation of the garnet led to its oxidation. Therefore, it is black in plane-polarised light. Long side of photo 7 mm.

g: A relict poikilitic garnet porpyroblast S2-aligned in a garnet quartzite, Siniscola schists (HH45b). The quartz in S2 has a strong lattice revered orientation (LPO), whereas the quartz inclusions in the garnet don’t show any LPO. They derived from the overgrown D1 fabric and have been protected from the D2 overprint by the garnet. Long side of photo 3 mm.

h: Poikilitic albite porphyroblasts in the microlithons of a D3 spaced cleavage, which is deflected around the porphyroblasts, Siniscola schists (HH402). The inclusion trails in the albite porphyroblasts derived from the overgrown S2 and are truncated at high-angle by S3. This overprinting relation constrains the albite porphyroblastesis as pre-D3 and post-D2. Long side of photo 7 mm.

PLATE 5.2

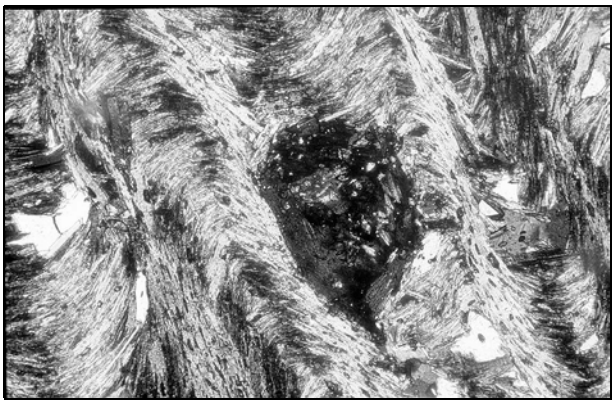

a

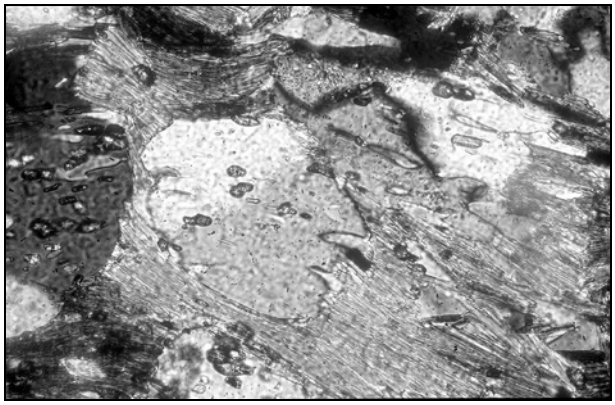

b

c

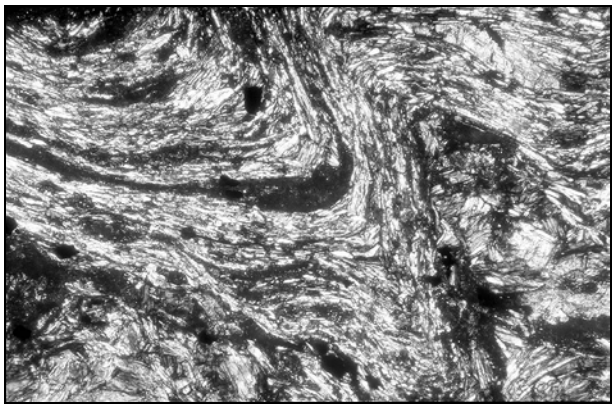

d

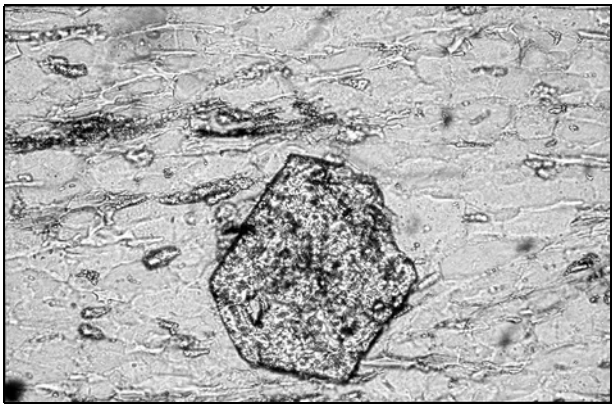

e

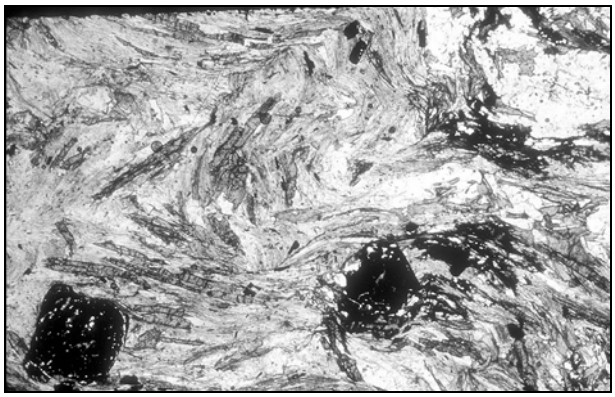

f

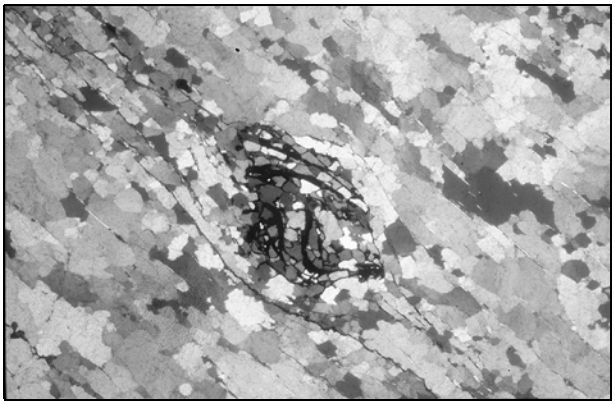

g

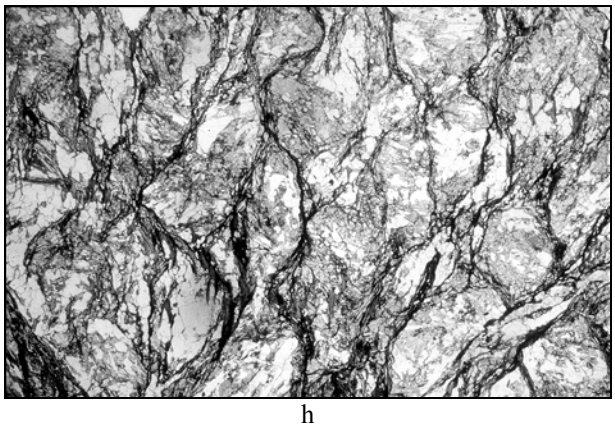

h

DESCRIPTION OF PHOTOS IN PLATE 5.3

a: D2 microfold and associated crenulation overprint the S1-transposed primary layering and garnet porphyroblasts, Siniscola schists (HH42d). Box in the upper middle indicates the detailed section shown in photo 'b' and the other smaller box at the half distance from this box in the middle to the left side of the photo marks a higher magnified section displayed in photo 'c'. Long side of photo 3 cm.

b: Detailed section of photo 'a' showing a garnet porphyroblast that caused deflection of the D2 cenulation cleavage, Siniscola schists (HH42d). Inclusion trails of the garnet porphyroblast remained from the overgrown S1. Therefore, the garnet blastesis can be constrained to be post-D1 and pre-D2. Long side of photo 3 mm.

c: Detailed section of photo 'a' showing a D2 crenulation cleavage in a mica-rich domain, which has been overgrown by an anhedral albite poikiloblast, Siniscola schists (HH42d). Thus, the albite blastesis is post-D2. Long side of photo 1 mm.

d: Albite porphyroblasts aligned in S2, Siniscola schists (HH162b). Inclusions trace overgrown earlier cleavage stages, which are truncated by the external S2. Oligoclase fringes (dark extinction) grew in the D2 pressure shadows. Therefore, the oligoclase appearance is syn-D2. Long side of photo 1 mm.

e: Detailed section of boundaries between quartz inclusions (1st order white) and poikilitic albite porphyroblast (1st order grey) showing oligoclase seams, which have a dark extinction in the photo and were altered in contrast to the clear albite, Siniscola schists (HH160b). Lobes of quartz head into the plagioclase. The lobed intergrowth might be caused by the prograde sodium-calcium substitution in plagioclase and related quartz release. Long side of photo 0,2 mm.

f: Detailed section of an albite porphyroblast that was marginally replaced by prograde myrmekite, Siniscola schists (HH184). The prograde myrmekite consists of oligoclase intergrown with vermicular rods of quartz. The oligoclase alterated subsequently, and therefore it contains cloudy zones of small mica inclusions. Long side of photo 0,5 mm.

g: Detailed section of a serrated phase boundary between quartz (dark) and plagioclase (bright) from a quartz inclusion in an albite porphyroblast of the oligoclase-in zone in Siniscola schists (HH190b). An increasing anorthite component due to rising temperatures liberated quartz from plagioclase in analogy to the formation of prograde myrmekite (Ashworth, 1986). The released quartz may could have nucleated more easily on an existing phase boundary to quartz and so, give rise eventually to the intergrowth of quartz and plagioclase. Long side of photo 0,2 mm.

h: Close-up of a quartz inclusion in a poikilitic albite porphyroblast from the oligoclase-in zone showing mushroom-shaped lobes of quartz progressing into the plagioclase, Siniscola schists (HH184). Long side of photo 0,2 mm.

PLATE 5.3

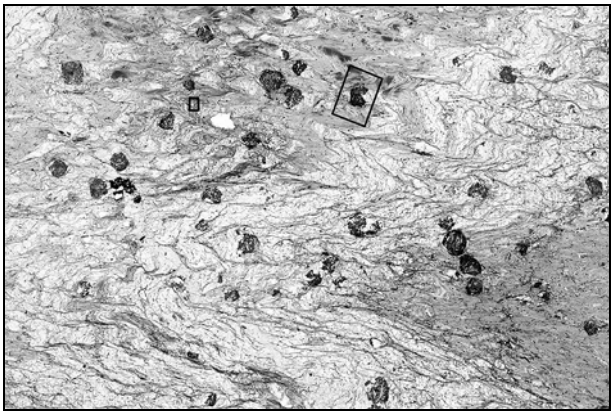

a

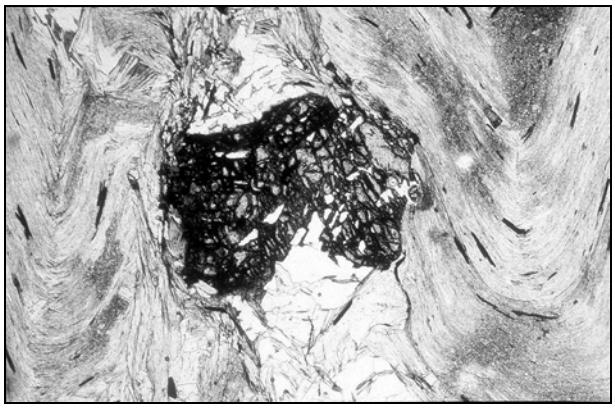

b

c

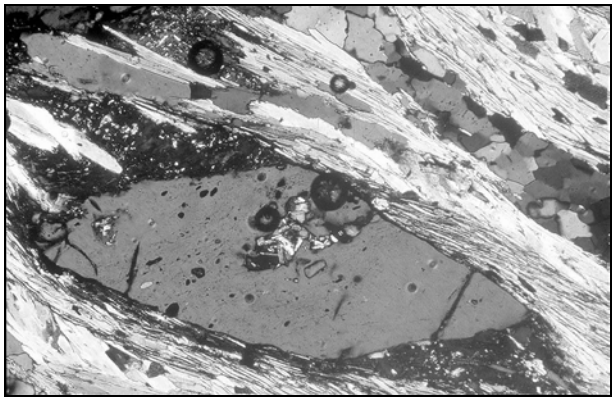

d

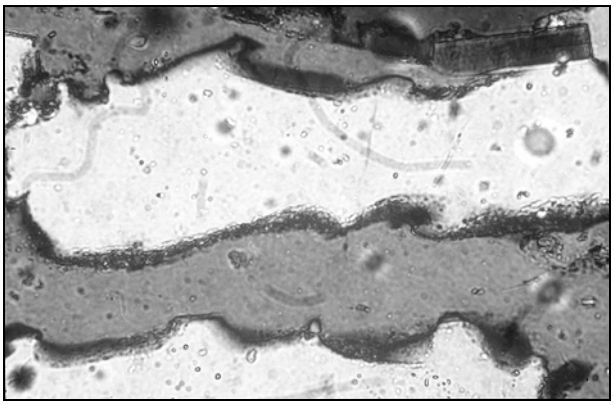

e

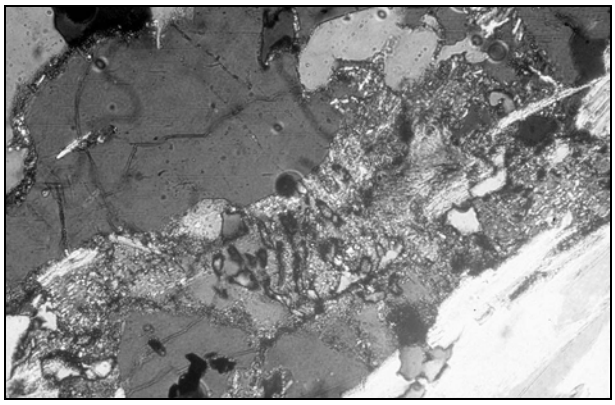

f

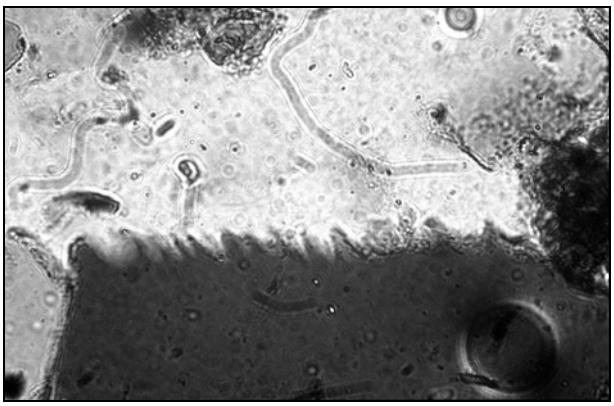

g

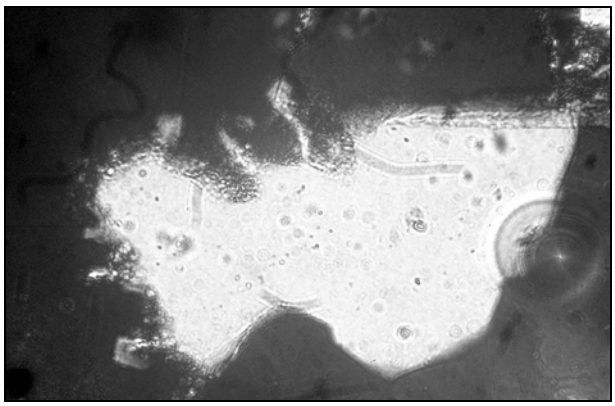

h

DESCRIPTION OF PHOTOS IN PLATE 5.4

a: This photo confirms that the sub- to euhedral fine-grained garnet grew after D2. Poikilitic albite porphyroblasts with oligoclase rim occur commonly in the microlithons of a D3 spaced cleavage, Siniscola schists (HH160b). S3 is deflected around the porphyroblasts. Inclusion traces, which derived from the overgrown S2, are truncated by the external S3. Small grained sub- to euhedral garnet occurs inside and outside of the albite porphyroblasts. It overgrew S2. S3 has been reactivated by S4, so that the garnet outside of the plagioclase porphyroblasts got partly retrogressed. Long side of photo 1,5 cm.

b: Detailed section of photo 'a' showing a poikilitic plagioclase porphyroblast with small grained sub- to euhedral garnet incorporated during progressive growth, Siniscola schists (HH160b). The inclusions trace the overgrown S2 and are truncated by the external S3. Long side of photo 3 mm.

c: Staurolite and garnet overgrew S2 that is marked by aligned white mica and chlorite, Siniscola schists (HH270a). Opaque inclusions in staurolite represent the continuation of the external S2. A slight deflection is caused by the later D4 overprint. The mineral assemblage staurolite, garnet and chlorite indicate conditions of lower amphibolite facies. Long side of photo 3 mm.

d: Normal D4 shear bands overprint the oligoclase + garnet assemblage and partly causes its retrogression, Siniscola schists (HH184). They are prevailingly developed in mica-rich domains, whereas its microlithons are beset by plagioclase porphyroblasts. Long side of photo 3 cm.

e: The K-feldspar phenocryst in is a remnant of the plutonic protolith, Lodè orthogneiss (HH19b). It is aligned in S2 and shows filled fractures. The fractures suggest a brittle deformation component at the south-eastern margin of the Lodè orthogneiss during D2. Long side of photo 7 mm.

f: Relict K-feldspar phenocrysts form rigid cores mantled by finely recrystallised feldspar, which is stretched out together with coarsely recrystallised quartz domains in trails and bands aligned parallel to S2, Lodè orthogneiss (HH7b). Long side of photo 3 cm.

g: The K-feldspar phenocrysts is surrounded by finely recrystallised feldspar and quartz in immediate vicinity, Lodè orthogneiss (HH7a). In more remote vicinity, quartz (bright grains in the top right corner and at the left side of the K-feldspar phenocryst) is generally coarser grained than plagioclase, because grain boundary migration recrystallisation allows coarsening of quartz, whereas prevailing subgrain rotation recrystallisation in plagioclase forbids major coarsening (chapter 5.5). This distinctive recrystallisation behaviour of quartz and feldspar is typical of the greenschist/amphibolite facies transition (Tullis & Yund 1985, Simpson & Wintsch 1989). Note the small myrmekite at the right margin of the K-feldspar auge. Long side of photo 3 mm.

h: Margin of a K-feldspar auge invaded by myrmekite, Lodè orthogneiss (HH19c3). This deformational induced replacement reaction (Simpson & Wintsch 1989) led to the differentiation in a core of K-feldspar and a mantle of plagioclase during D2. Long side of photo 1 mm.

PLATE 5.4

a

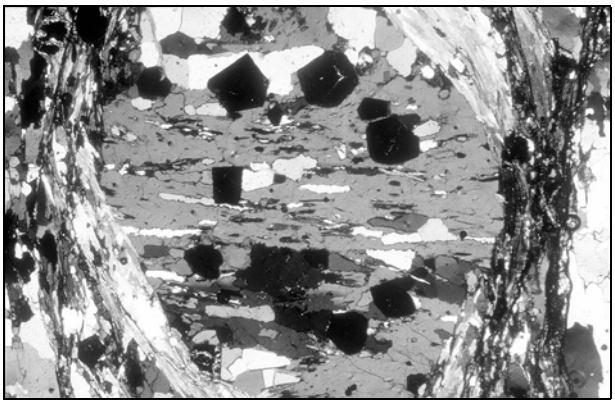

b

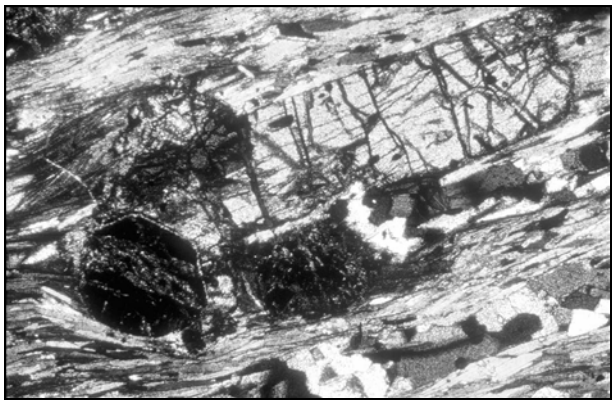

c

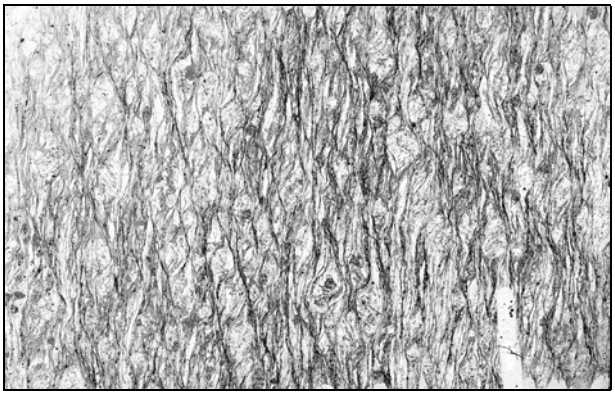

d

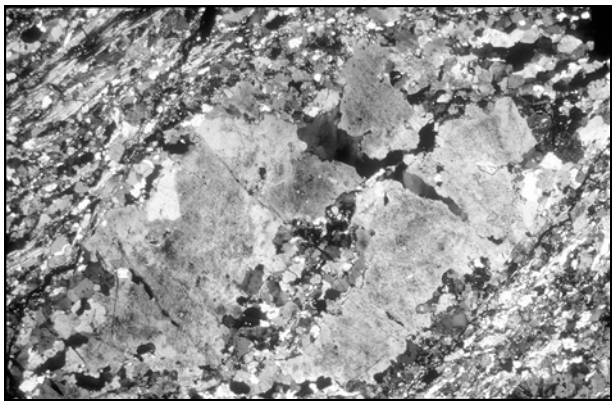

e

f

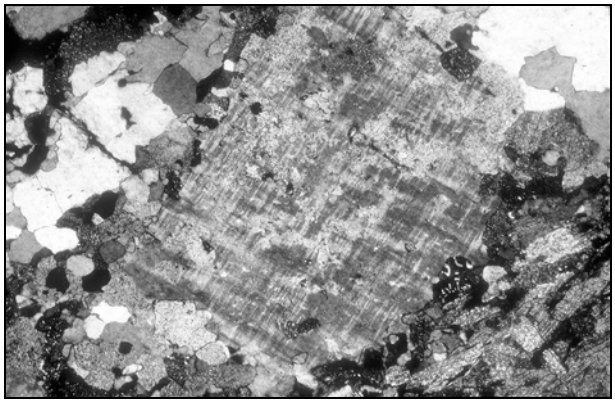

g

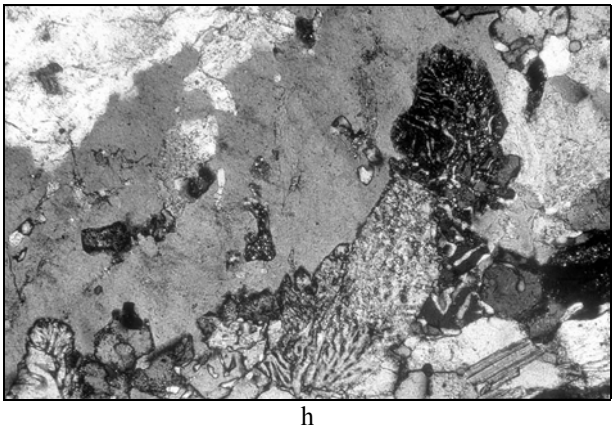

h

DESCRIPTION OF PHOTOS IN PLATE 5.5

a: S3 overprinted by D4 shear bands with sinistral asymmetry in the photo, Lodè orthogneiss (HH226). With the shear bands associated fabrics provide clear indicators of the shear sense operating during D4 (photo c) .The shear bands have generally accumulated more white mica than previous D2 or D3 fabrics in the Lodè orthogneiss. Long side of photo 7 mm.

b: Replacement of feldspar by white mica is a common reaction especially during D4 in the Lodè orthogneiss, and causes accumulation of white mica in shear bands (HH19). Long side of photo 0,2 mm.

c: Mica fish with a sinistral asymmetry in the photo, indicates top to the W sense of movement during D4, Lodè orthogneiss (HH7c). Long side of photo 1 mm.

d: D5 microfolds in Lodè orthogneiss (HH166). Long side of photo 3 cm.

e: Oligoclase porphyroblasts trace a recumbent D3-microfold, internal Siniscola schists (HH168). The internal foliation of the oligoclase porphyroblasts refers to S2. Therefore, the oligoclase blastesis can be constrained as pre-D3 and post-D2. Long side of photo 1 mm.

f: Detailed section of a poikilitic plagioclase porphyroblast showing lobate intergrowth of quartz (bright) and plagioclase (dark), internal Siniscola schists (HH290c1). The intergrowth progressed probably from quartz inclusions during prograde calcium enrichment of the plagioclase and related quartz release. Long side of photo 1 mm.

g: Close-up of a quartz-inclusion showing lobate intergrowth with the host plagioclase, Siniscola schists (HH290c1). The quartz inclusion consists of two grains (white and grey in photo). Compared with the lobate intergrowth of the external oligoclase-in zone (plate 5.3h), the lobes have coarsened northwards with the increased temperature. Long side of photo 0,5 mm.

h: Fine-grained sub- to euhedral garnet and anhedral grains of oligoclase (bright grains) overgrew S2, internal Siniscola schists (HH91). The anhedral oligoclase preserved inclusions, defining the overgrown S2. A further argument for post-D2 growth is, that S2 is not deflected around the minerals. Some slight bending or truncation refers to the D4 overprint. Long side of photo 1 mm.

PLATE 5.5

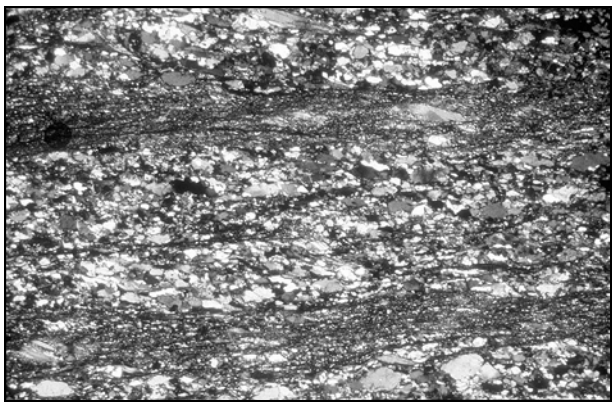

a

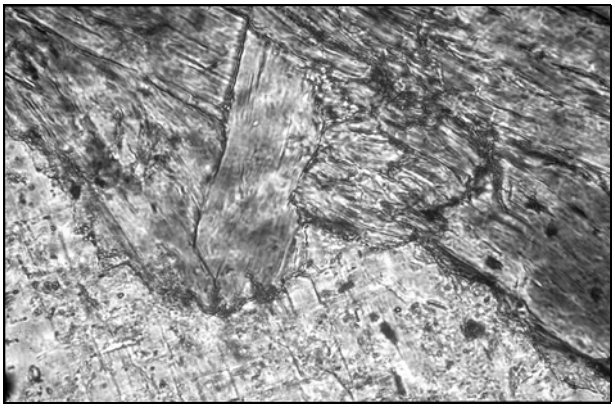

b

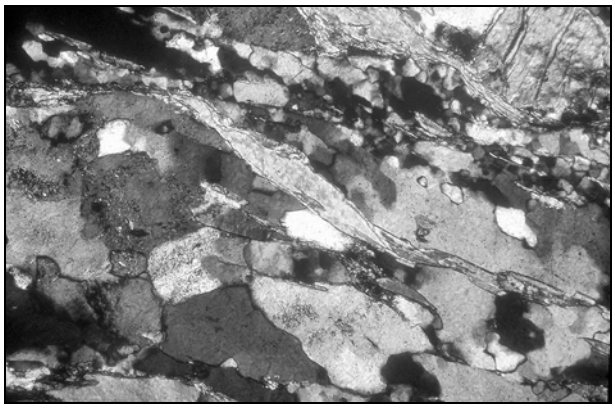

c

d

e

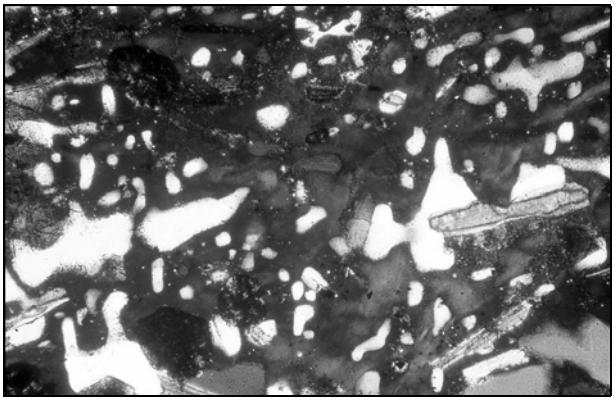

f

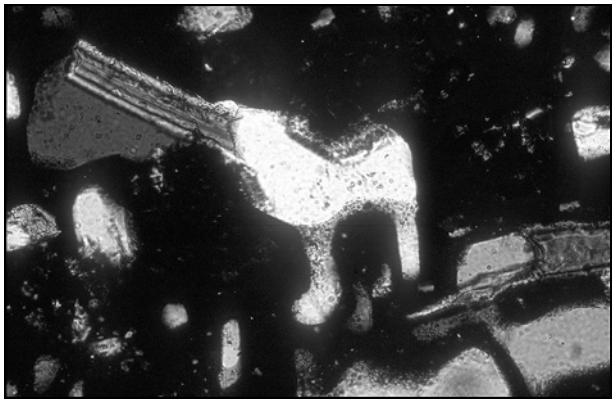

g

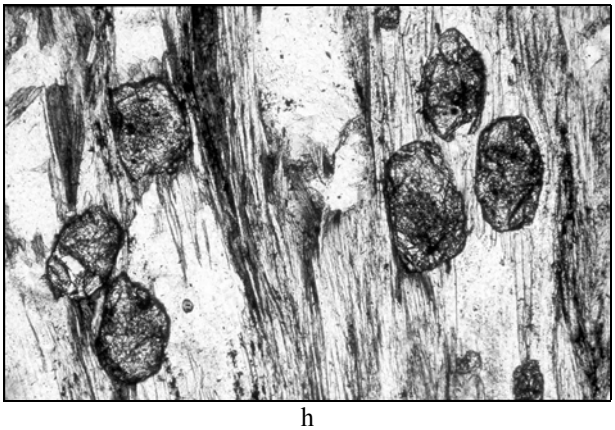

h

DESCRIPTION OF PHOTOS IN PLATE 5.6

a: Interpenetration twin in staurolite that overgrew S2, internal Siniscolaschists (HH91b). The external S2 is cut abruptly at a high-angle at the grain boundary of staurolite. Therefore, the staurolite is inferred to be post-D2. A slight deflection, that refers to D4, can be observed. Long side of photo 3 mm.

b: The staurolite porphyroblast has overgrown a fabric, which could be constrained in thin section as early D2 derived, internal Siniscola schists (HH15). It is preserved in the core. Following the inclusion trace of the internal fabric to the grain boundary of the staurolite fails, apparently due to a truncation at a core-rim interface. On the other hand the staurolite rim contains inclusion trails that continue into the external D2 fabric. Long side of photo 3 mm.

c: Staurolite porphyroblast with an internal foliation that dips to the left and refers to an early S2 stage, Siniscola schists (HH167). It is oblique to the external foliation S2 shown in the upper left corner of the photo. The internal foliation terminates abruptly at a truncation line between core and rim of the porphyroblast. Inclusion traces in the rim appear as a continuation of the external S2. Thus, the staurolite can be considered as syn-D2. Long side of photo 3 mm.

d: Zoned garnet porphyroblast in a D4 microlithon showing an internal foliation, which is truncated at the core-rim interface, internal Siniscola schists (HH214). The rim-garnet grew during D2. The core-garnet refers to an older post-D1/pre-D2 stage. Long side of photo 7 mm.

e: Parallel growth of staurolite (upper lath) and kyanite (lower lath) over S2, internal Siniscola schists (HH214). S2 is preserved as inclusions in the staurolite porphyroblast. During D4, the staurolite responded by brittle failure and marginal chloritisation, whereas the kyanite deformed by flexure-slip along (101) cleavage plane and marginal sericitisation. Long side of photo 1 mm.

f: D4 microlithon with porphyroblasts of kyanite in the upper part and of staurolite in the lower part of the photo, internal Siniscola schists (HH92). Previous biotite is strongly chloritisised in the dextral D4 shear bands. Deformation and retrogression is concentrated in the shear bands, but affected also the microlithons. Long side of photo 3 mm.

g: Close-up of a dextral D4 shear band in mica-rich domain, internal Siniscola schists (HH285b2). Focused deformation in the shear band caused comminution of mica. Long side of photo 7 mm.

h: Andalusite porphyroblast (middle of the photo) overgrew the previous D4 fabric during contact metamorphism in the contact aureole of the Concas granite, internal Siniscola schists (HH317b1). Long side of photo 3 mm.

PLATE 5.6

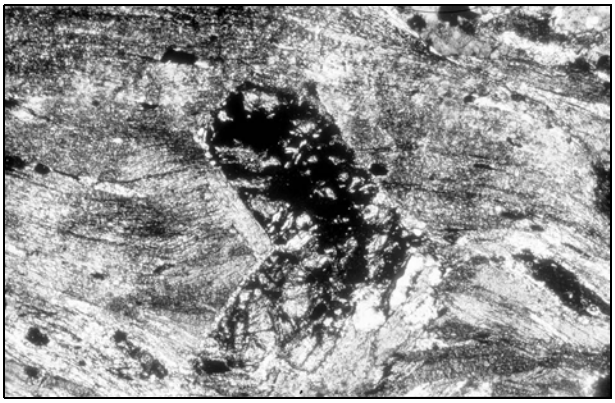

a

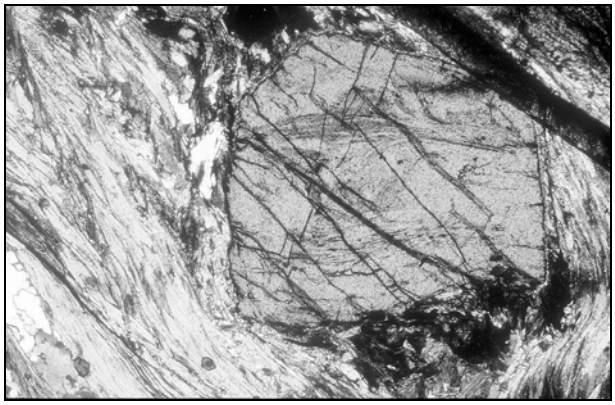

b

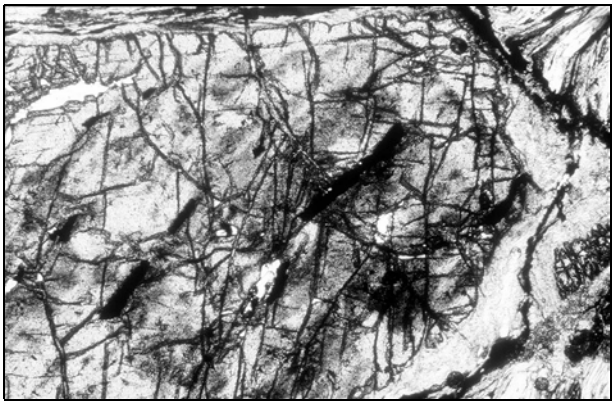

c

d

e

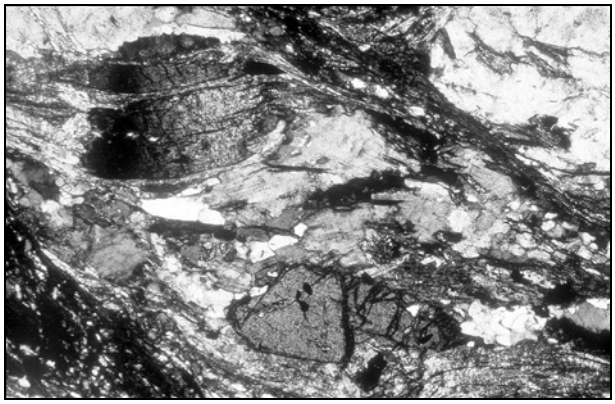

f

g

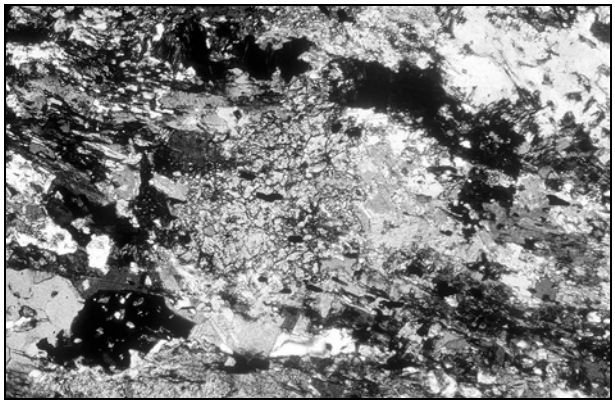

h

DESCRIPTION OF PHOTOS IN PLATE 5.7

a: Cordierite porphyroblast with laminar twinning grew during contact metamorphism in the contact aureole of the Concas granite, internal Siniscola schists (HH317b1). The Cordierite can be distinguished from plagioclase, because it is in places retrogressed marginally to chlorite, whereas plagioclase became sausuritisised and sericitisised. Long side of photo 3 mm.

b: Hornblende-rich and leucosome derived quartzo feldspathic domains are transposed by S4 in Torpè metabasite (HH67g). Feldspar occurs either as large clasts mantled by finely recrystallised grains or as finely recrystallised grains together with fine-grained dynamically recrystallised quartz in the matrix surrounding the hornblende lozenges. Long side of photo 1 cm.

c: Close-up of hornblende lozenges shown in photo 'b' in Torpè metabasite (HH67g). The hornblende lozenges are aligned in S4 and behaved as rigid porphyroclasts deformed to a certain extent by grain boundary sliding along their cleavage planes. They are surrounded by finely recrystallised grains of quartz and feldspar, which accumulated most of the deformation during D4. Long side of photo 1 mm.

d: Relict magmatic K-feldspar phenocrysts mantled by finely recrystallised K-feldspar grains, which are stretched out in trails together with quartz domains parallel to S4 in orthogneiss from the Posada fault (HH28). Long side of photo 7 mm.

e: Section of a mylonite showing a fine grained, well foliated D4 fabric, Posada fault (HH27). Three major compositional domains are recognisable: firstly, the quartz domains (white in photo), which are stretched out in bands and ribbons, secondly, feldspar-rich domains consisting of variably but generally coarser grained clasts, and thirdly, mica-rich domains (darker grey from biotite in photo) intercalated between quartz bands and feldspar clasts. These domains deformed by different deformation mechanisms during D4, as shown in the following photos. Long side of photo 3 cm.

f: Detailed section of a feldspar-rich domain in a mylonite showing numerous fine-grained feldspar clasts arranged in the mylonitic foliation S4, Posada fault (HH67d). Long side of photo 1 cm.

g: Section from a sheared pegmatite showing feldspar lozenges, which probably derived from a single phenocryst, Posada fault (HH71a). The phenocryst became divided by conjugating fracture sets during D4. The fractures are filled by recrystallised quartz and mica. Also, crystal-plastic deformation is suggested by the varying lattice orientation (dark and bright extinction colours in photo). Long side of photo 7 mm.

h: Array of feldspar lozenges within the mylonitic foliation, Posada fault (HH229). They may have developed from a single porphyroclast by comminution and extension. Long side of photo 3 mm.

PLATE 5.7

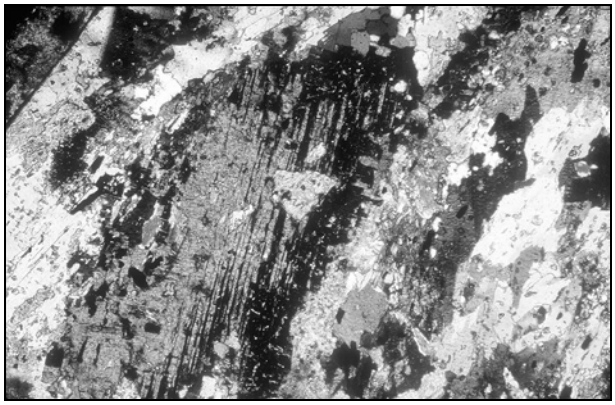

a

b

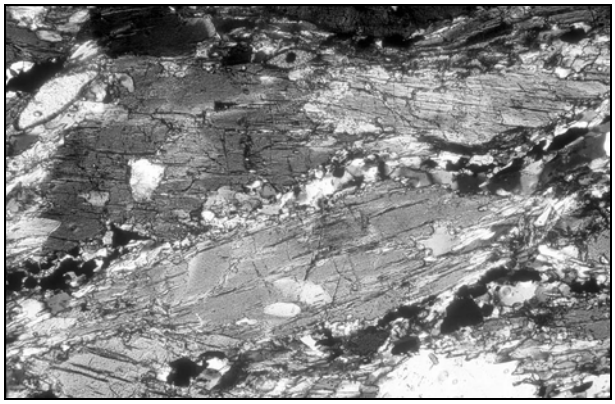

c

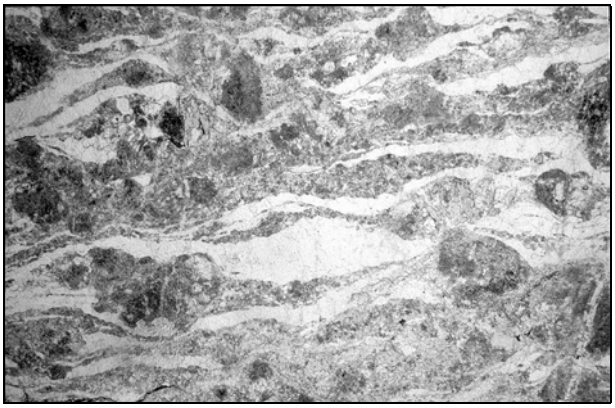

d

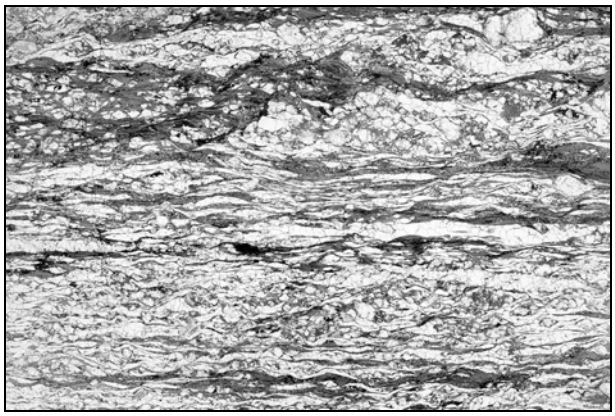

e

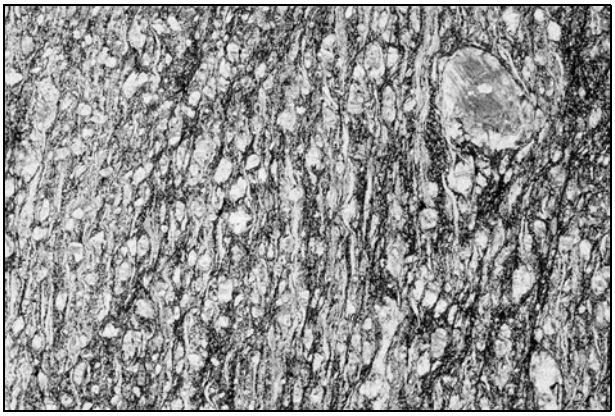

f

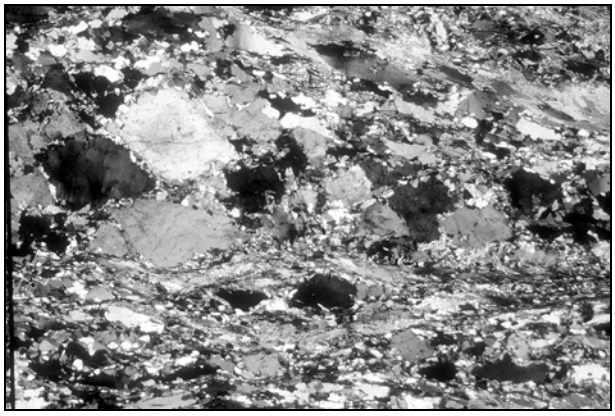

g

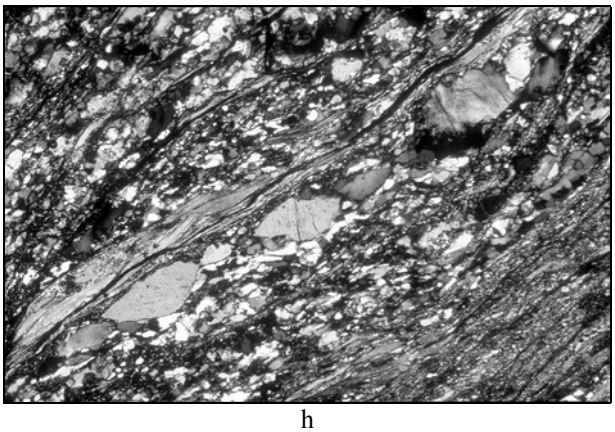

h

DESCRIPTION OF PHOTOS IN PLATE 5.8

a: Section of a feldspar-rich mylonite showing feldspar lozenges surrounded by a network of shear zones that contain prevailingly fine grained mica and quartz, Posada fault (HH30). The network pattern derived from a repeated reactivation of the main foliation and accompanying generations of normal slip crenulation. Long side of photo 7 mm.

b: Close-up of feldspar clast in a mylonite, Posada fault (HH288b2). The feldspar clast is mantled by mica, which formed especially in the D4 pressure shadow partly by retrograde replacement of the feldspar and partly by mass-transferring processes in a hydrous fluid, such as solution, diffusion from the high-strain zone away and precipitation in the pressure shadow. Long side of photo 0,5 mm.

c: Close-up of a zoned feldspar clast in a mylonite, Posada fault (HH288b2). The albite rim is thicker in the pressure shadow suggesting mass transfer in hydrous fluid from the high-strain sector away by solution, diffusion and precipitation. It could have been an originally or by retrogression zoned plagioclase. Long side of photo 0,5 mm.

d: Sheared mica porphyroclast in a mylonite, Posada fault (HH290b1). The mica porphyroblast deformed by grain boundary sliding along the cleavage planes. That is the main deformation mechanism that mica commonly shows in the D4 fabric. It gives rise to the abundant mica fishes, which indicate the D4 shear sense (plates 5.5c, 5.5e). Long side of photo 1 mm.

e: Mica fish in a phyllonite, Posada fault (HH67c). The white mica porphyroclast survived comminution and its asymmetric fish shape indicates a dextral displacement during D4. The surrounding fine grained matrix consists of white mica, chlorite and quartz. The phyllonite appears as final result of deformation-accompanying retrogression and comminution in feldspar- and mica-rich mylonites. Long side of photo 1 mm.

f: Section of a quartzitic mylonite showing a folded ribbon consisting of a single quartz crystal in a fine grained dynamically recrystallised matrix, Posada fault (HH67a). Long side of photo 1 mm.

g: Section of a quartzitic mylonite showing an array of boudinaged feldspar lozenges in a fine grained dynamically recrystallised quartz matrix, Posada fault (HH67b1). The feldspar appears cloudy and has white spots in the photo due to small white mica grains, which formed at the expense of feldspar during deformation-accompanying retrogression. The contact between the rigid feldspar and the ductile quartz is sharp and does not show any mantle, due to the high rheological contrast under the prevailing D4 conditions of greenschist facies. Long side of photo 0,5 mm.

h: Feldspar porphyroclast in a cataclasite showing brittle deformation during D4 accommodated by flexure slip along cleavage planes and fractures, Posada fault (HH243). Long side of photo 7 mm.

PLATE 5.8

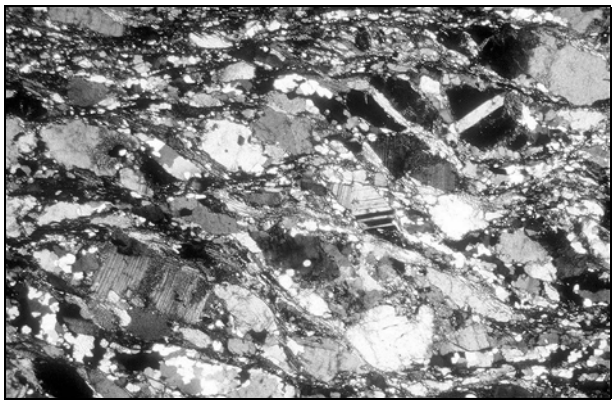

a

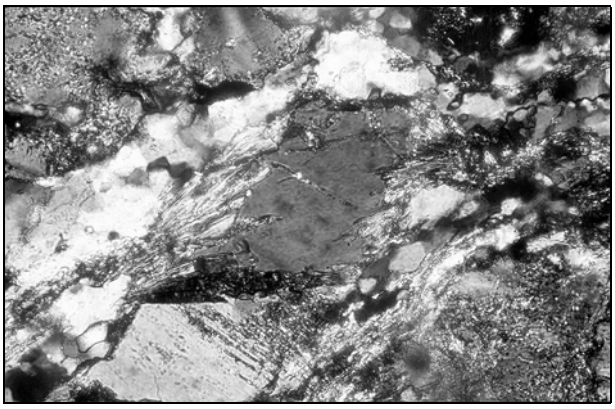

b

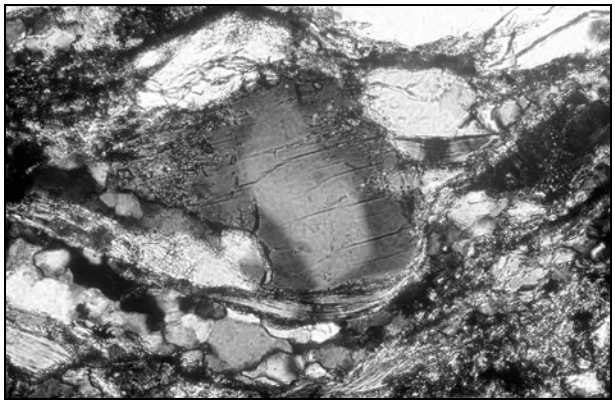

c

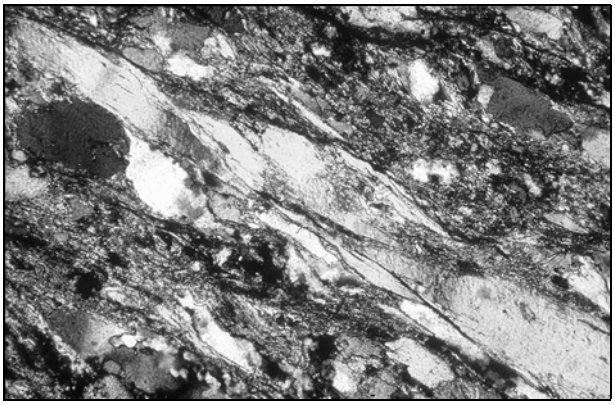

d

e

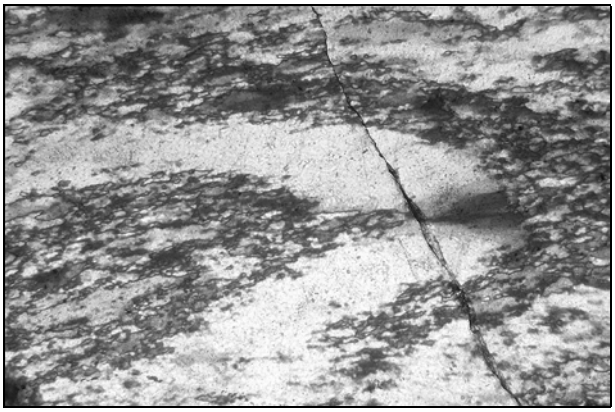

f

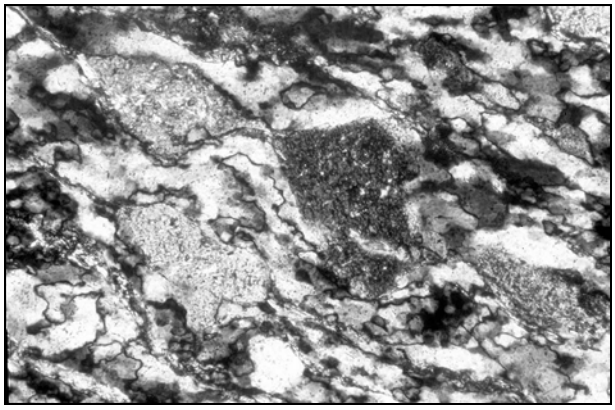

g

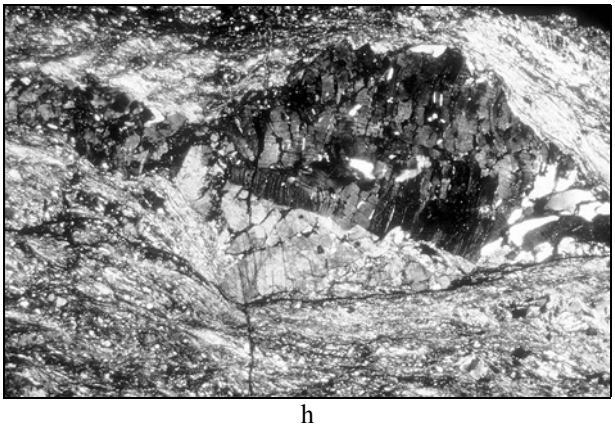

h

DESCRIPTION OF PHOTOS IN PLATE 5.9

a: Rock fragments in cataclasite derived from a quartzitic mylonite, Posada fault (HH243). After ductile deformation it experienced brittle deformation during the course of D4. Long side of photo 3 mm.

b: D5 microfold deforming the mylonitic foliation, Posada fault (HH67a). Long side of photo 1 mm.

c: Biotite selvages indicate the leucosome derived origin of the quartzofeldspathic layers in banded Brunella gneisses (HH40f1). In addition, they represent evidence of muscovite dehydration-melting, which left the biotite in the residue, but no garnet or cordierite. The magmatic fabric generated by anatexis in the leucosome was overprinted by S2, which has transposed the original stromatic migmatite. Long side of photo 3,5 cm.

d: A vein of leucosome slightly discordant with respect to S1 intruded in a Brunella gneiss (HH108B). The whole fabric was folded subsequently during D2. Long side of photo 4,5 cm.

e: Aggregate of fibrous sillimanite in S2 from Brunella zone (HH103). Sillimanite grew probably post-migmatic aligned in S2. Long side of photo 7 mm.

f: Fibrous sillimanite aligned in a microfold from Brunella zone (108A). Long side of photo 1 mm.

g: Chess board pattern in quartz remained in many Brunella gneisses (HH40c). It is made of subgrains with prismatic {hki0} and basal (0001) boundaries showing respectively traces parallel and normal to the c-axis. Chess board patterns in quartz is common in rocks that have experienced conditions of the high-quartz stability field and thus indicate high-grade conditions (Kruhl 1996). Long side of photo 1 mm.

h: Close-up of a coronitic garnet aggregate from P. de li Tulchi metabasite (HH115a). The inner zone of the corona consists of symplectic intergrown plagioclase and hornblende and the outer zone mainly of hornblende. The surrounding matrix is mainly made up of symplectitic intergrown clinopyroxene, hornblende and albite. Miller at al. (1976) found a clinopyroxen inclusion in garnet, which had a jadeite component of approx. 40 %. Corona and symplectite represent disequilibration fabrics of the retrogressed eclogite. Long side of photo 2 mm.

PLATE 5.9

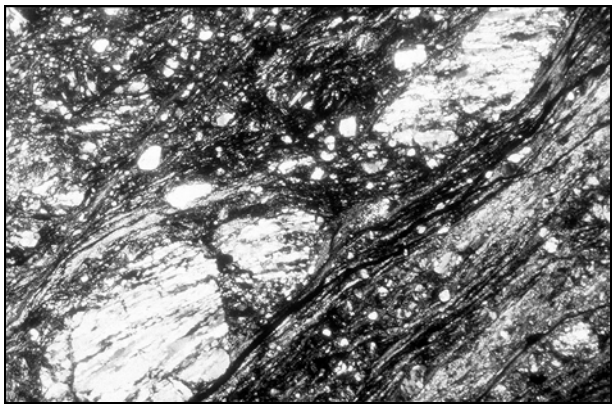

a

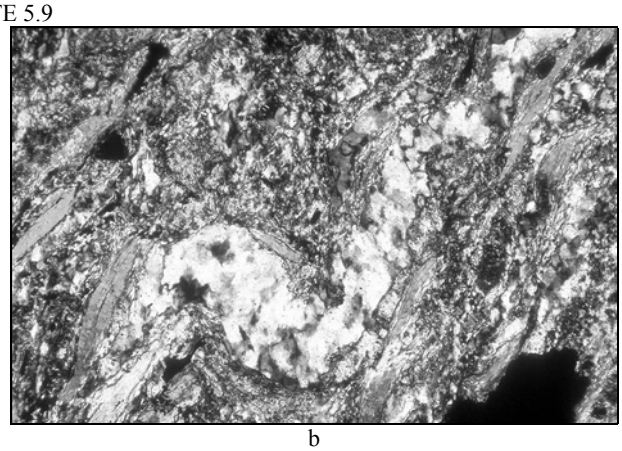

b

c

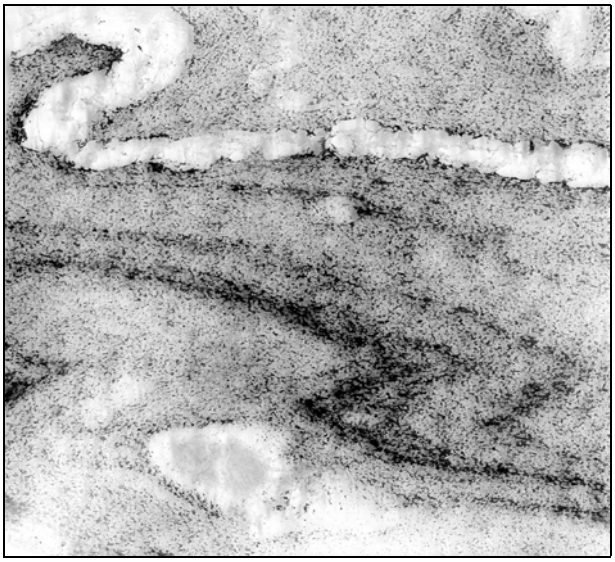

d

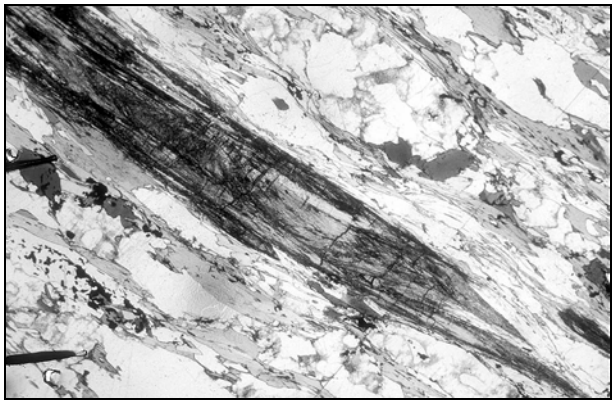

e

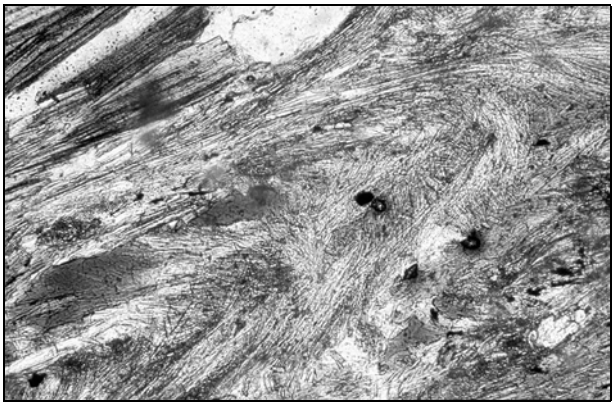

f

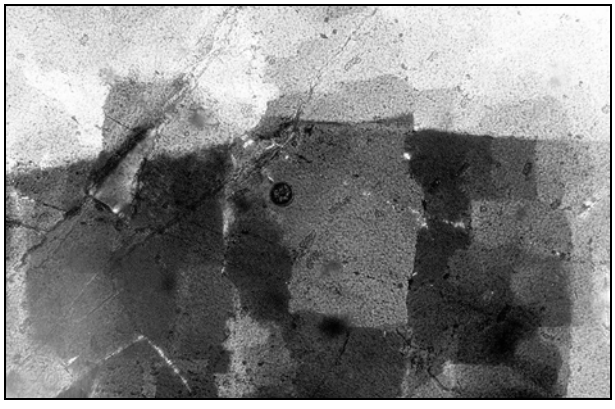

g

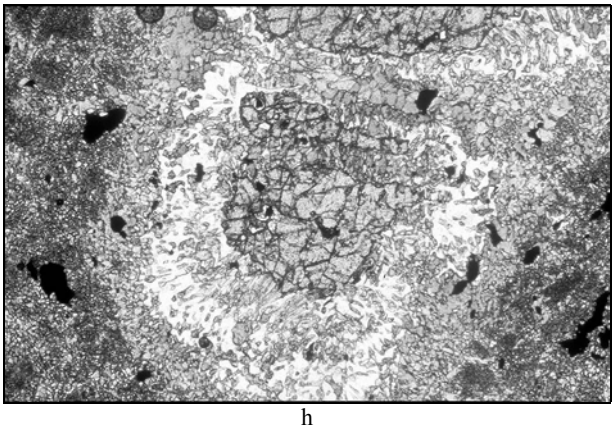

h

DESCRIPTION OF PHOTOS IN PLATE 5.10

a: Section with S2-parallel layering (horizontal in photo) crenulated by S3 (dips to the right in photo) in P. de li Tulchi metabasite (HH115c). The dark domains are richer in hornblende and the bright domains contain more plagioclase. The bright nodules mark probably the sites of garnet porphyroblasts prior the M2/3 retrogression. Long side of photo 3 cm.

b: Retrograde replacement of K-feldspar by myrmekite in a Brunella gneiss (HH117). Myrmekitic replacement is commonly associated with post-migmatic deformation in the Brunella gneisses. It indicates temperatures (approx. 500°C to 650°C) below the melting temperature of wet granite, but still in the stability field of plagioclase with a composition at the anorthite side of the peristerite gap. Long side of photo 0,5 mm.

c: Small sub- to euhedral garnet in the P. Orvili metabasite (HH99). Long side of photo 1 mm.

d: Lobate intergrowth of quartz (lower grain) and plagioclase (upper grain) in a Brunella gneiss (HH118A). Long side of photo 1 mm.

e: Symplectic intergrowth of quartz and muscovite in a Brunella gneiss (HH114A). It formed by retrograde replacement of K-feldspar (cloudy, grey grains at the upper side and in the right corner of photo). The vermicular rods of quartz are aligned in the basal (001) plane of the muscovite grain. They initiated apparently at a quartz grain boundary (white grain at the left side of the photo) and progressed from there. Long side of photo 0,5 mm.

f: Retrograde replacement of K-feldspar by muscovite in a Brunella gneiss (HH125a). Retrogression progressed from the spaced cleavage into the microlithon suggesting fluid supply via the foliation. The retrograde muscovite grew together with the sillimanite. Long side of photo 1 mm.

g: Biotite growing at the expense of feldspar in a Brunella gneiss (HH108A). Biotite grew prevailingly parallel to its cleavage planes. The replacement is most advanced along the grain boundaries of feldspar. Long side of photo 1 mm.

h: D4 micoshear zone with finely recrystallised grains of plagioclase and oblique biotite in Brunella gneiss (HH35). Quartz recrystallised distinctly coarser grained than plagioclase. Subgrain rotation recrystallisation prevailingly operating in feldspar forms small grains and dominating grain boundary migration recrystallisation in quartz led to grain-coarsening. This distinct recrystallisation behaviour of quartz and feldspar is characteristic for the transition between greenschist and amphibolite facies (Tullis & Yund 1985). Long side of photo 3 mm.

PLATE 5.10

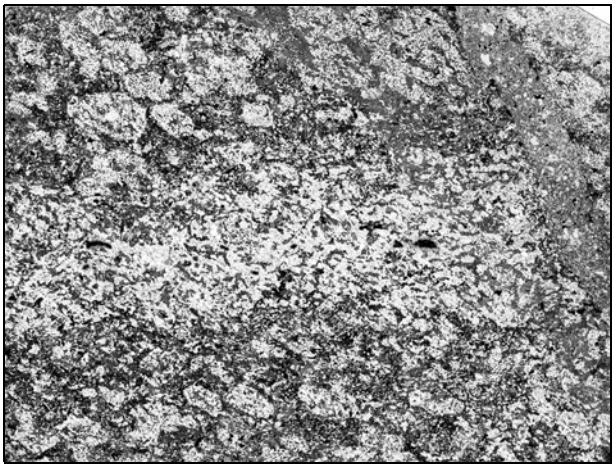

a

b

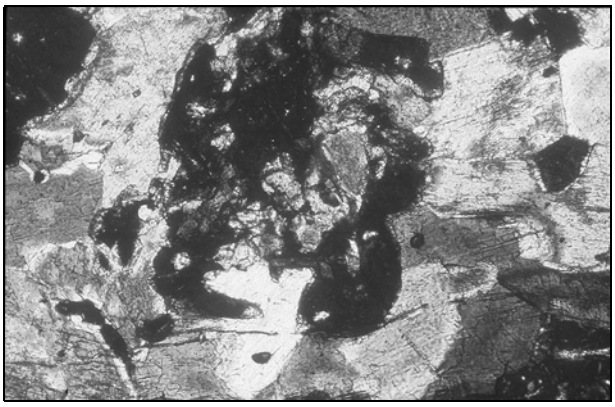

c

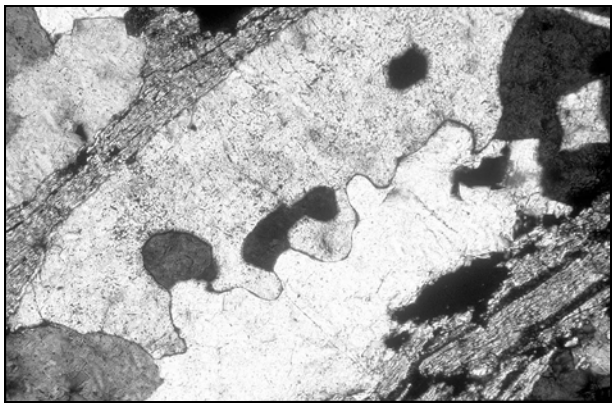

d

e

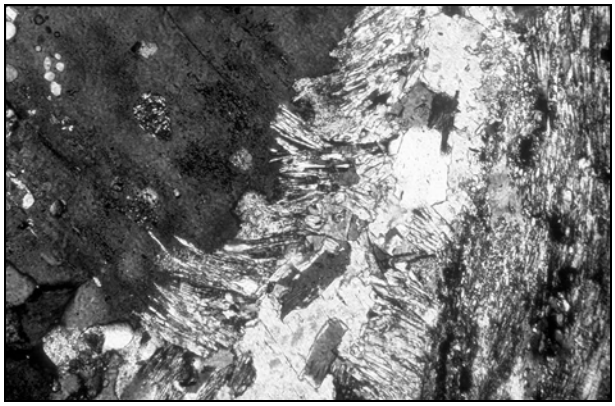

f

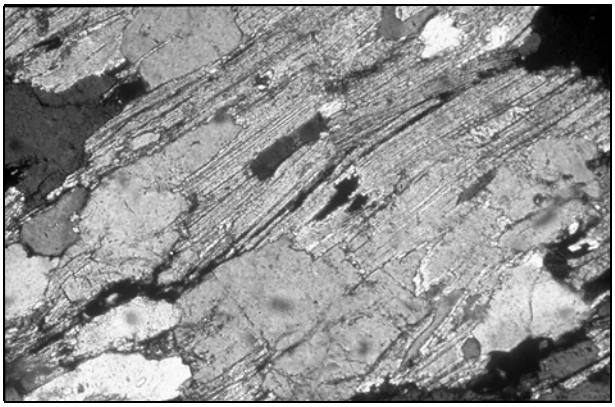

g

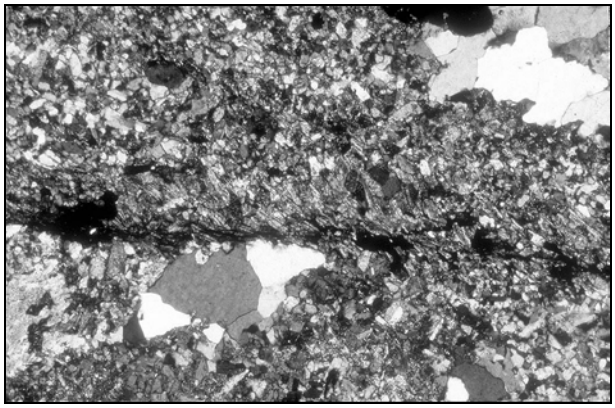

h

PLATE 5.11

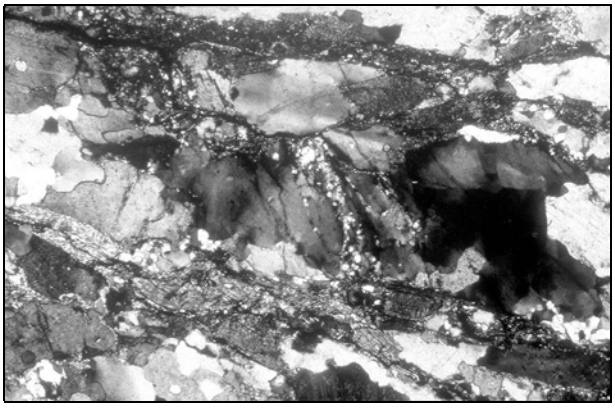

a: Late shear bands in a Brunella gneiss (HH121c). They mainly penetrate the rock along mica-rich domains and deformed the coarse quartz grain in the middle of photo. The quartz recrystallised finely while mica and feldspar show a brittle response to deformation along the during D5 operating shear bands. Long side of photo 3 mm.

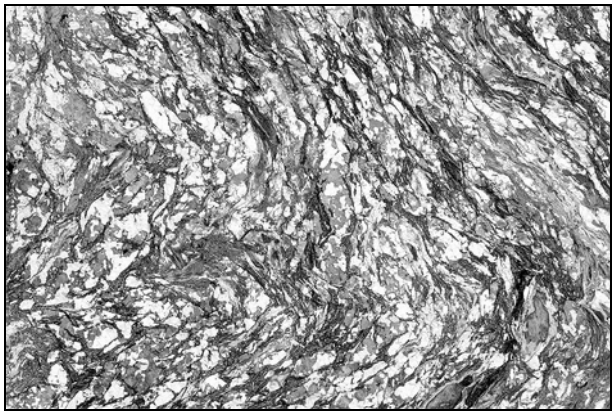

b: D5 microfold deforming S4 in a Brunella gneiss (HH68c). Long side of photo 3 cm.

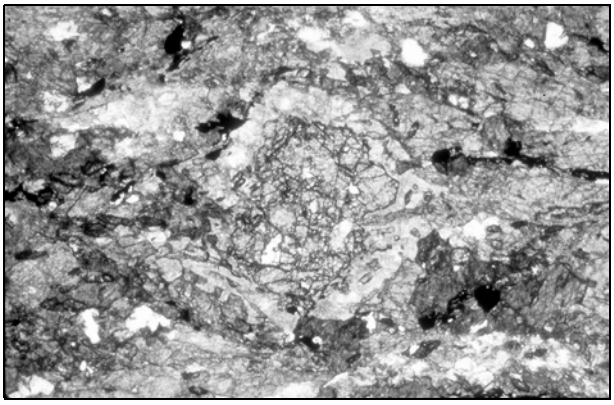

c: Corona-like plagioclase replacement of garnet in Torpè metabasite (HH97A2). Long side of photo 3 mm.

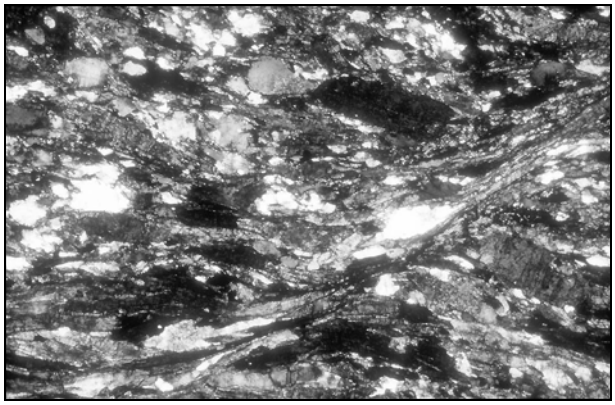

d: D4 shear band have reactivated the hornblende cleavage planes in Torpè metabasite (HH25A). Long side of photo 3 mm.

6 Geochronology

6.1 Previous work and open questions

The radiometric ages from the Paleozoic basement of Sardinia outline two events: an Ordovician to Silurian magmatism and the Variscan orogeny, which spans from Carboniferous to Permian times (fig. 6.1). The former event is manifested by numerous orthogneiss and porphyroid occurrences and has been dated radiometrically by orthogneiss Rb-Sr whole rock isochrons. However, it has been demonstrated that magmatic ages based on whole rock isochrons require backup measurements on minerals with high blocking temperatures, such as for instance on zircon, because an isotopically homogeneous magmatic body without post-magmatic resetting is a necessary but unfounded assumption in many cases (Hofmann 1993). So does the orthogneiss from Capo Spartivento (fig. 1.2) yield an Early Devonian age of 413 ± 33 Ma by whole rock Rb-Sr (Cocozza et al. 1977, Schabert 1978), but an Early Ordovician age of 478 ± 16 Ma by zircon U-Pb dating (Delaperrière & Lancelot 1989), and porphyroids from the Sarcidano and Gerrei (fig. 1.2) Late Devonian to Permian ages by whole rock K-Ar dating (Calderoni et al. 1984), but a pre-Caradocian age by stratigraphic correlation (Carmignani et al. 1982b).

In order to receive the required backup, the orthogneisses from Lodè and Tanaunella (fig. 6.2), which are already dated by Rb-Sr whole rock isochrons, yielding 441 ± 33 Ma (Ferrara et al. 1978) and 458 ± 31 Ma (Di Simplicio et al. 1974), have been chosen for in situ U-Pb measurements on zircon.

The orthogneisses are common in the internal part of the Sardinian Variscides and considered as plutonic equivalents to the calc-alkaline suite-derived porphyroids (Memmi et al. 1983), which are particularly common in the external parts of the nappe zone (fig. 1.2) and ascribed to a magmatic arc at the Gondwana margin (fig. 1.4b, Carmignani et al. 1992a). Towards the internal parts, the stratigraphy and the porphyroid occurrence become increasingly uncertain.

In order to resolve the stratigraphy also in the internal parts of the Sardinian Variscides, the discovered porphyroid near Lula (fig. 6.2), which is intercalated in the Orune schists, so far of unknown age, has been chosen for zircon U-Pb measurements. Moreover, the acquired radiometric age would be the first for the volcanic protoliths of the Sardinian porphyroids.

Cocozza et al. (1977) considered the Capo Spartivento orthogneiss, despite its Ordovician Rb-Sr whole rock isochron, as Precambrian basement overlain unconformably by a Cambrian cover. As mentioned above, the Ordovician age of the Capo Spartivento orthogneiss was confirmed and the precision of its age increased by zircon U-Pb backup measurements (Delaperrière & Lancelot 1989), but the classical basement problem, whether the Ordovician orthogneisses intruded in a sedimentary sequence or in an older basement, still remained unsolved.

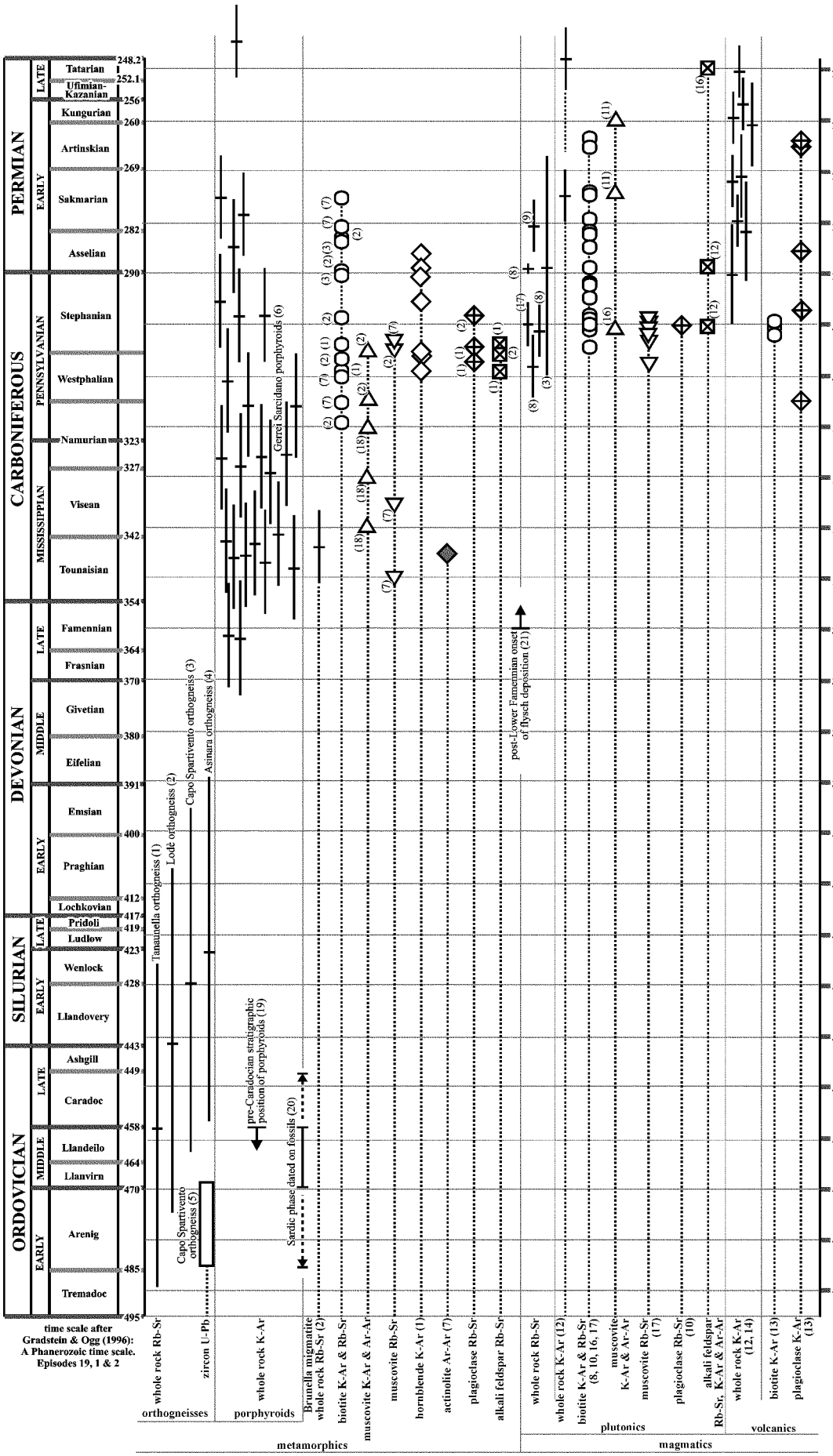

(1) Di Simplicio et al. (1974), **(2)** Ferrara et al. (1978), **(3)** Schabert et al. (1978), **(4)** Cappelli et al. (1992), **(5)** Delaperrière & Lancelot (1989), **(6)** Calderoni et al. (1984), **(7)** Del Moro et al. (1991), **(8)** Del Moro et al. (1975), **(9)** Cocherie (1984), **(10)** Nicoletti et al. (1982), **(11)** Cozzupoli et al. (1972), **(12)** Cozzupoli et al. (1971), **(13)** Edel et al. (1981), **(14)** Lombardi et al. (1974), **(15)** Cozzupoli et al. (1984), **(16)** Laurenzi et al. (1991), **(17)** Macera et al. (1989), **(18)** Carosi et al. (2002), **(19)** Carmignani et al. (1982b), **(20)** Barca et al. (1987), **(21)** Barca (1991).

Figure 6.1: Geochronology of Paleozoic Sardinia (Beccaluva et al. 1985 and others) plotted in time scale.

The structural investigations carried out in NE Sardinia show that the earliest foliation S1 is restricted to the host rocks of the orthogneisses from Lodè and Tanaunella, but is neither developed in the orthogneisses nor in the porphyroid-interlayered Orune schists. Dating the Lula porphyroid and the orthogneisses from Lodè and Tanaunella provides a further proof of this structurally indicated cover-basement relationship.

Although all metamorphic mineral ages fall in the Variscan time span (fig. 6.1), a pre-Variscan metamorphism cannot be excluded due to a possible Variscan resetting and the lack of radiometric measurements on metamorphic minerals with higher blocking temperatures. Besides the metamorphic extent, the tectonic extent of the pre-Variscan event is uncertain as well. The Sardic unconformity in the external zone of the Sardinian Variscides marks a hiatus from Arenigian to Caradocian (Barca et al. 1987), but the pre-Variscan magmatic event is mainly recorded in the nappe and axial zones, where such an unconformity as in the external zone is not exposed. Furthermore, geochemical differences between the Ordovician sequences of the external zone and the nappe/axial zones indicate two geodynamically distinct settings: the thinning Gondwana margin with a higher mantle input and the magmatic arc with a higher crustal input (Loi & Dabard 1997).

6.2 Sample location and description

The studied sequence in NE Sardinia represents a section from the axial zone of high-grade metamorphism through the internal nappe zone of medium-grade metamorphism to the external nappe zone of low-grade metamorphism (fig. 1.2), according to the anatomy of the Sardinian Variscides (Arthaud & Sauniac 1981, Carmignani et al. 1992a). In particular, the sequence comprises the migmatic Brunella gneisses overlain along the late Variscan Posada fault by the Siniscola schists, which in turn are overlain by the Orune schists (fig. 6.2). The structural investigations revealed a fivefold deformational history (chapter 3), and show that the earliest foliation S1 is restricted to the Brunella gneisses and Siniscola schists, but is neither developed in the intercalated orthogneisses from Tanaunella and Lodè nor in the porphyroid-interlayered Orune schists. Further evidence for a discontinuity between the Lodè orthogneiss-hosting Siniscola schists and the porphyroid-interlayered Orune schists provides their different composition. The metamorphic mineral assemblages of the Siniscola schists derive from high-Al pelites, those of the Orune schists from low-Al pelites (chapter 5). Supported by these structural and compositional relations, the Lula porphyroid could define a volcano-sedimentary cover and the protolith intrusions of the Lodè and Tanaunella orthogneisses an older basement below, if they formed during the same magmatic event.

The samples chosen for the radiometric age determination are described from internal to external positions as follows.

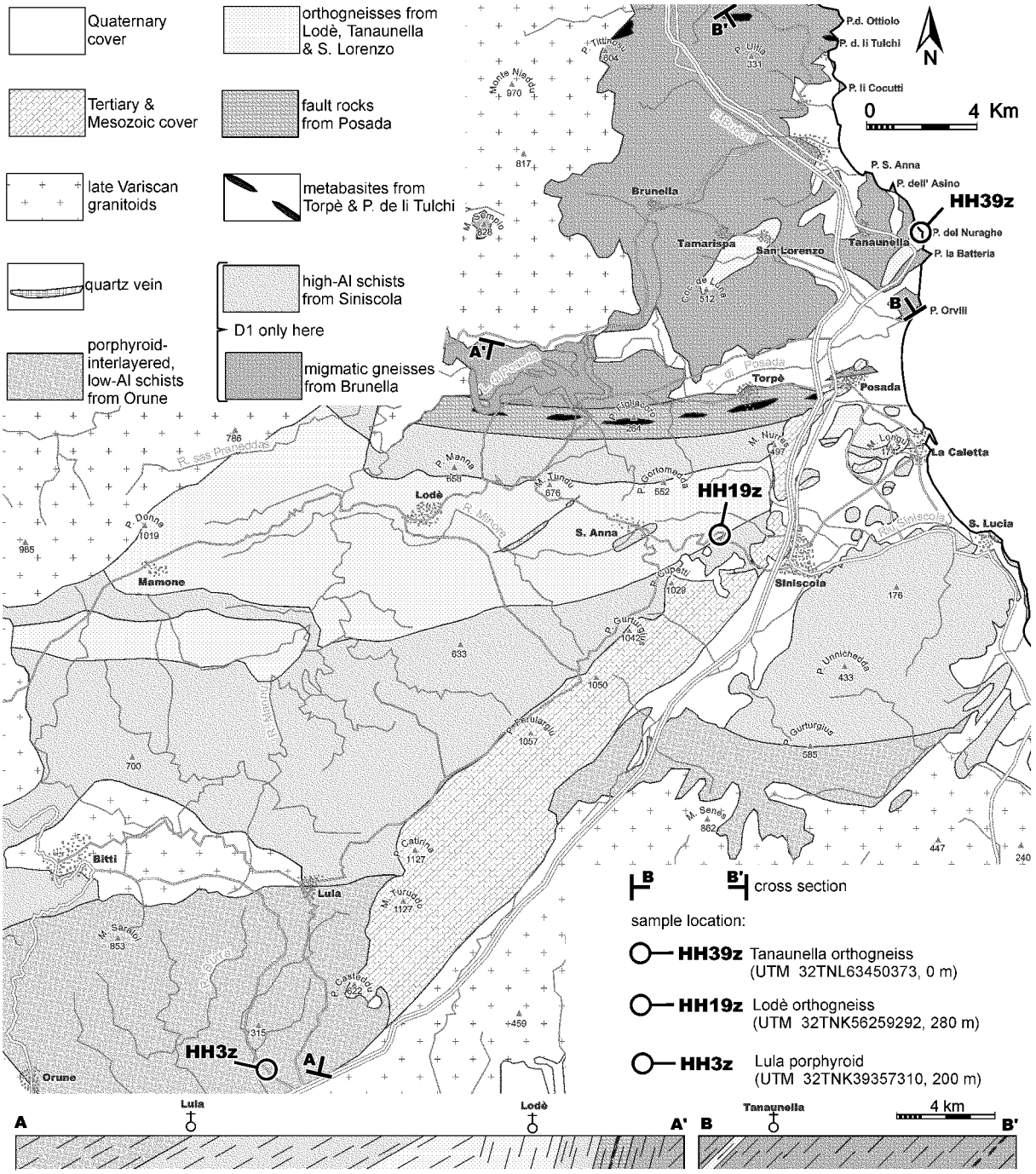

Figure 6.2: Sample location in geological sketch map of NE Sardinia with cross section.

6.2.1 Tanaunella orthogneiss

Sample HH39z was taken at Punta del Nuraghe (fig. 6.2). The main foliation S2 is commonly associated with a stretching lineation L2, which becomes particularly prominent where the crenulation cleavage S3 is developed with an intersection lineation subparallel to L2 (chapter 3). The trend of the moderately SE-dipping main foliation as well as of the shallowly NE-plunging stretching lineation is fairly the same as in the surrounding Brunella gneisses and follows the NE-SW long axis of the orthogneiss outline in the map (fig. 6.2). The aligned biotite dominates the anisotropy of the main foliation. Quartz and feldspar commonly occur in separated, centimetre-sized, elongated aggregates, which are aligned parallel to the main foliation and corresponding stretching lineation. The aggregates con-

sist commonly of smaller recrystallised grains. The aggregates display a weakly developed core-mantle structure with an old coarse grain partly surrounded by medium-sized recrystallised grains. Microcline and plagioclase of oligoclase composition can be identified according to the commonly clearly developed twinning. Some plagioclase grains preserved an oscillatory zoning of magmatic origin. Also, some idiomorphic apatite crystals remained from the magmatic fabric of the plutonic protolith. The grain boundaries of quartz and feldspar show in places lobate intergrowth (plate 5.10d), which is understood to be characteristic for diffusion creep under high-grade metamorphic conditions (Gower & Simpson 1992). Moreover, quartz subgrains have in places perpendicularly oriented optical axes, so that they reflect a chess board pattern (plate 5.9g), which is diagnostic for the stability field of high-quartz (Kruhl 1996). The high-grade fabric is randomly overgrown by some retrograde muscovite, biotite is partly chloritisised, and plagioclase partly saussuritisised.

Table 6.1: Rock-forming minerals of the granodioritic Tanaunella orthogneiss (sample HH39z)

qtz	kfs	olig	bt	chl	ms	ap	ep	zr	rt	opaques
35 %	10 %	15 %	25 %	8 %	5 %	2 %	✓	✓	✓	✓

6.2.2 Lodè orthogneiss

Sample HH19z was collected close to a roadside quarry at the south-eastern flank of the Lodè orthogneiss (fig. 6.2). The shallowly to moderately SE-dipping main foliation S2 and the associated subhorizontal stretching lineation follow fairly well the trend of the adjacent, concordant contact to the Siniscola schists (chapter 3). Extensional D4 shear bands (plate 3.2d), which are related to the Posada faulting, overprint the main foliation and indicate a displacement down to W. The Lodè orthogneiss is of granitic composition in the sample area (table 6.2), but changes to granodioritic composition towards Lodè. The sample exposes an augen gneiss fabric (plate 5.4f). The eye-shaped, centimetre-sized porphyroclasts of K-feldspar are aligned parallel to the main foliation and stretching lineation. The porphyroclasts might show in places an asymmetric morphology either as σ clasts in D2-derived S/C fabrics or as δ clasts commonly in the extensional D4 shear bands. The K-feldspar porphyroclasts are clearly structured in an old core with the coarse grain of magmatic origin and in a younger mantle of fine-grained recrystallised feldspar (plate 5.4g). In places, the K-feldspar is marginally invaded by myrmekites (plate 5.4h). The K-feldspar commonly shows the crosshatched twinning of microcline, and in comparison to the refraction indices of quartz, the plagioclase indicates an albite to oligoclase composition. The fine- to medium-grained matrix consists mainly of quartz and plagioclase, which tend to occur separated in bands aligned within the main foliation. The quartz grains related to the main fabric reflect a considerable annealing amount, which distinguishes them from the dynamically recrystallised fine-grained quartz related to the extensional D4 shear bands. According to the brittle response of feldspar to the D4-shearing, the temperature had already dropped below that of incipient feldspar recrystallisation, which is about 500 °C (Voll 1976). In particular, muscovite is preferentially involved in the D4 shear bands by kinking and slip along its basal plane. Retrogression is accompanied by chloritisation of biotite, saussuritisation of plagioclase and K-feldspar replacement by muscovite.

Table 6.2: Rock-forming minerals of the granitic Lodè orthogneiss (sample HH19z)

qtz	kfs	pl	ms	bt	chl	czo/ep	ap	tur	zr	opaques
25 %	30 %	25 %	10 %	10 %	✓	✓	✓	✓	✓	✓

6.2.3 Lula porphyroid

Sample HH3z is a porphyroid interlayered in the Orune schists. It was discovered in an outcrop at the new road to Bitti (fig. 6.2). The porphyroid-containing sequence is mainly made up by alternating metapsammopelites, some graphitic schists, and few greenschists. The main foliation S2 transposes the volcano-sedimentary bedding, contains intrafolial folds, and is commonly associated with a stretching lineation L2. The main foliation is deformed by cylindrical D3 folds of a half wavelength ranging from kilometre to centimetre size (chapter 3). The moderately SE-dipping axial plane cleavage S3 and the subhorizontal F3 axis show the same NE-SW trend as the subhorizontal stretching lineation L2. A steeply S-dipping crenulation cleavage S5 is restricted to the schistose domains. Up to centimetre-sized porphyroclast aggregates occur in the fine-grained schistose matrix of the porphyroids (plate 3.1a). These remnants of the former volcanic phenocrysts are composed either of feldspar or quartz. The quartz porphyroclast aggregates are commonly stretched out parallel to the main foliation and the associated stretching lineation. They consist of fine- to medium-sized recrystallised quartz grains (plate 5.1d). The feldspar porphyroclast aggregates are commonly made up by feldspar fragments. Recrystallised quartz and chlorite commonly fill the fractures between the fragments and occur in the strain caps of the porphyroclast aggregates (plate 5.1c). According to the recrystallised quartz and fractured feldspar, the temperatures overstepped the temperature of incipient quartz recrystallisation but not of incipient feldspar recrystallisation, which are 290 °C and 500 °C respectively (Voll 1976). The feldspar in the porphyroclast aggregates is strongly saussuritisised and sericitisised (plate 5.1e).

Table 6.3: Rock-forming minerals of the Lula porphyroid (sample HH3z)

qtz	ab	ms/ser	bt	chl	czo/ep	grs	ap	ttn	tur	zr	opaques
35 %	30 %	20 %	5 %	5 %	5 %	✓	✓	✓	✓	✓	✓

6.3 U-Pb dating on zircon

The mineral zircon ($ZrSiO_4$) incorporates U in its lattice structure where it replaces Zr, but accepts very little or no Pb at the time of crystallisation. The high resistance of zircon to metamorphism, chemical and physical weathering prevents the system from distortion, which makes it a favourite object for radiometric age determination.

The isotopes ^{238}U and ^{235}U decay to the stable isotopes ^{206}Pb and ^{207}Pb with half life times of 4,468 Ga and 0,704 Ga respectively. The two mother-daughter pairs yield two independent ages usually displayed in a $^{207}Pb/^{235}U$ versus $^{206}Pb/^{238}U$ diagram, where the points, having the same $^{207}Pb/^{235}U$ and $^{206}Pb/^{238}U$ ages, define the concordia line (Wetherill 1956). Open systems might suffer Pb loss and/or U gain or, less commonly, the other way around, so that the data plot below or, less commonly, above the concordia.

6.4 Laser ablation inductively coupled plasma mass spectrometry

By laser ablation inductively coupled plasma mass spectrometry (LA-ICP-MS) the isotopic composition can be measured. It comprises the laser ablation for sampling the matter, the inductively coupled plasma for ionisation of the matter, and the mass spectrometer for identification of the isotopes by their mass to charge ratio. The laser burns a crater in the sample. Attached to the cell that contains the sample is an optical microscope to locate the spot to be analysed and a gas flow of Argon. The vaporised particles from the crater are transported by the gas flow to the plasma. The diameter of the spot can be reduced commonly in the range from 100 μm down to 10 μm, which also reduces the analytical precision (Machado & Simonetti 2001).

The advantage of the LA-ICP-MS in comparison to the more precise and accurate isotope dilution thermal ionisation mass spectrometry (ID-TIMS, also known as conventional method) is the easier and faster sample preparation as well as the in-situ analysis, which might reveal that the single zircon crystal records more geological events than the rock containing it. In comparison to the secondary ionisation high resolution ion microprobe (SHRIMP), LA-ICP-MS is easier, cheaper, and faster.

6.5 Analytical procedure

Zircons were separated, using conventional separation techniques (Wilfley table, heavy liquids and magnetic separation). A final selection of the zircons was made with a binocular microscope, choosing the crystals according to criteria of morphology, size, colour, and clarity. 300 zircon crystals and/or fragments were mounted in 6 distinct epoxy resin discs, two discs per sample with 50 zircon pieces each, and then polished down to a surface roughness of 1 μm. The internal structure was imaged, using SEM-attached cathodoluminescence (CL).

The in-situ U-Pb isotope measurements on zircon were carried out by a single-collector double-focusing magnetic sector ICP-MS (Element I, ThermoFinnigan Mat.) coupled with a Q-switched Nd:YAG laser source (Brilliant, Quantel) at the C.N.R. – Istituto di Geoscience e Georisorse – Sezione di Pavia. Laser probe and analytical method are described in detail by Tiepolo et al. (2003). The laser operated at a frequency of 10 Hz with a fluency of 15 J/cm^2. Its fundamental emission in the near IR region was converted by harmonic generators into 213 nm. Spot sizes of 20 and 40 μm have been used with respect to the chosen spot location at the CL images. The $^{206}Pb/^{238}U$, $^{207}Pb/^{235}U$, $^{207}Pb/^{206}Pb$ and $^{208}Pb/^{232}Th$ ratios have been independently determined by acquiring masses ^{202}Hg, $^{204}(Pb+Hg)$, ^{206}Pb, ^{207}Pb, ^{208}Pb, ^{232}Th, ^{235}U and ^{238}U. For 20 μm spot size, the ICP-MS was run in magnetic scan mode, whereas at 40 μm spot size, the electronic scan mode was preferred due to higher performance. Mass bias, laser-induced elemental fractionation and sequential acquisition of transient signals are corrected by external standardisation, using zircon standard 91500 (Wiedenbeck et al. 1995), for which TIMS data furnish mean $^{206}Pb/^{238}U$ and $^{207}Pb/^{206}Pb$ apparent ages of 1062.4 ± 0.4 Ma and 1065.4 ± 0.3 Ma respectively. Zircon standard 02123, which is a pegmatitic gem zircon from Norway for which

TIMS data yield a concordant age of 295 ± 1 Ma (Ketchum et al. 2001), was used as reference material within the analytical run.

The analytical protocol of the data reduction software package LAMTRACE (developed by S. Jackson, Macquarie University, Sydney) was adopted for the off-line data procession the day after data acquisition. The ages were calculated from $^{206}Pb/^{238}U$ and $^{207}Pb/^{235}U$ ratios using the ISOPLOT software (Ludwig 2000).

6.6 Results

The zircons yielding concordant ages are shown in CL images (fig. 6.3), the isotopic data are listed in tables (table 6.4-6.6), plotted in concordia diagrams and cumulative probability histograms, and the weighted average ages were calculated (fig. 6.4). Discordant data are not considered. LA-ICP-MS data are affected by a larger analytical error with respect to TIMS. This prevents an accurate fit of the discordant data points on the concordia and the achievement of intercept values with geological meaning. On the basis of the reference zircon 02123 analysis, age determinations are estimated to be accurate within ± 1.5%.

6.6.1 Tanaunella orthogneiss (HH39z)

Half of the data from the Tanaunella orthogneiss (table 6.4) yield eleven concordant ages obtained on nine zircons. Continuous oscillatory zoning, such as shown by the zircons *b3*, *b16*, *b13*, *a22*, *a28*, and *a31* (fig. 6.3), is typical for growth in a melt (Hinton & Upton 1991, Hanchar & Miller 1993). Moreover, overlapping ages from core and rim of the zircons *b16* and *b13* suggest that the zircons crystallised entirely during the recorded magmatic event. Discontinuous zoning, to a minor extent at the tip of the zircon core *b7* and to a major extent at the zircon core *a18*, indicates a resorption phase. Despite this discontinuity, their ages overlap with the others, which suggests initial growth, subsequent resorption, and final overgrowth followed within the time span of a single magmatic event.

The concordant ages are distributed from Early to Late Ordovician times (fig. 6.4). However, a Middle to Late Ordovician age culmination can be distinguished. Taking the particularly low precision of zircon *b3* into account, the weighted average, calculated without this zircon, gives 453 ± 8 Ma (MSWD 0,63), inferred to be the protolith intrusion age for the Tanaunella orthogneiss.

6.6.2 Lodè orthogneiss (HH19z)

A quarter of the data from the Lodè orthogneiss (table 6.5) yield six concordant ages acquired on five zircons. The zircons are internally structured in core and rim (fig. 6.3). The oscillatory zoning of the idiomorphic rims suggests a magmatic origin. Also, the zircon cores *a19* and *a13* expose oscillatory zoning, which is truncated by a slight discontinuity towards the rim. A clear discontinuity towards the

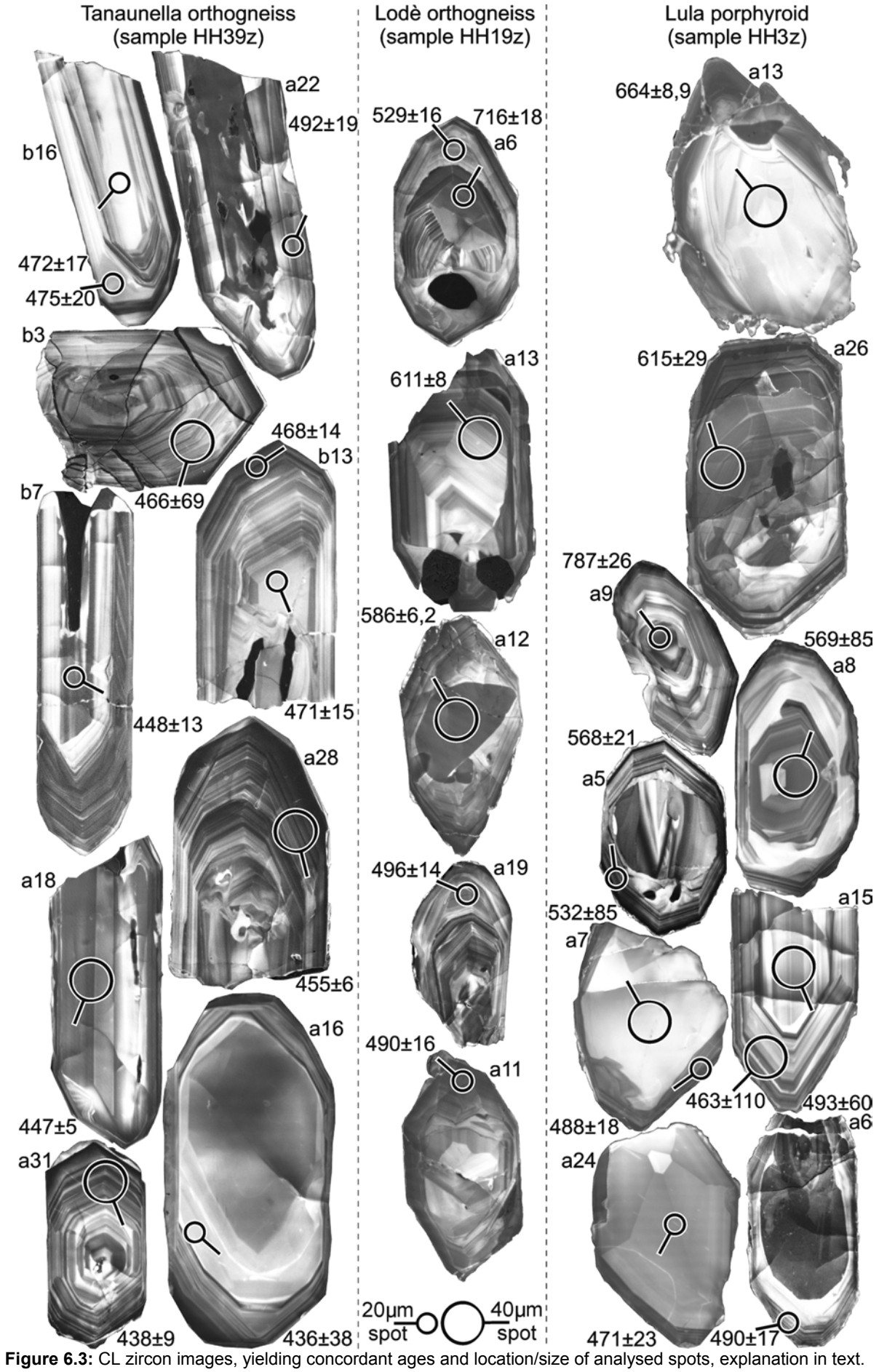

Figure 6.3: CL zircon images, yielding concordant ages and location/size of analysed spots, explanation in text.

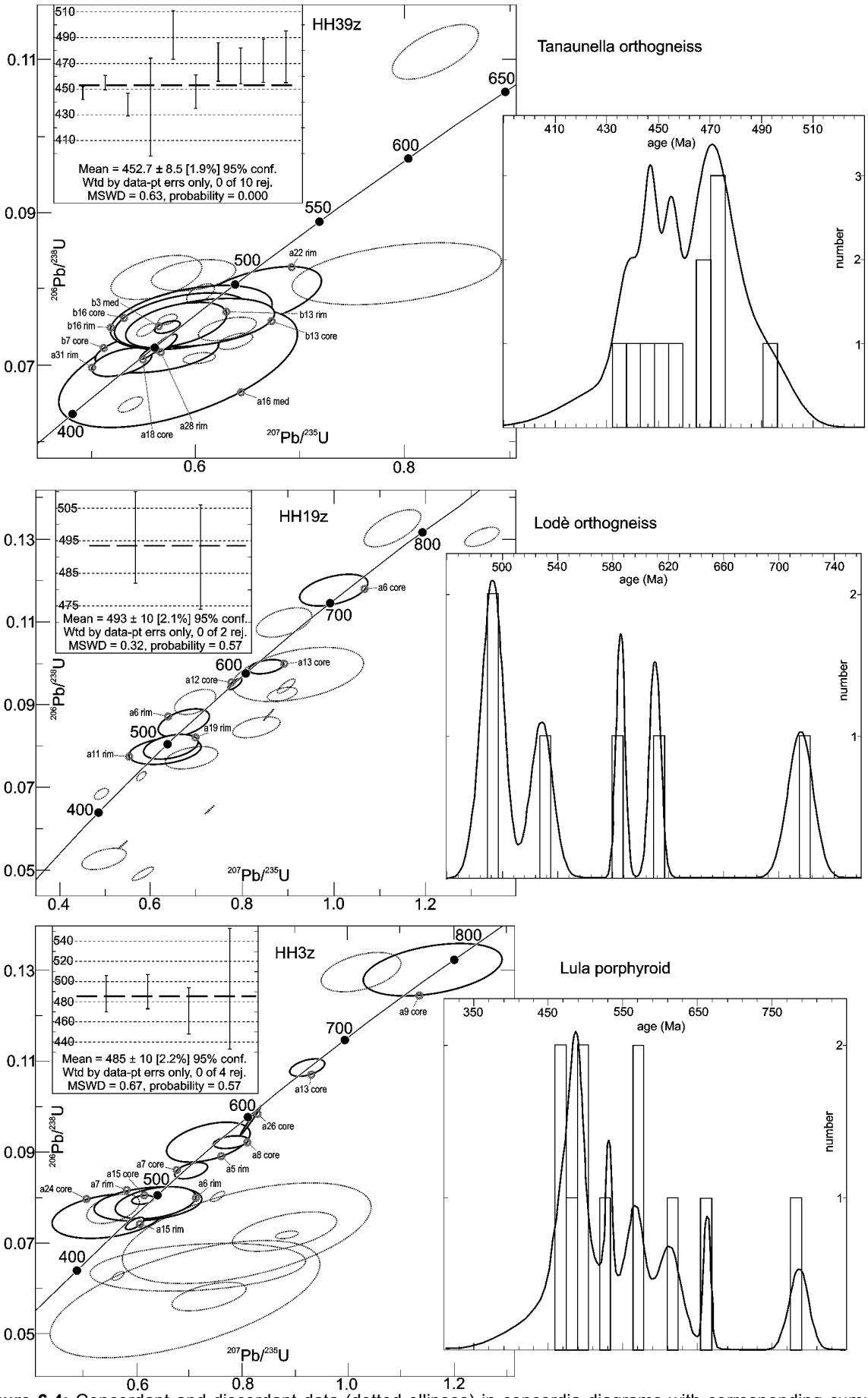

Figure 6.4: Concordant and discordant data (dotted ellipses) in concordia diagrams with corresponding cumulative probability histograms and weighted average plots, explanation in text.

Table 6.4: U-Pb isotopic data from the Tanaunella orthogneiss (sample HH39z)

Tanaunella orthogneiss		206/238		207/235		207/206		208/232		206/238		207/235		207/206		208/232		probability of		Concordant age	
sample HH39z	spot	ratio	R.S.D.	ratio	R.S.D.	ratio	R.S.D.	ratio	R.S.D.	age (Ma)	± 2 S.D.	age (Ma)	± 2 S.D.	age (Ma)	± 2 S.D.	age (Ma)	± 2 S.D.	concordance	MSWD	age (Ma)	± 2 S.D.
a16 core	40 µm	0,0649	0,006%	0,5365	0,0090%	0,0597	0,0098%	0,01988	0,0072%	405	5	436	6	592	42	398	6	---	---	----	----
a18 core	40 µm	0,0718	0,0059%	0,5539	0,0069%	0,0557	0,0075%	0,02099	0,0052%	447	5	448	5	440	34	420	4	0,69	0,16	447	4,9
a28 rim	40 µm	0,0730	0,0066%	0,5702	0,0084%	0,0564	0,0089%	0,02397	0,0071%	454	6	458	6	466	40	479	7	0,05	3,8	455	5,6
a26 core	40 µm	0,0795	0,0062%	0,6040	0,0093%	0,0548	0,0097%	0,02235	0,0134%	493	6	480	7	404	44	447	12	---	---	----	----
a31 rim	40 µm	0,0705	0,0106%	0,5285	0,0223%	0,054	0,0368%	0,02261	0,0768%	439	9	431	16	*372*	*166*	452	69	0,23	1,5	438	8,9
standard 2123	40 µm	0,0476	0,0062%	0,3408	0,013%	0,0516	0,0137%	0,01382	0,0057%	300	4	298	7	266	62	277	3	---	---	300	3,6
b02 core	40 µm	0,0732	0,0056%	0,6366	0,011%	0,0627	0,0106%	0,02983	0,0168%	456	5	500	9	696	44	594	20	---	---	----	----
b02 rim	40 µm	0,0747	0,0045%	0,5515	0,0069%	0,05320	0,0071%	0,02316	0,0083%	465	4	446	5	336	32	463	8	---	---	----	----
b03 med	40 µm	0,0751	0,0045%	0,5719	0,0087%	0,0549	0,0082%	0,02251	0,009%	467	4	459	6	408	36	450	8	0,007	7,3	466	69
b11 core	40 µm	0,0710	0,004%	0,6024	0,0103%	0,0613	0,0108%	0,02344	0,0111%	442	3	479	8	648	46	468	10	---	---	----	----
b11 rim	40 µm	0,0761	0,0036%	0,5722	0,0067%	0,0543	0,0061%	0,02148	0,0095%	473	3	459	5	382	28	430	8	---	---	----	----
b01 rim	40 µm	0,0748	0,0087%	0,6296	0,0179%	0,0609	0,0185%	0,02719	0,0144%	465	8	496	14	634	78	542	15	---	---	----	----
a16 rim	20 µm	0,0816	0,0143%	0,5617	0,0316%	*0,0499*	*0,0310%*	0,02407	0,0414%	506	14	453	23	*188*	*144*	481	39	---	---	----	----
a16 med	20 µm	0,0697	0,0453%	0,582	0,0802%	*0,0605*	*0,1427%*	0,02380	0,0607%	434	38	466	60	*622*	*622*	475	57	0,21	1,6	436	38
a19 core	20 µm	0,1112	0,0131%	0,8289	0,0202%	*0,054*	*0,0185%*	0,02873	0,0167%	680	17	613	19	*372*	*82*	572	19	---	---	----	----
a19 med	20 µm	0,0821	0,0202%	0,7919	0,0517%	*0,06990*	*0,0714%*	0,04259	0,0364%	509	20	592	46	*924*	*294*	843	60	---	---	----	----
a22 rim	20 µm	0,0791	0,0203%	0,6569	0,0391%	*0,0602*	*0,0546%*	0,02919	0,0382%	490	19	513	31	*612*	*236*	582	44	0,11	2,6	492	19
standard 2123	20 µm	0,0447	0,0315%	0,3597	0,0691%	*0,0583*	*0,1346%*	0,01323	0,0292%	282	17	312	37	*540*	*594*	266	15	---	---	282	17
b07 core	20 µm	0,0719	0,0156%	0,562	0,0431%	*0,0567*	*0,0442%*	0,01880	0,0199%	448	14	453	32	*478*	*196*	376	15	0,72	0,13	448	13
b07 rim	20 µm	0,0819	0,0102%	0,5968	0,0277%	*0,0529*	*0,0275%*	0,02019	0,0228%	507	10	475	21	*322*	*124*	404	18	---	---	----	----
b13 core	20 µm	0,0757	0,0169%	0,6055	0,0468%	*0,058*	*0,0463%*	0,02495	0,0439%	471	15	481	36	*528*	*204*	498	43	0,54	0,38	471	15
b13 rim	20 µm	0,0754	0,0158%	0,5806	0,0341%	*0,0558*	*0,0364%*	0,02489	0,0517%	469	14	465	25	*442*	*162*	497	51	0,74	0,11	468	14
b16 core	20 µm	0,0760	0,0193%	0,5881	0,0453%	*0,0559*	*0,0513%*	0,02380	0,0371%	472	18	468	34	*446*	*228*	475	35	0,8	0,06	472	17
b16 rim	20 µm	0,0764	0,0222%	0,595	0,0534%	*0,0565*	*0,0582%*	0,02444	0,0510%	475	20	474	40	*470*	*260*	488	49	0,98	0,0008	475	20

MSWD: mean square of weighted deviates, **R.S.D.**: ratio standard deviation given in percent, **± 2 S.D.**: double standard deviation given in Ma, *italic numbers in grey*: standard deviation too high

Table 6.5: U-Pb isotopic data from the Lodè orthogneiss (sample HH19z)

Lodè orthogneiss		206/238		207/235		207/206		208/232		206/238		207/235		207/206		208/232		probability of		Concordant age	
sample HH19z	spot	Ratio	R.S.D.	ratio	R.S.D.	ratio	R.S.D.	ratio	R.S.D.	age (Ma)	± 2 S.D.	age (Ma)	± 2 S.D.	age (Ma)	± 2 S.D.	age (Ma)	± 2 S.D.	concordance	MSWD	age	± 2 S.D.
a01 core	40 µm	0,0684	0,74%	0,4892	1,29%	0,05181	1,35%	0,02195	0,72%	427	6	404	9	276	62	439	6	---	---	----	----
a01 rim	40 µm	0,0728	0,60%	0,577	0,76%	0,0574	0,83%	0,02262	1,26%	453	5	463	6	506	36	450	11	---	---	----	----
a12 core	40 µm	0,095	0,57%	0,7821	0,79%	0,05966	0,93%	0,02681	0,67%	585	6	587	7	590	40	535	7	0,52	0,4	586	6,2
a13 core	40 µm	0,0992	0,69%	0,8512	1,80%	0,06211	1,89%	0,03122	0,71%	610	8	625	17	676	80	621	9	0,048	3,9	611	8
a04 core	40 µm	0,1306	0,71%	1,3244	1,17%	0,07345	1,25%	0,04232	0,90%	791	11	856	14	1026	50	838	15	---	---	----	----
standard 2123	40 µm	0,0472	0,85%	0,3358	1,56%	0,05156	1,55%	0,01422	0,76%	*297*	5	294	8	*264*	*72*	*285*	4	---	---	297	4,9
a20 core	40 µm	*0,0925*	*0,71%*	*0,8863*	*1,52%*	*0,0694*	*1,56%*	*0,03212*	*0,86%*	*570*	*8*	*644*	*14*	*908*	*64*	*639*	*11*	---	---	----	----
b03 core	40 µm	*0,0491*	*1,35%*	*0,5809*	*1,63%*	*0,0857*	*1,85%*	*0,01436*	*1,26%*	*309*	*8*	*465*	*12*	*1330*	*72*	*288*	*7*	---	---	----	----
b15 core	40 µm	*0,0646*	*0,66%*	*0,7267*	*0,53%*	*0,0814*	*0,73%*	*0,01722*	*0,71%*	*404*	*5*	*555*	*5*	*1230*	*28*	*345*	*5*	---	---	----	----
b17 core	40 µm	*0,0945*	*0,71%*	*0,8947*	*0,87%*	*0,0686*	*0,88%*	*0,02183*	*0,49%*	*582*	*8*	*649*	*8*	*886*	*38*	*436*	*4*	---	---	----	----
b17 rim	40 µm	*0,0563*	*0,62%*	*0,5389*	*0,57%*	*0,0694*	*0,72%*	*0,00588*	*0,75%*	*353*	*4*	*438*	*4*	*908*	*28*	*118*	*2*	---	---	----	----
b23 core	40 µm	*0,0875*	*0,66%*	*0,8555*	*0,54%*	*0,0709*	*0,45%*	*0,02947*	*0,39%*	*541*	*7*	*628*	*5*	*952*	*18*	*587*	*5*	---	---	----	----
a25 rim	20 µm	0,0772	1,37%	0,687	3,40%	0,06453	3,30%	0,01623	3,27%	479	13	531	28	*758*	*140*	325	21	---	---	----	----
a25 core	20 µm	0,0845	1,21%	0,828	2,57%	0,07106	3,27%	0,01388	1,76%	523	12	612	24	*958*	*134*	279	10	---	---	----	----
a12 rim	20 µm	0,0907	1,36%	0,6946	2,63%	0,05551	2,58%	0,01505	4,82%	560	15	536	22	*432*	*114*	302	29	---	---	----	----
a19 core	20 µm	0,1099	1,32%	0,8891	2,78%	0,05864	2,67%	0,02814	1,41%	672	17	646	27	*552*	*116*	561	16	---	---	----	----
a19 rim	20 µm	0,0799	1,52%	0,6422	3,81%	0,05825	3,55%	0,02078	4,51%	496	15	504	30	*538*	*156*	416	37	0,56	0,34	496	14
standard 2123	20 µm	0,0472	4,02%	0,3878	10,29%	0,05961	31,03%	0,01348	6,63%	*297*	*23*	*333*	*58*	*588*	*1148*	*271*	*36*	---	---	297	23
a06 med	20 µm	0,1177	1,31%	0,9993	3,01%	0,06155	3,01%	0,0192	3,47%	717	18	703	31	*658*	*128*	384	26	0,32	1,00	716	18
a06 core	20 µm	0,1326	1,38%	1,1267	2,22%	0,0616	1,97%	0,02853	4,50%	803	21	766	24	*660*	*84*	569	50	---	---	----	----
a06 rim	20 µm	0,0856	1,60%	0,6702	3,46%	0,05678	3,78%	0,03044	8,13%	529	16	521	28	*482*	*168*	606	97	0,49	0,47	529	16
a11 rim	20 µm	0,0789	1,68%	0,6283	5,12%	0,05774	5,20%	0,03024	4,90%	490	16	495	40	*518*	*228*	602	58	0,77	0,08	490	16
a11 med	20 µm	0,0973	2,70%	0,9197	6,38%	0,06852	12,14%	0,03048	6,94%	599	31	662	62	*884*	*506*	607	83	---	---	----	----
a04 rim	20 µm	0,0527	1,97%	0,495	4,00%	0,06805	3,40%	0,02088	4,70%	331	13	408	27	*870*	*140*	418	39	---	---	----	----

MSWD: mean square of weighted deviates, **R.S.D.**: ratio standard deviation given in percent, **± 2 S.D.**: double standard deviation given in Ma, *italic numbers in grey*: standard deviation too high

Table 6.6: U-Pb isotopic data from the Lula porphyroid (sample HH3z)

Lula porphyroid		206/238		207/235		207/206		208/232		206/238		207/235		207/206		208/232		probability of		Concordant age	
sample HH3z	spot	ratio	R.S.D.	ratio	R.S.D.	ratio	R.S.D.	ratio	R.S.D.	age (Ma)	± 2 S.D.	age (Ma)	± 2 S.D.	age (Ma)	± 2 S.D.	age (Ma)	± 2 S.D.	concordance	MSWD	age	± 2 S.D.
a08 rim	20 µm	0,072	6,2%	0,807	11,99%	*0,081*	*24,1%*	0,022	10,06%	450	54	600	109	*1218*	*980*	437	87	---	---	----	----
a09 core	20 µm	0,130	1,8%	1,159	4,62%	*0,065*	*6,7%*	0,033	2,99%	788	27	782	50	*762*	*284*	663	39	0,79	0,072	787	26
a09 rim	20 µm	0,078	1,7%	0,552	3,71%	*0,052*	*4,1%*	0,021	2,68%	481	15	446	27	*270*	*186*	422	22	---	---	----	----
a07 rim	20 µm	0,079	1,9%	0,619	6,74%	*0,057*	*6,8%*	0,022	4,66%	488	18	489	52	*492*	*298*	440	41	0,97	0,001	488	18
a06 rim	20 µm	0,079	1,8%	0,633	4,92%	*0,058*	*5,4%*	0,022	3,26%	489	17	498	39	*536*	*238*	434	28	0,64	0,22	490	17
standard 2123	20 µm	0,046	2,7%	0,358	7,00%	*0,056*	*9,5%*	0,014	3,48%	290	15	311	38	*468*	*422*	272	19	---	---	291	15
a05 rim	20 µm	0,092	1,9%	0,733	4,38%	*0,058*	*6,0%*	0,024	2,68%	569	21	559	38	*512*	*264*	476	25	0,53	0,39	568	21
a05 core	20 µm	0,130	1,3%	1,022	3,04%	*0,057*	*3,2%*	0,031	2,43%	785	20	715	31	*498*	*140*	625	30	---	---	----	----
a11 rim	20 µm	0,073	2,4%	0,877	4,63%	*0,088*	*8,0%*	0,031	3,57%	451	21	639	44	*1372*	*310*	617	43	---	---	----	----
a24 core	20 µm	0,076	2,6%	0,544	8,05%	*0,052*	*12,7%*	0,024	4,76%	473	24	441	58	*274*	*542*	487	46	0,24	1,4	471	23
a25 rim	20 µm	0,058	2,2%	0,735	3,87%	*0,091*	*14,0%*	0,029	2,94%	365	16	559	33	*1450*	*540*	583	34	---	---	----	----
a25 med	20 µm	0,058	9,1%	0,689	15,23%	*0,086*	*24,7%*	0,031	10,71%	362	64	532	126	*1346*	*984*	620	131	---	---	----	----
a08 core	40 µm	0,092	0,6%	0,776	1,75%	0,061	1,67%	0,027	0,97%	568	7	583	16	640	72	535	10	0,048	3,9	569	85
a07 core	40 µm	0,086	0,8%	0,700	1,80%	0,059	2,09%	0,026	1,37%	532	9	539	15	568	92	518	14	0,29	1,1	532	8,5
a06 core	40 µm	0,194	0,6%	2,815	0,75%	0,105	0,43%	0,061	0,51%	1145	12	1360	11	1714	16	1196	12	---	---	----	----
a11 core	40 µm	0,065	3,3%	0,713	11,75%	*0,080*	*60,12%*	0,027	11,00%	405	26	547	99	*1190*	*2066*	541	117	---	---	----	----
a13 core	40 µm	0,109	0,7%	0,921	1,47%	0,061	1,45%	0,035	0,85%	665	9	663	14	656	62	691	12	0,78	0,078	664	8,9
standard 2123	40 µm	0,047	0,6%	0,341	1,34%	0,053	1,26%	0,015	0,90%	294	3	298	7	322	58	293	5	---	---	294	3,3
a13 rim	40 µm	0,072	0,5%	0,882	1,01%	0,089	0,92%	0,041	0,96%	447	4	642	10	1406	34	816	15	---	---	----	----
a26 rim	40 µm	0,080	0,6%	0,751	0,75%	0,068	0,81%	0,025	0,75%	497	6	569	7	864	34	490	7	---	---	----	----
a26 core	40 µm	0,097	1,5%	0,815	1,08%	0,061	1,10%	0,029	0,57%	598	17	605	10	632	48	581	6	0,042	4,1	615	29
a15 rim	40 µm	0,074	0,7%	0,593	1,20%	0,058	1,00%	0,023	0,82%	463	6	473	9	520	42	452	7	0,006	7,5	463	110
a15 core	40 µm	0,080	0,5%	0,609	1,41%	0,055	1,43%	0,024	0,95%	494	4	483	11	430	64	476	9	0,035	4,5	493	60
a16 core	40 µm	0,063	0,7%	0,561	0,93%	0,065	0,64%	0,019	0,80%	392	5	452	7	768	26	389	6	---	---	----	----

MSWD: mean square of weighted deviates, **R.S.D.**: ratio standard deviation given in percent, **± 2 S.D.**: double standard deviation given in Ma, *italic numbers in grey*: standard deviation too high

rim is developed in the zircons *a12* and *a11* and in particular in *a6* and *a13*, where the cores suffered considerable resorption. Zircon core *a12* shows sector zoning, which indicates slow growth and low diffusivity in a fluid-enriched subsolidus reservoir (Watson & Liang 1995).

The zircon core *a11* is again structured in core and rim, both oscillatory-zoned, whereas the internal structure of the zircon core *a6* is structured in a sector and an oscillatory zone.

The concordant ages cover a wide time span (fig. 6.4), whereby the partly complexly structured cores refer to a polyphase Neoproterozoic crystallisation episode terminated in the early Paleozoic by the magmatic crystallisation of the rims. The overlapping ages obtained on the two zircon rims *a19* and *a11* line out an Early Ordovician age culmination that can be distinguished from the Early Cambrian age obtained on the zircon rim *a6*. The weighted average calculated from this age culmination yields 493 ± 10 Ma (MSWD 0,32) and is inferred to be the protolith intrusion age of the Lodè orthogneiss.

6.6.3 Lula porphyroid (HH3z)

Half of the data from the Lula porphyroid (table 6.6) yield eleven concordant ages obtained on nine zircons. Some zircons are clearly structured in core and rim, such as the zircons *a13*, *a5*, *a7*, *a6*, and *a24* (fig. 6.3), others are continuously oscillatory-zoned, such as zircon *a9* and *a15*. Zircon *a5* contains a particularly strong discontinuity between core and rim, which both show oscillatory zoning. The zircons *a13*, *a7* and *a6* exhibit sector-zoned cores surrounded by oscillatory-zoned rims, indicating terminal magmatic crystallisation. Most of these magmatic rims have an age, overlapping with the closely timed core and rim ages obtained on zircon *a15*, indicating that the entire zircon *a15* formed during the terminal magmatic crystallisation.

The concordant ages range from Neoproterozoic to early Paleozoic times (fig. 6.4), whereby the cores reflect the early crystallisation episode. However, this correlation is not always straight forward due to the zircons that crystallised entirely within a later time span. An Early Ordovician age culmination can be distinguished at the end of obtained age range. The weighted average for this terminal age culmination, which was calculated without the age on zircon rim *a15*, because of its extraordinarily low precision, yields 485 ± 10 Ma (MSWD 0,67), interpreted as the volcanic protolith age of the Lula porphyroid.

6.7 Discussion

The ages obtained by in-situ U-Pb isotopic analyses on zircons of the orthogneisses from Tanaunella (453 ± 8 Ma, MSWD 0,63) and Lodè (493 ± 10 Ma, MSWD 0,32) and of the Lula porphyroid (485 ± 10 Ma, MSWD 0,67) are interpreted as protolith ages. The widely distributed data of the Tanaunella orthogneiss (fig. 6.4), which all could be referred to the protolith intrusion, overlap with the data of the Lodè orthogneiss and Lula porphyroid. Therefore, the inferred protolith ages are likely to resolve a single Ordovician (Tremadocian to Caradocian) magmatism.

The age of the Tanaunella orthogneiss confirms and refines the Middle Ordovician age of the Rb-Sr whole rock isochron by Di Simplicio et al. (1974), which yields 458 ± 31 Ma. However, the age of the Lodè orthogneiss shows a discrepancy with the Early Silurian (441 ± 33 Ma) Rb-Sr whole rock age by Ferrara et al. (1978). As mentioned before, a discrepancy between U-Pb zircon and Rb-Sr whole rock ages is also known from the Capo Spartivento orthogneiss (Cocozza et al. 1977, Schabert 1978, Delaperrière & Lancelot 1989). According to the much higher reliability of the U-Pb zircon ages in comparison to the Rb-Sr whole rock ages (Hofmann 1993), the U-Pb age for the Lodè orthogneiss indi-

cates that the Rb-Sr age for the Lodè orthogneiss does not represent its intrusion age, but rather post-magmatic resetting of the Rb-Sr system.

The age for the Lula porphyroid is in agreement with the stratigraphically determined pre-Caradocian age (older than 458 Ma, fig. 6.1) of the porphyroids in the external nappe zone of the Sardinian Variscides (Carmignani et al. 1982b). Moreover, it confirms that the Devonian to Permian whole rock K-Ar dating of the porphyroids (Calderoni et al. 1984) refers to post-magmatic resetting of the K-Ar system. Thus, the age for the Lula porphyroid obtained in this study represents the first radiometric constraint of the Sardinian porphyroid volcanism to be of Early Ordovician age.

The classical basement problem, whether the protoliths of the orthogneisses intruded a sedimentary sequence or an older basement, has been solved. The new ages presented in this study in conjunction with the aforementioned structural and compositional relations in the studied sequence allow to define the porphyroid-interlayered Orune schists as volcano-sedimentary cover and the orthogneiss-intercalated Siniscola schists and Brunella gneisses as pre-Ordovician basement. The correlation of this cover-basement relationship with the Sardic unconformity in the external zone of the Sardinian Variscides is not straight forward due to the age discrepancy and the distinct geodynamic setting (fig. 6.5).

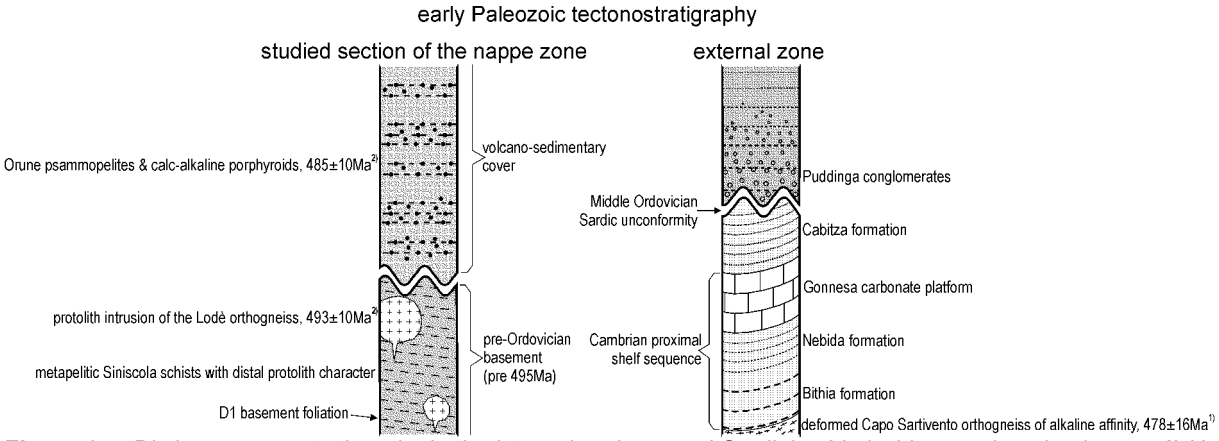

Figure 6.5: Distinct tectonostratigraphy in the internal and external Sardinian Variscides, explanation in text. **1)** U-Pb zircon (Delaperrière & Lancelot 1989), **2)** new U-Pb zircon ages presented in this study

The Sardic unconformity marks a Middle Ordovician (Arenigian to Caradocian) hiatus (Barca et al. 1987, fig. 6.1), whereas the D1 basement event has a pre-Ordovician age. On the one hand, the Cambrian tectonostratigraphy in the external zone comprises terrigenous siliciclastics and an overlying carbonate platform, displaying a proximal setting with respect to the Gondwanan continental shelf (Carmignani et al. 1994). On the other hand, the metapelites of the pre-Ordovician Siniscola schists in the study area rather have a distal character. Moreover, the Ordovician magmatism in the external zone is represented by the Capo Sartivento orthogneiss, which is of alkaline composition (Delaperrière & Lancelot 1989) and which is older than the Sardic deformation (fig. 6.1), whereas the Ordovician magmatism in the nappe zone shows calc-alkaline affinity (Memmi et al. 1983) and is younger than the pre-Ordovician basement documented in the study area.

These tectonostratigraphic differences between the nappe and external zones are ascribed by Carmignani et al. (1994) to distinct, but spatially associated arc and back arc settings respectively (fig. 1.4b). According to this point of view, the Ordovician magmatism in the study area could be related to an active margin setting, and the age discrepancy between the pre-Ordovician D1 basement event in the study area and the Middle Ordovician Sardic unconformity in the external zone expression of migrating, and thus diachronous arc tectonics. However, Loi & Dabard (1997) suggest to locate the nappe zone between Gondwana and Baltica separated from the Gondwanan shelf setting of the external zone, based on the occurrence of Baltic taxa in the nappe zone. Following this suggestion, a geodynamic setting of the nappe zone more separated from the external zone than ascribed by Carmignani et al. (1994) would be a reasonable assumption, questioning any correlation between the D1 basement event documented in the study area and the Sardic event recorded in the external zone.

According to the Early Cambrian ages measured on magmatic zircons (fig. 6.4), the Ordovician magmatism appears as the terminal phase of a longer period of magmatic activity. However, there is no magmatism older than Ordovician dated so far, although orthogneisses older than D1 are common, e.g. the Punta Orvili orthogneiss. Taking the possibility of an age significantly older than Ordovician into account, the D1 basement event could be expression of Cadomian/Pan-African tectonics.

The Neoproterozoic ages obtained on the partly complexly zoned zircon cores are probably inherited from a long-lasting, polyphase Pan-African episode. Thus, they represent the first radiometric proof of Sardinia's Gondwanan identity. This is likely to exclude a major geographical barrier between the nappe and external zones during Cambro-Ordovician times, because major break-off and separation of peri-Gondwanan terranes first started in Ordovician times (Raumer et al. 2003). On the other hand, such distinct geodynamic settings of active and passive margin regimes as probably represented by the nappe and external zones are not ruled out to have occurred during Cambro-Ordovician times within the Gondwanan vicinity.

The studied sequence can be inferred to represent an edifice of Ordovician magmatic belt upon older basement. The displacement along the late Variscan Posada fault did not exceed the dimension of this edifice, according to the Ordovician orthogneisses, occurring on both sides of the Posada fault. Contrary to Cappelli et al. (1992), there are no distinct tectonostratigraphic units juxtaposed along the Posada fault, but may be along the border between nappe and external zone.

6.8 Conclusion

The following conclusions can be drawn:

- The inferred protolith ages of the orthogneisses from Tanaunella (453 ± 8 Ma, MSWD 0,63) and Lodè (493 ± 10 Ma, MSWD 0,32) and of the Lula porphyroid (485 ± 10 Ma, MSWD 0,67) probably resolve a single Ordovician (Tremadocian to Caradocian) magmatic event.
- The Ordovician magmatism in addition to the structural and compositional relations defines a volcano-sedimentary cover and a pre-Ordovician basement below.

- An early volcanic stage of the Ordovician magmatism is constrained by the Lula porphyroid.
- The Ordovician magmatism consumed and/or assimilated polyphase Pan-African reworked crust.
- The displacement at the late Variscan Posada fault did not exceed the dimension of the inferred edifice of magmatic arc upon older basement.
- The nappe and external zones of the Sardinian Variscides probably refer to distinct geodynamic settings of active and passive margin regimes during Cambro-Ordovician times within the Gondwanan vicinity.

7 Final discussion

In order to prove, whether or not the Posada fault is superimposed on a Variscan suture, the geological record of the Posada fault/wall rocks has been studied. The results reflect an evolution that ranges from the early Paleozoic drift from the Gondwana margin away, via the accretion of Pangea at the south Variscan flank, to the deformation within the Alpine orogen. In addition to the Alpine overprint, a fivefold deformational history has been distinguished. After a brief review of the main results, the suture model by Cappelli et al. (1992) is refuted and an alternative model proposed and related to the neighbouring Variscan areas.

7.1 Alpine deformation

The Alpine reorientation of the Variscan structures has been estimated, based on the spatial relation between the Variscan basement layering and the post-Variscan cover bedding. So, the pre-Alpine recumbent attitude of the D3 folds and the gently inclined dip of the initial Posada fault have been revealed. Furthermore, the transtensive kinematics that led to the formation of the Monte Albo flower structure has been inferred from the Alpine structure, relief inversion, and basement-derived plateau gravel. In contrast to the transpressive model by Carmignani et al. (1992a, 1995), which relates the Alpine structure of E Sardinia to the Alpine collision in Corsica, the Alpine structure of E Sardinia has been explained by Miocene extension in the back arc of the retreating Apenninic-Maghrebidic arc, which eventually led to the Tyrrhenian basin opening (fig. 3.28, 3.29).

7.2 Ordovician magmatic belt upon older basement

The Variscan basement sequence can be described as an edifice of Ordovician magmatic belt upon older basement, according to the following evidences.

- The separate occurrence of metaplutonic and metavolcanic rocks defines intrusive and extrusive levels.
- The separate occurrence of metapelites with contrasting high- and low-Al composition correlates with the intrusive and extrusive levels respectively.
- D1 and the pre-D2 metamorphic mineral assemblage are restricted to those rocks, which host the metaplutonic rocks.
- The metavolcanic rocks interlayered with graphitic schists correlate lithostratigraphically with Ordovician to Silurian sequences in central Sardinia, whereas the Ordovician orthogneisses determinate their host rocks to be of pre-Ordovician age.
- In-situ U-Pb zircon ages reconfirm the age relations of the Ordovician magmatic belt upon older basement, yielding for the Lula porphyroid 485 ± 10 Ma (MSWD 0,67), for the Lodè orthogneiss 493 ± 10 Ma (MSWD 0,32), and for the Tanaunella orthogneiss 453 ± 8 Ma (MSWD 0,63).

The pre-Variscan cover-basement relationship explains the apparently lacking contact aureole of the metaplutonic rocks, the uncommon order of garnet and oligoclase appearance, as well as the partly contrasting deformational succession. The correlation of the pre-Ordovician D1 basement event with the Middle Ordovician Sardic unconformity in the external zone of the Sardinian Variscides is not straight forward due to the age discrepancy and contrasting tectonostratigraphy (fig. 6.5). Instead, a relation to the Cadomian/Pan-African orogeny appears to be equally justified.

7.3 Variscan deformation

It has been demonstrated that the studied sequence was subjected, during the main Variscan deformational event D2, to a foreland directed transport, accompanied by a prograde metamorphism that reached decompressional peak conditions, which ranged from low- to high-grade with increasingly deeper levels. The up to kilometre-scaled recumbent D3 folding coaxial with the D2 transport direction and the D4 Posada detachment faulting led to the formation of a mantled gneiss dome. The mantled gneiss dome comprises (1) the high-grade gneisses of the axial zone in the core, (2) the Posada fault-bounded contact between core and mantle, and (3) the medium- to low-grade schists of the nappe zone in the schistose mantle. The predominant orogen-parallel trend is related to the Posada shearing. S4 crosscut previous foliations at a low angle and retrogressed the high-grade Brunella gneisses under medium-grade conditions and the medium-grade Siniscola schists under low-grade conditions during early faulting stages. The initial temperature gradient across the fault was overcome with progressing retrogression. The Posada fault rocks evolved from the adjacent wall rocks by retrograde shearing. In response to the tectonic denudation further exhumation was accommodated by the large D5 flexure at the flank of the uplifting gneiss dome. D4 and D5 refer to the same exhumation process. The flexure axis is coaxial with the displacement direction in the Posada fault. In the steep limb of this flexure, the Posada fault became a dextral wrench fault and the F3 attitude changed from recumbent to reverse.

7.4 Variscan metamorphism

In the internal dome, peak metamorphic muscovite dehydration melting at about 760°C and 8 kbar led to the *K-feldspar + sillimanite* zone, on which the *muscovite + sillimanite* zone was retrogressively superimposed at the Posada fault, so that the metamorphic jump to the medium-grade Siniscola schists is less obvious. The latter expose a Barrovian metamorphic suite continuously developed from chloritoid disappearance to kyanite appearance. The *garnet + albite* zone results from the interference of Variscan and pre-Variscan metamorphic mineral assemblages. The *andalusite + cordierite* zone in the contact aureole of the Concas granite indicates that the studied sequence was already exhumed to shallow crustal levels when the Variscan deformational activity ceased.

Decreasing geobarometric, but increasing geothermometric values for the regional peak metamorphism from the hanging to the foot wall of the Posada fault (fig. 5.2) are likely to be caused by (1) a diachronous thermal peak at differently advanced exhumation stages, (2) retrograde re-equilibration, and (3) juxtaposition of distinct geothermal gradients during the D5 strike-slip stage. The lack of more

pressure-pronounced assemblages in the high-grade gneisses has been ascribed to the erasure by partial melting.

7.5 No suture

Tectonostratigraphic terranes are fault-bounded entities of regional extent, each characterised by a geological history distinct from the neighbouring terranes, and suture zones are commonly characterised by a belt of melange, blueschist and/or ophiolite (Howell et al. 1985). The results of this study rule out such a distinct geological history across the Posada fault that would be diagnostic of exotic terranes. The suture model by Cappelli et al. (1992) is particularly incompatible with the following facts.

- The main syn-peak metamorphic fabric is developed as D2 fabric superimposed on a D1 fabric and on pre-D2 porphyroblasts and/or nodules, indicating a similar tectono-metamorphic evolution across the Posada fault.
- Both wall rocks of the Posada fault belong to an Ordovician magmatic belt, suggesting a common pre-Variscan history.
- The Posada fault rocks derived from the adjacent gneisses and schists. The metabasite intercalations in the fault rocks are not particularly characteristic of the Posada fault, because metabasite intercalations occur in the wall rocks as well. Therefore, the Posada fault can not be inferred to be superimposed on an oceanic melange.

Further arguments against the suture model are:

- A fairly synchronous peak metamorphism at about 345 Ma is assumed for the high-grade gneisses on the one side (Rb-Sr whole rock, Ferrara et al. 1978) and for the medium-grade schists on the other side of the Posada fault (Rb-Sr muscovite, Del Morro et al. 1991).
- A magnetic anomaly, which was supposed to be caused by a remnant of a subducted oceanic slab in the upper mantle below the north Sardinian crust (Cassano et al. 1979, Cappelli et al. 1992), turned out as shallowly seated compositional variation within the late Variscan Sardinia-Corsica batholith (Fais et al. 1994), and therefore can not be related to an earlier suture.
- The geochemistry of the metabasites in the Posada fault is interpreted to be characteristic of ocean floor tholeiites (Cappelli et al. 1992), but the geochemical data are so ambiguous, that an alternative interpretation as continental rift tholeiitic basalts appears to be equally justified (Ricci & Sabatini 1978, Memmi et al. 1983).

Cappelli et al. (1992) delineate an ophiolitic suture sandwiched between an upper high-grade and lower medium- to low-grade plate. This proposal was probably inferred due to a too hypothetical approach. It is not in agreement with the structural record presented in this study. The most obvious structural mistakes in this suture model are as follows:

- The high-grade gneisses have not been recognised to be overlain by the medium- to low-grade schists.
- The overall dome structure has not been regarded.
- The exotic character, and thus the remote origin of the isolated eclogitic relics has been neglected.

The attempt by Cappelli et al. (1992) has failed, to establish a discrete ophiolitic suture zone in the Sardinian Variscides. The Variscan orogeny and the eclogitic relics in Sardinia have to be explained in another way, outlined henceforth.

7.6 The Variscan orogenic wedge in Sardinia

In order to explain the change from frontal to lateral tectonic transport, transpression resulting from oblique plate convergence (Harland 1971, Sanderson & Marchini 1984, Dewey et al. 1998) has been invoked (chapter 3). Moreover, the overall structure of a mantled gneiss dome as result of extensional collapse due to removal of the lithospheric mantle below the thickened orogen (Dewey 1988, Malavielle 1993) has been discussed. The critically tapered wedge concept (Chapple 1978, Davis et al. 1983, Platt 1986, Dahlen 1990) hereafter introduced, might provide the advantage to explain the various orogenic processes within a single geodynamic system. Accordingly, the sequences, which are presently exposed in the nappe/axial zones, became deformed and eventually emplaced as orogenic wedge on the sequences, which are presently exposed in the external zone (fig. 7.1). The wedge contains a magmatic belt upon pre-Ordovician basement, whereas the foreland comprises a Gondwanan shelf segment deformed during the Middle Ordovician Sardic event.

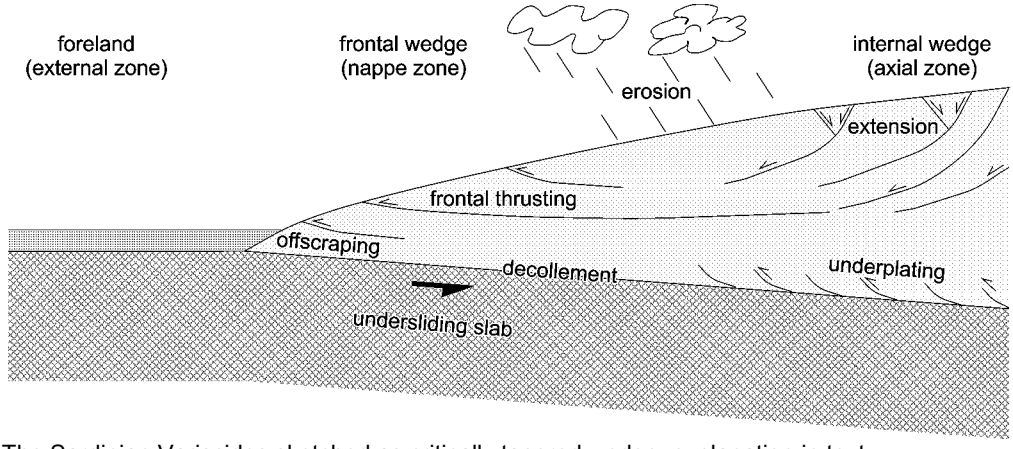

Fig. 7.1: The Sardinian Variscides sketched as critically tapered wedge, explanation in text.

The overriding wedge is considered as dynamic continuum, constantly adjusted to reach and maintain a stable shape, i.e. the critically tapered wedge, for which the gravitational forces balanced the traction exerted on the base of the wedge by the undersliding slab. Material was added to the wedge by (1) frontal offscraping, which lengthened the wedge and was balanced by folding and thrusting, (2) underplating at the underside of the wedge, which thickened the wedge and was balanced by unroofing, i.e. extension and erosion.

Prograde metamorphism of increasing grade associated with increasing deformation from frontal to internal parts of the wedge are ascribed to wedge growth due to progressing accretion. Supply of hydrous fluids by metamorphic dehydration reactions and increasing temperature enhanced deformation by pressure solution and crystal-plastic processes. Foredeep sediments were deposited and, with progressing convergence, successively added to the wedge. Folding and thrusting proceeded in the frontal parts of the wedge, while continued underplating at depth and compensating unroofing were bringing high-grade rocks up to shallower levels in the internal parts of the wedge. Underplating at depth and compensating normal faulting above are inferred to be the main exhumation mechanisms (Platt 1986, 1993) that juxtaposed dispersed eclogite intercalations against upper- to middle-crustal rocks. Exhumation started to trigger decompression-induced partial melting, when a thermally matured metamorphic stage has been reached in the internal wedge. In turn, the resulting buoyant ascent of the highly ductile, partially molten rocks enhanced exhumation. Moreover, a buoyancy-driven melt transfer might have caused further heating during exhumation, manifested in the decompressional peak metamorphism and in the elevated geothermal gradient of the axial zone.

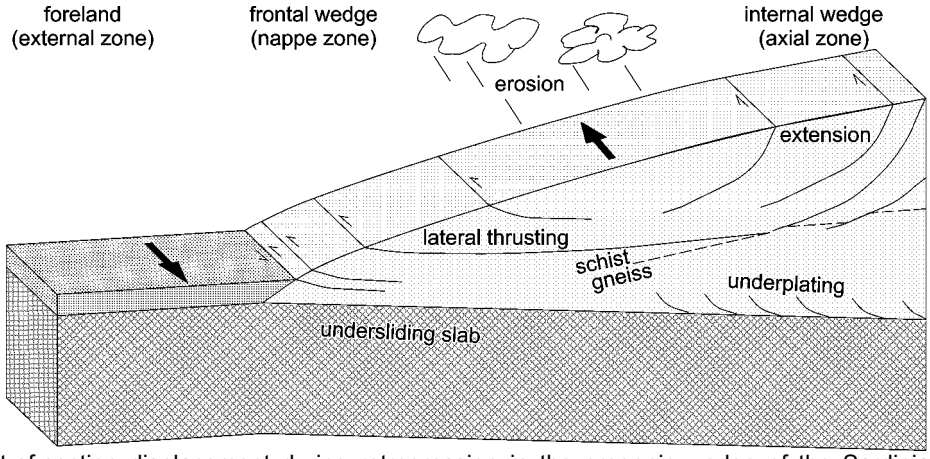

Fig. 7.2: Out-of-section displacement during retrogression in the orogenic wedge of the Sardinian Variscides, explanation in text.

The prograde and retrograde metamorphic record can be distinguished in increasingly greater detail towards the internal parts of the wedge. The post-peak metamorphic evolution of the wedge is characterised by a dextral rotation of the transport direction from frontal to lateral with respect to the orogenic anatomy (fig. 7.2). The rheological respond of feldspar changed from ductile to brittle due to the temperature drop below the low/medium-grade metamorphic transition and C'-type shear band cleavages preferentially accommodated extension with respect to the planar anisotropy in mica domains, while quartzofeldspathic domains commonly remained less affected by the retrograde deformation. Besides this arising rheological contrast, the limited supply of hydrous fluid due to the hydrous fluid-consuming retrogression led to an increased strain concentration in discrete retrograde shear zones. As consequence of this retrograde evolution, the dynamic continuum of the critical wedge became disturbed. The resulting accumulation of increasing stress inside the wedge eventually caused the detachment of the schists from the gneisses, and thus the final collapse of the wedge. The Posada detachment fault evolved in the rheological boundary layer between gneisses and schists. The detached

schistose envelope underwent gravitational spreading, denudating the gneiss core. When this collapse of the orogenic wedge ceased, the crust in the internal Sardinian Variscides has already been thinned to normal values, according to the shallowly seated intrusions of the Sardinia-Corsica batholith.

This Variscan evolution is geochronologically constrained as follows. The Variscan section of Sardinia and Corsica shows a foreland-directed younging of the orogenic events (Matte 1991). In Corsica, a Middle Devonian age is inferred for the Variscan peak metamorphism, yielding 375 Ma (Ar-Ar amphibole, Maluski 1977). The first granitic intrusions of the Sardinia-Corsica batholith are referred to an Early Carboniferous peraluminous pulse 345 Ma ago (U-Pb zircon, Paquette et al. 2003). In Sardinia, the Variscan peak metamorphism is ascribed to the Early Carboniferous migmatisation in the axial zone at about 345 Ma (Rb-Sr whole rock, Ferrara et al. 1978), and the first intrusions of the Sardinia-Corsica batholith are related to Late Carboniferous ages of 290-310 Ma (Rb-Sr whole rock, Del Moro et al. 1975). The age of the Posada detachment faulting correlates with the Late Carboniferous age culmination of metamorphic minerals (fig. 6.1, Beccaluva et al. 1985) with medium- to low-grade blocking temperatures, according to the corresponding retrograde metamorphism during faulting. Thus, suturing should have occurred sometime before or at the beginning of this event succession (pre-Middle Devonian) near the starting point of the migrating orogenic activity elsewhere more away from the foreland than the considered section. Assuming an active margin setting (fig. 1.4b, Carmignani et al. 1992a), in which the eclogites and the Ordovician magmatic belt have been formed, a margin segment might has been thrust onto a stable shelf segment of the same plate without that any ocean has been closed in the Sardinian Variscides.

7.7 Neighbouring areas

In order to define better Sardinia's place within the Variscan orogen, a correlation with its neighbouring areas shall be achieved. The early Paleozoic tectonostratigraphy is concerned, in order to increase the understanding about the relation between the pre-Ordovician basement event D1, the Ordovician magmatism, and the Sardic event. Furthermore, the Variscan structure, metamorphism and geochronology is considered to prove the significance of the Variscan evolution established in this study.

7.7.1 Maures massif

The Mauers massif is considered as immediate prolongation of the NW Sardinian section on the European mainland, extending further into the external massifs of the Alps (Alvarez 1972, Elter et al. 1991, Matte 1991, von Raumer et al. 1998).

- *Tectonostratigraphy:* A low- to medium-grade external and a high-grade internal part are distinguished. Basic and acidic metavolcanic and metaplutonic rocks are correlated with the leptyno-amphibolite association, widely common throughout the entire Variscan belt (Bellot et al. 2003). In the external part, an early Paleozoic low-grade succession overlies an older medium-grade basement of orthogneisses and kyanite-staurolite schists (Grevola & Pupin 1994).

- *Structure:* The kyanite-staurolite schists of the external part are juxtaposed against sillimanite-bearing migmatites of the internal part along the retrograde La Garde Freinet fault, which is interpreted as normal fault (Grevola & Pupin 1994, Morillon et al. 2000). D2 and D3 fold axes as well as stretching lineation have a coaxial orientation (Grevola & Pupin 1994, Bellot et al. 2003). A dextral rotation of the tectonic transport from orthogonal to parallel with respect to the orogenic trend is documented (Grevola & Pupin 1994, Morillon et al. 2000, Bellot et al. 2003).
- *Metamorphism:* The earliest metamorphic event is recorded by eclogitic relics in retrogressed metabasites that occur intercalated in the migmatic internal part. Anatexis in the internal part is related to low-pressure/high-temperature metamorphism (Bellot et al. 2003). A Barrovian metamorphism is documented by kyanite-staurolite schists in the external part.
- *Geochronology:* The eclogitic relics in retrogressed metabasites are referred to early Paleozoic ages of circa 430-450 Ma (U-Pb zircon upper intercept, Moussavou 1998). The Barrovian metamorphism has been dated on orthogneiss intercalations in the staurolite-kyanite schists, giving an Early Carboniferous age of about 345 Ma, whereas the migmatisation in the internal part provides younger ages of about 330 Ma (U-Pb monazite and zircon lower intercept, Moussavou & Lancelot 1996, Moussavou 1998). Late Carboniferous ages yield a younging of the cooling episode from 320 Ma in the external part to 303 Ma in the internal part (Ar-Ar biotite and muscovite, Morillon et al. 2000).

7.7.2 Montagne Noire

The connection between the Montagne Noire gneiss dome and the Sardinian section during Paleozoic times is not well established, despite a similar tectonic setting in a fold and thrust belt at the southern foreland of the Variscan chain (Arthaud & Sauniac 1981, Matte 1991).

- *Tectonostratigraphy:* The dome comprises a Precambrian axial zone and a Cambro-Ordovician envelope, in which locally occurring Middle Ordovician volcano-sedimentary sequences are overlain by Late Ordovician (Caradocian) conglomerates (Robardet et al. 1994).
- *Structure:* A foreland-directed transport, which started in Early Carboniferous times, as well as Late Carboniferous extension and retrograde lateral non-coaxial shearing are documented (Echtler & Malavieille 1990, Matte 1991). Stretching lineations and fold axes have an orthogonal orientation in the external nappe zone (Echtler 1990) and a coaxial orientation in the axial zone (Brun & Van den Driessche 1994). The ascent of the axial zone finds expression in normal shear fabrics in the envelope. Stephano-Permian extensional basin deposits attached to normal faults in the envelope indicate crustal extension and arose from tectonics, which is characterised by retrograde mylonitisation in strike-slip and normal faults (Echtler & Malavieille 1990, Brun & Van den Driessche 1994). The strike-slip faulting locally caused metamorphic gaps between core and the outer envelope. The inner envelope is best preserved in the strain shadow of the dome (Brun & Van den Driessche 1994).

- *Metamorphism:* A high-temperature/low-pressure overprint is documented by partial melting and anatectic granitoid intrusions in the axial zone as well as by an andalusite-sillimanite facies series in the inner envelope (Thompson & Bard 1982). It follows after a more pressure-pronounced event recorded by eclogites in the axial zone (Demange 1985) and a kyanite-sillimanite facies series in the envelope. Thermal peak conditions are characterised by a temperature gradient increasing from external to internal parts and by decreasing post-peak temperature and pressure in the axial zone, while the temperature increased and the pressure decreased less in the envelope than in the axial zone (Soula et al. 2001). Accordingly, the ascending axial zone had a thermal contact effect on the envelope.
- *Geochronology:* Syn-peak metamorphic anatectic granitoids yield Early Carboniferous ages of circa 320-340 Ma (U-Pb zircon and monazite, Matte et al. 1998). Late Carboniferous cooling provides ages of about 297-320 Ma (Ar-Ar muscovite and biotite, Maluski et al. 1991).

7.7.3 Pyrenees

The Variscan basement in the Pyrenees and Sardinia has been related to a single transpressive regime (Carreras & Capella 1994, Carosi & Oggiano 2002).

- *Tectonostratigraphy:* Besides the Pyrenees, the tectonostratigraphy of the Catalonian Coastal Range and the Central Iberian zone is introduced henceforth. In the Pyrenees, a Cambrian sequence is intruded by the protolith of the Canigou orthogneiss (Barbey et al. 2001) during Early Ordovician (Arenigian) times, giving about 475 Ma (U-Pb zircon, Deloule et al. 2002). Early Ordovician metavolcanics are common as well, e.g. in the Pierrefitte area (Calvet et al. 1988), below widely occurring conglomerates and a major discordance of Late Ordovician (Caradocian) age (Hartevelt 1970, Santanach 1974). In the Catalonian Coastal Range, Ordovician orthogneisses hosted in Cambrian sequences are considered as plutonic equivalents of metavolcanics with calc-alkaline affinity that are closely associated to Caradocian conglomerates (Gil Ibaruchi et al. 1990, Julivert and Duránd 1990). In the Ollo de Sapo domain of the Central Iberian zone, Early Ordovician orthogneisses widely occur and are overlain by the Sardic unconformity of middle to late Arenigian age (Valverde-Vaquero & Dunning 2000).
- *Structure:* The Pyrenean basement domes show an increasing metamorphic grade to the centre and a gently dipping foliation. They represent the so-called infrastructure and are distinguished from the surrounding steeply foliated suprastructure (Sitter & Zwart 1960). Thrusting oblique with respect to the orogenic trend (Kriegsman et al. 1989) is followed by a lateral transport. The latter has been related either to late orogenic extension (van den Eeckhout & Zwart 1988, Vissers 1992) or to dextral transpression (Carreras & Capella 1994).
- *Metamorphism:* In the Pyrenean section, a high-temperature/low-pressure metamorphism is closely associated with magmatism, reaching maximal conditions of amphibolite and granulite facies (Zwart 1962, 1986, Wickham & Oxburgh 1985, Vielzeuf & Pin 1989, de Saint Blanquat 1990,

Gibson 1991, Gleizes et al. 1998, Druguet 2001). Eclogites do not occur. The progressive metamorphism followed a clockwise P-T-t path (de Saint Blanquat 1990, Gibson 1991), reaching the thermal peak later with increasing metamorphic grade (van den Eeckhout & Zwart 1988).

- *Geochronology:* The Late Carboniferous deformation in the Pyrenees is dated on synkinematic granitoids, yielding about 310 Ma (U-Pb zircon, Paquette et al. 1997).

7.7.4 Calabria

The Variscan basement in Calabria belongs, besides the Variscan basement in Sardinia, the Pyrenees, and in the Alps, to a Late Carboniferous belt of I-type, calc-alkaline tonalites and granodiorites, which intruded the south Variscan flank circa 290-310 Ma ago (fig. 1.1).

- *Structure:* Peak metamorphic assemblages generally formed during the main deformation, but mineral growth lasted out deformation in response to advective heat input through granitoid intrusions (Gräßner & Schenk 1999).

- *Metamorphism:* In southern Calabria, Variscan low-pressure metamorphism achieves amphibolite facies conditions in shallow crustal levels and supplements granulite facies metamorphism in deeper crustal levels (Schenk 1981, Gräßner & Schenk 1999).

- *Geochronology:* The closely associated Late Carboniferous magmatism and metamorphism yield ages of about 300 Ma (U-Pb zircon and monazite Schenk 1981, Gräßner et al. 2000).

7.7.5 Alps

As outlined hereafter, the Variscan basement that is presently exposed in the Alps reflects an early Paleozoic active margin setting, such as proposed by Carmignani et al. (1992a, fig. 1.4b) for Sardinian nappe zone during Ordovician times.

- *Tectonostratigraphy:* Eclogitic metagabbros of island arc affinity, basaltic eclogites of MORB affinity, anatexis, and felsic magmatism are referred to an early Paleozoic active margin setting in the Central Alpine Aar and Gotthard massifs (Oberli et al. 1994, Schaltegger 1994). In the South Alpine Carnic Alps, lower Ordovician (Arenigian) porphyroids upon Cambrian sequences are common and can be distinguished from Late Ordovician (Caradocian) porphyroids (Meli & Klötzli 2001, Läufer et al. 2001). The South Alpine Strona-Ceneri zone consists of anatectic metapelites, ocean floor remnants and calc-alkaline intercalations that recorded early Paleozoic arc tectonics (Handy et al. 1999).

- *Structure:* A D1 basement foliation was crosscut by the Ordovician protolith intrusion of orthogneisses in the Strona-Ceneri zone (Zurbriggen et al. 1997). Handy et al. (1999) propose a late Carboniferous suture zone between the contrasting Strona-Ceneri and Ivrea-Verbano zones. The suture dip is suggested to be opposite to the direction of increasing metamorphism in the overlying Strona-Ceneri zone, which accommodated major crustal extension contemporaneous to suturing by a lateral operating retrograde normal fault (Val Colla shear zone) that detached greenschist facies from amphibolite facies rocks.

- *Metamorphism:* In the Aar and Gotthard massifs, an early Paleozoic succession of eclogite and granulite facies metamorphism, anatexis, and felsic magmatism has been documented (Biino 1994, Schaltegger 1994). Early Paleozoic eclogite to amphibolite facies metamorphism, anatexis, and magmatism are also reported from the Strona-Ceneri zone (Handy et al. 1999).
- *Geochronology:* The Variscan Aar and Gotthard massifs recorded an early and late Paleozoic metamorphic overprint (U-Pb and Sm-Nd, Schaltegger 1994 and references therein). Accordingly, the latter achieved an Early Carboniferous peak between 330-360 Ma. The early Paleozoic high-pressure and the subsequent high-temperature metamorphism occurred within a relatively short time span of 440-470 Ma, obtained on eclogitic metabasite and post-anatectic orthogneiss (U-Pb zircon, Oberli et al. 1994). In the Strona-Ceneri zone, early Paleozoic amphibolite facies metamorphism is constrained to 385 Ma (U-Pb staurolite, Romer & Franz 1998), and orthogneisses of anatectic origin yield Ordovician intrusion ages of about 480 Ma (U-Pb zircon lower intercept, Zurbriggen et al. 1997).

7.8 Sardinia's position within the Variscan orogen

According to this outline of the neighbouring areas, the early Paleozoic active margin setting, documented in the Variscan basement of the Alps and preceded by an older D1 foliation in the South Alpine Strona-Ceneri zone, correlates with the Ordovician magmatic belt upon older basement, delineated for the Sardinian nappe and axial zones. On the other hand, the early Paleozoic magmatism followed by the Sardic event, such as recorded by Arenigian to Caradocian conglomerates and/or unconformities upon older orthogneisses and metavolcanic rocks in the Pyrenees, Catalonian Coastal Range, Central Iberian zone, and in places of the Montagne Noire, correlate with the Sardinian external zone. Consequently, the Sardinian Variscides exhibit a section, in which a part of the Variscan domain that is mainly exposed in the present Alps has been thrust onto the Variscan domain that is mainly exposed in Iberia and Aquitaine.

The situation of the Sardinian section within the Variscan orogen is further constrained by its position with respect to the Variscan magmatic zoning (fig. 1.1). The two belts of high Mg-K magmatites and of I-type, calc-alkaline tonalites/granodiorites mark, probably as expression of the evolving orogenic wedge, an earlier more internal and a later more external setting respectively (Finger et al. 1997, Raumer 1998, Ferré & Leake 2001). The Variscan orogeny in the Pyrenees and Calabria appears closely associated with the later calc-alkaline magmatic event. On the other hand, this later calc-alkaline magmatic event led to intrusions after the deformational activity had already ceased in the Sardinian study area. Thus, the Sardinian section probably had a more internal setting than the Pyrenean and Calabrian sections.

The outlined similarities and differences between Sardinia and its neighbouring areas qualify the Sardinian section as exemplary study object, through without a suture, to constrain ubiquitous features of the Variscan orogeny, such as migrating orogenic activity, thermal doming, dextral rotation of the transport direction, etc..

8 Final conclusion

The model of Variscan collisional suturing in northern Sardinia by Cappelli et al. (1992) is not supported by the results of the presented study. Instead, the axial and nappe zones of the Sardinian Variscides are inferred to belong to the same tectonostratigraphic domain, which has been thrust as orogenic wedge onto the external zone. The isolated eclogitic intercalations and the Ordovician magmatites in the orogenic wedge might refer to an early Paleozoic active margin segment that might has been thrust on the early Paleozoic shelf segment, presently exposed in the external zone, without that any ocean has been closed in the Sardinian Variscides. Suturing is assumed to have occurred elsewhere more distant from the foreland than the Sardinian section. The isolated eclogitic intercalations became dismembered during thrusting and eventually exhumed in the axial zone. In the internal Variscides, exhumation was performed by the Posada detachment fault and led to the overall structure of a mantled gneiss dome.

References

Adam, J.F. 1989: Methoden und Algorythmen zur Verwaltung und Analyse axialer 3D-Richtungsdaten und ihrer Belegungsdichte. Göttinger Arb. Geol. Paläont. 40: 100S.

Ai Yang 1995. A revision of the garnet-clinopyroxene Fe2+-Mg exchange geothermometer. Contrib Mineral Petrol 115 : 467-150.

Alvarez, W. 1972. Rotation of the Corsica-Sardinia microplate. Nature, 235, 103-105.

Alvarez, W. & Cocozza, T. 1974. The tectonics of central-eastern Sardinia and the possible continuation of the Alpine Chain to the south of Corsica. In: Cherchi Pomesano A. (Ed.): Paleogeografia del Terziario Sardo nell'ambito del Mediterraneo occidentale, volume monografio, Cagliari 23-27 Luglio 1973, 5-34.

Arthaud F. & Matte, P. 1977. Late Paleozoic strike-slip faulting in southern Europe and northern Africa: result of a right lateral shear zone between the Appalachians and the Urals. Geol. Soc. Am. Bu.., 88: 1305-1320.

Arthaud F. & Sauniac S. 1981. Une coupe synthétique à travers la chaîne varisque de Sardaigne Commentaires sur l'évolution tectono-métamorphique. Bull. Soc. géol. Fr., t. XXIII, n° 5, p. 535-539.

Ashworth, J. R. 1986. Myrmekite replacing albite in prograde metamorphism. American Mineralogist, 71. 895-899.

Babin, C., Cock, L.R.R. & Walliser, H. 1980. Faciès, faunes et paléogéographie anté carbonifère de l'Europe. Mém. BRGM, 108, 90-111.

Ballèvre, M., Marchand, J., Godard, G., Goujou, J.C., Christian, J. & Wyns, R. 1994. Eo-Hercynian events in the Armorican massif. In: Keppie, J.D. (Ed.), Pre-Mesozoic Geology in France. Springer-Verlag, Berlin, pp. 183-194.

Barbey P., Cheilletz, A. & Laumonier B. 2001. The Canigou orthogneisses (Eastern Pyrenees, France, Spain): an early Ordovician rapakivi granite laccolith and its contact aureole. C. R. Acad. Sci. Paris 332. 129-136.

Barca, S. & Costamagna L. G. 1997. Compressive "Alpine" tectonics in Western Sardinia (Italy): geodynamic consequences. Comptes Rendus, Academie des Sciences Paris, série II a 325, 791-797.

Barca, S. & Palmerini, V. 1973. Contributo alla conoscenza degli ambienti di sedimentazione relativi alla 'formatione del Cixerri' (Sardegna sud-occidentale), Boll. Soc. Sarda Sc. Nat., 12, 13-50.

Barca, S., Cocozza, T., Del Rio, M., Pillola, G.L. & Pittau Demalia, P. 1987. Datation de l'Ordovicien inférieur par Dictyonema flabelliforme et Acritarches dans la partie supérieure de la formation "Cambrienne" de Cabitza (SW de la Sardaigne, Italie): Conséquences géodinamiques. C. R. Acad. Sc. Paris, t. 305, s. 2, 1109-1113.

Barca, S. 1991. Resedimentation and Hercynian flysch in Culm facies within the 'Sarrabus Syncline', SE Sardinia, Italy. Comptes-Rendus,-Academie-des-Sciences,-Serie-II a 313(9), 1051-1057.

Barca, S., Carmignani, L., Eltrudis, A., Gattiglio, M. & Pala, L. 1992. Relationships between foredeep deposits and Hercynian nappe building in south-eastern Sardinia. In: Carmignani, L. & Sassi, F.P. (Eds.) "Contributions to the geology of Italy with special regard to the Paleozoic basement" IGCP No 276, Newsletter 5, special issue, 23-44.

Barca, S., Carmignani, L., Eltrudis, A. & Franceschelli, M. 1995. Origin and evolution of the Permian-Carboniferous basin of Mulargia Lake (south-central Sardinia, Italy) related to the Late Hercynian extensional tectonics. Comptes Rendus, Academie des Sciences Paris, série II a 321, 171-178.

Barnes, H.L. 1997. Geochemistry of hydrothermal ore deposits. 3rd ed. Wiley, 972 p.

Beccaluva, L., Civetta, L., Macciotta, G. & Ricci, C. A. 1985. Geochronology in Sardinia; results and problems. In: Geochronology in Italy; results and problems. (edited by Fagnani, G.). Rendiconti della Societa Italiana di Mineralogia e Petrologia 40. Editrice Succ. Fusi., Pavia, Italy, 57-72.

Bellot, J.-P., Triboulet, C., Laverne, C. and Bronner, G. 2003. Evidence for two burial/exhumation stages during the evolution of the Variscan belt, as exemplified by P-T-t-d paths of metabasites in distinct allochthonous units of the Maures massif (SE France). Int J Earth Sci (Geol Rundsch) 92, 1: 7-26.

Berman, R.G., 1991. Thermobarometry using multi-equilibrium calculations: a new technique with petrological applications. Can. Mineral. 29, 833– 855.

Berthé, D., Choukroune, P. & Jegouzo, P. 1979. Orthogneiss, mylonite and non coaxial deformation of granites: the example of the South Armorican Shear Zone. Journal of Structural Geology 1(1), 31-42.

Bhattacharya A., Krishnakumar K.R., Raith M. & Sen S.K. 1991. An improved set of a-x parameters for Fe-Mg-Ca garnets and refinements of the orthopyroxene-garnet thermometer and the orthopyroxene-garnet-plagioclase-quartz barometer. J. Petrol. 22: 629-656.

Biino, G.G. 1994. The pre Late Ordovician metamorphic evolution of the Gotthard-Tavetsch massifs (Central Alps): from lawsonite to kyanite eclogites to granulite retrogression. Schweiz. Mineral. Petrogr. Mitt. 74, 87-104.

Bird, P. 1979. Continental delamination and the Colorado plateau. Geophys. Res., 84, 7561-7571.

Bouchez, J.L. 1977. Plastic deformation of quartzites at low temperatures in an area of natural strain gradient. Tectonophysics 39. 25-50.

Brown, E.H., 1977. The crossite content of Ca–amphibole as a guide to pressure of metamorphism. J. Petrol. 18, 53– 72.

Brun, J.-P. & Van den Driessche, J. 1994. Extensional gneiss domes and detachement fault systems: structure and kinematics. Bull. Soc. géol. France, t. 165,n° 6, pp. 519-530.

Brunet, C., Monié, P. & Jolivet, L. 1997. Geodynamic evolution of Alpine Corsica based on new Ar/Ar data. Terra Nova, 9, 493.

Bucher, K. & Frey, M. 1994. Petrogenesis of metamorphic rocks. Springer Verlag Heidelberg 1994. 318.

Calderoni G., Masi U., Maccioni L., Nicoletti M., Petrucciani C., Padalino 1984. Geochemistry and geochronology of the Caledonian <<Porphyroids>> from central Sardinia (Italy). Rend. Soc. It. Min. Petr., 39, 261-274.

Calvet P., Lapierre H. & Charvet J. 1988 Diversité du volcanisme Ordovicien dans la region de Pierrefitte (Hautes-Pyrénées) rhyolites calco-alcalines et basaltes alcalins. C. R. Acad. Sci. Paris, t. 307, Série II, p. 805-812

Calvino, F., Dieni, I., Ferasin, F. & Piccoli, G. 1958. Relazione preliminare sui rilevamenti geologici del foglio "195" Orosei (Sardegna). Boll. Soc. Geol. Ital., 77, 71-89.

Cappelli, B., Carmignani, L., Castorina, F., Di, P. A., Oggiano, G. & Petrini, R. 1992. A Hercynian suture zone in Sardinia; geological and geochemical evidence. Geodinamica Acta 5(1-2), 101-118.

Carreras, J. & Cappela, I. 1994. Tectonic levels in the Palaeozoic basement of the Pyrenees: a review and a new interpretation. 16, 11, 1509-1524.

Carmignani, L., Franceschelli, M., Pertusati, P. C., & Ricci, C. A. 1979. Evolutione tettonico-metamorphica del basamento ercinico della Nurra (Sardegna NW). Boll. Soc. Geol. It. 20. 55-81.

Carmignani, L., Franceschelli, M., Pertusati, P. C., Memmi, I. & Ricci, C. A. 1982a. An example of compositional control of the celadonitic content of muscovite and the incoming of biotite in metapelites (Nurra, NW Sardinia). N. Jb. Mineral. Mh. H. 7. 289-311.

Carmignani, L., Cocozza, T., Ghezzo, P. C., Pertusati, P. C. & Ricci, C. A. 1982b. Lineamenti del basamento sardo. In: Guida della geologia del Paleozoico sardo. Guide Geologiche Regionali. Soc. Geol. It., 11-23.

Carmignani, L., Cocozza, T., Ghezzo, P. C., Pertusati, P. C. & Ricci, C. A. 1986. Outlines of the Hercynian basement of Sardinia. In: Guide-book to the excursion on the Paleozoic basemant of Sardinia (edited by Carmingnani, L., Cocozza, T., Pertusati, P. C. & Ricci, C. A.). IGCP No. 5, Newsletter, special issue, Pisa, 11-21.

Carmignani, L. & Kligfield, R. 1990. Crustal extension in the northern Apennines: the transition from compression to extension in the Alpi Apuane core complex. Tectonics, 9, 1275-1303.

Carmignani L., Barca S., Cappelli A., Di Pisa A., Gattiglio M., Oggiano G. & Pertusati P.C. 1992a. A tentative geodynamic model for the Hercynian basement of Sardinia. In: Contributions to the geology of Italy with special regard to the paleozoic basements (edited by Carmignani, L. F. P. S.). IGCP No. 276, Newsletter 5, Siena, 61-82.

Carmignani, L., Carosi, R., Disperati, L., Funedda, A., Musumeci, G., Pasci, S. & Pertusati, P. C. 1992b. Tertiary transpressional tectonics in NE Sardinia. In: Contributions to the geology of Italy with special regard to the paleozoic basements (edited by Carmignani, L. F. P. S.). IGCP No. 276, Newsletter 5, Siena, 83-96.

Carmignani, L., Carosi, R., Di Pisa, A., Gattiglio, M., Musumeci, G., Oggiano, G. & Pertusati, P. C. 1994. The Hercynian Chain in Sardinia (Italy). Geodinamica Acta 7(1), 31-47.

Carmignani, L., Barca, S., Conti, P., Eltrudis, A., Funedda, A., Pasci, S., Oggiano, G., Pertusati, P. C. & Salvadori, I. 1996. Geological map of Sardinia. Scale 1 : 200.000. National geological survey of Italy. Firenze.

Carmignani, L., Decandia, F.A., Disperati, L., Fantozzi, P.L., Lazzarotto, A., Liotta, D. & Oggiano, G. 1995. Relationships between the Tertiary structural evolution of the Sardinia-Corsica-Provençal domain and the Northern Apennines. Terra Nova, 7, 128-137.

Carosi, R. & Elter, F. M. 1989. Le microstrutture deformative di alto grado delle anfiboliti di Torpé (Sardegna NE). Atti della Società Toscana di Science Nataturali Mememorie, A 96, 241-255.

Carosi, R., Gattiglio, M., Musumeci, G. & Oggiano, G. 1992. Geologia della catena Ercinica in Sardegna - zona a falde. In: Struttura della catena Ercinica in Sardegna – guida all'escursione. Gruppo informale di geologia strutturale (ed.). Siena Pisa. 78-145.

Carosi R., Di Vincenzo G. & Palmeri R. 2002. The relationship between metamorphic evolution and argon isotope records in white mica: constraints from the Variscan basement of Sardinia (Italy). Goldschmidt Conference Abstracts, A121.

Carosi R. & Oggiano, G. 2002. Transpressional deformation in northwestern Sardinia (Italy): insights on the tectonic evolution of the Variscan belt. Académie des science, C. R. Geoscience 334 (2002) 287-294.

Cassano, E., Marcello, A., Nannini, R., Pretti, S., Ranieri, G., Salvadori, R. & Salvadori, I. 1979. Rilievo aeromagnetico della Sardegna e del mare circostante. Ente Minerario Sardo. 3/4, 7-30.

Channell, J.E.T., D´Argenio, B. & Horváth, F. 1979. Adria, the African Promontory, in Mesozoic Mediterranean Palaeogeography. Earth Science Reviews, 15. 213-292.

Chapple, W.M. 1978. Mechanics of thin-skinned fold-and-thrust belts. Geol. Soc. Am. Bull. 89, 1189-1198.

Cherchi, A. & Montadert, L. 1982. Oligo-Miocene rift of Sardinia and the early history of the Western Mediterranean Basin. Nature 298. 736-739.

Cherchi, A. & Schröder, R. 1976. Presence de galets du Vraconien supérieur-Cénomanien basal de provenance du Sud-Ouest de la Sardaigne, Bull. Soc. Géol. Fr., 18, 1217-1219.

Cherchi, A. 1979. Microfaune aptiano (?) die ciottoli urgoniani della formazione del Cixerri (Sardegna SW) e loro interesse paleogeografico. Riv. It. Paleont. Strat. 35, 353-410.

Cocherie, A. 1978. Géochimie des terres rares dans les granodiorites. Thèse 3me cycle, Univ. Rennes.

Cocherie, A. 1984. Interaction manteau-croûte: son rôle dans la genèse d`associations plutoniques calco-alcalines, contrainets geochiniques (élément en traces et isotipes du strontium et de l´oxygen). Thèse, Doct. des Sciences, Univ. Rennes.

Cocherie, A., Rossi, P., Fouillac, A.M. & Vidal, P. 1994. Crust and mantle contributions to granite genesis – An example from the Variscan batholith of Corsica, France, studied by trace-element and Nd-Sr-O-isotope systematics. Chemical Geology 115. 173-211.

Cocozza, T. & Jacobacci, A. 1975. Geological outline of Sardinia. In: Geology of Italy. (edited by Squyres, C. H.). Earth Sci. Soc. Libyan Arab Rep., Tripoli, Libya, 49-81.

Cocozza, T., Conti, L. Cozzupoli, D., Lombradi, G. Scharbert, G. & Traversa, G. 1977. Rb/Sr age and geopetrologic evolution of crystalline rocks in southern Sulcis (Sardinia). N. Jb. Geol. Paläont. Mh., 1977, H2, 95-102.

Connolly J.A.D., Memmi I., Trommsdorff V., Franceschelli M. & Ricci C.A. 1994. Forward modeling of calc-silicate microinclusions and fluid evolution in a graphitic metapelite, northeastern Sardinia. American Mineralogist, 79, 960-972.

Conti, P. & Patta, E.D. 1998. Large scale Hercynian W-directed tectonics in southeastern Sardinia (Italy). Geodinamica Acta, 11, 217-231.

Conti, P., Carmignani, L., Oggiano, G., Funedda, A. & Eltrudis, A. 1999. From thickening to extension in the Variscan belt - kinematic evidence from Sardinia (Italy). Terra Nova 11, 93-99.

Conti, P., Funedda, A. & Cerbai, N. 1998. Mylonite development in the Hercynian basement of Sardinia (Italy). J. Struct. Geol., 20, 121-133.

Conti, P. Carmignani, L. & Funedda, A. 2001. Change of nappe transport direction during the Variscan collisional evolution of central-southern Sardinia (Italy). Tectonophysics 332. 255-273.

Costa, S. & Rey, P. 1995. Lower crustal rejuvenation and growth during post-thickening collapse; insights from a crustal cross section through a Variscan metamorphic core complex. Geology 23(10), 905-908.

Coward, M. & Dietrich, D. 1989. Alpine tectonics – an overview. In: Coward, M.P., Park, R.G. & Dietrich, D. (eds.) Alpine tectonics, Geological Society, London, Special Publications, 45, 1-29.

Cozzupoli D., Discendenti A., Lombardi G., Nicoletti M. 1971. Cronologia K-Ar delle manifestazioni eruttive del settore di Seui-Seulo (Barbagia –Sardegna). Period. Mineral., 40, 113-124.

Cozzupoli D., Discendenti A., Lombardi G., Nicoletti M. 1972. Datazione K-Ar di rocce granitoidi della Barbagia e dell'Ogliastra (Sardegna centro-orientale). Period. Mineral., 41, 113-124.

Cozzupoli D., Gerbasi G., Nicoletti M., Petrucciani C. 1984. Età K-Ar delle ignimbritti permiane di Galtellì (Orosei – Sardegna orientale). Rend. Soc. It. Min. Petr., 39, 471-476.

Cruciani, G., Franceschelli, M., Marchi, M. & Zucca, M. 2002. Geochemistry of metabasites from NE Sardinia, Italy: nature of the protoliths, magmatic trend, and geotectonic setting. Mineralogy and Petrology 74: 25-47.

Dahlen, F.A, 1990. Critical taper model of fold-and-thrust belts and accretionary wedges. Annu. Rev. Earth Planet. Sci. 18, 55-99.

Dalziel, I.W.D. 1997. Neoproterozoic-Paleozoic geography and tectonics: review, hypothesis, environmental speculation. Geological Society of America Bulletin 109. 16-42.

Dalziel, I.W.D., Dalla Salda, L.H. & Gahagan, L.M. 1994. Paleozoic Laurentia-Gondwana intercaction and the origin of the Appalachian-Andean mountain system. Geological Society of America Bulletin 106. 243-252.

Davis, D., Supp, J. & Dahlen, F.A. 1983. Mechanics of fold-and-thrust belts and accretionary wedges. J. Geophys. Res. 88, 1153-1172.

Del Moro, A., Di Simplicio, P., Ghezzo, C., Guasparri, G., Rita, F. & Sabatini, G. 1975. Radiometric data and intrusive sequence in the Sardinian Batholith. Neues Jahrbuch fuer Mineralogie. Abhandlungen 126(1), 28-44.

Del Morro, A., Di Pisa, A., Oggiano, G. & Villa, I. M. 1991. Isotopic ages of two contrasting tectonometamorphic episodes in the Variscan chain in northern Sardinia. In: Abstract, Geologia del Basamento Italiano (edited by Anonymous). Abstract, Convegno in memoria di Tommaso Cocozza, Siena.

Delaperrière, E. and Lancelot, J. 1989. Datation U-Pb sur zircon de l´orthogneiss du Capo Sartivento (Sardaigne, Italie), nouveau témoin d´un magmatisme alcaline ordovicien dans le Sud de l´Europe, C. R. Acad. Sci. Paris, 309, série II, 835-842.

Deloule E., Alexandrov P., Cheilletz B., Laumonier B. & Barbey P. 2002. In-situ U-Pb zircon ages for early Ordovician magmatism in the eastern Pyrenees, France: The Canigou orthogneisses. Int. J. Earth Science (Geol. Rundsch.) 91, 398-405.

Den Brok, S.W.J. 1989. Evidence for pre-Variscan deformation in the Lys-Caillaouas area, Central Pyrenees, France. Geologie en Mijnbouw 68. 377-380.

Demange, M. 1985. The eclogite-facies rocks of the Montagne Noire, France. Chemical Geology 50, 173-188.

Dennis, A. J. & Secor, D. T. 1987. A model for the development of crenulations in shear zones with applications from the Southern Appalachian Piedmont. Journal of Structural Geology 9(7), 809-817.

Dewey, J.F. 1988. Extensional collapse of orogens. Tectonics, 7, 1123-1139.

Dewey, J.F., Holdsworth, R.E. & Strachan R.A. 1998. Transpression and transtension zones. In: Holdsworth, R.E. & Strachan R.A. & Dewey, J.F. (eds). Continental transpressional and transtensional tectonics. Geological Society of London, Special Publications, 135, 1-14.

Dieni, I. & Massari, F. 1970. Tettogenesi gravitativa di età Oligocenica nella Sardegna centro-orientale. Boll. Soc. Geol. It. 89, 57-64.

Di Pisa, A., Gattiglio, M. & Oggiano, G. 1992. Pre-Hercynian magmatic activity in the nappe zone (internal and external) of Sardinia: Evidence of two within plate basaltic cycles. In: Contributions to the geology of Italy with special regard to the paleozoic basements (edited by Carmignani, L. F. P. S.). IGCP No. 276, Newsletter, special issue 5, Siena, 107-116.

Di Simplicio, P., Ferrara, G., Ghezzo, C., Guasparri, G., Pellizzer, R., Ricci, C. A., Rita, F. & Sabatini, G. 1974. Il metamorfismo e il magmatismo paleozoico della Sardegna. Rend. Soc. It. Min. Petr. 30, 979-1068.

Di Vincenzo, G., Ghezzo, C. & Tonarini, S. 1994. Geochemistry and Rb-Sr geochronology of the Hercynian peraluminous Sos Canales pluton (central Sardinia, Italy). Comptes Rendus, Academie des Sciences Paris, série II a 319 (7), 783-790.

Doglioni, C., Gueguen, E., Harabaglia, P. & Mongelli, F. 1999. On the origin of west-directed subduction zones and applications to the western Mediterranean. In: Durand, B., Jolivet, L., Horváth, F. & Séranne, M. (eds) The Mediterranean basins: Tertiary extension within the Alpine orogen. Geological Society, London, Special Publications, 156, 541-561.

Dooley, D.F. & Patiño Douce, A.E. 1996. Fluid-absent melting of F-rich phlogopite + rutile + quartz. American Mineralogist, 81, 202-212.

Druguet 2001. Development of high thermal gradients by coeval transpression and magmatism during the Variscan orogeny: insights from the Cap de Creus (Eastern Pyrenees). Tectonophysics 332, 275-293.

Durand-Delga, M. 1978. Corse. Guides géologiques régionaux. Masson, Paris, 208 pp.

Echtler, H. & Malavieille, J. 1990. Extensional tectonics, basement uplift and Stephano-Permian collapse basin in a late Variscan metamorphic core complex (Montagne Noire, southern Massif Central). Tectonophysics 177(1-3), 125-138.

Echtler, H. 1990. Geometry and kinematics of recumbent folding and low-angle detachment in the Pardailhan Nappe (Montagne Noire, southern French Massif Central). Tectonophysics 177(1-3), 109-123.

Edel J.B., Montigny R., Thuizat R. 1981. Late Paleozoic rotations of Corsica and Sardinia: New evidence from Paleomagnetic and K-Ar studies. Tectonophysics, 79, 210-223.

Edel, J.-B. 2001. The rotations of the Variscides during the Carboniferous collision: paleomagnetic constraints. Tectonophysics 332, 69-92.

Eeckhout, B. v. d. & Zwart, H.J. 1988. Hercynian crustal-scale extensional shear zone in the Pyrenees. Geology 16, 135-138.

Ellis, D.J. & Green, D.H., 1979. An experimental study of the effect of Ca upon garnet–clinopyroxene Fe –Mg exchange equilibria. Contrib. Mineral. Petrol. 71, 13– 22.

Elter, F. M., Franceschelli, M., Ghezzo, C., Memmi, I. & Ricci, C. A. 1986. The geology of northern Sardinia. In: Guide-book to the excursion on the Paleozoic basemant of Sardinia (edited by Carmingnani, L., Cocozza, T., Pertusati, P. C. & Ricci, C. A.). IGCP No. 5, Newsletter, special issue, Pisa, 87-102.

Elter, F. M., Musumeci, G. & Pertusati, P. C. 1990. Late Hercynian shear zones in Sardinia. Tectonophysics 176(3-4), 387-404.

Engel, W. 1984. Migration of folding and flysch sedimentation on the southern flank of the Variscan belt. Z. Dtsch. Geol. Ges. 135. 279-292.

Fais, S., Klingele, E. E. & Tocco, R. 1994. Geophysical interpretation of the Gallura magnetic anomaly (North-east Sardinia, Italy). Tectonophysics 233(1-2), 125-144.

Feraud, G. 1990. 39Ar/40Ar analysis on basaltic lavas series of Vavilov basin, Tyrrhenian sea (Ocean Drilling Program, Leg. 107, Holes 655B and 651A). In: Proceedings of the ODP Sci. Results, 107. 92-97.

Ferrara, G., Ricci, C. A. & Rita, F. 1978. Isotopic ages and tectono-metamorphic history of the metamorphic basement of northeastern Sardinia. Contributions to Mineralogy and Petrology 68(1), 99-106.

Ferré, E.C. & Leake, B.E 2001. Geodynamic significance of early orogenic high-K crustal and mantle melts: example of the Corsica batholith. Lithos 59, 47-67.

Ferry J.M. & Spear F.S. 1978. Experimental calibration of the partitioning of Fe and Mg between biotite and garnet. Contrib Mineral Petrol 66: 113-117.

Finger, F. & Steyrer, H. P. 1990. I-type granitoids as indicators of a late Paleozoic convergent ocean-continent margin along the southern flank of the central European Variscan orogen. Geology 18(12), 1207-1210.

Finger, F., Roberts, M.P., Haunschmidt, B., Schermaier, A. & Steyrer, H.P. 1997. Variscan granitoids of central Europe: their typology, potential sources and tectonothermal relations. Mineralogy & Petrology 61, 67-96.

Fleitout, L. & Froidevaux, C. 1982. Tectonics and topography for a lithosphere containing density heterogeneities. Tectonics, 1, 21-56.

Franceschelli, M., Memmi, I. & Ricci, C. A. 1982. Zoneografia metamorfica della Sardegna settentrionale. In: Guida alla geologia del Paleozoico Sardo (edited by Carmignani, L., Cocozza, T., Ghezzo, C., Pertusati, P. C. & Ricci, C. A.). Memorie della Societa Geologica Italiana. 24; Suppl B. Societa Geologica Italiana, Rome, Italy, 137-149.

Franceschelli, M., Memmi, I. & Ricci, C.A. 1982b. Ca distribution between almandine-rich garnet and plagioclase in pelitic and psammitic schists from the metamorphic basement of northeast Sardinia. Contrib Mineral Petrol 80: 285-295.

Franceschelli, M., Memmi, I., Pannuti, F. & Ricci, C. A. 1989. Diachronous metamorphic equilibria in the Hercynian basement of northern Sardinia, Italy. In: Evolution of metamorphic belts; proceedings of the 1987 joint meeting of the Metamorphic Studies Group and IGCP project 235. (edited by Daly, J. S., Cliff, R. A. & Yardley, B. W. D.). Geological Society Special Publications 43. Geological Society of London, London, United Kingdom, 371-375.

Franceschelli, M., Pannuti, F. & Puxeddu, M. 1990. Texture development and PT time path of psammitic schist from the Hercynian chain of NW Sardinia (Italy). European Journal of Mineralogy 2(3), 385-398.

Franceschelli, M., Pannuti F. & Carcangiu G. 1991. The formation of fibrolite nodules in a package of melanocratic gneisses from the Hercynian basement of NE Sardinia, Italy. Schweiz. Mineral. Petrogr. Mitt. 71, 427-439.

Franceschelli, M., Gattiglio, M., Pannuti, F. & Fadda, S. 1992. Illite crystallinity in pelitic rocks form the external and nappe zones of the Hercynian chain of Sardinia. In: Contributions to the geology of Italy with special regard to the paleozoic basements (edited by Carmignani, L. & Sassi, F. P.). IGCP No. 276, Newsletter, special issue 5, Siena, 127-135.

Franceschelli, M., Eltrudis, E., Memmi, I., Palmeri, R., Carcangiu, G., 1998. Multi-stage metamorphic re-equilibration in eclogitic rocks from the Hercynian basement of NE Sardinia, Italy. Mineral. Petrol. 62, 67–193.

Franke, W., Eder, W., Engel, W. & Langenstrassen, F. 1978. Main aspects of geosynclinal sedimentation in the Rhenohercynian zone. Z. dt. geol. Ges. 129, 201-216.

Franke, W. 1989. Variscan plate tectonics in Central Europe: current ideas and open questions. In: Palaeozoic plate tectonics with emphasis on the European Caledonian and Variscan belts. (edited by Matte, P. & Zwart, H. J.). Tectonophysics 169. Elsevier, Amsterdam, Netherlands, 221-228.

Frisch, W. & Neubauer, F. 1989. Pre-Alpine terranes and tectonic zoning in the eastern Alps. Geological Society of America, Special Paper 230, 92-100.

Fuhrman M.L. & Lindsley D.H. 1988. Ternary feldspar modeling and thermometry. Am Mineral 73: 201-215.

Ganguly, J. & Saxena, S. K. 1984. Mixing properties of aluminosilicate garnets: constaints from natural and experimental data, and application in geothermo-barometry. American Mineralogist 69. 88-97.

Ganguly, J. & Saxena, S. K. 1985. Mixing properties of aluminosilicate garnets: constaints from natural and experimental data, and application in geothermo-barometry: Clarifications. American Mineralogist 70, 1320.

Ghezzo, C., Memmi, I. & Ricci, C. A. 1979. Un evento granulitico nel basamento metamorphico della Sardegna nord-orientale. Mem Soc Geol It, 20. 23-38.

Ghiorso M.S., Evans B.W., Hirschmann M.M- & Yang H. 1995. Thermodynamics of the amphibole Fe-Mg cummingtonite solid solutions. Am Mineral 80: 502-519.

Gibson, R. L. 1991. Hercynian low-pressure-high-temperature regional metamorphism and subhorizontal foliation development in the Canigou Massif, Pyrenees, France; evidence for crustal extension. Geology 19(4), 380-383.

Gil Ibarguchi J.I., Navidad M. & Ortega L.A. 1990. Ordovician and Silurian igneous rocks and orthogneisses in the Catalonian Coastal Ranges. Acta Geol. Hisp. v. 25, n° 1-2, pàgs. 23-29.

Gleizes, G., Leblanc, D., Olivier, P. & Bouchez, J. L. 2001. Strain partitioning in a pluton during emplacement in transpressional regime: the example of the Néouvielle granite (Pyrenees). Int J Earth Sci 90. 325-340.

Gower R.J.W. & Simpson C. 1992. Phase boundary mobility in naturally deformed, high-grade quartzofeldspathic rocks: evidence for diffusional creep. J. Struct. Geol. 14, 301-314.

Graessner, T. & Schenk, V. 1999. Low-pressure metamorphism of Paleozoic pelites in the Aspromonte, southern Calabria: constraints for the thermal evolution in the Calbrian crustal cross-section during the Hercynian orogeny. Journal of Metamorphic Geology 17(2), 157-172.

Graessner, T., Schenk, V., Bröcker, M. & Mezger, K. 2000. Geochronological constraints on the timing of granitoid magmatism, metamorphism and post-metamorphic cooling in the Hercynian crustal cross-section of Calabria. J. metamorphic Geol. 18, 409-421.

Grevola, G. & Pupin, J.-P. 1994. Crystalline Provence: structure and Variscan evolution. In: Keppie (Ed.). Pre-Mesozoic geology in France and related areas. Springer-Verlag Berlin Heidelberg. 426-441.

Gross, A. F. K. & Van Heege, J. P. T. 1973. The high-low quartz transition up to 10 kb pressure. Journal of Geology 81, 717-724.

Hanchar J.M. & Miller C.F. 1993. Zircon zonation patterns as revealed by cathodoluminescence and backscattered electron images: implications for interpretation of complex crustal histories. Chem. Geol. 110, 1-3

Handy M.R., Franz L., Heller F., Janott B. & Zurbriggen R. 1999. Multistage accretion and exhumation of the continental crust (Ivrea crustal section, Italy and Switzerland). 18, 6, 1154-1177.

Harland, W.B. 1971. Tectonic transpression in Caledonian Spitzbergen. Geol. Mag. 108: 27-42.

Harley, S.L., 1984. The solubility of alumina in orthopyroxene coexisting with garnet in FeO–MgO–Al2O3–SiO2 and CaO–FeO–MgO–Al2O3–SiO2. J. Petrol. 25, 665– 696.

Harley, S.L., Green, D.H., 1982. Garnet– orthopyroxene barometry for granulites and peridotites. Nature 300, 697–701.

Hartevelt, J. J. A., 1970. Geology of the Upper Segre and Valira valleys, Central Pyrenees, Andora/Spain. Leidse Geol. Meded., 45, 167-236.

Hiller, O.K. 1981. Die Gebirgstreppe Ostsardiniens – Eine geomorphologische Analyse. Augsburger Geographische Hefte. ISBN 3-922481-02-7. Heft Nr. 3. 171 S.

Hinton R.W. & Upton B.G.J. 1991. The chemistry of zircon: variations within and between large crystals from syenite and alkali basalt xenoliths. Geochim. Cosmochim. Acta 55. 3287-3302.

Hodges, K. V. & Crowley, P. D. 1985. Error estimation and empirical geothermobarometry for pelitic systems. American Mineralogist 70. 702-9.

Hoeppener, R. 1955. Tektonik im Schiefergebirge. Geol Rundsch, 44. 26-58.

Hofmann, A. W. 1993. Limits of whole-rock dating methods: view of a geochemist. In: Radiometric Age Determinations in Orogenic Processes - Potentials and Limits (Funiciello, R., Ricci, C.A., and Trommsdorff, V., editors). Proceedings of the VI Summer School Earth and Planetary Sciences, Siena 1993, 53-65.

Hoisch, T.D. 1989. A muscovite-biotite geothermometer. Am. Mineral. 74, 565-572.

Hoisch, T.D. 1990. Empirical calibration of six geobarometers for the mineral assemblage quartz + muscovite + biotite + plagioclase + garnet. Contrib Mineral Petrol 104: 225-234.

Holdaway, M. J. 1971. Stability of andalusite and the aluminum silicate phase diagram. Am J Sci, 271, 97-131.

Holland, T.J.B., 1983. The experimental determination of activities in disordered and short-range ordered jadeitic pyroxenes. Contrib. Mineral. Petrol. 82, 214–220.

Houseman, G.A., McKenzie, D.P. & Molnar, P. 1981. Convective instability of a thickened boundary layer and its relevance for the thermal evolution of the continental crust. Journal of Geophysical Research, 86, 6115-6132.

Howell, D.G., Jones, D.L., Schermer, E.R. 1985. Tectonostratigraphic terranes of the circum-Pacific region. In: Howell, D.G. (Ed.), Tectonostratigraphic terranes of the circum-Pacific region. Circum-Pacific Council for Energy and Mineral Resources, Houtson, pp. 3-30.

Huang, W. L. & Wyllie, P. J. 1981. Phase relationship of S-type granite with H2O to 35 kbar: Muscovite granite from Harney Peak, South Dakota, J Geophys Res 86. 1,015-1,029.

Hunziker, J.C. & Zingg, A. 1980. Lower Palaeozoic amphibolite to granulite facies metamorphism in the Ivrea zone (southern Alps, northern Italy). Schweiz. Mineral. Petrogr. Mitt., 54, 229-242.

Indares A. & Martignole J. 1985. Biotite-garnet geothermometry in the ganulite facies: the influence of Ti and Al in biotite. Am Mineral 70: 272-278.

Jamieson R.A. & O´Beirne-Ryan A.M. 1991. Decompression-induced growth of albite porphyroblasts, Fleur de Lys supergroup, western Newfoundland. J. metamorphic Geol. 9, 433-439.

Jessell, M.W. 1988. Simulation of fabric development in recrystallizing aggregates:2 Example model runs. J Struct Geol 10. 779-793.

Jolivet, L., Daniel, J.M. & Fournier, M. 1991. Geometry and kinematics of extension in Alpine Corsica. Earth and Planetary Science Letters. 104. 278-291.

Jolivet, L., Frizon de Lamotte, D., Mascle, A. & Séranne, M. 1999. The Mediterranean basins: Tertiary extension within the Alpine orogen – an introduction. In: Durand, B., Jolivet, L., Horváth, F. & Séranne, M. (eds) The Mediterranean basins: Tertiary extension within the Alpine orogen. Geological Society, London, Special Publications, 156, 1-14.

Julivert M. & Durán H. 1990. Paleozoic stratigraphy of the Central and Northern part of the Catalonian Coastal Ranges (NE Spain). Acta Geol. Hisp. v. 25, n° 1-2, pàgs. 3-12.

Keller, J.V.A. & Lynch, G. 2000. Displacement transfer and forced folding in the Maritimes basin of Nova Scotia, eastern Canada. In: Forced folds and fractures. Cosgrove, J.W. & Ameen, M.S. (eds). Geological Society, London, Special Publication, 169. 87-101.

Kerrick, D. M. 1972. Experimental determination of muscovite + quartz stability with PH2O < Ptotal. Am J Sci 272. 946-958.

Ketchum J.W.F., Jackson S.E., Culshaw N.G. & Barr S.M. 2001. Depositional and tectonic setting of the Paleoproterozoic Lower Aillik Group, Makkovik Province, Canada: evolution of a passive margin – foredeep sequence based on petrochemistry and U-Pb (TIMS and LAM-ICP-MS) geochronology. Precambrian Research 105, 331-356.

Kretz, R. 1983. Symbols of rock-forming minerals. American Mineralogist, 68. 277-279.

Kriegsman, L. M., Aerden, D. G. A. M., Bakker, R. J., den Brok, S. W. J. & Schutjens, P. M. T. M. 1989. Variscan tectonometamorphic evolution of the eastern Lys-Caillaouas massif, Central Pyrenees – evidence for late orogenic extension prior to peak metamorphism. Geologie en Mijnbouw 68. 323-333. 1989.

Krogh E.J. 1988. The garnet-clinopyroxene Fe-Mg geothermometer – a reinterpretation of existing experimental data. Contrib Mineral Petrol 99: 44-48.

Kroll H., Evangelakakis C. & Voll G. 1993. Two-feldspar geothermometry: a review and revision for slowly cooled rocks. Contrib Mineral Petrol 114: 510-518.

Kruhl J.H. 1993. The P-T-t development at the basement-cover boundary in the north-eastern Tauern Window (Eastern Alps): Alpine continental collision. J. Metamorphic Geol. 11, 31-47.

Kruhl, J. H. 1996. Prism- and basal-plane parallel subgrain boundaries in quartz: a micro-structural geothermobarometer. Journal of Metamorphic Geology 14(5), 581-589.

Kruhl, J. H. 1998. Prism- and basal-plane parallel subgrain boundaries in quartz: a microstructural geothermobarometer: Reply. Journal of Metamorphic Geology 16, 142-146.

Läufer A.L., Hubich D. & Loeschke J. 2001. Variscan geodynamic evolution of the Carnic Alps (Austria/Italy). Int. J. Earth Science (Geol. Rundsch) 90, 855-870.

Laurent, P. & Arthaud, F. 1993. "Sardic Orogeny": a distictive event during Ordovician. Terra Abstracts 5(1), 207.

Laurenzi M.A., Del Moro A, Musumeci G. & Pardini G. 1991. Rb/Sr and Ar/Ar chronology of Monte Grighini intrusive complex (Sardinia, Italy), Terra abstract, 3, 1, 501-502.

Law, R.D. 1990. Crystallographic fabrics: a selective review of their applications to research in structural geology. In: Knipe, R.J., Rutter, E.H. (eds). Deformation mechanisms, reology and tectonics. Geol Soc Spec Publ 54. 335-352.

Le Breton, N. & Thompson, A. B. 1988. Fluid-absent (dehydration) melting of biotite in metapelites in the early stage of crustal anatexis. Contrib Mineral Petrol 99. 226-237.

Le Corre, C. 1994. Early tectonic events (Ordovician). In: Keppie, J.D. (Ed.), Pre-Mesozoic Geology in France. Springer-Verlag, Berlin, pp. 179-182.

Le Gall, B. 1990. Evidence of an imprecate crustal thrust belt: the south British Variscides. Contribution of SWAT deep seismic reflection profiles recorded through the English Channel and the Celtic sea. Tectonics, 9(2): 283-302.

Lee, H.Y., Ganguly, S., 1988. Equilibrium compositions of coexisting garnet and orthopyroxene: experimental determinations in the system FeO–MgO–Al2O3 –SiO2 and applications. J. Petrol. 29, 93– 113.

Leyreloup, A., Buscail, F., Motard, C., Ciancaléoni, l., Dumoulin-Thiault, C., Lavigne, J.F., Monié, P. & Brunel, M. 1996. Découvertes de paragenèse de types schists blancs dans les

Liou, J. G., Kuniyoshi, S. & Ito, K. 1974. Synthesis and stability reactions of epidote, Ca2Al2Si3O10(OH). J Petrol 14. 381-413.

Lister, G. S. & Snoke, A. W. 1984. S-C-Mylonites. Journal of Structural Geology 6(6), 617-638.

Lister, G.S. & Dornsiepen, U.F. 1982. Fabric transitions in the Saxony granulite terrain. J Struct Geol 41. 81-92.

Lister, G.S. & Hobbs, B.E. 1980. The simulation of fabric development and its application to quartzite; the influence of deformation history. J Struc Geol 2: 355-371.

Loi A. & Dabard M.P. 1997. Zircon typology and geochemistry in the paleogeographic reconstruction of the Late Ordovician of Sardinia (Italy). Sedimentary Geology 112, 263-279.

Lombardi G., Cozzupoli D., Nicoletti M. 1974. Notizie geopetrografiche e dati sulla cronologia K-Ar del vulcanesimo tardopaleozoico sardo. Period. Mineral., 43, 221-312.

Ludwig K.R. 2000. Isoplot – a geochronological toolkit for Microsoft Excel. Berkeley Geochronology Center, Special Publication No. 1a, 53 pp.

Lüneburg, C.M. & Lebit, H.D.W. 1998. The development of a single cleavage in an area of repeated folding. J. Structural Geol. 20, 11: 1531-1548.

Macera P., Conticelli S., Del Morro A., Di Pisa A., Oggiano G. & Squadrone A. 1989. Geochemistry and Rb-Sr age of syn-tectonic peraluminous granites of Western Gallura, Northern Sardinia: constraints on their genesis. Per. Mineral, 58, 25-43.

Machado N. & Simonetti A. 2001. U-Pb dating and Hf isotopic composition of zircon by Laser-Ablation-MC-ICP-MS. In: Laser-Ablation-ICPMS in the earth science principles and applications. Sylvester P. (Ed.), Short Course Series Volum 29, Mineralogical Association of Canada, 121-147.

Malavielle, J. 1993. Late orogenic extension in mountain belts: insights from the basin and range and the late Paleocoic Variscan belt. Tectonics 12, 1115-1130.

Malinverno, A. & Ryan, W.B.F. 1986. Extension in the Tyrrhenian sea and shortening in the Apennines as a result of arc migration driven by sinking of the lithosphere, Tectonics, 5, 227-245.

Maluski, H. 1977. Application de la méthode ^{40} Ar-^{39}Ar aux minéraux des roches cristallines perturbées par des événements thermiques en Corse. Bull. Soc. Géol. Fr., 7, 4: 849-855.

Maluski H., Costa, S. & Echtler, H. 1991. Late Variscan tectonic evolution by thinning of earlier thickened crust. An ^{40} Ar-^{39}Ar study of the Montagne Noire, southern Massif Central, France. Lithos 26, 287-304.

Marjoribanks, R.W. 1976. The relation between microfabric and strain in a progressively deformed quartzite sequence from central Australia. Tectonophysics 32. 269-293.

Massari, F. & Dieni I. 1983. Pelagic Oncoids and Ooids in the Middle-Upper Jurassic of eastern Sardinia. In: Coated Grains (ed. by T.M. Peryt). Spinger-Verlag Berlin Heidelberg. 367-376.

Massone, H.J. & Schreyer, W. 1987. Phengite geobarometry based on the limiting assemblage with K-feldspar, phlogopite and quartz. Contrib. Mineral. Petrol., 96, 212-24.

Matte, P. 1991. Accretionary history and crustal evolution of the Variscan Belt in Western Europe. In: Accretionary tectonics and composite continents. (edited by Hatcher, R. D., Jr. & Zonenshain, L.). Tectonophysics 196. Elsevier, Amsterdam, Netherlands, 309-337.

Matte, P., Lancelot, J. & Mattauer, M. 1998. La zone axiale hercynienne de la Montagne Noire n'est pas un "metamorphic core complex" extensive mais un anticlinal post-nappe à Coeur anatectique. Geodinamica Acta 11 (1), 13-22.

Matte, P. 2001. The Variscan collage and orogeny (480-290 Ma) and the tectonic definition of the Armorica microplate: a review. Terra Nova 13. 122-128.

Meli S. & Klötzli U.S. 2001. Evidence for lower Paleozoic magmatism in the eastern Southalpine basement: zircon geochronology from Comelico porphyroids. Schweiz. Mineral. Petrogr. Mitt. 81, 147-157.

Memmi, I., Barca, S., Carmignani, L., Coccozza, T., Elter, F. M., Franceschelli, M., Gattiglio, M., Ghezzo, C., Minzoni, N., Naud, G., Pertusati, P. & Ricci, C. A. 1983. Further geochemical data on the Pre-Hercynian igneous activities of Sardinia and on their geodynamic significance (edited by Sassi & Szederkenyi). IGCP 5, Newsletter 5, 87-93.

Miller, C., Sassi, F. P. & Armari, G. 1976. On the occurrence of altered eclogitic rocks in north-eastern Sardinia and their implications. N. Jb. Geol. Paläont. Mh., H. 11, 683-689.

Molnar, P. & Tapponnier, P. 1975. Cenozoic tectonics of Asia: Effects of a continental collision. Science 189, 419-426.

Morillon A.-C., Féraud, G., Sosson, M., Ruffet, G., Grevola, G. & Lerouge, G. 2000. Diachronous cooling on both sides of a major strike slip fault in the Variscan Maures massif (southeast France), as deduced from a detailed $^{40}Ar/^{39}Ar$ study. Tectonophysics 321, 103-126.

Moussavou, M. 1998. Contribution à l'histoire thermo-tectonique varisque du massif des Maures, par la typologie du zircon et la geochronology U-Pb sur minéraux accessoires. Ph.D. thesis, Université Montpellier II. 187 pp.

Musumeci, G. 1992. Ductile wrench tectonics and exhumation of Hercynian metamorphic basement in Sardinia; Monte Grighini Complex. In: Symposium "Palaeozoic orogenies in Europe; Tectonics, magmatism and evolution". (edited by Anonymous). Geodinamica Acta 5. Masson, Paris, France, 119-133.

Nägler, T.F., Schäfer, H.J. & Gebauer, D. 1995. Evolution of the western European continental crust: implications from Nd and Pb isotopes in Iberian sediments. Chemical Geology 121, 345-357.

Nardi, R., Puccinelli, A. & Verani, M. 1979. Carta geologica della Balagne "sedimentaria" (Corsica). Alla scala 1:25000 e note illustrative. Bull. Soc. Geol. Italia 97: 11-30.

Newton, R. C. & Haselton, H. T. 1981. Thermodynamics of the garnet-plagioclase-Al2SiO5-quartz geobarometer. In: Newton, R. C., Navrotsky, A. & Wood, J. (eds) Thermodynamics of minerals and melts, Springer-Verlag, New York. 131-47.

Newton, R.C., Perkins, D., 1982. Thermodynamic calibration of geobarometers based on the assemblages garnet–plagioclase–orthopyroxene – (clinopyroxene)–quartz. Am. Mineral. 67, 203– 222.

Nicoletti M., Ardanese L.R., Colasanti S. 1982. La granodioritie di Capo Carbonara (Sardegna – Italy). Età K/Ar di fasi minerali in paragneiss. Rend. Soc. It. Min. Petr., 38, 765-769.

Oberli F., Meier M. & Biino G.G. 1994. Time constraints on the pre-Variscan magmatic/metamorphic evolution of the Gotthard and Tavetsch units derived from single-zircon U-Pb results. Schweiz. Mineral. Petrogr. Mitt. 74, 483-488.

Oggiano, G. & Di Pisa, A. 1988. I graniti peralluminiferi sin-tettonici nell' area di Aggius-Trinita d'Agultu e loro rapporti con le metamorfiti di alto grado della bassa Gallura (Sardegna settentrionale). Boll. Soc. Geol. It 107, 471-480.

Oggiano, G. & Di Pisa, A. 1992. Geologia della catena Ercinica in Sardegna - zona assinale. In: Struttura della catena Ercinica in Sardegna – guida all'escursione. Gruppo informale di geologia strutturale (ed.). Siena Pisa. 147-177.

Palmeri, R., Fanning, M., Franceschelli, M., Memmi, I., Ricci, C.A. 1997. New petrological and geochronological data on the eclogite of Pta de Li Tulchi, NE Sardinia (Italy). IEC97: Fifth International Eclogite Conference, Ascona, CH.

Paquette, J.-L., Peucat, J.J., Bernard-Griffiths, J. & Marchand, J., J. 1985. Evidence for old pre-Cambrian relics shown by U-Pb zircon dating of eclogites and associated rocks in the Hercynian belt of Brittany, France. Chemical Geology 52, 203-216.

Paquette, J.-L., Gleizes, G., Leblanc, D. & Bouchez, J.L. 1997. Le granite de Bassiès (Pyrénées): un pluton syntectonique d'âge westphalien. Comptes Rendus de l'Académie des Siences 324, 387-392.

Paquette, J.-L., Ménot, R.P. & Peucat, J.J. 1989. REE, Sm-Nd and U-Pb zircon study of eclogites from the Alpine External Massifs (Western Alps): evidence for crustal contamination. Earth Planet Sic Lett 96: 181-198.

Paquette, J.-L., Ménot, R.-P., Pin, C. & Orsini, J.-B. 2003. Episodic and short-lived granitic pulses in a post-collsional setting: evidence from precise U-Pb zircon dating through a crustal cross-section in Corsica. Chemical geology 198, 1-20.

Passchier, C.W. & Trouw, R.A.J. 1996. Microtectonics. Springer-Verlag Heidelberg 1996. 289.

Patiño Douce A.E., Johnston A.D. & Rice J.M. 1993. Octahedral excess mixing properties in biotite: a working model with applications to geobarometry and geothermometry. Am Mineral 78: 113-131.

Patiño Douce, A. E. & Harris, N. 1998. Experimental constraints on Himalayan anatexis. J Petrol 39. 689-710.

Perkins, D., Chipera, S.J., 1985. Garnet – orthopyroxene – quartz barometry refinement and application to the English River subprovince and the Minnesota River Valley. Contrib. Mineral. Petrol. 89, 69– 80.

Peucat, J.J., Paris, F., & Chalet, M. 1986: U-Pb zircon dating of volcanic rocks close to the Silurian-Devonian boundary from Vendée (western France). Chemical Geology 59, 133-142.

Phillips, E. R., Ransom, D. M. & Vernon, R. H. 1972. Myrmekite and muscovite developed by retrograde metamorphism at Broken hill, New South Wales. Min Mag 38. 570-8.

Pin, C. & Marini, F. 1993. Early Ordovician continental break-up in Variscan Europe: Nd-Sr isotope and trace element evidence for bimodal igneous associations of the Southern Massif Central, France. Lithos 29: 177-196.

Platt, J. P. & Vissers, R. L. M. 1980. Extensional structures in anisotropic rocks. Journal of Structural Geology 2(4), 397-410.

Platt, J.P. & England, P. 1994. Convective removal of lithosphere beneath mountain belt: thermal and mechanical consequences. American Journal of Science, 294, 307-336.

Platt, J.P. 1986. Dynamics of orogenic wedges and uplift of high-pressure metamorphic rocks. Geol. Soc. Am. Bull. 79, 1037-1053.

Platt, J.P. 1993. Exhumation of high-pressure rocks: a review of concepts and processes. Terra Nova 5, 119-133.

Plyusnina L.P. 1982. Geothermometry and gerobarometry of plagioclase-hornblende-bearing assemblages. Contrib Mineral Petrol 80: 140-146.

Poli, G., Ghezzo, C. & Conticelli, S. 1989. Geochemistry of granitic rocks from the Hercynian Sardinia-Corsica batholith: Implication for magma genesis. Lithos 23, 247-266.

Poll, J.J.K. & Zwart, H.J. 1964. On the tectonics of the Sulcis area, S. Sardinia. Geol. En Mijnbow 43, 4, 144-146.

Poll, J.J.K. 1966. The geology of the Rosas-Terreseo area (Sulcis, South Sardinia). Leidse Geologische Mededelingen, deel 35. 117-208.

Powell R. & Holland T.J.B. 1988. An internally consistent thermodynamic data set with uncertainties and corrections. 3. Applications to geobarometry, worked examples and a computer program. J. Metam. Geol. 6: 173-204.

Powell, R., 1985. Regression diagnostics and robust regression in geothermometer/geobarometer calibration: the garnet–clinopyroxene geothermometer revisited. J. Metamorph. Geol. 2, 231–243.

Ramsay J.G. 1967. Folding and fracturing of rocks. McGraw Hill, New York.

Raumer J.F. von 1998. The Palaeozoic evolution in the Alps: from Gondwana to Pangea. Geol Runsch 87. 407-435.

Raumer J.F. von, Stampfli G.M., Borel G. & Bussy, F. 2002. Organization of pre-Variscan basement areas at the north-Gondwanan margin. Int. J. Earth Science (Geol. Rundsch) 91, 35-52.

Rehault, J.P., Boillot, G. & Mauffret, A. 1984. The Western Mediterranean basin geological evolution. Marine Geology, 55. 447-477.

Ricci, C. A. 1992. From crustal thickening to exhumation: petrological, structural and geochronological records in the crystalline basement of Northern Sardinia. In: Contributions to the geology of Italy with special regard to the paleozoic basements, A volume dedicated to Tommaso Cocozza (edited by Carmignani, L. & Sassi, F. P.). IGCP No. 276, Newsletter 5, Siena, 187-197.

Ricci, C.A. & Sabatini, G. 1978. Petrogenetic affinity and geodynamic significance of metabasic rocks from Sardinia, Corsica and Provence. N. Jb. Miner. Mh., 1, 23-38.

Robardet, M., Paris, F. & Racheboeuf, P. R. 1990. Palaeogeographic evolution of southwestern Europe during early Palaeozoic times. In: Palaeozoic palaeogeography and biogeography. (edited by McKerrow, W. S. & Scotese, C. R.). Memoir - Geological Society of London 12. Blackwell [for the] Geological Society of London, London, United Kingdom, 411-419.

Robardet M., Verniers, J., Feist R. & Paris F. 1994. Le Paleozoique ante-varisique de France, contexte paleogeographique et geodynamique. Geologie de la France, 3, 3-31.

Robardet, M. 2003. The Amorican 'microplate': fact or fiction? Critical review of the concept and contradictory palaeobiogeographical data. Palaeogeography, Palaeoclimatology, Palaeoecology 3076: 1-24.

Romer, R.L. & Franz, L. 1998. Ordovician Barrow-type metamorphism in the Strona-Ceneri Zone (northern Italy) dated by U-Pb on staurolite, Schweiz. Mineral. Petrogr. Mitt. 78 (3)383-395.

Rottura, A., Bargossi, G.M., Caironi, V., Del Moro, A., Maccarrone, E., Macera, P., Paglionico, A., Petrini, R., Piccaretta, G. & Poli, G. 1990. Petrogenesis of contrasting Hercynian granitoids from the Calabrian Arc, southern Italy. Lithos 24, 97-119.

Saint Blanquat, M. de, Lardeaux, J. M. & Brunel, M. 1990. Petrological arguments for high-temperature extensional deformation in the Pyrenean Variscan crust (Saint Barthélémy Massif, Ariège, France). Tectonophysics 177. 245-262.

Sanderson, D.J. & W.R.D. Marchini 1984. Transpression. J. Struct. Geol. 6: 449-485.

Santanach, P. 1974. Estudi tectónic del Paleozoic inferior del Pirineu entre la Cerdanya i el riu Ter. Tesis, Univ. Barcelona, Pub. Fund. S. Vives Casajuana, pp. 1-131.

Scandone, P. 1979. Origin of the Tyrrhenian sea and the Calabrian arc. Boll. Soc. Geol. Ital., 98, 27-34.

Schaltegger, U. 1994. Unravelling the pre-Mesozoic history of Aar and Gotthard massifs (Central Alps) by isotopic dating – a review. Schweiz. Mineral. Petrogr. Mitt. 74, 41-51.

Scharbert, S. 1978. Supplementary remarks on the "Rb/Sr age and geopetrologic evolution of crystalline rocks in southern Sulcis (Sardinia)" by Cocozza et al. (1977). N. Jb. Geol. Paläont. Mh., 1978, h, 1, 59-64.

Schenk, V. 1981. Synchronous uplift of the lower crust of the Ivrea zone and of Southern Calabria and its possible consequences for the Hercynian orogeny in Southern Europe. Earth and Planetary Science Letters, 56. 305-320.

Schmid, S.M. & Casey, M. 1986. Complete fabric analysis of some commonly observed quartz C-axis patterns. Geophys Monogr 36. 263-286.

Searl, M.P. & Rex, A.J. 1989. Thermal model for the Zanskar Himalaya. J.Metam. Geol. 7, 127-134.

Selverstone, J. 1988. Evidence for east-west crustal extension in the Eastern Alps: Implications for the unroofing history of the Tauern Window. Tectonics 7. 87-105.

Sen, S.K., Bhattacharya, A., 1984. An orthopyroxene–garnet thermometer and its application to Madras charnockites. Contrib. Mineral. Petrol. 86, 359– 373.

Séranne, M. 1999. The gulf of Lion continental margin (NW Mediterranean) revisited by IBS: An overview. In: Durand, B., Jolivet, L., Horváth, F. & Séranne, M. (eds) The Mediterranean basins: Tertiary extension within the Alpine orogen. Geological Society, London, Special Publications, 156, 15-36.

Shelley, D. 1993. Igneous and metamorphic rocks under the microscope. Chapman and Hall, London 1993. 445.

Shelley, D. & Bossière, G. 2000. A new model for the Hercynian Orogen of Gondwanan France and Iberia. J. Structural Geol. 22. 757-776.

Simpson, C. & Wintsch, R. P. 1989. Evidence for deformation-induced K-feldspar replacement by myrmekite. Journal of Metamorphic Geology 7, 261-275.

Simpson, G. D. H. 1998. Dehydration-related deformation during regional metamorphism, NW Sardinia, Italy. Journal of Metamorphic Geology 16(3), 457-472.

Sitter, L.U. & Zwart H.J. 1960. Tectonic development in supra and infra-structures of a mountain chain. Proc. 21st, Int. Congr. Copenhagen 18, 248-256.

Soliva, J., Salel, J.F. & Brunel, M. 1989. Shear deformation and emplacement of the gneissic Canigou thrust nappe (Eastern Pyrenees). Geologie en Mijnbouw 68. 357-366.

Soula J.-C., Debat, P., Brusset, S., Bessière, G. Christophoul, F. & Déramond, J. 2001. Thrust-related, diapiric, and extensional doming in a frontal orogenic wedge: example of the Montagne Noire, southern France Hercynian belt. J. Struc. Geol. 23. 1677-1699.

Spear F.S. 1980. NaSi-CaAl exchange equilibrium between plagioclase and amphiboles. An empirical model. Contrib Mineral Petrol 72: 33-41.

Spear, F. S. & Cheney, T. J. 1989. A petrogenetic grid for pelitic schists in the systhem SiO2-Al2O3-FeO-MgO-K2O-H2O. Contrib Mineral. Petrol. 101. 149-164.

Spear, F. S. 1981. An experimental study of hornblende stability and compositional variability in amphibolite. Am J Sci 281.697-734.

Spear, F. S. 1993. Metamorphic phase equilibria and pressure-temperature-time paths. Mineralogical Society of America, Washington, D.C. 1993. 799.

Stampfli, G. M. 1996. The Intra-Alpine terrain; a Paleotethyan remnant in the Alpine Variscides. In: Alpine geology; proceedings of the second workshop. (edited by Schmid, S. M., Frey, M., Froitzheim, N., Heilbronner, R. & Stuenitz, H.). Eclogae Geologicae Helvetiae 89. Birkhaeuser Verlag, Basel, Switzerland, 13-42.

Stampfli, G.M., von Raumer, J.F. & Borel, G.D. 2002. The Palaeozoic evolution of pre-Variscan terranes: from Gondwana to the Variscan collision. Geological Society of America, Special Paper 364, 263-280.

Stewart M., Holdsworth, R. E. & Strachan, R. A. 2000. Deformation processes and weakening mechanisms within the frictional-viscous transition zone of major crustal-scale faults: inights from the Great Glen Fault Zone, Scotland. J Struct Geol 22. 543-560.

Stille, H. 1939. Bemerkungen betreffend die Sardische Faultung und den Ausdruck Ophiolitisch. Z. dt. geol. Ges., 91, 771-773.

Teichmüller, R. 1931. Zur Geologie des Tyrrhenisgebietes No. 1, Alte und junge Krustenbewegungen im südlichen Sardinien. Abh. Der Gesellschaft der Wissensch. Zu Göttingen, 857-950.

Thompson, P. H. & Bard, J. P. 1982. Isograds and mineral assemblages in the eastern Axial Zone, Montagne Noire (France). Implications for temperature gradients and P/T history. Can J Eath Sci 19(1). 129-143.

Tiepolo M., Bottazzi P., Palenzona M. 6 Vannucci R., 2003. A laser probe coupled with ICP-double-focusing sector-field mass spectrometer from in situ analysis of geological samples and U-Pb dating of zircons. Can. Mineral. In press.

Tommasini, S., Poli, G. & Halliday, A. N. 1995. The role of sediment subduction and crustal growth in Hercynian plutonism; isotopic and trace element evidence from the Sardinia-Corsica Batholith. Journal of Petrology 36(5), 1305-1332.

Traversa, G. & Vaccaro, C. 1992. REE distribution in the late Hercynian dykes from Sardinia. In: Carmignani, L. & Sassi, F.P. (Eds.) "Contributions to the geology of Italy with special regard to the Paleozoic basement" IGCP No 276, Newsletter 5, special issue, 215-226.

Tullis, J. & Yund, R. A. 1985. Dynamic recrystallization of feldspar: A mechanism for ductile shear zone deformation. Geology 13, 238-241.

Tullis, J., Christie, J.M. Giggs, D.T. 1973. Microstructures and preferred orientations of experimentally deformed quartzites. Bull Geol Soc Am 84. 297-314.

Vai G.B. & Cocozza, T. 1986. Tentative schematic zonation of the Hercynian chain in Italy. Bull. Soc. géol. France. t. II, n° 1, p. 95-114.

Valverde-Vaquero P. & Dunning G.R. 2000. New U–Pb ages for Early Ordovician magmatism in Central Spain. Journal of the Geological Society London, 157: 15-26.

Vernon, R.H. 1979. Formation of late sillimanite by hydrogen metasomatism (base-leaching) in some high-grade gneisses. Lithos 12, 143-152.

Vidal, P., Auvray, B., Charlot, R. & Cogné, J. 1981. Pre-Cadomian relicts in the Armorican Massif: their age and role in the evolution of the western and central European Cadomian-Hercynian belt. Precambrian Research 14, 1-20.

Vigliotti, L. & Langenheim, V.E. 1995. When did Sardinia stop rotating? New palaeomagnetic results. Terra Nova 7, 424-435.

Vielzeuf D. & Pin C. 1989. Geodynamic implications of granulitic rocks in the Hercynian belt. In: Daly, J.S., Cliff R.A., & Yardley, B.W.D. (eds.) Evolution of metamorphic belts. Geol. Soc. Spec. Publ. 43, 343-348.

Vissers, R.L.M. 1992. Variscan extension in the Pyrenees. Tectonics 11, 1369-1384.

Voll, G. 1976. Recrystallization of quartz, biotite and feldspars from Erstfeld to the Leventina nappe, Swiss alps, and its geological significance. Schweizerische mineralogische und petrographische Mitteilungen 56, 641-647.

Watson E.B. & Yan Liang 1995. A simple model for sector zoning in slowly grown crystals: implications for growth rate and lattice diffusion, with emphasis on accessory minerals in crustal rocks. Am. Mineral. 80, 1179-1187.

Weisbrod, A. 1973. Refinements of the equilibrium conditions of the reaction Fe cordierite = almandine + quartz + sillimanite + H2O. Carnegie Inst Washington, Yearb 72. 518-521.

Wells P.R.A. 1977. Pyroxene thermometry in simple and complex systems. Contrib Mineral Petrol 62: 129-239.

Wenzel, T., Mertz, D.F., Oberhänsli, R., Becker, T. & Renne, P.R. 1997. Age, geodynamic setting, and mantle enrichment processes of a K-rich intrusion from the Meissen massif (northern Bohemian massif) and implications for related occurrences from the mid-European Hercynian. Geol Rundsch 86: 556-570.

Wetherill G.W 1956. Discordant uranium-lead ages. Trans. Amer. Geophys. Union 37, 320-326.

Williams, H. 1985. Paleozoic miogeoclines and suspect terranes of the north Atlantic region: Cordilleran comparisons. In: Howell, D.G. (Ed.), Tectonostratigraphic terranes of the circum-Pacific region. Circum-Pacific Council for Energy and Mineral Resources, Houtson, pp. 71-75.

Wilson, CJL 1975. Preferred orientation in quartz ribbon mylonites. Bull Geol Soc Am 86. 968-974.

Wilson, M. & Bianchini, G. 1999. Tertiary-Quaternary magmatism within the Mediterranean and surrounding regions. In: Durand, B., Jolivet, L., Horváth, F. & Séranne, M. (eds) The Mediterranean basins: Tertiary extension within the Alpine orogen. Geological Society, London, Special Publications, 156, 141-168.

Winchester, J.A., The PACE TMR Network Team 2002. Palaeozoic amalgamation of Central Europe - new results from recent geological & geophysical investigations. Tectonophysics 360. 5-21.

Wickham, S.M. & Oxburgh, E.R. 1985. Continental rifts as a setting for regional metamorphism. Nature 318, 330-333.

Wong a Ton, S.Y.M. & Wortel, M.J.R. 1997. Slab detachment in continental collision zones: An analysis of controlling parameters, Geoph. Res. Lett., 24 (16), 2095-2098.

Wood B.J. & Banno S. 1973. Garnet-orthopyroxene and orthopyroxene-clinopyroxene relationships in single and complex systems. Contrib Mineral Petrol 42: 109-124.

Woodcock, N.H 1977. Specification of fabric shapes using an Eigenvalue Method. Geol. Soc. Am. Bull. 88. 1231-1236.

Wortel, M.J.R. & Sparkman, W. 1992. Structure and dynamics of subducted lithoshere in the Mediterranean region. Verhandelingen der Koninklijke Nederlandse Akademie van Wetenschappen, Amsterdam, 95, 325-347.

Yorder, H. S. & Tilley, C. E. 1962. Origin of basalt magmas: an experimental study of natural and synthetic rock systems. J Petrol 3(3). 342-532.

Zeck, H.P. 1999. Alpine plate kinematics in the western Mediterranean: a westward-directed subduction regime followed by slab roll-back and slab detachment. In: Durand, B., Jolivet, L., Horváth, F. & Séranne, M. (eds) The Mediterranean basins: Tertiary extension within the Alpine orogen. Geological Society, London, Special Publications, 156, 109-120.

Zurbriggen R., Franz L. & Handy M.R. 1997. Pre-Variscan deformation, metamorphism and magmatism in the Strona-Ceneri zone (southern Alps of northern Italy and southern Switzerland). Schweiz. Mineral. Petrogr. Mitt. 77, 361-380.

Zwart H.J. & Dornsiepen U.F. 1978. The tectonic framework of central and western Europe. Geol. Mijnbouw 57. 627-654.

Appendix

- **field data, orientation**

- **thin section data**

structural field data, NE-Sardinia, n: 3600 (approx.)

outcrop	structural zone/lithology	dipping-direction	dipping-angle	fabric
HH001	SZ I	**020**	**45**	B3

HH001	SZ I	**060**	**05**	B3
HH001	SZ I	**020**	**45**	B3
HH001	SZ I	**038**	**35**	B3
HH001	SZ I	**025**	**11**	B3
HH001	SZ I	**026**	**24**	B3
HH001	SZ I	**222**	**30**	B3
HH001	SZ I	**043**	**43**	B3
HH001	SZ I	**040**	**10**	B3
HH001	SZ I	**037**	**35**	B3
HH001	SZ I	**038**	**07**	B3
HH001	SZ I	**229**	**40**	B3
HH001	SZ I	**030**	**23**	B3
HH001	SZ I	**216**	**33**	B3
HH001	SZ I	**085**	**14**	B5
HH001	SZ I	**218**	**01**	L2
HH001	SZ I	**041**	**25**	L2
HH001	SZ I	**252**	**20**	L2
HH001	SZ I	**033**	**15**	L2
HH001	SZ I	**134**	**80**	S2
HH001	SZ I	**116**	**74**	S2
HH001	SZ I	**102**	**83**	S2
HH001	SZ I	**071**	**30**	S2
HH001	SZ I	**128**	**75**	S2
HH001	SZ I	**280**	**75**	S2
HH001	SZ I	**165**	**75**	S2
HH001	SZ I	**321**	**85**	S2
HH001	SZ I	**102**	**83**	S2
HH001	SZ I	**328**	**80**	S2
HH001	SZ I	**123**	**80**	S2
HH001	SZ I	**130**	**65**	S3
HH001	SZ I	**124**	**85**	S3
HH002	SZ I	**240**	**18**	B2
HH002	SZ I	**045**	**27**	B3
HH002	SZ I	**045**	**15**	B3
HH002	SZ I	**046**	**22**	B3
HH002	SZ I	**060**	**20**	B3
HH002	SZ I	**045**	**15**	B3
HH002	SZ I	**042**	**02**	B3
HH002	SZ I	**042**	**06**	B3
HH002	SZ I	**040**	**02**	B3
HH002	SZ I	**026**	**13**	B3
HH002	SZ I	**218**	**02**	B3
HH002	SZ I	**059**	**17**	B3
HH002	SZ I	**051**	**13**	B3
HH002	SZ I	**047**	**32**	B3
HH002	SZ I	**053**	**02**	L2
HH002	SZ I	**045**	**08**	L2
HH002	SZ I	**138**	**90**	S2
HH002	SZ I	**325**	**58**	S2
HH002	SZ I	**121**	**36**	S2
HH002	SZ I	**125**	**23**	S2
HH002	SZ I	**133**	**84**	S2
HH002	SZ I	**140**	**86**	S2
HH002	SZ I	**146**	**88**	S2
HH002	SZ I	**291**	**84**	S2
HH002	SZ I	**126**	**25**	S2
HH002	SZ I	**308**	**74**	S2
HH002	SZ I	**088**	**13**	S2
HH002	SZ I	**048**	**25**	S2
HH002	SZ I	**130**	**76**	S2
HH002	SZ I	**128**	**60**	S3
HH002	SZ I	**132**	**62**	S3
HH002	SZ I	**308**	**60**	S3
HH002	SZ I	**105**	**45**	S3
HH002	SZ I	**128**	**54**	S3
HH002	SZ I	**134**	**43**	S3
HH002	SZ I	**130**	**76**	S3

HH002	SZ I	**113**	**57**	S3
HH002	SZ I	**138**	**74**	S3
HH002	SZ I	**140**	**72**	S3
HH002	SZ I	**145**	**64**	S3
HH002	SZ I	**129**	**50**	S3
HH002	SZ I	**130**	**62**	S3
HH003	SZ I	**222**	**16**	B2
HH003	SZ I	**203**	**11**	B2
HH003	SZ I	**050**	**17**	B3
HH003	SZ I	**070**	**32**	B3
HH003	SZ I	**213**	**04**	B3
HH003	SZ I	**070**	**20**	B3
HH003	SZ I	**104**	**50**	B3
HH003	SZ I	**060**	**30**	B3
HH003	SZ I	**110**	**70**	B5
HH003	SZ I	**057**	**30**	L2
HH003	SZ I	**072**	**31**	L2
HH003	SZ I	**050**	**26**	L2
HH003	SZ I	**132**	**63**	S2
HH003	SZ I	**136**	**61**	S2
HH003	SZ I	**129**	**66**	S2
HH003	SZ I	**110**	**30**	S2
HH003	SZ I	**116**	**60**	S2
HH003	SZ I	**130**	**44**	S2
HH003	SZ I	**125**	**43**	S2
HH003	SZ I	**129**	**60**	S2
HH003	SZ I	**128**	**44**	S3
HH003	SZ I	**112**	**83**	S3
HH003	SZ I	**122**	**63**	S3
HH003	SZ I	**141**	**76**	S3
HH003	SZ I	**114**	**36**	S3
HH004	SZ I	**252**	**22**	B3
HH004	SZ I	**082**	**05**	B5
HH004	SZ I	**086**	**11**	B5
HH004	SZ I	**335**	**75**	S2
HH004	SZ I	**170**	**45**	S3
HH004	SZ I	**165**	**20**	S3
HH004	SZ I	**155**	**37**	S3
HH004	SZ I	**169**	**36**	S3
HH004	SZ I	**168**	**41**	S3
HH004	SZ I	**358**	**60**	S5
HH004	SZ I	**350**	**60**	S5
HH004	SZ I	**008**	**40**	S5
HH005	SZ I	**077**	**38**	L2
HH005	SZ I	**112**	**40**	S2
HH005	SZ I	**090**	**73**	S2
HH006	SZ II	**078**	**11**	B3
HH006	SZ II	**086**	**05**	L2/4
HH006	SZ II	**077**	**08**	L2/4
HH006	SZ II	**086**	**05**	L2/4
HH006	SZ II	**145**	**33**	S3
HH006	SZ II	**128**	**45**	S3
HH006	SZ II	**182**	**13**	S3
HH006	SZ II	**150**	**36**	S3
HH006	SZ II	**155**	**40**	S3
HH006	SZ II	**132**	**35**	S3
HH007	SZ III	**197**	**14**	L2
HH007	SZ III	**180**	**20**	L2
HH007	SZ III	**200**	**15**	L2
HH007	SZ III	**190**	**35**	L2
HH007	SZ III	**208**	**32**	L2
HH007	SZ III	**210**	**36**	L2
HH007	SZ III	**211**	**24**	L2
HH007	SZ III	**139**	**10**	L2/4
HH007	SZ III	**140**	**15**	L2/4
HH007	SZ III	**180**	**16**	S2
HH007	SZ III	**160**	**20**	S2
HH007	SZ III	**140**	**22**	S2

BA: basalt dike, **CO**: cover, **PE**: pegmatite dike, **SB**: shear band, **SZ I**: structural zone I, **SZ II**: structural zone II, **SZ III**: structural zone III, **SZ IV**: structural zone IV, **SZ V**: structural zone V, **SZ VI**: structural zone VI, **SZ VII**: structural zone VII, **TM**: Punta de li Tulchi metabasite, **TO**: Tanaunella orthogneiss

structural field data, NE-Sardinia, n: 3600 (approx.)

outcrop	structural zone/lithology	dipping-direction	dipping-angle	fabric
HH001	SZ I	**020**	**45**	B3

HH007	SZ III	**182**	**37**	S2
HH007	SZ III	**200**	**35**	S2
HH007	SZ III	**196**	**32**	S2
HH007	SZ III	**200**	**23**	S2
HH007	SZ III	**228**	**48**	SB
HH008	SZ III	**202**	**17**	L2
HH008	SZ III	**198**	**22**	L2
HH008	SZ III	**123**	**25**	L2/4
HH008	SZ III	**125**	**25**	L2/4
HH008	SZ III	**125**	**39**	S2
HH008	SZ III	**144**	**24**	S2
HH009	SZ IV	**090**	**57**	B3
HH009	SZ IV	**108**	**45**	L2/4
HH009	SZ IV	**105**	**40**	L2/4
HH009	SZ IV	**087**	**54**	L2/4
HH009	SZ IV	**178**	**85**	S2/4
HH009	SZ IV	**025**	**74**	S2/4
HH009	SZ IV	**032**	**80**	S2/4
HH009	SZ IV	**022**	**74**	S2/4
HH010	SZ II	**059**	**25**	S2
HH010	SZ II	**084**	**26**	S2
HH010	SZ II	**099**	**26**	S3
HH010	SZ II	**100**	**32**	S3
HH010	SZ II	**115**	**45**	S3
HH011	SZ II	**080**	**09**	L2/4
HH011	SZ II	**072**	**14**	L2/4
HH011	SZ II	**086**	**05**	L2/4
HH011	SZ II	**280**	**10**	L2/4
HH011	SZ II	**128**	**21**	S3
HH011	SZ II	**158**	**20**	S3
HH011	SZ II	**100**	**10**	S3
HH011	SZ II	**125**	**16**	S3
HH012	SZ IV	**108**	**28**	L2/4
HH012	SZ IV	**113**	**22**	L2/4
HH012	SZ IV	**198**	**70**	S2/4
HH012	SZ IV	**188**	**72**	S2/4
HH012	SZ IV	**195**	**76**	S2/4
HH013	SZ IV	**288**	**10**	B3
HH013	SZ IV	**080**	**15**	B3
HH013	SZ IV	**095**	**20**	B3
HH013	SZ IV	**105**	**26**	B3
HH013	SZ IV	**092**	**32**	B3
HH013	SZ IV	**287**	**14**	B3
HH013	SZ IV	**106**	**19**	L2/4
HH013	SZ IV	**137**	**40**	L2/4
HH013	SZ IV	**191**	**64**	S2/4
HH013	SZ IV	**191**	**68**	S3
HH014	SZ IV	**120**	**02**	B3
HH014	SZ IV	**119**	**03**	B3
HH014	SZ IV	**115**	**10**	L2/4
HH014	SZ IV	**120**	**06**	L2/4
HH014	SZ IV	**034**	**54**	S2/4
HH014	SZ IV	**198**	**75**	S2/4
HH014	SZ IV	**180**	**43**	S2/4
HH014	SZ IV	**048**	**50**	S2/4
HH014	SZ IV	**208**	**83**	S3
HH014	SZ IV	**205**	**70**	S3
HH014	SZ IV	**220**	**59**	S3
HH015	SZ V	**090**	**03**	L2/4
HH015	SZ V	**094**	**15**	L2/4
HH015	SZ V	**075**	**18**	L2/4
HH015	SZ V	**190**	**45**	S2/3/4
HH015	SZ V	**134**	**25**	S2/3/4
HH015	SZ V	**172**	**58**	S2/3/4
HH015	SZ V	**160**	**44**	S2/3/4
HH015	SZ V	**137**	**30**	SB
HH016	SZ IV	**104**	**24**	L2/4
HH016	SZ IV	**090**	**22**	L2/4
HH016	SZ IV	**174**	**55**	S2/4
HH016	SZ IV	**172**	**73**	S2/4
HH016	SZ IV	**168**	**78**	S2/4
HH016	SZ IV	**172**	**77**	S2/4
HH016	SZ IV	**171**	**71**	S2/4
HH016	SZ IV	**001**	**84**	S2/4
HH016	SZ IV	**170**	**58**	S2/4
HH017	SZ III	**068**	**10**	L2/4
HH017	SZ III	**098**	**05**	L2/4
HH017	SZ III	**110**	**00**	L2/4
HH017	SZ III	**088**	**10**	L2/4
HH017	SZ III	**065**	**20**	S2
HH017	SZ III	**208**	**20**	S2
HH017	SZ III	**181**	**22**	S2/4
HH017	SZ III	**168**	**20**	S2/4
HH017	SZ III	**138**	**30**	S2/4
HH017	SZ III	**205**	**17**	S2/4
HH017	SZ III	**180**	**25**	S2/4
HH017	SZ III	**152**	**20**	S2/4
HH018	SZ III	**112**	**15**	L2/4
HH018	SZ III	**081**	**03**	L2/4
HH018	SZ III	**175**	**25**	S2/4
HH018	SZ III	**172**	**22**	S2/4
HH018	SZ III	**165**	**20**	SB
HH018	SZ III	**211**	**34**	SB
HH019	SZ III	**045**	**13**	L2
HH019	SZ III	**055**	**09**	L2
HH019	SZ III	**074**	**08**	L2
HH019	SZ III	**083**	**23**	L2/4
HH019	SZ III	**085**	**23**	L2/4
HH019	SZ II	**105**	**15**	L2/4
HH019	SZ III	**138**	**28**	S2
HH019	SZ III	**128**	**27**	S2
HH019	SZ III	**138**	**28**	S2
HH019	SZ III	**129**	**29**	S2
HH019	SZ III	**154**	**21**	S2
HH019	SZ II	**160**	**20**	S2
HH019	SZ II	**098**	**34**	S2
HH019	SZ II	**134**	**38**	S2
HH019	SZ II	**155**	**31**	S2
HH019	SZ II	**120**	**30**	S2
HH019	SZ II	**133**	**29**	S2
HH019	SZ II	**020**	**05**	S2
HH019	SZ II	**030**	**02**	S2
HH019	SZ III	**105**	**26**	S2/4
HH019	SZ III	**107**	**25**	S2/4
HH019	SZ II	**188**	**15**	SB
HH019	SZ II	**189**	**16**	SB
HH021	SZ V	**271**	**04**	L2/4
HH021	SZ V	**179**	**53**	S2/3/4
HH021	SZ V	**150**	**37**	S2/3/4
HH021	SZ V	**160**	**80**	S2/3/4
HH022	SZ V	**221**	**20**	B2/3
HH022	SZ V	**322**	**20**	B2/3
HH022	SZ V	**205**	**66**	BA
HH022	SZ V	**205**	**66**	S2/3/4
HH022	SZ V	**226**	**70**	S2/3/4
HH023	SZ V	**240**	**45**	S2/3/4
HH024	SZ V	**088**	**38**	B2/3
HH024	SZ V	**172**	**64**	S2/3/4
HH024	SZ V	**172**	**80**	S2/3/4
HH024	SZ V	**178**	**80**	S2/3/4
HH025	SZ V	**096**	**16**	B2/3
HH025	SZ V	**075**	**65**	B2/3
HH025	SZ V	**091**	**23**	L2/4
HH025	SZ V	**109**	**26**	L2/4
HH025	SZ V	**088**	**19**	L2/4
HH025	SZ V	**185**	**55**	S2/3/4
HH025	SZ V	**172**	**67**	S2/3/4
HH025	SZ V	**144**	**34**	S2/3/4

BA: basalt dike, **CO**: cover, **PE**: pegmatite dike, **SB**: shear band, **SZ I**: structural zone I, **SZ II**: structural zone II, **SZ III**: structural zone III, **SZ IV**: structural zone IV, **SZ V**: structural zone V, **SZ VI**: structural zone VI, **SZ VII**: structural zone VII, **TM**: Punta de li Tulchi metabasite, **TO**: Tanaunella orthogneiss

structural field data, NE-Sardinia, n: 3600 (approx.)

outcrop	structural zone/lithology	dipping-direction	dipping-angle	fabric
HH001	SZ I	**020**	**45**	B3

HH025	SZ V	**065**	**50**	S2/3/4
HH025	SZ V	**208**	**80**	S2/3/4
HH025	SZ V	**175**	**75**	S2/3/4
HH025	SZ V	**020**	**82**	S2/3/4
HH025	SZ V	**164**	**43**	S2/3/4
HH025	SZ V	**010**	**65**	S2/3/4
HH025	SZ V	**165**	**70**	S2/3/4
HH025	SZ V	**038**	**33**	S2/3/4
HH025	SZ V	**190**	**65**	S2/3/4
HH025	SZ V	**218**	**72**	S2/3/4
HH026	SZ V	**090**	**50**	B2/3
HH026	SZ V	**195**	**72**	S2/3/4
HH026	SZ V	**190**	**70**	S2/3/4
HH027	SZ V	**310**	**05**	L2/4
HH027	SZ V	**309**	**15**	L2/4
HH027	SZ V	**220**	**73**	S2/3/4
HH027	SZ V	**215**	**80**	S2/3/4
HH028	SZ V	**102**	**18**	L2/4
HH028	SZ V	**120**	**15**	L2/4
HH028	SZ V	**212**	**83**	S2/3/4
HH028	SZ V	**039**	**88**	S2/3/4
HH028	SZ V	**040**	**80**	S2/3/4
HH029	SZ V	**086**	**25**	B2/3
HH029	SZ V	**080**	**04**	B2/3
HH029	SZ V	**088**	**10**	B2/3
HH029	SZ V	**107**	**17**	B2/3
HH029	SZ V	**100**	**10**	B2/3
HH029	SZ V	**078**	**20**	B2/3
HH029	SZ V	**070**	**25**	B2/3
HH029	SZ V	**058**	**20**	B2/3
HH029	SZ V	**084**	**27**	B2/3
HH029	SZ V	**144**	**17**	B5
HH029	SZ V	**115**	**11**	B5
HH029	SZ V	**093**	**10**	B5
HH029	SZ V	**086**	**37**	B5
HH029	SZ V	**100**	**13**	B5
HH029	SZ V	**090**	**02**	L2/4
HH029	SZ V	**080**	**00**	L2/4
HH029	SZ V	**126**	**07**	L2/4
HH029	SZ V	**102**	**22**	L2/4
HH029	SZ V	**161**	**33**	S2/3/4
HH029	SZ V	**138**	**06**	S2/3/4
HH029	SZ V	**040**	**33**	S2/3/4
HH029	SZ V	**070**	**21**	S2/3/4
HH029	SZ V	**178**	**45**	S2/3/4
HH029	SZ V	**096**	**11**	S2/3/4
HH029	SZ V	**150**	**55**	S2/3/4
HH029	SZ V	**154**	**12**	S2/3/4
HH029	SZ V	**165**	**20**	S2/3/4
HH029	SZ V	**160**	**26**	S2/3/4
HH029	SZ V	**104**	**10**	S2/3/4
HH029	SZ V	**150**	**05**	S2/3/4
HH029	SZ V	**185**	**76**	S2/3/4
HH029	SZ V	**090**	**30**	S2/3/4
HH029	SZ V	**160**	**15**	S2/3/4
HH029	SZ V	**154**	**68**	S5
HH029	SZ V	**187**	**50**	S5
HH030	SZ V	**113**	**20**	L2/4
HH030	SZ V	**111**	**25**	L2/4
HH030	SZ V	**198**	**80**	S2/3/4
HH030	SZ V	**202**	**67**	S2/3/4
HH030	SZ V	**234**	**66**	SB
HH031	SZ V	**093**	**06**	B2/3
HH031	SZ V	**105**	**15**	B2/3
HH031	SZ V	**095**	**05**	L2/4
HH031	SZ V	**102**	**08**	L2/4
HH031	SZ V	**195**	**89**	S2
HH031	SZ V	**358**	**85**	S2
HH031	SZ V	**176**	**70**	S2/3/4

HH031	SZ V	**195**	**66**	S2/3/4
HH032	SZ V	**118**	**01**	L2/4
HH032	SZ V	**200**	**75**	S2/3/4
HH034	SZ V	**263**	**04**	B5
HH034	SZ V	**258**	**17**	B5
HH034	SZ V	**280**	**05**	L2/4
HH034	SZ V	**273**	**20**	L2/4
HH034	SZ V	**190**	**60**	S2/3/4
HH034	SZ V	**203**	**72**	S2/3/4
HH035	SZ V	**324**	**70**	BA
HH035	SZ V	**025**	**89**	BA
HH035	SZ V	**088**	**12**	L2/4
HH035	SZ V	**135**	**25**	S2/3/4
HH035	SZ V	**188**	**56**	S2/3/4
HH035	SZ V	**174**	**50**	S2/3/4
HH035	SZ V	**190**	**38**	S2/3/4
HH035	SZ V	**198**	**38**	S2/3/4
HH035	SZ V	**180**	**45**	S2/3/4
HH035	SZ V	**170**	**35**	S2/3/4
HH035	SZ V	**163**	**28**	S2/3/4
HH036	SZ VII	**066**	**25**	L2
HH036	SZ VII	**210**	**20**	L2
HH036	SZ VII	**225**	**35**	L2
HH036	SZ VII	**205**	**50**	S2
HH036	SZ VII	**166**	**55**	S2
HH036	SZ VII	**162**	**53**	S2
HH036	SZ VII	**116**	**43**	S2
HH036	SZ VII	**165**	**42**	S2
HH036	SZ VII	**162**	**40**	S2
HH036	SZ VII	**180**	**37**	S2
HH037	SZ VII	**162**	**53**	S2
HH037	SZ VII	**162**	**34**	S2
HH037	SZ VII	**190**	**55**	S2
HH037	SZ VII	**186**	**43**	S2
HH038	SZ VII	**095**	**25**	B2
HH038	SZ VII	**098**	**26**	B2
HH038	SZ VII	**225**	**36**	L2
HH038	SZ VII	**216**	**33**	L2
HH038	SZ VII	**160**	**55**	S2
HH038	SZ VII	**161**	**43**	S2
HH039	TO	**078**	**03**	B3
HH039	TO	**078**	**15**	B3
HH039	TO	**080**	**40**	B3
HH039	TO	**082**	**58**	B3
HH039	TO	**099**	**38**	B3
HH039	TO	**028**	**36**	L2
HH039	TO	**034**	**25**	L2
HH039	TO	**036**	**05**	L2
HH039	TO	**060**	**34**	L2
HH039	TO	**063**	**15**	L2
HH039	TO	**065**	**36**	L2
HH039	TO	**200**	**05**	L2
HH039	TO	**248**	**05**	L2
HH039	SZ VII	**185**	**78**	PE
HH039	SZ VII	**210**	**80**	PE
HH039	SZ VII	**030**	**36**	PE
HH039	SZ VII	**192**	**67**	PE
HH039	TO	**098**	**45**	S2
HH039	TO	**100**	**34**	S2
HH039	TO	**108**	**60**	S2
HH039	TO	**108**	**42**	S2
HH039	TO	**114**	**48**	S2
HH039	TO	**120**	**60**	S2
HH039	TO	**122**	**58**	S2
HH039	TO	**128**	**40**	S2
HH039	TO	**131**	**13**	S2
HH039	TO	**132**	**66**	S2
HH039	TO	**134**	**35**	S2
HH039	TO	**142**	**60**	S2

BA: basalt dike, **CO**: cover, **PE**: pegmatite dike, **SB**: shear band, **SZ I**: structural zone I, **SZ II**: structural zone II, **SZ III**: structural zone III, **SZ IV**: structural zone IV, **SZ V**: structural zone V, **SZ VI**: structural zone VI, **SZ VII**: structural zone VII, **TM**: Punta de li Tulchi metabasite, **TO**: Tanaunella orthogneiss

structural field data, NE-Sardinia, n: 3600 (approx.)

outcrop	structural zone/lithology	dipping-direction	dipping-angle	fabric
HH001	SZ I	**020**	**45**	B3

HH039	TO	**142**	**33**	S2
HH039	TO	**155**	**30**	S2
HH039	TO	**160**	**53**	S2
HH039	TO	**168**	**33**	S2
HH039	TO	**188**	**33**	S2
HH039	TO	**188**	**70**	S2
HH039	TO	**236**	**11**	S2
HH039	TO	**122**	**58**	S3
HH039	TO	**160**	**53**	S3
HH04	SZ I	**090**	**05**	B5
HH040	SZ VII	**098**	**25**	B2
HH040	SZ VII	**202**	**05**	B2
HH040	SZ VII	**100**	**30**	B2
HH040	SZ VII	**093**	**36**	B2
HH040	SZ VII	**062**	**02**	B2
HH040	SZ VII	**023**	**01**	B2
HH040	SZ VII	**198**	**82**	BA
HH040	SZ VII	**206**	**20**	B-kink
HH040	SZ VII	**200**	**15**	B-kink
HH040	SZ VII	**203**	**29**	B-kink
HH040	SZ VII	**212**	**05**	L2
HH040	SZ VII	**218**	**02**	L2
HH040	SZ VII	**216**	**03**	L2
HH040	SZ VII	**035**	**07**	L2
HH040	SZ VII	**220**	**06**	L2
HH040	SZ VII	**041**	**01**	L2
HH040	SZ VII	**072**	**13**	L2
HH040	SZ VII	**116**	**54**	S2
HH040	SZ VII	**120**	**45**	S2
HH040	SZ VII	**118**	**33**	S2
HH040	SZ VII	**120**	**36**	S2
HH040	SZ VII	**111**	**40**	S2
HH040	SZ VII	**135**	**50**	S2
HH040	SZ VII	**120**	**28**	S2
HH040	SZ VII	**112**	**70**	S2
HH040	SZ VII	**112**	**25**	S2
HH040	SZ VII	**135**	**40**	S2
HH040	SZ VII	**128**	**42**	S2
HH040	SZ VII	**146**	**35**	S2
HH040	SZ VII	**122**	**47**	S2
HH040	SZ VII	**125**	**55**	S2
HH040	SZ VII	**120**	**30**	S2
HH041	SZ II	**050**	**05**	B2
HH041	SZ II	**072**	**25**	B2
HH041	SZ II	**160**	**35**	B3
HH041	SZ II	**120**	**25**	B3
HH041	SZ II	**140**	**30**	B3
HH041	SZ II	**148**	**15**	B3
HH041	SZ II	**112**	**25**	S2
HH041	SZ II	**116**	**20**	S2
HH041	SZ II	**116**	**25**	S2
HH041	SZ II	**130**	**25**	S2
HH041	SZ II	**110**	**35**	S2
HH041	SZ II	**078**	**15**	S2
HH041	SZ II	**048**	**15**	S2
HH041	SZ II	**070**	**13**	S2
HH041	SZ II	**068**	**29**	S2
HH042	SZ II	**096**	**20**	B2
HH042	SZ II	**118**	**23**	B2
HH042	SZ II	**090**	**25**	B2
HH042	SZ II	**112**	**25**	B2
HH042	SZ II	**096**	**22**	B2
HH042	SZ II	**083**	**27**	B3
HH042	SZ II	**102**	**20**	B3
HH042	SZ II	**150**	**30**	S1
HH042	SZ II	**072**	**20**	S1
HH042	SZ II	**092**	**18**	S1
HH042	SZ II	**156**	**25**	S1
HH042	SZ II	**157**	**28**	S1

HH042	SZ II	**108**	**40**	S2
HH042	SZ II	**129**	**18**	S2
HH042	SZ II	**111**	**17**	S2
HH042	SZ II	**130**	**30**	S2
HH042	SZ II	**110**	**26**	S2
HH042	SZ II	**136**	**25**	S2
HH042	SZ II	**088**	**20**	S2
HH042	SZ II	**090**	**15**	S2
HH042	SZ II	**114**	**15**	S2
HH042	SZ II	**097**	**20**	S2
HH042	SZ II	**105**	**10**	S2
HH042	SZ II	**079**	**10**	S2
HH042	SZ II	**097**	**30**	S2
HH042	SZ II	**128**	**25**	S3
HH043	SZ II	**102**	**07**	B2
HH043	SZ II	**110**	**12**	B2
HH043	SZ II	**096**	**02**	B2
HH043	SZ II	**114**	**05**	B2
HH043	SZ II	**180**	**25**	S2
HH043	SZ II	**050**	**16**	S2
HH043	SZ II	**190**	**35**	S2
HH043	SZ II	**022**	**01**	S2
HH043	SZ II	**338**	**08**	S2
HH043	SZ II	**142**	**01**	S2
HH043	SZ II	**128**	**01**	S2
HH043	SZ II	**093**	**10**	S2
HH043	SZ II	**112**	**29**	S2
HH043	SZ II	**025**	**15**	S2
HH043	SZ II	**165**	**04**	S2
HH043	SZ II	**350**	**05**	S2
HH043	SZ II	**100**	**11**	S2
HH043	SZ II	**085**	**15**	S2
HH044	SZ II	**099**	**09**	B2
HH044	SZ II	**118**	**13**	B2
HH044	SZ II	**110**	**13**	S2
HH044	SZ II	**188**	**43**	S2
HH044	SZ II	**095**	**18**	S2
HH045	SZ II	**082**	**02**	B2
HH045	SZ II	**155**	**16**	S2
HH045	SZ II	**092**	**14**	S2
HH045	SZ II	**088**	**03**	S2
HH045	SZ II	**062**	**13**	S2
HH046	SZ II	**170**	**58**	S2
HH046	SZ II	**168**	**54**	S2
HH046	SZ II	**098**	**25**	S2
HH047	SZ II	**248**	**05**	B2
HH047	SZ II	**248**	**11**	B2
HH047	SZ II	**230**	**08**	S2
HH048	SZ II	**302**	**15**	B2
HH048	SZ II	**270**	**14**	B2
HH048	SZ II	**105**	**13**	S2
HH048	SZ II	**120**	**15**	S2
HH048	SZ II	**201**	**05**	S2
HH048	SZ II	**080**	**25**	S2
HH048	SZ II	**085**	**25**	S2
HH048	SZ II	**291**	**07**	S2
HH048	SZ II	**148**	**10**	S2
HH048	SZ II	**078**	**14**	S2
HH049	SZ III	**192**	**05**	L2
HH049	SZ III	**195**	**07**	L2
HH049	SZ III	**210**	**10**	L2
HH049	SZ III	**275**	**15**	S2
HH049	SZ III	**262**	**17**	S2
HH049	SZ III	**240**	**10**	S2
HH051	SZ III	**078**	**06**	L2/4
HH051	SZ III	**099**	**02**	L2/4
HH051	SZ III	**050**	**00**	S2/4
HH051	SZ III	**066**	**09**	S2/4
HH051	SZ III	**072**	**03**	S2/4

BA: basalt dike, **CO**: cover, **PE**: pegmatite dike, **SB**: shear band, **SZ I**: structural zone I, **SZ II**: structural zone II, **SZ III**: structural zone III, **SZ IV**: structural zone IV, **SZ V**: structural zone V, **SZ VI**: structural zone VI, **SZ VII**: structural zone VII, **TM**: Punta de li Tulchi metabasite, **TO**: Tanaunella orthogneiss

structural field data, NE-Sardinia, n: 3600 (approx.)

outcrop	structural zone/lithology	dipping-direction	dipping-angle	fabric
HH001	SZ I	**020**	**45**	B3

HH052	SZ III	**135**	**20**	L2/4
HH052	SZ III	**105**	**25**	S2/4
HH055	SZ II	**166**	**05**	B3
HH055	SZ II	**162**	**04**	S2
HH055	SZ II	**162**	**17**	S2
HH055	SZ II	**135**	**03**	S2
HH055	SZ II	**110**	**01**	S2
HH055	SZ II	**220**	**35**	SB
HH055	SZ II	**223**	**40**	SB
HH056	SZ II	**165**	**40**	S2
HH056	SZ II	**168**	**50**	S2
HH056	SZ II	**172**	**25**	S2
HH056	SZ II	**193**	**50**	S2
HH056	SZ II	**062**	**33**	S2
HH056	SZ II	**240**	**13**	S2
HH056	SZ II	**058**	**22**	S2
HH056	SZ II	**239**	**15**	S2
HH057	SZ II	**145**	**39**	S2
HH057	SZ II	**155**	**42**	S2
HH057	SZ II	**162**	**41**	S2
HH057	SZ II	**264**	**03**	S2
HH057	SZ II	**180**	**65**	SB
HH058	SZ III	**225**	**26**	L2
HH058	SZ III	**219**	**09**	L2
HH058	SZ III	**232**	**15**	L2
HH058	SZ III	**230**	**10**	L2
HH058	SZ III	**154**	**36**	S2
HH058	SZ III	**158**	**36**	S2
HH058	SZ III	**168**	**28**	S2
HH058	SZ III	**176**	**21**	S2
HH058	SZ III	**155**	**34**	S2
HH058	SZ III	**163**	**25**	S2
HH059	SZ III	**201**	**11**	L2
HH059	SZ III	**220**	**16**	L2
HH059	SZ III	**122**	**10**	L2/4
HH059	SZ III	**181**	**16**	S2
HH059	SZ III	**222**	**21**	S2
HH059	SZ III	**180**	**20**	S2
HH060	SZ VI	**280**	**30**	B5
HH060	SZ VI	**275**	**37**	B5
HH060	SZ VI	**181**	**75**	S2/3/4
HH060	SZ VI	**200**	**80**	S2/3/4
HH060	SZ VI	**195**	**89**	S2/3/4
HH060	SZ VI	**240**	**65**	S2/3/4
HH060	SZ VI	**185**	**57**	S2/3/4
HH060	SZ VI	**162**	**33**	S2/3/4
HH061	SZ VI	**258**	**45**	L2
HH061	SZ VI	**270**	**37**	L2/4
HH061	SZ VI	**198**	**64**	S2/3/4
HH061	SZ VI	**172**	**90**	S2/3/4
HH061	SZ VI	**202**	**65**	S2/3/4
HH062	SZ III	**172**	**02**	L2
HH062	SZ III	**172**	**09**	L2
HH062	SZ III	**050**	**02**	L2/4
HH062	SZ III	**250**	**24**	S2
HH062	SZ III	**252**	**46**	S2
HH062	SZ III	**244**	**04**	S2
HH062	SZ III	**230**	**20**	S2
HH063	SZ VI	**206**	**11**	B2/3
HH063	SZ VI	**222**	**17**	B2/3
HH063	SZ VI	**238**	**17**	L2/4
HH063	SZ VI	**142**	**67**	S2/3/4
HH063	SZ VI	**155**	**43**	S2/3/4
HH063	SZ VI	**164**	**35**	S2/3/4
HH063	SZ VI	**160**	**65**	S2/3/4
HH063	SZ VI	**162**	**67**	S2/3/4
HH063	SZ VI	**140**	**55**	S2/3/4
HH063	SZ VI	**141**	**61**	S2/3/4
HH064	SZ VI	**222**	**78**	B2/3
HH064	SZ VI	**355**	**25**	B5
HH064	SZ VI	**054**	**02**	L2/4
HH064	SZ VI	**028**	**82**	S2/3/4
HH064	SZ VI	**162**	**67**	S2/3/4
HH064	SZ VI	**160**	**65**	S2/3/4
HH064	SZ VI	**140**	**55**	S2/3/4
HH064	SZ VI	**141**	**61**	S2/3/4
HH065	SZ VI	**042**	**00**	L2/4
HH065	SZ VI	**162**	**45**	S2/3/4
HH065	SZ VI	**196**	**26**	S2/3/4
HH065	SZ VI	**277**	**15**	S2/3/4
HH065	SZ VI	**190**	**33**	S2/3/4
HH065	SZ VI	**150**	**67**	S2/3/4
HH065	SZ VI	**176**	**45**	S2/3/4
HH066	SZ VI	**230**	**30**	L2/4
HH066	SZ VI	**165**	**50**	S2/3/4
HH066	SZ VI	**165**	**20**	S2/3/4
HH067	SZ VI	**062**	**15**	B5
HH067	SZ VI	**138**	**87**	BA
HH067	SZ VI	**248**	**10**	L2/4
HH067	SZ VI	**080**	**05**	L2/4
HH067	SZ VI	**237**	**14**	L2/4
HH067	SZ VI	**236**	**11**	L2/4
HH067	SZ VI	**065**	**02**	L2/4
HH067	SZ VI	**218**	**10**	L2/4
HH067	SZ VI	**242**	**10**	L2/4
HH067	SZ VI	**248**	**13**	L2/4
HH067	SZ VI	**045**	**01**	L2/4
HH067	SZ VI	**048**	**05**	L2/4
HH067	SZ VI	**055**	**41**	L2/4
HH067	SZ VI	**310**	**85**	S2
HH067	SZ VI	**150**	**73**	S2/3/4
HH067	SZ VI	**170**	**40**	S2/3/4
HH067	SZ VI	**186**	**89**	S2/3/4
HH067	SZ VI	**146**	**65**	S2/3/4
HH067	SZ VI	**005**	**37**	S2/3/4
HH067	SZ VI	**142**	**64**	S2/3/4
HH067	SZ VI	**006**	**45**	S2/3/4
HH067	SZ VI	**174**	**50**	S2/3/4
HH067	SZ VI	**151**	**60**	S2/3/4
HH067	SZ VI	**170**	**59**	S2/3/4
HH067	SZ VI	**148**	**45**	S2/3/4
HH067	SZ VI	**158**	**68**	S2/3/4
HH067	SZ VI	**168**	**50**	S2/3/4
HH067	SZ VI	**152**	**55**	S2/3/4
HH067	SZ VI	**126**	**42**	S2/3/4
HH067	SZ VI	**134**	**37**	S2/3/4
HH067	SZ VI	**160**	**42**	S2/3/4
HH067	SZ VI	**145**	**36**	S2/3/4
HH067	SZ VI	**158**	**40**	S2/3/4
HH067	SZ VI	**173**	**40**	S2/3/4
HH067	SZ VI	**168**	**36**	S2/3/4
HH067	SZ VI	**166**	**32**	S2/3/4
HH067	SZ VI	**146**	**50**	S2/3/4
HH067	SZ VI	**151**	**74**	S2/3/4
HH067	SZ VI	**154**	**75**	S2/3/4
HH067	SZ VI	**161**	**83**	S2/3/4
HH067	SZ VI	**165**	**40**	S2/3/4
HH068	SZ VI	**260**	**50**	B5
HH068	SZ VI	**247**	**49**	B5
HH068	SZ VI	**268**	**14**	B5
HH068	SZ VI	**250**	**35**	B5
HH068	SZ VI	**230**	**09**	B5
HH068	SZ VI	**244**	**58**	B5
HH068	SZ VI	**250**	**17**	L2/4
HH068	SZ VI	**250**	**22**	L2/4
HH068	SZ VI	**265**	**05**	L2/4
HH068	SZ VI	**255**	**20**	L2/4
HH068	SZ VI	**075**	**20**	L2/4

BA: basalt dike, **CO**: cover, **PE**: pegmatite dike, **SB**: shear band, **SZ I**: structural zone I, **SZ II**: structural zone II, **SZ III**: structural zone III, **SZ IV**: structural zone IV, **SZ V**: structural zone V, **SZ VI**: structural zone VI, **SZ VII**: structural zone VII, **TM**: Punta de li Tulchi metabasite, **TO**: Tanaunella orthogneiss

structural field data, NE-Sardinia, n: 3600 (approx.)

outcrop	structural zone/lithology	dipping-direction	dipping-angle	fabric
HH001	SZ I	**020**	**45**	B3

HH068	SZ VI	**230**	**35**	L2/4
HH068	SZ VI	**218**	**35**	L2/4
HH068	SZ VI	**240**	**20**	L2/4
HH068	SZ VI	**330**	**88**	S2/3/4
HH068	SZ VI	**161**	**66**	S2/3/4
HH068	SZ VI	**161**	**80**	S2/3/4
HH068	SZ VI	**143**	**87**	S2/3/4
HH068	SZ VI	**162**	**74**	S2/3/4
HH068	SZ VI	**162**	**72**	S2/3/4
HH068	SZ VI	**155**	**59**	S2/3/4
HH068	SZ VI	**162**	**73**	S2/3/4
HH068	SZ VI	**352**	**75**	S2/3/4
HH068	SZ VI	**196**	**65**	S2/3/4
HH068	SZ VI	**320**	**64**	S2/3/4
HH068	SZ VI	**185**	**57**	S2/3/4
HH068	SZ VI	**295**	**51**	S2/3/4
HH068	SZ VI	**155**	**85**	S2/3/4
HH068	SZ VI	**158**	**80**	S2/3/4
HH069	SZ VI	**101**	**10**	L2/4
HH069	SZ VI	**195**	**55**	S2/3/4
HH069	SZ VI	**190**	**66**	S2/3/4
HH070	SZ VI	**076**	**15**	L2/4
HH070	SZ VI	**086**	**09**	L2/4
HH070	SZ VI	**087**	**11**	L2/4
HH070	SZ VI	**104**	**10**	L2/4
HH070	SZ VI	**095**	**15**	L2/4
HH070	SZ VI	**176**	**83**	L2/4
HH070	SZ VI	**264**	**17**	L2/4
HH070	SZ VI	**252**	**05**	L2/4
HH070	SZ VI	**086**	**03**	L2/4
HH070	SZ VI	**104**	**12**	L2/4
HH070	SZ VI	**106**	**05**	L2/4
HH070	SZ VI	**113**	**22**	L2/4
HH070	SZ VI	**168**	**80**	S2/3/4
HH070	SZ VI	**182**	**80**	S2/3/4
HH070	SZ VI	**168**	**80**	S2/3/4
HH070	SZ VI	**004**	**85**	S2/3/4
HH070	SZ VI	**183**	**84**	S2/3/4
HH070	SZ VI	**164**	**67**	S2/3/4
HH070	SZ VI	**176**	**83**	S2/3/4
HH070	SZ VI	**178**	**86**	S2/3/4
HH070	SZ VI	**164**	**77**	S2/3/4
HH070	SZ VI	**191**	**76**	S2/3/4
HH071	SZ VI	**274**	**25**	L2/4
HH071	SZ VI	**093**	**17**	L2/4
HH071	SZ VI	**188**	**70**	S2/3/4
HH071	SZ VI	**016**	**74**	S2/3/4
HH071	SZ VI	**012**	**84**	S2/3/4
HH071	SZ VI	**168**	**74**	S2/3/4
HH071	SZ VI	**192**	**75**	S2/3/4
HH071	SZ VI	**190**	**78**	S2/3/4
HH071	SZ VI	**180**	**80**	S2/3/4
HH072	SZ VI	**275**	**10**	B2/3
HH072	SZ VI	**195**	**57**	S2/3/4
HH072	SZ VI	**178**	**57**	S2/3/4
HH072	SZ VI	**302**	**43**	S2/3/4
HH073	SZ V	**155**	**82**	S2/3/4
HH074	SZ V	**215**	**89**	S2/3/4
HH074	SZ V	**215**	**37**	S2/3/4
HH075	SZ V	**258**	**20**	L2/4
HH075	SZ V	**195**	**75**	S2/3/4
HH076	SZ V	**304**	**14**	B5
HH076	SZ V	**307**	**13**	B5
HH076	SZ V	**260**	**14**	B5
HH076	SZ V	**230**	**16**	B5
HH076	SZ V	**255**	**05**	B5
HH076	SZ V	**278**	**15**	B5
HH076	SZ V	**225**	**54**	S2/3/4
HH076	SZ V	**228**	**66**	S2/3/4

HH076	SZ V	**320**	**21**	S2/3/4
HH076	SZ V	**186**	**84**	S2/3/4
HH076	SZ V	**190**	**64**	S2/3/4
HH076	SZ V	**195**	**85**	S2/3/4
HH076	SZ V	**353**	**73**	S2/3/4
HH076	SZ V	**350**	**55**	S2/3/4
HH076	SZ V	**312**	**01**	S2/3/4
HH076	SZ V	**175**	**35**	S2/3/4
HH076	SZ V	**356**	**80**	S2/3/4
HH076	SZ V	**188**	**87**	S2/3/4
HH077	SZ V	**113**	**20**	B2/3
HH077	SZ V	**255**	**05**	B2/3
HH077	SZ V	**108**	**10**	L2/4
HH077	SZ V	**205**	**75**	S2/3/4
HH077	SZ V	**172**	**68**	S2/3/4
HH077	SZ V	**164**	**75**	S2/3/4
HH077	SZ V	**193**	**64**	S2/3/4
HH078	SZ V	**265**	**13**	B2/3
HH078	SZ V	**274**	**30**	B2/3
HH078	SZ V	**120**	**14**	L2/4
HH078	SZ V	**120**	**05**	L2/4
HH078	SZ V	**208**	**70**	S2/3/4
HH078	SZ V	**212**	**47**	S2/3/4
HH078	SZ V	**171**	**89**	S2/3/4
HH079	SZ V	**110**	**15**	B5
HH079	SZ V	**110**	**23**	S2/3/4
HH079	SZ V	**194**	**47**	S2/3/4
HH079	SZ V	**186**	**79**	S2/3/4
HH079	SZ V	**210**	**37**	S2/3/4
HH080	SZ V	**121**	**05**	L2/4
HH080	SZ V	**215**	**87**	S2/3/4
HH081	SZ V	**032**	**81**	S2/3/4
HH082	SZ V	**104**	**50**	L2/4
HH082	SZ V	**189**	**75**	S2/3/4
HH082	SZ V	**195**	**85**	S2/3/4
HH082	SZ V	**190**	**81**	S2/3/4
HH082	SZ V	**184**	**86**	S2/3/4
HH082	SZ V	**008**	**85**	S2/3/4
HH082	SZ V	**138**	**45**	S2/3/4
HH082	SZ V	**146**	**75**	S2/3/4
HH082	SZ V	**154**	**37**	S2/3/4
HH083	SZ V	**184**	**72**	S2/3/4
HH083	SZ V	**178**	**63**	S2/3/4
HH083	SZ V	**182**	**56**	S2/3/4
HH083	SZ V	**233**	**75**	S2/3/4
HH083	SZ V	**176**	**56**	S2/3/4
HH084	SZ V	**102**	**35**	B2/3
HH084	SZ V	**198**	**89**	S2/3/4
HH084	SZ V	**177**	**81**	S2/3/4
HH084	SZ V	**347**	**85**	S2/3/4
HH084	SZ V	**163**	**85**	S2/3/4
HH084	SZ V	**183**	**80**	S2/3/4
HH085	SZ V	**096**	**35**	B2/3
HH085	SZ V	**008**	**85**	S2/3/4
HH085	SZ V	**328**	**85**	S2/3/4
HH085	SZ V	**172**	**72**	S2/3/4
HH085	SZ V	**178**	**57**	S2/3/4
HH085	SZ V	**185**	**59**	S2/3/4
HH086	SZ V	**095**	**30**	B2/3
HH086	SZ V	**210**	**75**	S2/3/4
HH086	SZ V	**202**	**55**	S2/3/4
HH086	SZ V	**200**	**89**	S2/3/4
HH087	SZ V	**122**	**17**	B2/3
HH087	SZ V	**090**	**20**	B2/3
HH087	SZ V	**108**	**10**	L2/4
HH087	SZ V	**043**	**68**	S2/3/4
HH088	SZ V	**112**	**86**	L2/4
HH088	SZ V	**222**	**75**	S2/3/4
HH088	SZ V	**220**	**73**	S2/3/4

BA: basalt dike, **CO**: cover, **PE**: pegmatite dike, **SB**: shear band, **SZ I**: structural zone I, **SZ II**: structural zone II, **SZ III**: structural zone III, **SZ IV**: structural zone IV, **SZ V**: structural zone V, **SZ VI**: structural zone VI, **SZ VII**: structural zone VII, **TM**: Punta de li Tulchi metabasite, **TO**: Tanaunella orthogneiss

structural field data, NE-Sardinia, n: 3600 (approx.)

outcrop	structural zone/lithology	dipping-direction	dipping-angle	fabric
HH001	SZ I	**020**	**45**	B3

HH088	SZ V	**210**	**55**	S2/3/4
HH088	SZ V	**212**	**65**	S2/3/4
HH089	SZ V	**120**	**15**	L2/4
HH089	SZ V	**204**	**67**	S2/3/4
HH089	SZ V	**058**	**78**	S2/3/4
HH089	SZ V	**234**	**87**	S2/3/4
HH090	SZ V	**216**	**72**	S2/3/4
HH090	SZ V	**222**	**72**	S2/3/4
HH090	SZ V	**213**	**60**	S2/3/4
HH090	SZ V	**202**	**85**	S2/3/4
HH090	SZ V	**006**	**75**	S2/3/4
HH090	SZ V	**205**	**72**	S2/3/4
HH090	SZ V	**200**	**87**	S2/3/4
HH091	SZ V	**136**	**13**	L2/4
HH091	SZ V	**217**	**45**	S2/3/4
HH092	SZ V	**128**	**28**	L2/4
HH092	SZ V	**180**	**45**	S2/3/4
HH093	SZ V	**090**	**15**	L2/4
HH093	SZ V	**172**	**67**	S2/3/4
HH093	SZ V	**172**	**80**	S2/3/4
HH094	SZ V	**106**	**29**	L2/4
HH094	SZ V	**185**	**54**	S2/3/4
HH095	SZ VI	**099**	**55**	B5
HH095	SZ VI	**090**	**55**	L2/4
HH095	SZ VI	**162**	**81**	S2/3/4
HH096	SZ VI	**048**	**25**	B2/3
HH096	SZ VI	**070**	**26**	S2/3/4
HH096	SZ VI	**076**	**32**	S2/3/4
HH097	SZ V	**240**	**83**	B2/3
HH097	SZ V	**272**	**40**	L2
HH097	SZ V	**108**	**07**	L2
HH097	SZ V	**280**	**10**	L2
HH097	SZ V	**278**	**24**	L2
HH097	SZ V	**204**	**72**	S2
HH097	SZ V	**200**	**64**	S2
HH097	SZ V	**198**	**80**	S2
HH097	SZ V	**191**	**75**	S2
HH097	SZ V	**135**	**83**	S2
HH097	SZ V	**330**	**85**	S2
HH097	SZ V	**184**	**75**	S2
HH097	SZ V	**223**	**57**	S2
HH097	SZ V	**205**	**67**	S2
HH097	SZ V	**170**	**78**	S2/3/4
HH098	SZ VII	**238**	**32**	B2
HH098	SZ VII	**202**	**55**	B3
HH098	SZ VII	**224**	**36**	L2
HH098	SZ VII	**230**	**30**	L2
HH098	SZ VII	**178**	**47**	S2
HH098	SZ VII	**240**	**47**	S2
HH098	SZ VII	**235**	**85**	S2
HH098	SZ VII	**176**	**55**	S2
HH099	SZ VII	**104**	**01**	B2
HH099	SZ VII	**164**	**74**	S2
HH099	SZ VII	**190**	**65**	S2
HH099	SZ VII	**140**	**81**	S2
HH099	SZ VII	**208**	**60**	S2
HH099	SZ VII	**175**	**81**	S2
HH099	SZ VII	**142**	**88**	S2
HH100	SZ VII	**215**	**34**	L2
HH100	SZ VII	**105**	**50**	L2
HH100	SZ VII	**142**	**50**	S2
HH101	SZ VII	**260**	**74**	B3
HH101	SZ VII	**300**	**82**	B3
HH101	SZ VII	**155**	**72**	B3
HH101	SZ VII	**075**	**55**	B3
HH101	SZ VII	**251**	**70**	B3
HH101	SZ VII	**260**	**70**	B3
HH101	SZ VII	**098**	**35**	B3
HH101	SZ VII	**092**	**16**	B3

HH101	SZ VII	**095**	**15**	B3
HH101	SZ VII	**118**	**34**	B3
HH101	SZ VII	**220**	**37**	B3
HH101	SZ VII	**246**	**50**	B3
HH101	SZ VII	**250**	**27**	L2
HH101	SZ VII	**238**	**45**	L2
HH101	SZ VII	**227**	**50**	L2
HH101	SZ VII	**233**	**45**	L2
HH101	SZ VII	**164**	**72**	S2
HH101	SZ VII	**157**	**67**	S2
HH101	SZ VII	**155**	**72**	S2
HH101	SZ VII	**163**	**62**	S2
HH101	SZ VII	**188**	**59**	S2
HH101	SZ VII	**154**	**70**	S2
HH101	SZ VII	**138**	**81**	S2
HH101	SZ VII	**139**	**63**	S2
HH101	SZ VII	**196**	**85**	S2
HH101	SZ VII	**195**	**80**	S2
HH101	SZ VII	**015**	**64**	S2
HH101	SZ VII	**024**	**55**	S2
HH101	SZ VII	**196**	**77**	S2
HH101	SZ VII	**024**	**55**	S2
HH101	SZ VII	**196**	**77**	S2
HH101	SZ VII	**012**	**82**	S2
HH101	SZ VII	**177**	**76**	S2
HH101	SZ VII	**181**	**60**	S2
HH101	SZ VII	**174**	**57**	S2
HH101	SZ VII	**170**	**67**	S2
HH101	SZ VII	**184**	**65**	S2
HH102	SZ VII	**238**	**61**	B3
HH102	SZ VII	**202**	**47**	B3
HH102	SZ VII	**220**	**36**	L2
HH102	SZ VII	**210**	**34**	L2
HH102	SZ VII	**128**	**70**	S2
HH102	SZ VII	**158**	**55**	S2
HH102	SZ VII	**142**	**59**	S2
HH103	SZ VII	**175**	**35**	B-kink
HH103	SZ VII	**184**	**33**	B-kink
HH103	SZ VII	**220**	**15**	L2
HH103	SZ VII	**155**	**53**	S2
HH103	SZ VII	**163**	**43**	S2
HH103	SZ VII	**118**	**52**	S2
HH104	TO	**050**	**12**	L2
HH104	TO	**230**	**01**	L2
HH104	TO	**232**	**05**	L2
HH104	SZ VII	**360**	**70**	PE
HH104	SZ VII	**035**	**85**	PE
HH104	TO	**123**	**40**	S2
HH104	TO	**142**	**30**	S2
HH104	TO	**148**	**30**	S2
HH104	TO	**148**	**38**	S2
HH104	TO	**148**	**43**	S2
HH104	TO	**152**	**30**	S2
HH105	TO	**072**	**24**	L2
HH105	SZ VII	**218**	**85**	PE
HH105	TO	**126**	**38**	S2
HH106	SZ VII	**092**	**43**	B2
HH106	SZ VII	**060**	**10**	B2
HH106	SZ VII	**172**	**20**	B2
HH106	SZ VII	**172**	**21**	B2
HH106	SZ VII	**124**	**15**	B2
HH106	SZ VII	**061**	**22**	L2
HH106	SZ VII	**110**	**46**	S2
HH106	SZ VII	**106**	**27**	S2
HH106	SZ VII	**092**	**30**	S2
HH106	SZ VII	**120**	**32**	S2
HH106	SZ VII	**105**	**42**	S2
HH106	SZ VII	**110**	**40**	S2
HH106	SZ VII	**111**	**55**	S2

BA: basalt dike, **CO**: cover, **PE**: pegmatite dike, **SB**: shear band, **SZ I**: structural zone I, **SZ II**: structural zone II, **SZ III**: structural zone III, **SZ IV**: structural zone IV, **SZ V**: structural zone V, **SZ VI**: structural zone VI, **SZ VII**: structural zone VII, **TM**: Punta de li Tulchi metabasite, **TO**: Tanaunella orthogneiss

structural field data, NE-Sardinia, n: 3600 (approx.)

outcrop	structural zone/lithology	dipping-direction	dipping-angle	fabric
HH001	SZ I	**020**	**45**	B3

HH106	SZ VII	**108**	**82**	S2
HH106	SZ VII	**107**	**43**	S2
HH106	SZ VII	**107**	**43**	S2
HH106	SZ VII	**105**	**30**	S2
HH107	TO	**055**	**19**	L2
HH107	TO	**128**	**35**	S2
HH108	SZ VII	**073**	**22**	B2
HH108	SZ VII	**062**	**10**	B2
HH108	SZ VII	**095**	**37**	B2
HH108	SZ VII	**140**	**30**	B2
HH108	SZ VII	**125**	**27**	B3
HH108	SZ VII	**120**	**30**	B3
HH108	SZ VII	**070**	**25**	L2
HH108	SZ VII	**058**	**05**	L2
HH108	SZ VII	**059**	**10**	L2
HH108	SZ VII	**093**	**31**	L2
HH108	SZ VII	**096**	**30**	L2
HH108	SZ VII	**134**	**35**	S2
HH108	SZ VII	**130**	**27**	S2
HH108	SZ VII	**108**	**26**	S2
HH108	SZ VII	**118**	**21**	S2
HH108	SZ VII	**105**	**42**	S2
HH108	SZ VII	**110**	**37**	S2
HH108	SZ VII	**104**	**30**	S2
HH109	SZ VII	**070**	**29**	B2
HH109	SZ VII	**212**	**15**	B2
HH109	SZ VII	**191**	**16**	B-kink
HH109	SZ VII	**180**	**10**	B-kink
HH109	SZ VII	**064**	**20**	L2
HH109	SZ VII	**070**	**24**	L2
HH109	SZ VII	**226**	**05**	L2
HH109	SZ VII	**055**	**09**	L2
HH109	SZ VII	**070**	**15**	L2
HH109	SZ VII	**078**	**16**	L2
HH109	SZ VII	**213**	**18**	L2
HH109	SZ VII	**082**	**27**	L2
HH109	SZ VII	**145**	**50**	S2
HH109	SZ VII	**118**	**31**	S2
HH109	SZ VII	**120**	**30**	S2
HH109	SZ VII	**117**	**25**	S2
HH109	SZ VII	**100**	**85**	S2
HH109	SZ VII	**140**	**42**	S2
HH109	SZ VII	**140**	**38**	S2
HH109	SZ VII	**135**	**27**	S2
HH110	SZ VII	**118**	**37**	B2
HH110	SZ VII	**090**	**66**	PE
HH110	SZ VII	**115**	**31**	PE
HH110	SZ VII	**125**	**38**	S2
HH110	SZ VII	**108**	**34**	S2
HH110	SZ VII	**142**	**46**	S2
HH111	SZ VII	**087**	**35**	B3
HH111	SZ VII	**108**	**43**	B3
HH111	SZ VII	**076**	**34**	B3
HH111	SZ VII	**083**	**05**	B3
HH111	SZ VII	**075**	**34**	B3
HH111	SZ VII	**065**	**30**	B3
HH111	SZ VII	**087**	**35**	B3
HH111	SZ VII	**097**	**26**	B3
HH111	SZ VII	**077**	**16**	B3
HH111	SZ VII	**075**	**31**	B3
HH111	SZ VII	**076**	**30**	B3
HH111	SZ VII	**101**	**81**	PE
HH111	SZ VII	**180**	**81**	S2
HH111	SZ VII	**355**	**87**	S2
HH111	SZ VII	**176**	**87**	S2
HH111	SZ VII	**190**	**53**	S2
HH111	SZ VII	**110**	**26**	S2
HH111	SZ VII	**166**	**85**	S2
HH111	SZ VII	**327**	**86**	S2

HH111	SZ VII	**158**	**74**	S2
HH111	SZ VII	**136**	**63**	S2
HH111	SZ VII	**168**	**71**	S2
HH111	SZ VII	**161**	**68**	S2
HH112	SZ VII	**078**	**17**	B3
HH112	SZ VII	**085**	**25**	B3
HH112	SZ VII	**058**	**40**	B3
HH112	SZ VII	**081**	**42**	B3
HH112	SZ VII	**106**	**26**	L2
HH112	SZ VII	**088**	**22**	L2
HH112	SZ VII	**051**	**26**	L2
HH112	SZ VII	**135**	**40**	S2
HH112	SZ VII	**145**	**34**	S2
HH112	SZ VII	**356**	**80**	S2
HH112	SZ VII	**170**	**63**	S2
HH112	SZ VII	**080**	**19**	S2
HH112	SZ VII	**159**	**70**	S2
HH112	SZ VII	**327**	**79**	S2
HH113	SZ VII	**083**	**44**	B3
HH113	SZ VII	**052**	**39**	B3
HH113	SZ VII	**078**	**46**	B3
HH113	SZ VII	**082**	**35**	B3
HH113	SZ VII	**048**	**27**	L2
HH113	SZ VII	**073**	**29**	L2
HH113	SZ VII	**112**	**63**	S2
HH113	SZ VII	**073**	**64**	S2
HH113	SZ VII	**031**	**74**	S2
HH113	SZ VII	**033**	**85**	S2
HH113	SZ VII	**048**	**36**	S2
HH113	SZ VII	**077**	**46**	S2
HH113	SZ VII	**108**	**45**	S2
HH113	SZ VII	**135**	**58**	S2
HH114	SZ VII	**125**	**65**	B3
HH114	SZ VII	**087**	**65**	B3
HH114	SZ VII	**061**	**53**	B3
HH114	SZ VII	**072**	**71**	B3
HH114	SZ VII	**116**	**45**	B3
HH114	SZ VII	**035**	**43**	S2
HH114	SZ VII	**068**	**45**	S2
HH114	SZ VII	**116**	**86**	S2
HH114	SZ VII	**098**	**67**	S2
HH114	SZ VII	**108**	**65**	S2
HH114	SZ VII	**109**	**75**	S2
HH114	SZ VII	**106**	**73**	S2
HH114	SZ VII	**091**	**66**	S2
HH114	SZ VII	**087**	**42**	S2
HH115	TM	**259**	**17**	B2
HH115	TM	**284**	**29**	B2
HH115	TM	**090**	**05**	B3
HH115	TM	**158**	**25**	B3
HH115	TM	**033**	**10**	L2
HH115	TM	**040**	**55**	L2
HH115	TM	**041**	**40**	L2
HH115	TM	**048**	**37**	L2
HH115	TM	**145**	**15**	L2
HH115	TM	**001**	**52**	S2
HH115	TM	**002**	**73**	S2
HH115	TM	**006**	**69**	S2
HH115	TM	**008**	**52**	S2
HH115	TM	**017**	**68**	S2
HH115	TM	**180**	**80**	S2
HH115	TM	**188**	**55**	S2
HH115	TM	**218**	**40**	S2
HH115	TM	**330**	**45**	S2
HH115	TM	**331**	**61**	S2
HH115	TM	**335**	**70**	S2
HH115	TM	**340**	**64**	S2
HH115	TM	**340**	**80**	S2
HH115	TM	**345**	**67**	S2

BA: basalt dike, **CO**: cover, **PE**: pegmatite dike, **SB**: shear band, **SZ I**: structural zone I, **SZ II**: structural zone II, **SZ III**: structural zone III, **SZ IV**: structural zone IV, **SZ V**: structural zone V, **SZ VI**: structural zone VI, **SZ VII**: structural zone VII, **TM**: Punta de li Tulchi metabasite, **TO**: Tanaunella orthogneiss

structural field data, NE-Sardinia, n: 3600 (approx.)

outcrop	structural zone/lithology	dipping-direction	dipping-angle	fabric
HH001	SZ I	**020**	**45**	B3

HH115	TM	**345**	**66**	S2
HH115	TM	**346**	**63**	S2
HH115	TM	**348**	**63**	S2
HH115	TM	**348**	**71**	S2
HH115	TM	**349**	**70**	S2
HH115	TM	**349**	**86**	S2
HH115	TM	**350**	**59**	S2
HH115	TM	**350**	**75**	S2
HH115	TM	**351**	**62**	S2
HH115	TM	**351**	**68**	S2
HH115	TM	**352**	**68**	S2
HH115	TM	**354**	**57**	S2
HH115	TM	**355**	**58**	S2
HH115	TM	**355**	**57**	S2
HH115	TM	**360**	**65**	S2
HH115	TM	**360**	**64**	S2
HH115	TM	**186**	**56**	S3
HH116	SZ VII	**172**	**30**	B3
HH116	SZ VII	**118**	**16**	B3
HH116	SZ VII	**126**	**13**	B3
HH116	SZ VII	**138**	**19**	B3
HH116	SZ VII	**248**	**29**	B3
HH116	SZ VII	**103**	**06**	B3
HH116	SZ VII	**141**	**11**	B3
HH116	SZ VII	**118**	**21**	B3
HH116	SZ VII	**110**	**12**	B3
HH116	SZ VII	**142**	**30**	B3
HH116	SZ VII	**085**	**01**	B3
HH116	SZ VII	**226**	**30**	B-kink
HH116	SZ VII	**242**	**14**	B-kink
HH116	SZ VII	**232**	**34**	L2
HH116	SZ VII	**224**	**01**	L2
HH116	SZ VII	**100**	**15**	L2
HH116	SZ VII	**168**	**49**	S2
HH116	SZ VII	**292**	**51**	S2
HH116	SZ VII	**141**	**69**	S2
HH116	SZ VII	**161**	**50**	S2
HH116	SZ VII	**166**	**51**	S2
HH116	SZ VII	**154**	**40**	S2
HH116	SZ VII	**183**	**76**	S2
HH116	SZ VII	**190**	**56**	S2
HH116	SZ VII	**115**	**15**	S2
HH116	SZ VII	**152**	**15**	S2
HH116	SZ VII	**130**	**16**	S2
HH116	SZ VII	**026**	**65**	S2
HH116	SZ VII	**125**	**25**	S2
HH116	SZ VII	**150**	**28**	S2
HH116	SZ VII	**221**	**59**	S2
HH116	SZ VII	**188**	**75**	S2
HH116	SZ VII	**174**	**70**	S2
HH116	SZ VII	**181**	**65**	S2
HH116	SZ VII	**198**	**47**	S2
HH116	SZ VII	**182**	**50**	S2
HH116	SZ VII	**162**	**53**	S2
HH116	SZ VII	**185**	**63**	S2
HH117	SZ VII	**038**	**40**	B3
HH117	SZ VII	**240**	**26**	B3
HH117	SZ VII	**303**	**60**	B-kink
HH117	SZ VII	**044**	**10**	L2
HH117	SZ VII	**240**	**20**	L2
HH117	SZ VII	**335**	**57**	S2
HH117	SZ VII	**326**	**60**	S2
HH117	SZ VII	**298**	**55**	S2
HH117	SZ VII	**280**	**59**	S2
HH117	SZ VII	**297**	**55**	S2
HH117	SZ VII	**328**	**75**	S2
HH117	SZ VII	**014**	**80**	S2
HH117	SZ VII	**312**	**67**	S2
HH117	SZ VII	**145**	**81**	S2

HH118	SZ VII	**211**	**09**	L2
HH118	SZ VII	**200**	**15**	L2
HH118	SZ VII	**143**	**35**	S2
HH118	SZ VII	**131**	**47**	S2
HH118	SZ VII	**127**	**41**	S2
HH118	SZ VII	**129**	**36**	S2
HH119	SZ VII	**125**	**40**	B3
HH119	SZ VII	**180**	**32**	B3
HH119	SZ VII	**135**	**27**	B3
HH119	SZ VII	**145**	**36**	B-kink
HH119	SZ VII	**270**	**05**	L2
HH119	SZ VII	**222**	**20**	L2
HH119	SZ VII	**208**	**27**	L2
HH119	SZ VII	**066**	**62**	PE
HH119	SZ VII	**062**	**56**	PE
HH119	SZ VII	**147**	**63**	S2
HH119	SZ VII	**172**	**75**	S2
HH119	SZ VII	**198**	**49**	S2
HH119	SZ VII	**218**	**36**	S2
HH119	SZ VII	**190**	**28**	S2
HH119	SZ VII	**212**	**25**	S2
HH119	SZ VII	**200**	**45**	S2
HH120	SZ VII	**265**	**05**	L2
HH120	SZ VII	**236**	**23**	L2
HH120	SZ VII	**225**	**17**	L2
HH120	SZ VII	**033**	**12**	L2
HH120	SZ VII	**028**	**07**	L2
HH120	SZ VII	**080**	**11**	S2
HH120	SZ VII	**322**	**35**	S2
HH120	SZ VII	**052**	**10**	S2
HH120	SZ VII	**157**	**15**	S2
HH120	SZ VII	**205**	**13**	S2
HH120	SZ VII	**225**	**15**	S2
HH120	SZ VII	**348**	**05**	S2
HH120	SZ VII	**208**	**43**	S2
HH120	SZ VII	**194**	**35**	S2
HH121	SZ VII	**089**	**06**	B3
HH121	SZ VII	**082**	**25**	B3
HH121	SZ VII	**178**	**48**	L2
HH121	SZ VII	**150**	**42**	L2
HH121	SZ VII	**210**	**54**	L2
HH121	SZ VII	**208**	**38**	L2
HH121	SZ VII	**192**	**52**	L2
HH121	SZ VII	**200**	**32**	L2
HH121	SZ VII	**191**	**33**	L2
HH121	SZ VII	**182**	**40**	L2
HH121	SZ VII	**208**	**50**	L2
HH121	SZ VII	**143**	**20**	L2
HH121	SZ VII	**196**	**62**	S2
HH121	SZ VII	**178**	**48**	S2
HH121	SZ VII	**171**	**48**	S2
HH121	SZ VII	**258**	**08**	S2
HH121	SZ VII	**158**	**41**	S2
HH121	SZ VII	**164**	**77**	S2
HH121	SZ VII	**014**	**74**	S2
HH121	SZ VII	**358**	**61**	S2
HH121	SZ VII	**181**	**64**	S2
HH121	SZ VII	**138**	**21**	S2
HH121	SZ VII	**178**	**57**	S2
HH121	SZ VII	**133**	**69**	S2
HH122	SZ VII	**070**	**05**	B3
HH122	SZ VII	**170**	**38**	L2
HH122	SZ VII	**225**	**20**	L2
HH122	SZ VII	**166**	**30**	L2
HH122	SZ VII	**185**	**25**	L2
HH122	SZ VII	**133**	**39**	S2
HH122	SZ VII	**143**	**46**	S2
HH122	SZ VII	**128**	**46**	S2
HH122	SZ VII	**128**	**36**	S2

BA: basalt dike, **CO**: cover, **PE**: pegmatite dike, **SB**: shear band, **SZ I**: structural zone I, **SZ II**: structural zone II, **SZ III**: structural zone III, **SZ IV**: structural zone IV, **SZ V**: structural zone V, **SZ VI**: structural zone VI, **SZ VII**: structural zone VII, **TM**: Punta de li Tulchi metabasite, **TO**: Tanaunella orthogneiss

structural field data, NE-Sardinia, n: 3600 (approx.)

outcrop	structural zone/lithology	dipping-direction	dipping-angle	fabric
HH001	SZ I	**020**	**45**	B3

HH122	SZ VII	**127**	**40**	S2
HH123	SZ VII	**246**	**06**	B3
HH123	SZ VII	**254**	**08**	B3
HH123	SZ VII	**244**	**26**	B3
HH123	SZ VII	**200**	**13**	B3
HH123	SZ VII	**150**	**37**	B-kink
HH123	SZ VII	**319**	**03**	B-kink
HH123	SZ VII	**250**	**05**	L2
HH123	SZ VII	**244**	**12**	L2
HH123	SZ VII	**211**	**06**	L2
HH123	SZ VII	**231**	**18**	L2
HH123	SZ VII	**208**	**19**	L2
HH123	SZ VII	**200**	**18**	S2
HH123	SZ VII	**182**	**34**	S2
HH123	SZ VII	**188**	**15**	S2
HH123	SZ VII	**165**	**40**	S2
HH123	SZ VII	**030**	**04**	S2
HH124	SZ VII	**088**	**06**	L2
HH124	SZ VII	**055**	**50**	L2
HH124	SZ VII	**110**	**48**	L2
HH124	SZ VII	**180**	**80**	S2
HH124	SZ VII	**020**	**85**	S2
HH124	SZ VII	**315**	**77**	S2
HH124	SZ VII	**118**	**59**	S2
HH124	SZ VII	**146**	**45**	S2
HH124	SZ VII	**154**	**64**	S2
HH125	SZ VII	**042**	**05**	B3
HH125	SZ VII	**212**	**04**	B3
HH125	SZ VII	**041**	**14**	B3
HH125	SZ VII	**100**	**65**	BA
HH125	SZ VII	**270**	**82**	BA
HH125	SZ VII	**082**	**84**	BA
HH125	SZ VII	**234**	**10**	L2
HH125	SZ VII	**228**	**20**	L2
HH125	SZ VII	**081**	**41**	L2
HH125	SZ VII	**230**	**09**	L2
HH125	SZ VII	**238**	**24**	L2
HH125	SZ VII	**255**	**08**	L2
HH125	SZ VII	**071**	**11**	L2
HH125	SZ VII	**077**	**15**	L2
HH125	SZ VII	**245**	**02**	L2
HH125	SZ VII	**132**	**50**	S2
HH125	SZ VII	**198**	**23**	S2
HH125	SZ VII	**210**	**53**	S2
HH125	SZ VII	**171**	**23**	S2
HH125	SZ VII	**145**	**39**	S2
HH125	SZ VII	**181**	**42**	S2
HH125	SZ VII	**178**	**41**	S2
HH125	SZ VII	**135**	**44**	S2
HH125	SZ VII	**159**	**67**	S2
HH125	SZ VII	**160**	**59**	S2
HH125	SZ VII	**162**	**55**	S2
HH126	SZ VII	**222**	**07**	B3
HH126	SZ VII	**214**	**10**	B3
HH126	SZ VII	**192**	**17**	B3
HH126	SZ VII	**052**	**05**	B3
HH126	SZ VII	**072**	**37**	L2
HH126	SZ VII	**106**	**05**	L2
HH126	SZ VII	**033**	**60**	PE
HH126	SZ VII	**144**	**53**	S2
HH126	SZ VII	**126**	**58**	S2
HH126	SZ VII	**122**	**60**	S2
HH126	SZ VII	**265**	**80**	S2
HH126	SZ VII	**122**	**40**	S2
HH126	SZ VII	**145**	**47**	S2
HH126	SZ VII	**120**	**89**	S2
HH126	SZ VII	**188**	**32**	S2
HH127	SZ VII	**256**	**25**	L2
HH127	SZ VII	**088**	**26**	L2
HH127	SZ VII	**093**	**27**	L2
HH127	SZ VII	**088**	**05**	L2
HH127	SZ VII	**160**	**60**	S2
HH127	SZ VII	**155**	**60**	S2
HH127	SZ VII	**160**	**64**	S2
HH127	SZ VII	**170**	**59**	S2
HH127	SZ VII	**146**	**50**	S2
HH128	SZ VII	**245**	**20**	B3
HH128	SZ VII	**231**	**14**	L2
HH128	SZ VII	**171**	**56**	S2
HH128	SZ VII	**162**	**61**	S2
HH128	SZ VII	**145**	**60**	S2
HH128	SZ VII	**145**	**49**	S2
HH128	SZ VII	**150**	**62**	S2
HH129	SZ VII	**075**	**33**	L2
HH129	SZ VII	**093**	**20**	L2
HH129	SZ VII	**064**	**15**	L2
HH129	SZ VII	**075**	**29**	L2
HH129	SZ VII	**135**	**50**	S2
HH129	SZ VII	**162**	**48**	S2
HH129	SZ VII	**135**	**60**	S2
HH129	SZ VII	**146**	**66**	S2
HH130	SZ VII	**075**	**60**	L2
HH130	SZ VII	**105**	**45**	L2
HH130	SZ VII	**120**	**66**	S2
HH130	SZ VII	**140**	**49**	S2
HH132	SZ V	**257**	**26**	B5
HH132	SZ V	**240**	**35**	B5
HH132	SZ V	**118**	**10**	L2/4
HH132	SZ V	**117**	**10**	L2/4
HH132	SZ V	**110**	**06**	L2/4
HH132	SZ V	**110**	**08**	L2/4
HH132	SZ V	**185**	**25**	S2/3/4
HH132	SZ V	**190**	**41**	S2/3/4
HH132	SZ V	**200**	**35**	S2/3/4
HH132	SZ V	**185**	**31**	S2/3/4
HH132	SZ V	**195**	**27**	S2/3/4
HH132	SZ V	**208**	**20**	S2/3/4
HH132	SZ V	**330**	**40**	S2/3/4
HH132	SZ V	**330**	**36**	S2/3/4
HH132	SZ V	**328**	**20**	S2/3/4
HH132	SZ V	**205**	**50**	S2/3/4
HH132	SZ V	**190**	**46**	S2/3/4
HH133	SZ V	**063**	**01**	L2
HH133	SZ V	**045**	**48**	L2
HH133	SZ V	**047**	**03**	L2
HH133	SZ V	**280**	**40**	L2/4
HH133	SZ V	**275**	**40**	L2/4
HH133	SZ V	**306**	**36**	L2/4
HH133	SZ V	**320**	**66**	L2/4
HH133	SZ V	**328**	**40**	L2/4
HH133	SZ V	**330**	**70**	S2/3/4
HH133	SZ V	**331**	**56**	S2/3/4
HH133	SZ V	**150**	**81**	S2/3/4
HH133	SZ V	**335**	**63**	S2/3/4
HH133	SZ V	**142**	**85**	S2/3/4
HH133	SZ V	**131**	**75**	S2/3/4
HH133	SZ V	**136**	**78**	S2/3/4
HH133	SZ V	**120**	**75**	S2/3/4
HH133	SZ V	**134**	**47**	S2/3/4
HH133	SZ V	**340**	**44**	S2/3/4
HH134	CO	**115**	**26**	S0
HH134	CO	**190**	**15**	S0
HH134	CO	**130**	**13**	S0
HH134	CO	**142**	**12**	S0
HH134	CO	**162**	**01**	S0
HH134	CO	**120**	**09**	S0
HH134	CO	**135**	**12**	S0
HH134	CO	**167**	**12**	S0

BA: basalt dike, **CO**: cover, **PE**: pegmatite dike, **SB**: shear band, **SZ I**: structural zone I, **SZ II**: structural zone II, **SZ III**: structural zone III, **SZ IV**: structural zone IV, **SZ V**: structural zone V, **SZ VI**: structural zone VI, **SZ VII**: structural zone VII, **TM**: Punta de li Tulchi metabasite, **TO**: Tanaunella orthogneiss

structural field data, NE-Sardinia, n: 3600 (approx.)

outcrop	structural zone/lithology	dipping-direction	dipping-angle	fabric
HH001	SZ I	**020**	**45**	B3

HH134	CO	**146**	**14**	S0
HH134	CO	**154**	**22**	S0
HH135	SZ II	**130**	**40**	B3
HH135	SZ II	**128**	**40**	B3
HH135	SZ II	**106**	**25**	L2/4
HH135	SZ II	**114**	**40**	L2/4
HH135	SZ II	**097**	**34**	L2/4
HH135	SZ II	**182**	**51**	S2
HH135	SZ II	**164**	**45**	S2
HH135	SZ II	**178**	**57**	S3
HH135	SZ II	**170**	**53**	S3
HH135	SZ II	**176**	**50**	S3
HH135	SZ II	**160**	**33**	S3
HH135	SZ II	**166**	**48**	S3
HH135	SZ II	**155**	**45**	S3
HH135	SZ II	**173**	**45**	S3
HH135	SZ II	**156**	**42**	S3
HH135	SZ II	**195**	**55**	S3
HH136	SZ III	**120**	**32**	L2/4
HH136	SZ III	**243**	**11**	L2/4
HH136	SZ III	**260**	**02**	L2/4
HH136	SZ III	**160**	**47**	S2/4
HH136	SZ III	**155**	**38**	S2/4
HH136	SZ III	**110**	**33**	S2/4
HH136	SZ III	**180**	**32**	S2/4
HH136	SZ III	**172**	**36**	S2/4
HH136	SZ III	**180**	**35**	S2/4
HH136	SZ III	**178**	**28**	S2/4
HH137	SZ II	**084**	**14**	L2/4
HH137	SZ II	**092**	**12**	L2/4
HH137	SZ II	**175**	**44**	S2
HH137	SZ II	**205**	**36**	S2
HH137	SZ II	**202**	**40**	S2
HH137	SZ II	**166**	**44**	S3
HH138	SZ I	**052**	**15**	B3
HH138	SZ I	**054**	**28**	B3
HH138	SZ I	**054**	**30**	B3
HH138	SZ I	**054**	**10**	B3
HH138	SZ I	**048**	**07**	B3
HH138	SZ I	**083**	**19**	B5
HH138	SZ I	**087**	**28**	B5
HH138	SZ I	**050**	**13**	L2
HH138	SZ I	**111**	**32**	S2
HH138	SZ I	**112**	**28**	S2
HH138	SZ I	**104**	**19**	S2
HH138	SZ I	**106**	**68**	S2
HH138	SZ I	**053**	**27**	S2
HH138	SZ I	**122**	**27**	S2
HH138	SZ I	**337**	**87**	S2
HH138	SZ I	**327**	**75**	S2
HH138	SZ I	**155**	**85**	S2
HH138	SZ I	**088**	**24**	S2
HH138	SZ I	**338**	**45**	S2
HH138	SZ I	**112**	**20**	S2
HH138	SZ I	**091**	**18**	S2
HH138	SZ I	**086**	**56**	S2
HH138	SZ I	**119**	**50**	S3
HH138	SZ I	**125**	**47**	S3
HH138	SZ I	**120**	**50**	S3
HH138	SZ I	**140**	**75**	S3
HH138	SZ I	**118**	**40**	S3
HH138	SZ I	**129**	**24**	S3
HH138	SZ I	**114**	**41**	S3
HH138	SZ I	**109**	**21**	S3
HH138	SZ I	**100**	**57**	S3
HH139	SZ I	**220**	**02**	L2
HH139	SZ I	**235**	**05**	L2
HH139	SZ I	**136**	**79**	S2
HH139	SZ I	**113**	**66**	S2
HH139	SZ I	**314**	**84**	S2
HH139	SZ I	**312**	**60**	S2
HH139	SZ I	**302**	**34**	S2
HH139	SZ I	**001**	**05**	S2
HH140	SZ I	**052**	**01**	B3
HH140	SZ I	**220**	**06**	L2
HH140	SZ I	**300**	**37**	S2
HH140	SZ I	**126**	**89**	S2
HH140	SZ I	**128**	**76**	S2
HH140	SZ I	**312**	**86**	S2
HH140	SZ I	**119**	**45**	S3
HH141	SZ I	**044**	**04**	B3
HH141	SZ I	**049**	**07**	B3
HH141	SZ I	**045**	**11**	B3
HH141	SZ I	**051**	**01**	B3
HH141	SZ I	**040**	**07**	B3
HH141	SZ I	**044**	**04**	B3
HH141	SZ I	**040**	**04**	L2
HH141	SZ I	**358**	**17**	S2
HH141	SZ I	**116**	**21**	S2
HH141	SZ I	**128**	**89**	S2
HH141	SZ I	**138**	**83**	S2
HH141	SZ I	**330**	**60**	S2
HH141	SZ I	**096**	**13**	S2
HH141	SZ I	**105**	**12**	S2
HH141	SZ I	**315**	**86**	S2
HH141	SZ I	**306**	**85**	S2
HH141	SZ I	**115**	**27**	S2
HH141	SZ I	**104**	**13**	S2
HH141	SZ I	**309**	**63**	S2
HH141	SZ I	**126**	**87**	S2
HH141	SZ I	**110**	**32**	S2
HH141	SZ I	**111**	**14**	S2
HH141	SZ I	**096**	**08**	S2
HH141	SZ I	**312**	**62**	S2
HH141	SZ I	**128**	**44**	S3
HH141	SZ I	**123**	**55**	S3
HH141	SZ I	**128**	**34**	S3
HH141	SZ I	**130**	**42**	S3
HH141	SZ I	**129**	**55**	S3
HH141	SZ I	**130**	**49**	S3
HH141	SZ I	**135**	**45**	S3
HH142	SZ I	**028**	**10**	B3
HH142	SZ I	**048**	**07**	B3
HH142	SZ I	**057**	**13**	B3
HH142	SZ I	**048**	**05**	L2
HH142	SZ I	**048**	**07**	L2
HH142	SZ I	**303**	**64**	S2
HH142	SZ I	**310**	**71**	S2
HH142	SZ I	**212**	**01**	S2
HH142	SZ I	**109**	**10**	S2
HH142	SZ I	**328**	**24**	S2
HH142	SZ I	**296**	**70**	S2
HH142	SZ I	**130**	**17**	S2
HH142	SZ I	**120**	**52**	S3
HH142	SZ I	**123**	**35**	S3
HH143	SZ I	**232**	**06**	B3
HH143	SZ I	**051**	**02**	B3
HH143	SZ I	**203**	**01**	B3
HH143	SZ I	**138**	**89**	S2
HH143	SZ I	**072**	**04**	S2
HH143	SZ I	**326**	**49**	S2
HH143	SZ I	**132**	**77**	S2
HH143	SZ I	**122**	**58**	S3
HH144	SZ I	**052**	**07**	B3
HH144	SZ I	**123**	**36**	S3
HH145	SZ I	**043**	**03**	B3
HH145	SZ I	**032**	**05**	B3
HH145	SZ I	**216**	**04**	B3

BA: basalt dike, **CO**: cover, **PE**: pegmatite dike, **SB**: shear band, **SZ I**: structural zone I, **SZ II**: structural zone II, **SZ III**: structural zone III, **SZ IV**: structural zone IV, **SZ V**: structural zone V, **SZ VI**: structural zone VI, **SZ VII**: structural zone VII, **TM**: Punta de li Tulchi metabasite, **TO**: Tanaunella orthogneiss

structural field data, NE-Sardinia, n: 3600 (approx.)

outcrop	structural zone/lithology	dipping-direction	dipping-angle	fabric
HH001	SZ I	**020**	**45**	B3

HH145	SZ I	**074**	**47**	B5
HH145	SZ I	**128**	**77**	S2
HH145	SZ I	**135**	**65**	S2
HH145	SZ I	**140**	**57**	S2
HH145	SZ I	**125**	**64**	S2
HH146	SZ I	**053**	**09**	B3
HH146	SZ I	**136**	**46**	S3
HH147	SZ I	**030**	**15**	B3
HH147	SZ I	**028**	**24**	B3
HH147	SZ I	**035**	**39**	B3
HH147	SZ I	**017**	**50**	B3
HH147	SZ I	**032**	**30**	B3
HH147	SZ I	**042**	**13**	L2
HH147	SZ I	**031**	**22**	L2
HH147	SZ I	**126**	**85**	S2
HH147	SZ I	**109**	**70**	S2
HH147	SZ I	**050**	**21**	S2
HH147	SZ I	**120**	**57**	S2
HH147	SZ I	**119**	**67**	S2
HH147	SZ I	**128**	**64**	S2
HH147	SZ I	**129**	**87**	S2
HH147	SZ I	**113**	**79**	S2
HH147	SZ I	**306**	**83**	S3
HH147	SZ I	**163**	**42**	S3
HH148	SZ I	**220**	**04**	B3
HH148	SZ I	**210**	**05**	B3
HH148	SZ I	**208**	**07**	B3
HH148	SZ I	**133**	**70**	S2
HH148	SZ I	**147**	**21**	S2
HH148	SZ I	**120**	**75**	S2
HH148	SZ I	**140**	**40**	S3
HH149	SZ I	**230**	**01**	B3
HH149	SZ I	**036**	**17**	L2
HH149	SZ I	**046**	**07**	L2
HH149	SZ I	**294**	**45**	S2
HH149	SZ I	**055**	**19**	S2
HH149	SZ I	**127**	**78**	S2
HH149	SZ I	**324**	**74**	S2
HH151	SZ I	**062**	**07**	B3
HH151	SZ I	**060**	**22**	B3
HH151	SZ I	**084**	**21**	B5
HH151	SZ I	**085**	**29**	B5
HH151	SZ I	**053**	**10**	L2
HH151	SZ I	**052**	**05**	L2
HH151	SZ I	**132**	**34**	S2
HH151	SZ I	**156**	**50**	S2
HH151	SZ I	**137**	**33**	S2
HH151	SZ I	**123**	**24**	S3
HH152	SZ I	**040**	**27**	B3
HH152	SZ I	**035**	**02**	B3
HH152	SZ I	**042**	**11**	B3
HH152	SZ I	**045**	**26**	B3
HH152	SZ I	**070**	**40**	L2
HH152	SZ I	**070**	**27**	L2
HH152	SZ I	**070**	**22**	L2
HH152	SZ I	**330**	**50**	S2
HH152	SZ I	**135**	**30**	S3
HH152	SZ I	**108**	**50**	S3
HH152	SZ I	**151**	**60**	S3
HH152	SZ I	**138**	**85**	S3
HH152	SZ I	**138**	**47**	S3
HH152	SZ I	**146**	**45**	S3
HH152	SZ I	**140**	**46**	S3
HH153	SZ II	**270**	**12**	B2
HH153	SZ II	**249**	**21**	B2
HH153	SZ II	**262**	**13**	B2
HH153	SZ II	**090**	**04**	B2
HH153	SZ II	**270**	**05**	B2
HH153	SZ II	**082**	**25**	B3

HH153	SZ II	**082**	**26**	B3
HH153	SZ II	**078**	**08**	B5
HH153	SZ II	**110**	**14**	B5
HH153	SZ II	**164**	**80**	S2
HH153	SZ II	**150**	**58**	S2
HH153	SZ II	**002**	**60**	S2
HH153	SZ II	**170**	**54**	S2
HH153	SZ II	**335**	**55**	S2
HH153	SZ II	**156**	**70**	S2
HH153	SZ II	**180**	**75**	S2
HH153	SZ II	**155**	**32**	S2
HH153	SZ II	**157**	**67**	S2
HH153	SZ II	**155**	**58**	S2
HH153	SZ II	**180**	**66**	S2
HH153	SZ II	**172**	**70**	S2
HH153	SZ II	**140**	**50**	S2
HH153	SZ II	**072**	**01**	S2
HH153	SZ II	**078**	**09**	S2
HH153	SZ II	**263**	**10**	S2
HH153	SZ II	**166**	**60**	S3
HH153	SZ II	**132**	**50**	S3
HH153	SZ II	**150**	**59**	S3
HH153	SZ II	**162**	**77**	S3
HH153	SZ II	**138**	**76**	S3
HH153	SZ II	**005**	**34**	S5
HH154	SZ II	**064**	**35**	B3
HH154	SZ II	**068**	**50**	B3
HH154	SZ II	**075**	**29**	B3
HH154	SZ II	**076**	**45**	L2/4
HH154	SZ II	**083**	**41**	L2/4
HH154	SZ II	**150**	**75**	S2
HH154	SZ II	**346**	**81**	S2
HH154	SZ II	**144**	**76**	S2
HH154	SZ II	**142**	**71**	S2
HH154	SZ II	**068**	**35**	S2
HH154	SZ II	**064**	**32**	S2
HH154	SZ II	**164**	**80**	S3
HH154	SZ II	**010**	**56**	S3
HH154	SZ II	**162**	**85**	S3
HH155	SZ II	**092**	**30**	L2/4
HH155	SZ II	**085**	**35**	L2/4
HH155	SZ II	**101**	**37**	S3
HH155	SZ II	**093**	**33**	S3
HH156	SZ II	**073**	**06**	L2/4
HH156	SZ II	**085**	**10**	L2/4
HH156	SZ II	**050**	**25**	S2
HH156	SZ II	**080**	**27**	S2
HH156	SZ II	**020**	**25**	S2
HH156	SZ II	**350**	**20**	S2
HH156	SZ II	**100**	**02**	S2
HH156	SZ II	**272**	**01**	S2
HH156	SZ II	**086**	**26**	S2
HH156	SZ II	**093**	**15**	S2
HH156	SZ II	**100**	**28**	S3
HH156	SZ II	**084**	**10**	S3
HH157	SZ II	**092**	**21**	B3
HH157	SZ II	**095**	**35**	L2/4
HH157	SZ II	**097**	**26**	L2/4
HH157	SZ II	**148**	**39**	S3
HH157	SZ II	**150**	**45**	S3
HH157	SZ II	**164**	**47**	S3
HH157	SZ II	**146**	**37**	S3
HH157	SZ II	**157**	**37**	S3
HH158	SZ II	**158**	**45**	S2
HH158	SZ II	**098**	**23**	S2
HH159	SZ II	**072**	**01**	B3
HH159	SZ II	**072**	**28**	B3
HH159	SZ II	**084**	**12**	B3
HH159	SZ II	**052**	**06**	B3

BA: basalt dike, **CO**: cover, **PE**: pegmatite dike, **SB**: shear band, **SZ I**: structural zone I, **SZ II**: structural zone II, **SZ III**: structural zone III, **SZ IV**: structural zone IV, **SZ V**: structural zone V, **SZ VI**: structural zone VI, **SZ VII**: structural zone VII, **TM**: Punta de li Tulchi metabasite, **TO**: Tanaunella orthogneiss

structural field data, NE-Sardinia, n: 3600 (approx.)

outcrop	structural zone/lithology	dipping-direction	dipping-angle	fabric
HH001	SZ I	**020**	**45**	B3

HH159	SZ II	**069**	**13**	S2
HH159	SZ II	**076**	**04**	S2
HH159	SZ II	**135**	**30**	S3
HH159	SZ II	**135**	**67**	S3
HH159	SZ II	**154**	**37**	S3
HH159	SZ II	**152**	**53**	S3
HH159	SZ II	**140**	**32**	S3
HH160	SZ III	**078**	**13**	L2/4
HH160	SZ III	**245**	**09**	L2/4
HH160	SZ III	**082**	**06**	L2/4
HH160	SZ II	**060**	**28**	L2/4
HH160	SZ II	**097**	**03**	L2/4
HH160	SZ II	**264**	**26**	L2/4
HH160	SZ II	**070**	**20**	L2/4
HH160	SZ III	**185**	**14**	S2/4
HH160	SZ III	**186**	**18**	S2/4
HH160	SZ III	**161**	**20**	S2/4
HH160	SZ III	**108**	**26**	S2/4
HH160	SZ II	**124**	**45**	S3
HH160	SZ II	**128**	**35**	S3
HH160	SZ II	**145**	**40**	S3
HH160	SZ II	**138**	**45**	S3
HH160	SZ II	**133**	**44**	S3
HH160	SZ II	**133**	**40**	S3
HH160	SZ II	**081**	**58**	S3
HH160	SZ III	**210**	**25**	SB
HH160	SZ II	**181**	**20**	SB
HH162	SZ II	**076**	**25**	L2/4
HH162	SZ II	**070**	**15**	L2/4
HH162	SZ II	**092**	**22**	L2/4
HH162	SZ II	**135**	**46**	S3
HH162	SZ II	**125**	**41**	S3
HH162	SZ II	**130**	**36**	S3
HH163	SZ II	**050**	**22**	B3
HH163	SZ II	**074**	**28**	B3
HH163	SZ II	**068**	**28**	B3
HH163	SZ II	**060**	**22**	L2/4
HH163	SZ II	**122**	**35**	S3
HH163	SZ II	**129**	**42**	S3
HH165	SZ III	**080**	**30**	L2/4
HH165	SZ III	**081**	**01**	L2/4
HH165	SZ III	**205**	**31**	S2/4
HH165	SZ III	**124**	**40**	S2/4
HH165	SZ III	**160**	**30**	S2/4
HH165	SZ III	**360**	**75**	S5
HH165	SZ III	**170**	**80**	S5
HH166	SZ IV	**109**	**25**	B3
HH166	SZ IV	**115**	**24**	B3
HH166	SZ IV	**115**	**06**	L2/4
HH166	SZ IV	**190**	**69**	S2/4
HH166	SZ IV	**196**	**86**	S2/4
HH167	SZ V	**302**	**04**	L2/4
HH167	SZ V	**298**	**13**	L2/4
HH167	SZ V	**117**	**14**	L2/4
HH167	SZ V	**227**	**48**	S2/3/4
HH167	SZ V	**200**	**66**	S2/3/4
HH167	SZ V	**180**	**80**	S2/3/4
HH167	SZ V	**210**	**85**	SB
HH168	SZ V	**280**	**10**	B2
HH168	SZ V	**284**	**10**	B2
HH168	SZ V	**092**	**14**	B2/3
HH168	SZ V	**104**	**01**	L2/4
HH168	SZ V	**104**	**00**	L2/4
HH168	SZ V	**100**	**15**	L2/4
HH168	SZ V	**092**	**10**	L2/4
HH168	SZ V	**194**	**85**	S2/3/4
HH168	SZ V	**202**	**74**	S2/3/4
HH168	SZ V	**010**	**75**	S2/3/4
HH168	SZ V	**186**	**83**	S2/3/4
HH168	SZ V	**226**	**75**	SB
HH168	SZ V	**215**	**75**	SB
HH168	SZ V	**215**	**80**	SB
HH168	SZ V	**111**	**12**	SB
HH168	SZ V	**224**	**73**	SB
HH169	SZ IV	**106**	**06**	L2/4
HH169	SZ IV	**096**	**15**	L2/4
HH169	SZ IV	**006**	**80**	S2/4
HH169	SZ IV	**170**	**70**	S2/4
HH169	SZ IV	**185**	**74**	SB
HH169	SZ IV	**196**	**79**	SB
HH169	SZ IV	**189**	**52**	SB
HH170	SZ VII	**178**	**24**	S4
HH170	SZ VII	**155**	**27**	S4
HH170	SZ VII	**176**	**28**	S4
HH171	SZ V	**280**	**12**	B2/3
HH171	SZ VII	**098**	**20**	L2
HH171	SZ VII	**096**	**09**	L2
HH171	SZ V	**272**	**09**	L2/4
HH171	SZ V	**282**	**10**	L2/4
HH171	SZ VII	**168**	**30**	S2
HH171	SZ VII	**156**	**33**	S2
HH171	SZ VII	**144**	**28**	S2
HH171	SZ V	**190**	**57**	S2/3/4
HH171	SZ V	**200**	**85**	S2/3/4
HH171	SZ V	**200**	**77**	S2/3/4
HH171	SZ V	**198**	**87**	S2/3/4
HH171	SZ V	**224**	**80**	SB
HH172	SZ V	**178**	**55**	S2/3/4
HH173	SZ V	**274**	**06**	B2/3
HH173	SZ V	**279**	**17**	L2/4
HH173	SZ V	**174**	**60**	S2/3/4
HH173	SZ V	**195**	**56**	S2/3/4
HH174	SZ V	**111**	**06**	L2/4
HH174	SZ V	**108**	**07**	L2/4
HH174	SZ V	**276**	**07**	L2/4
HH174	SZ V	**284**	**01**	L2/4
HH174	SZ V	**275**	**04**	L2/4
HH174	SZ V	**204**	**64**	S2/3/4
HH174	SZ V	**200**	**85**	S2/3/4
HH174	SZ V	**200**	**85**	S2/3/4
HH174	SZ V	**190**	**63**	S2/3/4
HH174	SZ V	**182**	**76**	S2/3/4
HH174	SZ V	**185**	**55**	S2/3/4
HH174	SZ V	**294**	**10**	S2/3/4
HH174	SZ V	**190**	**40**	S2/3/4
HH174	SZ V	**195**	**39**	S2/3/4
HH174	SZ V	**182**	**40**	S2/3/4
HH174	SZ V	**210**	**64**	S2/3/4
HH174	SZ V	**205**	**65**	S2/3/4
HH175	SZ V	**098**	**02**	B2/3
HH175	SZ V	**099**	**06**	B2/3
HH175	SZ V	**288**	**04**	B2/3
HH175	SZ V	**276**	**04**	L2
HH175	SZ V	**280**	**04**	L2/4
HH175	SZ V	**198**	**59**	S2
HH175	SZ V	**193**	**04**	S2
HH175	SZ V	**203**	**70**	S2
HH175	SZ V	**160**	**62**	S2
HH175	SZ V	**195**	**45**	S2
HH175	SZ V	**012**	**51**	S2
HH175	SZ V	**020**	**43**	S2
HH175	SZ V	**195**	**40**	S2
HH175	SZ V	**026**	**31**	S2
HH175	SZ V	**188**	**35**	S2
HH175	SZ V	**212**	**10**	S2
HH175	SZ V	**203**	**75**	S2/3/4
HH175	SZ V	**010**	**76**	S2/3/4
HH176	SZ V	**258**	**35**	B5

BA: basalt dike, **CO**: cover, **PE**: pegmatite dike, **SB**: shear band, **SZ I**: structural zone I, **SZ II**: structural zone II, **SZ III**: structural zone III, **SZ IV**: structural zone IV, **SZ V**: structural zone V, **SZ VI**: structural zone VI, **SZ VII**: structural zone VII, **TM**: Punta de li Tulchi metabasite, **TO**: Tanaunella orthogneiss

structural field data, NE-Sardinia, n: 3600 (approx.)

outcrop	structural zone/lithology	dipping-direction	dipping-angle	fabric
HH001	SZ I	**020**	**45**	B3

HH176	SZ V	**260**	**18**	B5
HH176	SZ V	**258**	**32**	B5
HH176	SZ V	**260**	**25**	B5
HH176	SZ V	**255**	**30**	B5
HH176	SZ V	**253**	**34**	B5
HH176	SZ V	**262**	**23**	B5
HH176	SZ V	**091**	**02**	L2/4
HH176	SZ V	**111**	**05**	L2/4
HH176	SZ V	**102**	**05**	L2/4
HH176	SZ V	**182**	**71**	S2/3/4
HH176	SZ V	**308**	**50**	S2/3/4
HH176	SZ V	**184**	**67**	S2/3/4
HH176	SZ V	**306**	**35**	S2/3/4
HH176	SZ V	**180**	**70**	S2/3/4
HH176	SZ V	**292**	**40**	S2/3/4
HH176	SZ V	**178**	**71**	S2/3/4
HH176	SZ V	**255**	**33**	S2/3/4
HH176	SZ V	**174**	**71**	S2/3/4
HH176	SZ V	**003**	**60**	S5
HH176	SZ V	**346**	**68**	S5
HH177	SZ V	**248**	**20**	L2/4
HH177	SZ V	**258**	**17**	L2/4
HH177	SZ V	**157**	**80**	S2/3/4
HH177	SZ V	**352**	**85**	S2/3/4
HH177	SZ V	**150**	**70**	S2/3/4
HH177	SZ V	**178**	**70**	S2/3/4
HH178	SZ V	**108**	**01**	L2
HH178	SZ V	**270**	**12**	L2/4
HH178	SZ V	**098**	**07**	L2/4
HH178	SZ V	**195**	**54**	S2
HH178	SZ V	**208**	**48**	S2/3/4
HH178	SZ V	**190**	**37**	S2/3/4
HH178	SZ V	**208**	**37**	S2/3/4
HH178	SZ V	**245**	**04**	S2/3/4
HH178	SZ V	**182**	**10**	S2/3/4
HH178	SZ V	**220**	**20**	S2/3/4
HH178	SZ V	**194**	**53**	S2/3/4
HH178	SZ V	**180**	**59**	S2/3/4
HH178	SZ V	**215**	**85**	SB
HH179	SZ V	**109**	**03**	B5
HH179	SZ V	**010**	**80**	S2/3/4
HH180	SZ V	**268**	**15**	B5
HH180	SZ V	**254**	**20**	B5
HH180	SZ V	**280**	**04**	L2/4
HH180	SZ V	**190**	**66**	S2/3/4
HH180	SZ V	**356**	**70**	S2/3/4
HH180	SZ V	**200**	**64**	S2/3/4
HH180	SZ V	**202**	**40**	S2/3/4
HH180	SZ V	**230**	**20**	S2/3/4
HH180	SZ V	**204**	**66**	S2/3/4
HH180	SZ V	**280**	**14**	S2/3/4
HH180	SZ V	**355**	**89**	S2/3/4
HH180	SZ V	**208**	**17**	S2/3/4
HH181	SZ V	**208**	**40**	S2/3/4
HH181	SZ V	**194**	**76**	S2/3/4
HH181	SZ V	**192**	**54**	S2/3/4
HH181	SZ V	**360**	**73**	S2/3/4
HH182	SZ V	**161**	**64**	S2/3/4
HH183	SZ V	**267**	**05**	B5
HH183	SZ V	**086**	**04**	B5
HH183	SZ V	**085**	**30**	B5
HH183	SZ V	**080**	**25**	B5
HH183	SZ V	**080**	**60**	B5
HH183	SZ V	**330**	**85**	BA
HH183	SZ V	**004**	**89**	BA
HH183	SZ V	**080**	**28**	L2/4
HH183	SZ V	**085**	**35**	L2/4
HH183	SZ V	**270**	**05**	L2/4
HH183	SZ V	**094**	**27**	L2/4

HH183	SZ V	**180**	**15**	S2/3/4
HH183	SZ V	**010**	**03**	S2/3/4
HH183	SZ V	**168**	**52**	S2/3/4
HH183	SZ V	**116**	**24**	S2/3/4
HH183	SZ V	**010**	**44**	S2/3/4
HH183	SZ V	**165**	**65**	S2/3/4
HH183	SZ V	**152**	**65**	S2/3/4
HH183	SZ V	**200**	**25**	S2/3/4
HH183	SZ V	**190**	**41**	S2/3/4
HH183	SZ V	**181**	**45**	S2/3/4
HH183	SZ V	**180**	**79**	S2/3/4
HH183	SZ V	**160**	**38**	S2/3/4
HH183	SZ V	**160**	**13**	S2/3/4
HH183	SZ V	**177**	**81**	S2/3/4
HH183	SZ V	**200**	**90**	S2/3/4
HH183	SZ V	**183**	**49**	S2/3/4
HH183	SZ V	**180**	**50**	S2/3/4
HH183	SZ V	**190**	**41**	S2/3/4
HH183	SZ V	**160**	**35**	S2/3/4
HH183	SZ V	**170**	**47**	S2/3/4
HH183	SZ V	**174**	**88**	S2/3/4
HH183	SZ V	**160**	**25**	S2/3/4
HH183	SZ V	**170**	**47**	S2/3/4
HH183	SZ V	**360**	**77**	S2/3/4
HH183	SZ V	**164**	**80**	S2/3/4
HH184	SZ II	**073**	**23**	B2
HH184	SZ II	**062**	**07**	B2
HH184	SZ II	**042**	**00**	B2
HH184	SZ II	**060**	**11**	B3
HH184	SZ II	**054**	**06**	B3
HH184	SZ II	**221**	**04**	B3
HH184	SZ II	**054**	**10**	L2/4
HH184	SZ II	**048**	**04**	L2/4
HH184	SZ II	**067**	**05**	L2/4
HH184	SZ II	**128**	**30**	S2
HH184	SZ II	**125**	**26**	S2
HH184	SZ II	**132**	**37**	S2
HH184	SZ II	**134**	**41**	S2
HH184	SZ II	**126**	**30**	S2
HH184	SZ II	**046**	**03**	S2
HH184	SZ II	**060**	**08**	S2
HH184	SZ II	**132**	**45**	S3
HH184	SZ II	**139**	**50**	S3
HH184	SZ II	**148**	**53**	SB
HH185	SZ II	**030**	**20**	B3
HH185	SZ II	**042**	**25**	B3
HH185	SZ II	**345**	**15**	S2
HH185	SZ II	**290**	**04**	S2
HH185	SZ II	**352**	**20**	S2
HH185	SZ II	**210**	**07**	S2
HH185	SZ II	**085**	**34**	S2
HH185	SZ II	**125**	**51**	S2
HH185	SZ II	**108**	**28**	S2
HH185	SZ II	**050**	**05**	S2
HH185	SZ II	**048**	**12**	S2
HH185	SZ II	**057**	**07**	S2
HH185	SZ II	**210**	**07**	S2
HH185	SZ II	**056**	**20**	S2
HH185	SZ II	**112**	**50**	S3
HH185	SZ II	**113**	**33**	S3
HH185	SZ II	**100**	**36**	S3
HH186	SZ II	**072**	**37**	B3
HH186	SZ II	**055**	**12**	B3
HH186	SZ II	**102**	**35**	S2
HH186	SZ II	**098**	**33**	S2
HH186	SZ II	**097**	**42**	S2
HH186	SZ II	**068**	**31**	S2
HH186	SZ II	**090**	**32**	S2
HH186	SZ II	**138**	**30**	S2

BA: basalt dike, **CO**: cover, **PE**: pegmatite dike, **SB**: shear band, **SZ I**: structural zone I, **SZ II**: structural zone II, **SZ III**: structural zone III, **SZ IV**: structural zone IV, **SZ V**: structural zone V, **SZ VI**: structural zone VI, **SZ VII**: structural zone VII, **TM**: Punta de li Tulchi metabasite, **TO**: Tanaunella orthogneiss

structural field data, NE-Sardinia, n: 3600 (approx.)

outcrop	structural zone/lithology	dipping-direction	dipping-angle	fabric
HH001	SZ I	**020**	**45**	B3

HH186	SZ II	**155**	**23**	S2
HH186	SZ II	**128**	**47**	S2
HH186	SZ II	**138**	**50**	S2
HH186	SZ II	**128**	**34**	S2
HH186	SZ II	**115**	**48**	S2
HH186	SZ II	**046**	**25**	S2
HH186	SZ II	**066**	**07**	S2
HH187	SZ II	**035**	**23**	B3
HH187	SZ II	**022**	**30**	B3
HH187	SZ II	**069**	**27**	B3
HH187	SZ II	**032**	**30**	B3
HH187	SZ II	**135**	**73**	S2
HH187	SZ II	**140**	**78**	S2
HH187	SZ II	**135**	**71**	S2
HH187	SZ II	**125**	**71**	S2
HH187	SZ II	**116**	**50**	S2
HH187	SZ II	**117**	**57**	S2
HH187	SZ II	**109**	**67**	S2
HH187	SZ II	**118**	**47**	S2
HH187	SZ II	**110**	**55**	S2
HH187	SZ II	**122**	**70**	S2
HH187	SZ II	**116**	**30**	S2
HH187	SZ II	**108**	**55**	S2
HH187	SZ II	**110**	**45**	S2
HH187	SZ II	**118**	**49**	S2
HH187	SZ II	**045**	**43**	S2
HH187	SZ II	**030**	**15**	S2
HH187	SZ II	**065**	**40**	S2
HH187	SZ II	**134**	**39**	S3
HH187	SZ II	**095**	**68**	S3
HH188	SZ II	**100**	**54**	S2
HH188	SZ II	**120**	**47**	S2
HH188	SZ II	**130**	**45**	S2
HH188	SZ II	**100**	**42**	S2
HH188	SZ II	**115**	**34**	S2
HH188	SZ II	**100**	**35**	S2
HH188	SZ II	**098**	**34**	S2
HH188	SZ II	**070**	**30**	S2
HH188	SZ II	**144**	**45**	S2
HH188	SZ II	**041**	**30**	S2
HH188	SZ II	**050**	**29**	S2
HH189	SZ II	**048**	**14**	L2/4
HH189	SZ II	**068**	**24**	L2/4
HH189	SZ II	**074**	**20**	L2/4
HH189	SZ II	**240**	**04**	L2/4
HH189	SZ II	**118**	**37**	S3
HH189	SZ II	**122**	**30**	S3
HH189	SZ II	**122**	**42**	S3
HH189	SZ II	**132**	**55**	S3
HH189	SZ II	**130**	**62**	S3
HH189	SZ II	**135**	**50**	S3
HH189	SZ II	**123**	**33**	S3
HH189	SZ II	**128**	**23**	S3
HH189	SZ II	**122**	**23**	S3
HH189	SZ II	**108**	**20**	S3
HH189	SZ II	**090**	**28**	S3
HH189	SZ II	**160**	**14**	S3
HH189	SZ II	**140**	**47**	S3
HH189	SZ II	**134**	**46**	S3
HH189	SZ II	**102**	**16**	S3
HH189	SZ II	**314**	**65**	S3
HH189	SZ II	**320**	**89**	S3
HH189	SZ II	**172**	**07**	S3
HH189	SZ II	**170**	**40**	S3
HH189	SZ II	**158**	**15**	S3
HH189	SZ II	**070**	**14**	S3
HH190	SZ II	**045**	**14**	L2/4
HH190	SZ II	**026**	**16**	L2/4
HH190	SZ II	**050**	**10**	L2/4

HH190	SZ II	**087**	**25**	S3
HH190	SZ II	**080**	**25**	S3
HH190	SZ II	**079**	**32**	S3
HH190	SZ II	**100**	**23**	S3
HH190	SZ II	**115**	**33**	S3
HH190	SZ II	**065**	**38**	S3
HH190	SZ II	**050**	**18**	S3
HH191	SZ II	**065**	**40**	S2
HH191	SZ II	**132**	**24**	S2
HH191	SZ II	**130**	**32**	S2
HH191	SZ II	**112**	**34**	S2
HH191	SZ II	**145**	**16**	S2
HH191	SZ II	**108**	**70**	S2
HH191	SZ II	**088**	**33**	S2
HH191	SZ II	**080**	**46**	S2
HH191	SZ II	**072**	**37**	S2
HH191	SZ II	**360**	**24**	S2
HH191	SZ II	**088**	**24**	S2
HH191	SZ II	**100**	**31**	S2
HH191	SZ II	**136**	**07**	S2
HH191	SZ II	**068**	**25**	S2
HH191	SZ II	**030**	**30**	S2
HH191	SZ II	**053**	**15**	S2
HH191	SZ II	**055**	**14**	S2
HH191	SZ II	**066**	**32**	SB
HH192	SZ III	**042**	**18**	L2
HH192	SZ III	**030**	**10**	L2
HH192	SZ III	**110**	**14**	S2
HH192	SZ III	**122**	**08**	S2
HH192	SZ III	**098**	**11**	S2
HH192	SZ III	**120**	**30**	S2
HH192	SZ III	**105**	**30**	S2
HH192	SZ III	**104**	**30**	S2
HH192	SZ III	**103**	**28**	S2
HH192	SZ III	**105**	**35**	S2
HH192	SZ III	**108**	**15**	S2
HH192	SZ III	**058**	**27**	S2
HH192	SZ III	**135**	**20**	S2
HH192	SZ III	**030**	**30**	S2
HH192	SZ III	**103**	**27**	S2
HH192	SZ III	**096**	**37**	S2
HH193	SZ III	**275**	**20**	L2/4
HH193	SZ III	**248**	**16**	L2/4
HH193	SZ III	**278**	**31**	S2/4
HH193	SZ III	**279**	**30**	S2/4
HH193	SZ III	**268**	**24**	S2/4
HH193	SZ III	**248**	**19**	S2/4
HH193	SZ III	**278**	**17**	S2/4
HH193	SZ III	**132**	**12**	S2/4
HH193	SZ III	**198**	**08**	S2/4
HH193	SZ III	**255**	**17**	S2/4
HH193	SZ III	**190**	**22**	S2/4
HH193	SZ III	**098**	**23**	S2/4
HH193	SZ III	**212**	**20**	S2/4
HH193	SZ III	**335**	**12**	S2/4
HH193	SZ III	**075**	**16**	S2/4
HH193	SZ III	**140**	**27**	S2/4
HH193	SZ III	**272**	**26**	S2/4
HH193	SZ III	**263**	**23**	S2/4
HH193	SZ III	**272**	**37**	S2/4
HH193	SZ III	**274**	**22**	S2/4
HH193	SZ III	**252**	**25**	S2/4
HH193	SZ III	**262**	**32**	S2/4
HH194	SZ III	**050**	**08**	L2
HH194	SZ III	**078**	**37**	S2
HH194	SZ III	**076**	**20**	S2
HH194	SZ III	**114**	**30**	S2
HH194	SZ III	**110**	**21**	S2
HH194	SZ III	**130**	**26**	S2

BA: basalt dike, **CO**: cover, **PE**: pegmatite dike, **SB**: shear band, **SZ I**: structural zone I, **SZ II**: structural zone II, **SZ III**: structural zone III, **SZ IV**: structural zone IV, **SZ V**: structural zone V, **SZ VI**: structural zone VI, **SZ VII**: structural zone VII, **TM**: Punta de li Tulchi metabasite, **TO**: Tanaunella orthogneiss

structural field data, NE-Sardinia, n: 3600 (approx.)

outcrop	structural zone/lithology	dipping-direction	dipping-angle	fabric
HH001	SZ I	**020**	**45**	B3

HH195	SZ III	**302**	**04**	L2/4
HH195	SZ III	**270**	**14**	L2/4
HH195	SZ III	**094**	**05**	L2/4
HH195	SZ III	**278**	**06**	L2/4
HH195	SZ III	**128**	**24**	S2/4
HH195	SZ III	**094**	**28**	S2/4
HH195	SZ III	**285**	**12**	S2/4
HH195	SZ III	**205**	**34**	S2/4
HH195	SZ III	**009**	**10**	S2/4
HH195	SZ III	**265**	**15**	S2/4
HH195	SZ III	**330**	**06**	S2/4
HH195	SZ III	**310**	**05**	S2/4
HH195	SZ III	**170**	**20**	S2/4
HH195	SZ III	**164**	**19**	S2/4
HH195	SZ III	**190**	**24**	S2/4
HH195	SZ III	**211**	**30**	S2/4
HH195	SZ III	**200**	**15**	S2/4
HH195	SZ III	**208**	**27**	SB
HH196	SZ III	**272**	**18**	L2/4
HH196	SZ III	**234**	**24**	S2/4
HH196	SZ III	**230**	**36**	S2/4
HH196	SZ III	**078**	**20**	S2/4
HH196	SZ III	**220**	**12**	S2/4
HH196	SZ III	**210**	**32**	S2/4
HH197	SZ III	**064**	**34**	L2/4
HH197	SZ III	**260**	**09**	L2/4
HH197	SZ III	**257**	**01**	L2/4
HH197	SZ III	**112**	**01**	L2/4
HH197	SZ III	**270**	**04**	L2/4
HH197	SZ III	**211**	**05**	S2/4
HH197	SZ III	**173**	**06**	S2/4
HH197	SZ III	**107**	**17**	S2/4
HH197	SZ III	**245**	**06**	S2/4
HH197	SZ III	**210**	**10**	S2/4
HH197	SZ III	**220**	**10**	S2/4
HH197	SZ III	**315**	**05**	S2/4
HH197	SZ III	**339**	**03**	S2/4
HH197	SZ III	**140**	**18**	S2/4
HH197	SZ III	**130**	**20**	S2/4
HH197	SZ III	**114**	**24**	S2/4
HH197	SZ III	**117**	**36**	S2/4
HH197	SZ III	**100**	**37**	S2/4
HH197	SZ III	**140**	**28**	S2/4
HH197	SZ III	**125**	**20**	S2/4
HH197	SZ III	**108**	**32**	S2/4
HH197	SZ III	**134**	**16**	S2/4
HH198	SZ III	**170**	**30**	S2/4
HH199	SZ III	**088**	**18**	L2/4
HH199	SZ III	**108**	**22**	L2/4
HH199	SZ III	**081**	**19**	L2/4
HH199	SZ III	**091**	**34**	L2/4
HH199	SZ III	**152**	**15**	S2/4
HH199	SZ III	**143**	**25**	S2/4
HH199	SZ III	**115**	**26**	S2/4
HH199	SZ III	**130**	**27**	S2/4
HH199	SZ III	**128**	**26**	S2/4
HH199	SZ III	**030**	**12**	S2/4
HH199	SZ III	**120**	**30**	S2/4
HH199	SZ III	**142**	**24**	S2/4
HH199	SZ III	**125**	**30**	S2/4
HH199	SZ III	**145**	**35**	S2/4
HH200	SZ III	**300**	**75**	BA
HH200	SZ III	**088**	**01**	L2/4
HH200	SZ III	**086**	**11**	L2/4
HH200	SZ III	**158**	**24**	S2/4
HH200	SZ III	**132**	**25**	S2/4
HH200	SZ III	**132**	**20**	S2/4
HH200	SZ III	**148**	**24**	S2/4
HH200	SZ III	**232**	**36**	S2/4

HH200	SZ III	**230**	**16**	S2/4
HH200	SZ III	**212**	**08**	S2/4
HH200	SZ III	**175**	**10**	S2/4
HH200	SZ III	**256**	**60**	S2/4
HH200	SZ III	**208**	**47**	S2/4
HH200	SZ III	**100**	**45**	S2/4
HH200	SZ III	**113**	**28**	S2/4
HH201	SZ III	**142**	**58**	BA
HH201	SZ III	**082**	**11**	L2/4
HH201	SZ III	**285**	**04**	L2/4
HH201	SZ III	**230**	**31**	S2/4
HH201	SZ III	**151**	**30**	S2/4
HH201	SZ III	**125**	**38**	S2/4
HH201	SZ III	**140**	**20**	S2/4
HH201	SZ III	**150**	**27**	S2/4
HH201	SZ III	**155**	**18**	S2/4
HH201	SZ III	**006**	**18**	S2/4
HH201	SZ III	**140**	**20**	S2/4
HH202	SZ III	**154**	**87**	BA
HH202	SZ III	**192**	**17**	S2/4
HH202	SZ III	**160**	**07**	S2/4
HH202	SZ III	**086**	**12**	S2/4
HH202	SZ III	**190**	**17**	S2/4
HH202	SZ III	**050**	**24**	S2/4
HH202	SZ III	**092**	**15**	S2/4
HH202	SZ III	**164**	**17**	S2/4
HH203	SZ II	**248**	**08**	B3
HH203	SZ II	**300**	**70**	BA
HH203	SZ II	**108**	**34**	L2/4
HH203	SZ II	**200**	**08**	S2
HH203	SZ II	**160**	**18**	S2
HH203	SZ II	**172**	**08**	S2
HH203	SZ II	**201**	**12**	S2
HH203	SZ II	**205**	**24**	S2
HH203	SZ II	**184**	**25**	S2
HH203	SZ II	**216**	**26**	S2
HH203	SZ II	**200**	**45**	S2
HH203	SZ II	**220**	**49**	S2
HH203	SZ II	**201**	**30**	S2
HH203	SZ II	**150**	**75**	S2
HH203	SZ II	**153**	**37**	S2
HH203	SZ II	**100**	**33**	S2
HH203	SZ II	**210**	**12**	S2
HH203	SZ II	**208**	**11**	S2
HH203	SZ II	**222**	**07**	S2
HH203	SZ II	**216**	**12**	S2
HH203	SZ II	**330**	**09**	S3
HH203	SZ II	**200**	**16**	SB
HH204	SZ II	**034**	**04**	L2/4
HH204	SZ II	**044**	**04**	L2/4
HH204	SZ II	**220**	**05**	L2/4
HH204	SZ II	**053**	**09**	L2/4
HH204	SZ II	**142**	**50**	S3
HH204	SZ II	**123**	**48**	S3
HH204	SZ II	**126**	**50**	S3
HH204	SZ II	**138**	**35**	S3
HH204	SZ II	**111**	**42**	S3
HH204	SZ II	**117**	**55**	S3
HH204	SZ II	**125**	**48**	S3
HH204	SZ II	**142**	**49**	S3
HH204	SZ II	**137**	**46**	S3
HH204	SZ II	**134**	**42**	S3
HH204	SZ II	**150**	**20**	S3
HH205	SZ III	**087**	**06**	L2/4
HH205	SZ III	**160**	**35**	S2/4
HH206	SZ II	**147**	**51**	S3
HH206	SZ II	**148**	**41**	S3
HH206	SZ II	**141**	**50**	S3
HH206	SZ II	**148**	**37**	S3

BA: basalt dike, **CO**: cover, **PE**: pegmatite dike, **SB**: shear band, **SZ I**: structural zone I, **SZ II**: structural zone II, **SZ III**: structural zone III, **SZ IV**: structural zone IV, **SZ V**: structural zone V, **SZ VI**: structural zone VI, **SZ VII**: structural zone VII, **TM**: Punta de li Tulchi metabasite, **TO**: Tanaunella orthogneiss

structural field data, NE-Sardinia, n: 3600 (approx.)

outcrop	structural zone/lithology	dipping-direction	dipping-angle	fabric
HH001	SZ I	**020**	**45**	B3

HH206	SZ II	**134**	**27**	S3
HH206	SZ II	**176**	**56**	S3
HH207	SZ IV	**093**	**10**	L2/4
HH207	SZ IV	**093**	**19**	L2/4
HH207	SZ IV	**097**	**15**	L2/4
HH207	SZ IV	**091**	**07**	L2/4
HH207	SZ IV	**175**	**47**	S2/4
HH207	SZ IV	**170**	**60**	S2/4
HH207	SZ IV	**160**	**60**	S2/4
HH207	SZ IV	**177**	**48**	S2/4
HH207	SZ IV	**190**	**71**	SB
HH207	SZ IV	**186**	**82**	SB
HH208	SZ IV	**270**	**06**	L2/4
HH208	SZ IV	**186**	**86**	S2/4
HH208	SZ IV	**023**	**84**	S2/4
HH208	SZ IV	**176**	**62**	S2/4
HH208	SZ IV	**188**	**82**	S2/4
HH208	SZ IV	**182**	**86**	S2/4
HH208	SZ IV	**172**	**83**	S2/4
HH210	SZ IV	**106**	**14**	L2/4
HH210	SZ IV	**015**	**88**	S2/4
HH210	SZ IV	**186**	**89**	S2/4
HH210	SZ IV	**180**	**68**	S2/4
HH210	SZ IV	**198**	**88**	S2/4
HH211	SZ IV	**100**	**07**	L2/4
HH211	SZ IV	**105**	**05**	L2/4
HH211	SZ IV	**105**	**04**	L2/4
HH211	SZ IV	**105**	**03**	L2/4
HH211	SZ IV	**103**	**13**	L2/4
HH211	SZ IV	**107**	**15**	L2/4
HH211	SZ IV	**185**	**70**	S2/4
HH211	SZ IV	**186**	**84**	S2/4
HH211	SZ IV	**186**	**71**	S2/4
HH211	SZ IV	**186**	**84**	S2/4
HH211	SZ IV	**196**	**74**	S2/4
HH211	SZ IV	**194**	**83**	S2/4
HH211	SZ IV	**200**	**86**	S2/4
HH211	SZ IV	**030**	**85**	SB
HH211	SZ IV	**192**	**71**	SB
HH211	SZ IV	**028**	**70**	SB
HH211	SZ IV	**050**	**75**	SB
HH212	SZ IV	**108**	**19**	B3
HH212	SZ IV	**105**	**29**	B3
HH212	SZ IV	**108**	**07**	B3
HH212	SZ IV	**100**	**05**	B3
HH212	SZ IV	**107**	**06**	B3
HH212	SZ IV	**100**	**10**	B3
HH212	SZ IV	**106**	**10**	B3
HH212	SZ IV	**116**	**08**	B3
HH212	SZ IV	**094**	**16**	B3
HH212	SZ IV	**103**	**08**	L2/4
HH212	SZ IV	**108**	**04**	L2/4
HH212	SZ IV	**278**	**09**	L2/4
HH212	SZ IV	**091**	**04**	L2/4
HH212	SZ IV	**090**	**07**	L2/4
HH212	SZ IV	**033**	**35**	S2/4
HH212	SZ IV	**020**	**42**	S2/4
HH212	SZ IV	**032**	**48**	S2/4
HH212	SZ IV	**061**	**25**	S2/4
HH212	SZ IV	**120**	**12**	S2/4
HH212	SZ IV	**172**	**48**	S2/4
HH212	SZ IV	**180**	**59**	S2/4
HH212	SZ IV	**172**	**59**	S2/4
HH212	SZ IV	**197**	**70**	S2/4
HH212	SZ IV	**200**	**67**	S2/4
HH212	SZ IV	**167**	**15**	S2/4
HH212	SZ IV	**062**	**07**	S2/4
HH212	SZ IV	**196**	**61**	S2/4
HH212	SZ IV	**190**	**48**	S2/4
HH212	SZ IV	**052**	**34**	S2/4
HH212	SZ IV	**172**	**23**	S2/4
HH212	SZ IV	**040**	**34**	S2/4
HH212	SZ IV	**023**	**53**	S2/4
HH212	SZ IV	**090**	**23**	S2/4
HH212	SZ IV	**190**	**73**	S2/4
HH212	SZ IV	**190**	**86**	S2/4
HH212	SZ IV	**006**	**40**	S2/4
HH212	SZ IV	**010**	**62**	S2/4
HH212	SZ IV	**016**	**78**	S2/4
HH212	SZ IV	**196**	**89**	S2/4
HH212	SZ IV	**202**	**67**	S3
HH212	SZ IV	**204**	**69**	S3
HH212	SZ IV	**208**	**75**	S3
HH212	SZ IV	**172**	**60**	S3
HH212	SZ IV	**197**	**87**	S3
HH212	SZ IV	**188**	**57**	SB
HH213	SZ IV	**115**	**12**	B3
HH213	SZ IV	**105**	**04**	B3
HH213	SZ IV	**100**	**09**	B3
HH213	SZ IV	**100**	**04**	B3
HH213	SZ IV	**100**	**05**	B3
HH213	SZ IV	**118**	**14**	B3
HH213	SZ IV	**098**	**07**	B3
HH213	SZ IV	**097**	**04**	B3
HH213	SZ IV	**100**	**05**	B3
HH213	SZ IV	**104**	**02**	B3
HH213	SZ IV	**109**	**04**	B3
HH213	SZ IV	**110**	**07**	L2/4
HH213	SZ IV	**285**	**13**	L2/4
HH213	SZ IV	**118**	**37**	L2/4
HH213	SZ IV	**110**	**27**	L2/4
HH213	SZ IV	**103**	**15**	L2/4
HH213	SZ IV	**304**	**02**	L2/4
HH213	SZ IV	**096**	**02**	L2/4
HH213	SZ IV	**106**	**01**	L2/4
HH213	SZ IV	**293**	**02**	L2/4
HH213	SZ IV	**101**	**10**	L2/4
HH213	SZ IV	**110**	**18**	L2/4
HH213	SZ IV	**284**	**18**	L2/4
HH213	SZ IV	**110**	**16**	L2/4
HH213	SZ IV	**095**	**16**	L2/4
HH213	SZ IV	**177**	**52**	S2/4
HH213	SZ IV	**200**	**25**	S2/4
HH213	SZ IV	**155**	**22**	S2/4
HH213	SZ IV	**194**	**24**	S2/4
HH213	SZ IV	**010**	**39**	S2/4
HH213	SZ IV	**174**	**37**	S2/4
HH213	SZ IV	**182**	**46**	S2/4
HH213	SZ IV	**018**	**45**	S2/4
HH213	SZ IV	**188**	**55**	S2/4
HH213	SZ IV	**118**	**04**	S2/4
HH213	SZ IV	**042**	**36**	S2/4
HH213	SZ IV	**186**	**70**	S2/4
HH213	SZ IV	**185**	**76**	S2/4
HH213	SZ IV	**200**	**66**	S2/4
HH213	SZ IV	**197**	**86**	S2/4
HH213	SZ IV	**027**	**50**	S2/4
HH213	SZ IV	**170**	**17**	S2/4
HH213	SZ IV	**012**	**59**	S2/4
HH213	SZ IV	**170**	**29**	S2/4
HH213	SZ IV	**002**	**54**	S2/4
HH213	SZ IV	**190**	**36**	S2/4
HH213	SZ IV	**196**	**60**	S2/4
HH213	SZ IV	**182**	**62**	S2/4
HH213	SZ IV	**215**	**65**	S2/4
HH213	SZ IV	**210**	**30**	S2/4
HH213	SZ IV	**194**	**30**	S2/4
HH213	SZ IV	**194**	**51**	S2/4

BA: basalt dike, **CO**: cover, **PE**: pegmatite dike, **SB**: shear band, **SZ I**: structural zone I, **SZ II**: structural zone II, **SZ III**: structural zone III, **SZ IV**: structural zone IV, **SZ V**: structural zone V, **SZ VI**: structural zone VI, **SZ VII**: structural zone VII, **TM**: Punta de li Tulchi metabasite, **TO**: Tanaunella orthogneiss

structural field data, NE-Sardinia, n: 3600 (approx.)

outcrop	structural zone/lithology	dipping-direction	dipping-angle	fabric
HH001	SZ I	**020**	**45**	B3

HH213	SZ IV	**012**	**54**	S2/4
HH213	SZ IV	**174**	**31**	S2/4
HH213	SZ IV	**178**	**25**	S2/4
HH213	SZ IV	**013**	**30**	S2/4
HH213	SZ IV	**180**	**35**	S2/4
HH213	SZ IV	**175**	**46**	S2/4
HH213	SZ IV	**186**	**55**	S2/4
HH213	SZ IV	**178**	**47**	S2/4
HH213	SZ IV	**125**	**05**	S2/4
HH213	SZ IV	**012**	**48**	S2/4
HH213	SZ IV	**188**	**36**	S2/4
HH213	SZ IV	**185**	**46**	S2/4
HH213	SZ IV	**203**	**31**	S2/4
HH213	SZ IV	**175**	**40**	S2/4
HH213	SZ IV	**220**	**64**	S2/4
HH213	SZ IV	**162**	**30**	S2/4
HH213	SZ IV	**130**	**20**	S2/4
HH213	SZ IV	**190**	**20**	S2/4
HH213	SZ IV	**174**	**30**	S2/4
HH213	SZ IV	**065**	**05**	S2/4
HH213	SZ IV	**192**	**54**	S2/4
HH213	SZ IV	**020**	**02**	S2/4
HH213	SZ IV	**192**	**41**	S2/4
HH213	SZ IV	**090**	**02**	S2/4
HH213	SZ IV	**180**	**36**	S2/4
HH213	SZ IV	**160**	**46**	S2/4
HH213	SZ IV	**065**	**15**	S2/4
HH213	SZ IV	**190**	**05**	S2/4
HH213	SZ IV	**196**	**77**	S2/4
HH213	SZ IV	**190**	**36**	S2/4
HH213	SZ IV	**188**	**81**	S2/4
HH213	SZ IV	**195**	**83**	S2/4
HH213	SZ IV	**188**	**63**	S2/4
HH213	SZ IV	**185**	**60**	S2/4
HH213	SZ IV	**192**	**78**	S2/4
HH213	SZ IV	**190**	**64**	S2/4
HH213	SZ IV	**180**	**78**	S2/4
HH213	SZ IV	**192**	**66**	S2/4
HH213	SZ IV	**178**	**62**	S2/4
HH213	SZ IV	**189**	**75**	S2/4
HH213	SZ IV	**002**	**85**	S2/4
HH213	SZ IV	**008**	**86**	S2/4
HH213	SZ IV	**198**	**67**	S2/4
HH213	SZ IV	**198**	**84**	S2/4
HH213	SZ IV	**178**	**88**	S2/4
HH213	SZ IV	**195**	**68**	S3
HH213	SZ IV	**195**	**75**	S3
HH213	SZ IV	**200**	**90**	S3
HH213	SZ IV	**213**	**51**	S3
HH213	SZ IV	**198**	**52**	S3
HH213	SZ IV	**195**	**55**	S3
HH213	SZ IV	**204**	**45**	S3
HH213	SZ IV	**194**	**78**	S3
HH213	SZ IV	**196**	**83**	S3
HH213	SZ IV	**188**	**85**	S3
HH213	SZ IV	**206**	**64**	S3
HH213	SZ IV	**197**	**57**	S3
HH213	SZ IV	**190**	**90**	S3
HH213	SZ IV	**010**	**85**	S3
HH213	SZ IV	**008**	**86**	S3
HH213	SZ IV	**190**	**65**	S3
HH213	SZ IV	**190**	**90**	S3
HH213	SZ IV	**006**	**85**	S3
HH213	SZ IV	**190**	**80**	S3
HH213	SZ IV	**015**	**87**	S3
HH213	SZ IV	**202**	**79**	S3
HH213	SZ IV	**188**	**84**	S3
HH213	SZ IV	**198**	**65**	S3
HH213	SZ IV	**190**	**85**	S3

HH213	SZ IV	**095**	**16**	S3
HH213	SZ IV	**205**	**85**	S3
HH213	SZ IV	**193**	**85**	S3
HH213	SZ IV	**200**	**63**	S3
HH213	SZ IV	**200**	**70**	S3
HH213	SZ IV	**208**	**76**	S3
HH213	SZ IV	**015**	**89**	S3
HH213	SZ IV	**192**	**82**	S3
HH213	SZ IV	**197**	**67**	S3
HH213	SZ IV	**198**	**73**	S3
HH213	SZ IV	**194**	**77**	S3
HH213	SZ IV	**195**	**64**	S3
HH213	SZ IV	**200**	**69**	S3
HH213	SZ IV	**187**	**75**	S3
HH213	SZ IV	**195**	**77**	S3
HH213	SZ IV	**205**	**64**	S3
HH213	SZ IV	**207**	**85**	S3
HH213	SZ IV	**192**	**75**	S3
HH213	SZ IV	**192**	**70**	S3
HH213	SZ IV	**210**	**56**	S3
HH213	SZ IV	**182**	**72**	S3
HH213	SZ IV	**201**	**85**	S3
HH213	SZ IV	**200**	**60**	S3
HH213	SZ IV	**205**	**62**	S3
HH213	SZ IV	**198**	**62**	S3
HH213	SZ IV	**200**	**70**	S3
HH213	SZ IV	**198**	**81**	SB
HH213	SZ IV	**188**	**57**	SB
HH213	SZ IV	**210**	**65**	SB
HH213	SZ IV	**212**	**50**	SB
HH213	SZ IV	**208**	**45**	SB
HH213	SZ IV	**200**	**47**	SB
HH213	SZ IV	**215**	**64**	SB
HH213	SZ IV	**215**	**66**	SB
HH213	SZ IV	**215**	**64**	SB
HH213	SZ IV	**210**	**65**	SB
HH213	SZ IV	**200**	**73**	SB
HH213	SZ IV	**015**	**70**	SB
HH213	SZ IV	**015**	**74**	SB
HH214	SZ V	**112**	**20**	L2/4
HH214	SZ V	**112**	**19**	L2/4
HH214	SZ IV	**295**	**02**	L2/4
HH214	SZ V	**206**	**73**	S2/3/4
HH214	SZ V	**180**	**61**	S2/3/4
HH214	SZ IV	**208**	**71**	S3
HH214	SZ IV	**210**	**63**	S3
HH214	SZ V	**206**	**73**	S5
HH214	SZ V	**180**	**61**	S5
HH215	SZ V	**200**	**74**	L2/4
HH215	SZ V	**199**	**65**	L2/4
HH215	SZ V	**198**	**73**	S2/3/4
HH215	SZ V	**200**	**74**	S2/3/4
HH215	SZ V	**199**	**65**	S2/3/4
HH216	SZ V	**099**	**45**	B2/3
HH216	SZ V	**080**	**51**	B2/3
HH216	SZ V	**085**	**31**	B2/3
HH216	SZ V	**121**	**20**	L2/4
HH216	SZ V	**201**	**68**	S2/3/4
HH216	SZ V	**202**	**70**	S2/3/4
HH216	SZ V	**205**	**70**	S2/3/4
HH216	SZ V	**315**	**84**	S2/3/4
HH217	SZ V	**106**	**17**	L2/4
HH217	SZ V	**188**	**62**	S2/3/4
HH217	SZ V	**004**	**37**	S2/3/4
HH217	SZ V	**356**	**38**	S2/3/4
HH217	SZ V	**009**	**57**	S2/3/4
HH217	SZ V	**188**	**59**	S2/3/4
HH217	SZ V	**195**	**60**	S2/3/4
HH218	SZ IV	**093**	**26**	B3

BA: basalt dike, **CO**: cover, **PE**: pegmatite dike, **SB**: shear band, **SZ I**: structural zone I, **SZ II**: structural zone II, **SZ III**: structural zone III, **SZ IV**: structural zone IV, **SZ V**: structural zone V, **SZ VI**: structural zone VI, **SZ VII**: structural zone VII, **TM**: Punta de li Tulchi metabasite, **TO**: Tanaunella orthogneiss

structural field data, NE-Sardinia, n: 3600 (approx.)

outcrop	structural zone/lithology	dipping-direction	dipping-angle	fabric
HH001	SZ I	**020**	**45**	B3

HH218	SZ V	**083**	**18**	L2/4
HH218	SZ IV	**105**	**19**	L2/4
HH218	SZ IV	**112**	**20**	L2/4
HH218	SZ V	**025**	**60**	S2/3/4
HH218	SZ IV	**178**	**88**	S2/4
HH218	SZ IV	**174**	**60**	S2/4
HH218	SZ IV	**197**	**86**	S2/4
HH218	SZ IV	**188**	**90**	S2/4
HH218	SZ IV	**192**	**78**	S3
HH218	SZ IV	**195**	**86**	S3
HH218	SZ IV	**190**	**89**	S3
HH218	SZ IV	**122**	**89**	S3
HH218	SZ IV	**019**	**87**	S3
HH218	SZ IV	**196**	**71**	S3
HH218	SZ IV	**175**	**80**	S3
HH218	SZ V	**025**	**60**	S5
HH218	SZ V	**190**	**70**	S5
HH218	SZ V	**221**	**84**	S5
HH218	SZ V	**006**	**90**	S5
HH218	SZ IV	**245**	**87**	SB
HH218	SZ V	**246**	**56**	SB
HH218	SZ V	**230**	**86**	SB
HH218	SZ V	**240**	**66**	SB
HH218	SZ V	**246**	**56**	SB
HH218	SZ V	**230**	**86**	SB
HH218	SZ V	**240**	**66**	SB
HH219	SZ IV	**107**	**30**	B3
HH219	SZ IV	**090**	**26**	L2/4
HH219	SZ IV	**152**	**53**	S2/4
HH219	SZ IV	**170**	**66**	S2/4
HH219	SZ IV	**172**	**84**	S2/4
HH219	SZ IV	**180**	**81**	S2/4
HH220	SZ IV	**096**	**25**	B3
HH220	SZ V	**312**	**52**	S2/3/4
HH220	SZ V	**324**	**43**	S2/3/4
HH220	SZ IV	**005**	**80**	S2/4
HH220	SZ IV	**158**	**64**	S3
HH220	SZ IV	**186**	**58**	S3
HH220	SZ V	**312**	**52**	S5
HH220	SZ V	**324**	**43**	S5
HH221	SZ V	**169**	**86**	S2/3/4
HH221	SZ V	**160**	**67**	S2/3/4
HH221	SZ V	**165**	**66**	S2/3/4
HH221	SZ V	**169**	**86**	S5
HH221	SZ V	**160**	**67**	S5
HH221	SZ V	**165**	**66**	S5
HH222	SZ V	**072**	**09**	L2/4
HH222	SZ V	**084**	**32**	L2/4
HH222	SZ V	**095**	**27**	L2/4
HH222	SZ V	**072**	**09**	L2/4
HH222	SZ V	**084**	**32**	L2/4
HH222	SZ V	**095**	**27**	L2/4
HH222	SZ IV	**112**	**23**	L2/4
HH222	SZ IV	**107**	**15**	L2/4
HH222	SZ IV	**094**	**30**	L2/4
HH222	SZ IV	**080**	**50**	L2/4
HH222	SZ V	**160**	**48**	S2/3/4
HH222	SZ V	**148**	**57**	S2/3/4
HH222	SZ V	**139**	**54**	S2/3/4
HH222	SZ V	**152**	**55**	S2/3/4
HH222	SZ V	**170**	**52**	S2/3/4
HH222	SZ V	**168**	**80**	S2/3/4
HH222	SZ IV	**171**	**69**	S3
HH222	SZ IV	**190**	**70**	S3
HH222	SZ IV	**174**	**64**	S3
HH222	SZ V	**148**	**57**	S5
HH222	SZ V	**139**	**54**	S5
HH222	SZ V	**160**	**48**	S5
HH222	SZ V	**152**	**55**	S5
HH222	SZ V	**168**	**80**	S5
HH223	SZ V	**120**	**19**	L2/4
HH223	SZ V	**107**	**16**	L2/4
HH223	SZ V	**120**	**19**	L2/4
HH223	SZ V	**107**	**16**	L2/4
HH223	SZ IV	**106**	**27**	L2/4
HH223	SZ V	**201**	**55**	S2/3/4
HH223	SZ V	**196**	**85**	S2/3/4
HH223	SZ V	**186**	**75**	S2/3/4
HH223	SZ IV	**197**	**83**	S3
HH223	SZ V	**201**	**55**	S5
HH223	SZ V	**196**	**85**	S5
HH223	SZ V	**186**	**75**	S5
HH224	SZ V	**198**	**51**	S2/3/4
HH224	SZ V	**190**	**70**	SB
HH225	SZ V	**110**	**01**	B2/3
HH225	SZ V	**172**	**06**	S2
HH225	SZ V	**180**	**73**	S2/3/4
HH226	SZ IV	**096**	**14**	L2/4
HH226	SZ IV	**109**	**16**	L2/4
HH226	SZ IV	**288**	**04**	L2/4
HH226	SZ IV	**196**	**80**	S2/4
HH226	SZ IV	**194**	**87**	S2/4
HH226	SZ IV	**200**	**81**	S2/4
HH226	SZ IV	**201**	**89**	S2/4
HH227	SZ IV	**100**	**19**	B3
HH227	SZ IV	**107**	**22**	L2/4
HH227	SZ IV	**125**	**14**	L2/4
HH227	SZ IV	**128**	**09**	L2/4
HH227	SZ IV	**117**	**23**	L2/4
HH227	SZ IV	**109**	**20**	L2/4
HH227	SZ IV	**038**	**77**	S2/4
HH227	SZ IV	**028**	**62**	S2/4
HH227	SZ IV	**020**	**86**	S2/4
HH227	SZ IV	**192**	**88**	S2/4
HH227	SZ IV	**183**	**77**	S2/4
HH227	SZ IV	**191**	**86**	S2/4
HH227	SZ IV	**030**	**59**	S2/4
HH227	SZ IV	**002**	**84**	S3
HH227	SZ IV	**205**	**73**	S3
HH227	SZ IV	**215**	**70**	S3
HH227	SZ IV	**192**	**69**	SB
HH228	SZ IV	**108**	**18**	L2/4
HH228	SZ IV	**102**	**06**	L2/4
HH228	SZ IV	**120**	**11**	L2/4
HH228	SZ IV	**108**	**19**	L2/4
HH228	SZ IV	**206**	**74**	S2/4
HH228	SZ IV	**190**	**79**	S2/4
HH228	SZ IV	**210**	**84**	S2/4
HH228	SZ IV	**186**	**86**	S2/4
HH228	SZ IV	**197**	**70**	SB
HH228	SZ IV	**194**	**68**	SB
HH229	SZ IV	**120**	**15**	L2/4
HH229	SZ IV	**119**	**22**	L2/4
HH229	SZ IV	**106**	**03**	L2/4
HH229	SZ IV	**110**	**06**	L2/4
HH229	SZ IV	**022**	**85**	S2/4
HH229	SZ IV	**045**	**76**	S2/4
HH229	SZ IV	**033**	**78**	S2/4
HH229	SZ IV	**034**	**88**	S2/4
HH229	SZ IV	**197**	**89**	S2/4
HH229	SZ IV	**197**	**85**	S2/4
HH230	SZ IV	**116**	**09**	L2/4
HH230	SZ IV	**136**	**17**	L2/4
HH230	SZ IV	**085**	**55**	S2
HH230	SZ IV	**125**	**45**	S2
HH230	SZ IV	**116**	**65**	S2
HH230	SZ IV	**106**	**77**	S2
HH230	SZ IV	**107**	**85**	S2

BA: basalt dike, **CO**: cover, **PE**: pegmatite dike, **SB**: shear band, **SZ I**: structural zone I, **SZ II**: structural zone II, **SZ III**: structural zone III, **SZ IV**: structural zone IV, **SZ V**: structural zone V, **SZ VI**: structural zone VI, **SZ VII**: structural zone VII, **TM**: Punta de li Tulchi metabasite, **TO**: Tanaunella orthogneiss

structural field data, NE-Sardinia, n: 3600 (approx.)

outcrop	structural zone/lithology	dipping-direction	dipping-angle	fabric
HH001	SZ I	**020**	**45**	B3

HH230	SZ IV	**116**	**73**	S2
HH230	SZ IV	**092**	**63**	S2
HH230	SZ IV	**033**	**73**	S2
HH230	SZ IV	**045**	**83**	S2/4
HH230	SZ IV	**209**	**86**	S2/4
HH231	SZ IV	**110**	**20**	L2/4
HH231	SZ IV	**191**	**85**	S2/4
HH232	SZ IV	**108**	**19**	B3
HH232	SZ IV	**100**	**04**	B3
HH232	SZ IV	**101**	**04**	B3
HH232	SZ IV	**103**	**01**	B3
HH232	SZ IV	**104**	**01**	B3
HH232	SZ IV	**287**	**06**	L2/4
HH232	SZ IV	**102**	**04**	L2/4
HH232	SZ IV	**051**	**39**	S2/4
HH232	SZ IV	**104**	**09**	S2/4
HH232	SZ IV	**190**	**45**	S2/4
HH232	SZ IV	**192**	**58**	S2/4
HH232	SZ IV	**204**	**80**	S2/4
HH232	SZ IV	**160**	**32**	S2/4
HH232	SZ IV	**018**	**36**	S2/4
HH232	SZ IV	**182**	**41**	S2/4
HH232	SZ IV	**077**	**14**	S2/4
HH232	SZ IV	**177**	**30**	S2/4
HH232	SZ IV	**356**	**30**	S2/4
HH232	SZ IV	**104**	**75**	S2/4
HH232	SZ IV	**210**	**89**	S3
HH232	SZ IV	**201**	**87**	S3
HH232	SZ IV	**010**	**82**	S3
HH232	SZ IV	**193**	**86**	S3
HH232	SZ IV	**174**	**82**	S3
HH232	SZ IV	**210**	**70**	SB
HH233	SZ IV	**101**	**06**	B3
HH233	SZ IV	**313**	**62**	BA
HH233	SZ IV	**116**	**10**	L2/4
HH233	SZ IV	**105**	**07**	L2/4
HH233	SZ IV	**087**	**04**	L2/4
HH233	SZ IV	**108**	**15**	L2/4
HH233	SZ IV	**196**	**66**	S2/4
HH233	SZ IV	**205**	**34**	S2/4
HH233	SZ IV	**210**	**21**	S2/4
HH233	SZ IV	**090**	**16**	S2/4
HH233	SZ IV	**168**	**39**	S2/4
HH233	SZ IV	**182**	**62**	S2/4
HH233	SZ IV	**179**	**72**	S3
HH233	SZ IV	**170**	**79**	S3
HH233	SZ IV	**181**	**80**	S3
HH233	SZ IV	**196**	**63**	SB
HH234	SZ IV	**098**	**27**	L2/4
HH234	SZ IV	**036**	**44**	S2/4
HH234	SZ IV	**030**	**51**	S2/4
HH234	SZ IV	**038**	**64**	S2/4
HH234	SZ IV	**003**	**81**	SB
HH235	SZ IV	**108**	**13**	L2/4
HH235	SZ IV	**034**	**47**	S2/4
HH235	SZ IV	**036**	**48**	S2/4
HH236	SZ IV	**185**	**53**	B3
HH236	SZ IV	**102**	**10**	L2/4
HH236	SZ IV	**185**	**53**	S2/4
HH236	SZ IV	**032**	**45**	S2/4
HH237	SZ IV	**113**	**31**	B3
HH237	SZ IV	**136**	**36**	S2/4
HH237	SZ IV	**142**	**40**	S2/4
HH237	SZ IV	**030**	**80**	S2/4
HH238	SZ VI	**180**	**85**	S2/3/4
HH238	SZ VI	**176**	**85**	S2/3/4
HH238	SZ VI	**190**	**60**	S2/3/4
HH241	SZ III	**160**	**28**	S2/4
HH241	SZ III	**150**	**29**	S2/4

HH243	SZ VI	**055**	**10**	L2/4
HH243	SZ VI	**084**	**35**	L2/4
HH243	SZ VI	**131**	**47**	S2/3/4
HH243	SZ VI	**108**	**40**	S2/3/4
HH243	SZ VI	**135**	**47**	S2/3/4
HH243	SZ VI	**202**	**22**	SB
HH243	SZ VI	**180**	**24**	SB
HH244	SZ I	**052**	**28**	B3
HH244	SZ I	**052**	**36**	B3
HH244	SZ I	**042**	**35**	B3
HH244	SZ I	**060**	**44**	B3
HH244	SZ I	**052**	**12**	B3
HH244	SZ I	**059**	**25**	B3
HH244	SZ I	**055**	**28**	B3
HH244	SZ I	**066**	**34**	B3
HH244	SZ I	**035**	**32**	L2
HH244	SZ I	**042**	**29**	S2
HH244	SZ I	**130**	**75**	S2
HH244	SZ I	**090**	**36**	S2
HH244	SZ I	**120**	**65**	S2
HH244	SZ I	**128**	**88**	S2
HH244	SZ I	**130**	**35**	S2
HH244	SZ I	**062**	**35**	S2
HH244	SZ I	**125**	**66**	S2
HH244	SZ I	**020**	**45**	S2
HH244	SZ I	**097**	**37**	S2
HH244	SZ I	**059**	**25**	S2
HH244	SZ I	**062**	**29**	S2
HH244	SZ I	**002**	**36**	S2
HH244	SZ I	**107**	**46**	S3
HH244	SZ I	**102**	**58**	S3
HH244	SZ I	**120**	**40**	S3
HH244	SZ I	**096**	**49**	S3
HH244	SZ I	**063**	**34**	S3
HH244	SZ I	**110**	**35**	S3
HH245	SZ I	**034**	**16**	B3
HH245	SZ I	**040**	**22**	B3
HH245	SZ I	**042**	**25**	B3
HH245	SZ I	**130**	**75**	S2
HH245	SZ I	**315**	**80**	S2
HH245	SZ I	**126**	**80**	S3
HH245	SZ I	**118**	**90**	S3
HH245	SZ I	**090**	**70**	S3
HH245	SZ I	**100**	**50**	S3
HH246	SZ I	**049**	**14**	B3
HH246	SZ I	**035**	**30**	B3
HH246	SZ I	**040**	**25**	B3
HH246	SZ I	**130**	**30**	S2
HH246	SZ I	**011**	**56**	S2
HH246	SZ I	**122**	**70**	S3
HH246	SZ I	**115**	**50**	S3
HH246	SZ I	**133**	**80**	S3
HH246	SZ I	**122**	**82**	S3
HH247	SZ I	**046**	**01**	B3
HH247	SZ I	**226**	**09**	B3
HH247	SZ I	**226**	**21**	B3
HH247	SZ I	**096**	**45**	B5
HH247	SZ I	**068**	**11**	L2
HH247	SZ I	**056**	**16**	L2
HH247	SZ I	**063**	**10**	L2
HH247	SZ I	**135**	**34**	S2
HH247	SZ I	**131**	**41**	S2
HH247	SZ I	**124**	**57**	S2
HH247	SZ I	**137**	**52**	S2
HH247	SZ I	**144**	**67**	S3
HH248	SZ I	**062**	**27**	B3
HH248	SZ I	**052**	**10**	B3
HH248	SZ I	**067**	**04**	B3
HH248	SZ I	**045**	**27**	L2

BA: basalt dike, **CO**: cover, **PE**: pegmatite dike, **SB**: shear band, **SZ I**: structural zone I, **SZ II**: structural zone II, **SZ III**: structural zone III, **SZ IV**: structural zone IV, **SZ V**: structural zone V, **SZ VI**: structural zone VI, **SZ VII**: structural zone VII, **TM**: Punta de li Tulchi metabasite, **TO**: Tanaunella orthogneiss

structural field data, NE-Sardinia, n: 3600 (approx.)

outcrop	structural zone/lithology	dipping-direction	dipping-angle	fabric
HH001	SZ I	**020**	**45**	B3

HH248	SZ I	**132**	**55**	S2
HH248	SZ I	**120**	**50**	S2
HH248	SZ I	**070**	**32**	S2
HH249A	SZ I	**068**	**20**	B3
HH249A	SZ I	**063**	**18**	B3
HH249A	SZ I	**041**	**44**	B3
HH249A	SZ I	**090**	**25**	B5
HH249A	SZ I	**088**	**36**	B5
HH249A	SZ I	**030**	**42**	L2
HH249A	SZ I	**055**	**13**	L2
HH249A	SZ I	**061**	**18**	L2
HH249A	SZ I	**125**	**35**	S2
HH249A	SZ I	**126**	**44**	S2
HH249A	SZ I	**076**	**23**	S3
HH249A	SZ I	**155**	**33**	S3
HH249B	SZ I	**076**	**13**	B3
HH249B	SZ I	**062**	**07**	B3
HH249B	SZ I	**066**	**00**	B3
HH249B	SZ I	**059**	**06**	B3
HH249B	SZ I	**148**	**29**	S2
HH249B	SZ I	**138**	**22**	S2
HH249B	SZ I	**130**	**20**	S3
HH249B	SZ I	**155**	**50**	S3
HH250	SZ I	**090**	**10**	B3
HH250	SZ I	**080**	**01**	B3
HH250	SZ I	**081**	**10**	B3
HH250	SZ I	**086**	**02**	B5
HH250	SZ I	**080**	**12**	L2
HH250	SZ I	**150**	**47**	S2
HH250	SZ I	**068**	**01**	S3
HH250	SZ I	**154**	**35**	S3
HH250	SZ I	**120**	**10**	S3
HH250	SZ I	**010**	**55**	S5
HH251	SZ I	**066**	**15**	B3
HH251	SZ I	**061**	**17**	B3
HH251	SZ I	**063**	**23**	B3
HH251	SZ I	**088**	**34**	B5
HH251	SZ I	**038**	**08**	L2
HH251	SZ I	**132**	**43**	S2
HH251	SZ I	**110**	**20**	S3
HH251	SZ I	**114**	**36**	S3
HH251	SZ I	**350**	**40**	S5
HH252	SZ I	**055**	**25**	B3
HH252	SZ I	**050**	**21**	B3
HH252	SZ I	**115**	**50**	S2
HH252	SZ I	**133**	**48**	S2
HH253	SZ I	**046**	**07**	B3
HH253	SZ I	**068**	**18**	B3
HH253	SZ I	**080**	**17**	B5
HH253	SZ I	**142**	**36**	S2
HH253	SZ I	**125**	**20**	S2
HH253	SZ I	**131**	**33**	S2
HH253	SZ I	**325**	**10**	S3
HH253	SZ I	**340**	**25**	S3
HH253	SZ I	**001**	**36**	S5
HH254	SZ I	**060**	**06**	B3
HH254	SZ I	**044**	**09**	B3
HH254	SZ I	**064**	**10**	B3
HH254	SZ I	**100**	**37**	S2
HH254	SZ I	**124**	**29**	S3
HH255	SZ I	**060**	**16**	B2
HH255	SZ I	**062**	**16**	B3
HH255	SZ I	**053**	**09**	B3
HH255	SZ I	**050**	**18**	B3
HH255	SZ I	**210**	**20**	L2
HH255	SZ I	**132**	**39**	S2
HH255	SZ I	**174**	**25**	S2
HH255	SZ I	**124**	**36**	S3
HH255	SZ I	**170**	**40**	S3
HH255	SZ I	**140**	**27**	S3
HH256	SZ I	**090**	**35**	S3
HH256	SZ I	**124**	**45**	S3
HH257	SZ I	**030**	**16**	B3
HH257	SZ I	**222**	**03**	B3
HH257	SZ I	**055**	**21**	B3
HH257	SZ I	**042**	**12**	B3
HH257	SZ I	**062**	**18**	B3
HH257	SZ I	**094**	**45**	B5
HH257	SZ I	**134**	**50**	S2
HH257	SZ I	**127**	**66**	S2
HH257	SZ I	**117**	**56**	S2
HH257	SZ I	**132**	**64**	S3
HH257	SZ I	**131**	**60**	S3
HH257	SZ I	**128**	**45**	S3
HH257	SZ I	**112**	**32**	S3
HH258	SZ I	**050**	**32**	B3
HH258	SZ I	**064**	**17**	B3
HH258	SZ I	**233**	**02**	L2
HH258	SZ I	**110**	**24**	S2
HH258	SZ I	**155**	**60**	S2
HH258	SZ I	**124**	**28**	S2
HH258	SZ I	**120**	**40**	S3
HH258	SZ I	**124**	**28**	S3
HH259	SZ I	**045**	**02**	L2
HH259	SZ I	**136**	**53**	S2
HH259	SZ I	**160**	**52**	S2
HH259	SZ I	**135**	**44**	S2
HH260	SZ I	**075**	**10**	L2
HH260	SZ I	**158**	**36**	S2
HH260	SZ I	**151**	**34**	S2
HH261	SZ I	**162**	**36**	S2
HH263	SZ II	**162**	**50**	S2
HH263	SZ II	**154**	**48**	S2
HH263	SZ II	**068**	**00**	S2
HH264	SZ II	**064**	**38**	B3
HH264	SZ II	**080**	**41**	B3
HH264	SZ II	**094**	**35**	B3
HH264	SZ II	**152**	**42**	S2
HH264	SZ II	**148**	**52**	S2
HH264	SZ II	**136**	**37**	S2
HH264	SZ II	**230**	**12**	S2
HH264	SZ II	**064**	**18**	S2
HH264	SZ II	**162**	**32**	S3
HH264	SZ II	**175**	**35**	S3
HH264	SZ II	**158**	**69**	S3
HH265	SZ II	**077**	**25**	B3
HH265	SZ II	**125**	**37**	B3
HH265	SZ II	**070**	**20**	B3
HH265	SZ II	**083**	**16**	B5
HH265	SZ II	**150**	**42**	S1
HH265	SZ II	**138**	**58**	S2
HH265	SZ II	**150**	**42**	S2
HH265	SZ II	**048**	**09**	S2
HH265	SZ II	**070**	**16**	S2
HH265	SZ II	**134**	**35**	S3
HH265	SZ II	**160**	**47**	S3
HH265	SZ II	**155**	**55**	S3
HH265	SZ II	**350**	**40**	S3
HH265	SZ II	**354**	**80**	S5
HH266	SZ II	**235**	**01**	B3
HH266	SZ II	**050**	**04**	B3
HH266	SZ II	**156**	**53**	S2
HH266	SZ II	**150**	**36**	S2
HH266	SZ II	**138**	**35**	S2
HH266	SZ II	**166**	**52**	S2
HH266	SZ II	**140**	**38**	S2
HH266	SZ II	**088**	**37**	S2
HH266	SZ II	**145**	**45**	S3

BA: basalt dike, **CO**: cover, **PE**: pegmatite dike, **SB**: shear band, **SZ I**: structural zone I, **SZ II**: structural zone II, **SZ III**: structural zone III, **SZ IV**: structural zone IV, **SZ V**: structural zone V, **SZ VI**: structural zone VI, **SZ VII**: structural zone VII, **TM**: Punta de li Tulchi metabasite, **TO**: Tanaunella orthogneiss

structural field data, NE-Sardinia, n: 3600 (approx.)

outcrop	structural zone/lithology	dipping-direction	dipping-angle	fabric
HH001	SZ I	**020**	**45**	B3

HH266	SZ II	**140**	**40**	S3
HH267	SZ II	**082**	**22**	B3
HH267	SZ II	**166**	**59**	S2
HH267	SZ II	**164**	**64**	S2
HH267	SZ II	**180**	**90**	S3
HH267	SZ II	**180**	**90**	S3
HH268	SZ II	**072**	**02**	B3
HH268	SZ II	**162**	**85**	S2
HH268	SZ II	**169**	**64**	S2
HH268	SZ II	**160**	**50**	S3
HH268	SZ II	**190**	**60**	S3
HH269	SZ II	**200**	**06**	B3
HH269	SZ II	**205**	**13**	B3
HH269	SZ II	**240**	**45**	S2
HH269	SZ II	**290**	**60**	S3
HH269	SZ II	**297**	**80**	S3
HH269	SZ II	**292**	**70**	S3
HH270	SZ II	**172**	**36**	S2
HH270	SZ II	**200**	**50**	S2
HH270	SZ II	**172**	**35**	S2
HH270	SZ II	**103**	**08**	S2
HH270	SZ II	**111**	**14**	S2
HH270	SZ II	**170**	**29**	S3
HH270	SZ II	**159**	**24**	S3
HH271	SZ III	**260**	**15**	L2/4
HH271	SZ III	**104**	**05**	L2/4
HH271	SZ II	**260**	**15**	L2/4
HH271	SZ II	**104**	**05**	L2/4
HH271	SZ III	**182**	**47**	S2
HH271	SZ III	**184**	**46**	S2
HH271	SZ II	**184**	**46**	S3
HH271	SZ II	**182**	**47**	S3
HH272	SZ III	**214**	**35**	L2
HH272	SZ III	**214**	**35**	L2
HH272	SZ III	**188**	**42**	S2
HH272	SZ III	**184**	**46**	S2
HH272	SZ III	**188**	**42**	S2
HH272	SZ III	**184**	**46**	S2
HH273	SZ II	**190**	**44**	S2
HH273	SZ II	**150**	**40**	S2
HH273	SZ II	**113**	**33**	S2
HH273	SZ II	**105**	**30**	S2
HH273	SZ II	**224**	**45**	S3
HH273	SZ II	**225**	**50**	S3
HH274	SZ II	**243**	**22**	B2
HH274	SZ II	**246**	**15**	B2
HH274	SZ II	**234**	**37**	B3
HH274	SZ II	**158**	**59**	S2
HH274	SZ II	**160**	**61**	S2
HH274	SZ II	**234**	**37**	SB
HH275	SZ III	**224**	**18**	L2
HH275	SZ III	**050**	**20**	L2
HH275	SZ III	**156**	**40**	S2
HH275	SZ III	**158**	**24**	S2
HH276	SZ III	**123**	**05**	L2/4
HH276	SZ III	**108**	**05**	L2/4
HH276	SZ III	**217**	**18**	S2
HH276	SZ III	**180**	**15**	S2
HH276	SZ III	**228**	**46**	SB
HH277	SZ II	**060**	**05**	L2/4
HH277	SZ II	**060**	**10**	L2/4
HH277	SZ II	**142**	**26**	S3
HH277	SZ II	**138**	**30**	S3
HH278	SZ III	**084**	**12**	L2/4
HH278	SZ III	**087**	**16**	L2/4
HH278	SZ III	**105**	**14**	S2/4
HH278	SZ III	**117**	**17**	S2/4
HH278	SZ III	**090**	**24**	S2/4
HH279	SZ III	**079**	**05**	L2/4
HH279	SZ III	**100**	**08**	L2/4
HH279	SZ III	**114**	**60**	S2/4
HH279	SZ III	**160**	**15**	S2/4
HH279	SZ III	**170**	**45**	SB
HH279	SZ III	**150**	**58**	SB
HH280	SZ IV	**110**	**30**	L2/4
HH280	SZ IV	**104**	**41**	L2/4
HH280	SZ IV	**104**	**27**	L2/4
HH280	SZ IV	**110**	**21**	L2/4
HH280	SZ IV	**185**	**76**	S2
HH280	SZ IV	**162**	**80**	S2
HH280	SZ IV	**204**	**86**	S2/4
HH280	SZ IV	**198**	**82**	S2/4
HH280	SZ IV	**188**	**86**	S2/4
HH281	SZ IV	**175**	**66**	S2/4
HH281	SZ IV	**220**	**45**	SB
HH281	SZ IV	**192**	**61**	SB
HH282	SZ VI	**162**	**75**	S2/3/4
HH282	SZ VI	**174**	**65**	S2/3/4
HH282	SZ VI	**180**	**65**	S2/3/4
HH282	SZ VI	**166**	**80**	SB
HH282	SZ VI	**187**	**85**	SB
HH283	SZ V	**112**	**33**	L2/4
HH283	SZ V	**090**	**04**	L2/4
HH283	SZ V	**091**	**17**	L2/4
HH283	SZ V	**013**	**83**	S2
HH283	SZ V	**002**	**58**	S2
HH283	SZ V	**010**	**80**	S2/3/4
HH283	SZ V	**198**	**84**	S2/3/4
HH283	SZ V	**215**	**73**	SB
HH283	SZ V	**198**	**84**	SB
HH284	SZ V	**095**	**06**	B2/3
HH284	SZ V	**091**	**18**	L2/4
HH284	SZ V	**094**	**09**	L2/4
HH284	SZ V	**182**	**76**	S2/3/4
HH284	SZ V	**190**	**83**	S2/3/4
HH284	SZ V	**002**	**83**	S2/3/4
HH284	SZ V	**230**	**75**	SB
HH284	SZ V	**233**	**80**	SB
HH285	SZ V	**292**	**05**	B2/3
HH285	SZ V	**275**	**05**	B2/3
HH285	SZ V	**088**	**05**	B5
HH285	SZ V	**100**	**05**	B5
HH285	SZ V	**090**	**08**	B5
HH285	SZ V	**092**	**05**	B5
HH285	SZ V	**084**	**14**	L2/4
HH285	SZ V	**097**	**07**	L2/4
HH285	SZ V	**185**	**65**	S2/3/4
HH285	SZ V	**186**	**70**	S2/3/4
HH285	SZ V	**190**	**65**	S2/3/4
HH285	SZ V	**186**	**82**	S2/3/4
HH285	SZ V	**188**	**70**	S2/3/4
HH285	SZ V	**194**	**84**	S2/3/4
HH285	SZ V	**185**	**85**	S5
HH285	SZ V	**002**	**85**	S5
HH285	SZ V	**355**	**80**	S5
HH285	SZ V	**220**	**75**	SB
HH285	SZ V	**228**	**85**	SB
HH285	SZ V	**220**	**60**	SB
HH285	SZ V	**225**	**50**	SB
HH285	SZ V	**230**	**76**	SB
HH286	SZ V	**109**	**10**	B2/3
HH286	SZ V	**100**	**02**	B2/3
HH286	SZ V	**100**	**14**	B2/3
HH286	SZ V	**116**	**19**	B2/3
HH286	SZ V	**200**	**90**	S2/3/4
HH286	SZ V	**202**	**83**	S2/3/4
HH286	SZ V	**224**	**75**	SB
HH286	SZ V	**235**	**65**	SB

BA: basalt dike, **CO**: cover, **PE**: pegmatite dike, **SB**: shear band, **SZ I**: structural zone I, **SZ II**: structural zone II, **SZ III**: structural zone III, **SZ IV**: structural zone IV, **SZ V**: structural zone V, **SZ VI**: structural zone VI, **SZ VII**: structural zone VII, **TM**: Punta de li Tulchi metabasite, **TO**: Tanaunella orthogneiss

structural field data, NE-Sardinia, n: 3600 (approx.)

outcrop	structural zone/lithology	dipping-direction	dipping-angle	fabric
HH001	SZ I	**020**	**45**	B3

HH287	SZ V	**110**	**08**	L2/4
HH287	SZ V	**105**	**05**	L2/4
HH287	SZ V	**190**	**55**	S2/3/4
HH287	SZ V	**199**	**77**	S2/3/4
HH287	SZ V	**202**	**80**	S2/3/4
HH287	SZ V	**225**	**35**	SB
HH287	SZ V	**221**	**69**	SB
HH287	SZ V	**215**	**74**	SB
HH288	SZ V	**108**	**02**	L2/4
HH288	SZ V	**108**	**02**	L2/4
HH288	SZ V	**117**	**25**	L2/4
HH288	SZ V	**210**	**70**	S2/3/4
HH288	SZ V	**222**	**71**	S2/3/4
HH288	SZ V	**180**	**70**	S2/3/4
HH288	SZ V	**198**	**78**	S2/3/4
HH288	SZ V	**235**	**55**	SB
HH288	SZ V	**234**	**76**	SB
HH288	SZ V	**180**	**75**	SB
HH289	SZ V	**111**	**10**	L2/4
HH289	SZ V	**113**	**10**	L2/4
HH289	SZ V	**193**	**65**	S2/3/4
HH289	SZ V	**205**	**72**	S2/3/4
HH289	SZ V	**232**	**58**	SB
HH289	SZ V	**232**	**55**	SB
HH290	SZ V	**081**	**27**	B2/3
HH290	SZ V	**122**	**03**	L2/4
HH290	SZ V	**138**	**27**	L2/4
HH290	SZ V	**122**	**03**	L2/4
HH290	SZ V	**290**	**08**	L2/4
HH290	SZ V	**114**	**03**	L2/4
HH290	SZ V	**207**	**71**	S2/3/4
HH290	SZ V	**200**	**85**	S2/3/4
HH290	SZ V	**195**	**61**	S2/3/4
HH290	SZ V	**210**	**66**	SB
HH290	SZ V	**212**	**68**	SB
HH291	SZ V	**118**	**06**	L2/4
HH291	SZ V	**209**	**80**	S2/3/4
HH291	SZ V	**168**	**75**	S2/3/4
HH291	SZ V	**202**	**70**	SB
HH292	SZ V	**110**	**16**	L2/4
HH292	SZ V	**290**	**23**	L2/4
HH292	SZ V	**194**	**83**	S2/3/4
HH292	SZ V	**198**	**82**	S2/3/4
HH292	SZ V	**188**	**84**	S2/3/4
HH293	SZ V	**087**	**05**	L2/4
HH293	SZ V	**196**	**80**	S2/3/4
HH293	SZ V	**176**	**79**	S2/3/4
HH294	SZ V	**113**	**15**	L2/4
HH294	SZ V	**112**	**12**	L2/4
HH294	SZ V	**194**	**64**	S2
HH294	SZ V	**188**	**77**	S2
HH294	SZ V	**210**	**90**	S2/3/4
HH294	SZ V	**190**	**63**	S2/3/4
HH294	SZ V	**185**	**62**	S2/3/4
HH294	SZ V	**240**	**45**	SB
HH294	SZ V	**215**	**55**	SB
HH295	SZ V	**190**	**76**	S2/3/4
HH295	SZ V	**192**	**84**	S2/3/4
HH295	SZ V	**187**	**78**	S2/3/4
HH296	SZ V	**082**	**26**	B2/3
HH296	SZ V	**103**	**20**	L2/4
HH296	SZ V	**010**	**79**	S2/3/4
HH296	SZ V	**175**	**84**	S2/3/4
HH296	SZ V	**170**	**83**	S2/3/4
HH296	SZ V	**185**	**62**	S2/3/4
HH297	SZ V	**185**	**80**	S2/3/4
HH297	SZ V	**220**	**90**	SB
HH298	SZ V	**172**	**78**	S2/3/4
HH298	SZ V	**176**	**73**	S2/3/4

HH299	SZ V	**275**	**29**	B5
HH299	SZ V	**190**	**90**	S2/3/4
HH299	SZ V	**360**	**81**	S5
HH299	SZ V	**220**	**80**	SB
HH300	SZ V	**260**	**25**	B5
HH300	SZ V	**257**	**27**	L2/4
HH300	SZ V	**173**	**80**	S2/3/4
HH300	SZ V	**180**	**80**	S5
HH300	SZ V	**215**	**55**	SB
HH300	SZ V	**200**	**75**	SB
HH301	SZ VII	**215**	**39**	S3
HH301	SZ VII	**210**	**35**	S3
HH301	SZ VII	**201**	**20**	S3
HH301	SZ VII	**240**	**50**	SB
HH302	SZ V	**273**	**07**	S2
HH302	SZ V	**205**	**46**	S2
HH303	SZ V	**290**	**02**	L2/4
HH303	SZ V	**111**	**04**	L2/4
HH303	SZ V	**198**	**36**	S2/3/4
HH304	SZ V	**273**	**05**	L2
HH304	SZ V	**006**	**86**	S2
HH304	SZ V	**276**	**06**	S2
HH304	SZ V	**190**	**40**	S2
HH304	SZ V	**208**	**85**	SB
HH306	SZ V	**104**	**06**	B2/3
HH306	SZ V	**190**	**55**	S2/3/4
HH306	SZ V	**172**	**56**	S2/3/4
HH307	SZ V	**298**	**09**	L2/4
HH307	SZ V	**198**	**63**	S2/3/4
HH307	SZ V	**195**	**45**	S2/3/4
HH307	SZ V	**206**	**68**	S2/3/4
HH307	SZ V	**192**	**63**	S2/3/4
HH307	SZ V	**235**	**79**	SB
HH308	SZ V	**112**	**04**	L2/4
HH308	SZ V	**197**	**57**	S2/3/4
HH309	SZ V	**092**	**32**	L2
HH309	SZ V	**098**	**07**	L2
HH309	SZ V	**184**	**72**	S2
HH309	SZ V	**168**	**63**	S2
HH310	SZ V	**100**	**28**	L2/4
HH310	SZ V	**183**	**90**	S2/3/4
HH310	SZ V	**199**	**80**	SB
HH311	SZ V	**282**	**11**	L2/4
HH311	SZ V	**192**	**40**	S2/3/4
HH311	SZ V	**230**	**62**	SB
HH312	SZ V	**107**	**12**	B2/3
HH312	SZ V	**115**	**12**	L2/4
HH312	SZ V	**100**	**15**	L2/4
HH312	SZ V	**202**	**63**	S2/3/4
HH312	SZ V	**192**	**70**	S2/3/4
HH313	SZ V	**118**	**10**	B2/3
HH314	SZ V	**002**	**87**	S2/3/4
HH314	SZ V	**220**	**81**	SB
HH316	SZ IV	**272**	**40**	L2/4
HH316	SZ IV	**087**	**02**	L2/4
HH316	SZ IV	**188**	**86**	S2/4
HH316	SZ IV	**178**	**80**	S2/4
HH316	SZ IV	**000**	**89**	S2/4
HH316	SZ IV	**012**	**86**	S2/4
HH316	SZ IV	**218**	**79**	SB
HH316	SZ IV	**212**	**70**	SB
HH317	SZ V	**240**	**55**	BA
HH317	SZ V	**210**	**82**	BA
HH317	SZ V	**128**	**30**	L2/4
HH317	SZ V	**210**	**82**	S2/3/4
HH317	SZ V	**201**	**72**	S2/3/4
HH317	SZ V	**205**	**72**	S2/3/4
HH318	SZ IV	**111**	**33**	L2/4
HH318	SZ IV	**187**	**74**	S2/4

BA: basalt dike, **CO**: cover, **PE**: pegmatite dike, **SB**: shear band, **SZ I**: structural zone I, **SZ II**: structural zone II, **SZ III**: structural zone III, **SZ IV**: structural zone IV, **SZ V**: structural zone V, **SZ VI**: structural zone VI, **SZ VII**: structural zone VII, **TM**: Punta de li Tulchi metabasite, **TO**: Tanaunella orthogneiss

structural field data, NE-Sardinia, n: 3600 (approx.)

outcrop	structural zone/lithology	dipping-direction	dipping-angle	fabric
HH001	SZ I	**020**	**45**	B3

HH319	SZ IV	**109**	**21**	L2/4
HH319	SZ IV	**113**	**33**	L2/4
HH319	SZ IV	**193**	**65**	S2/4
HH320	SZ IV	**175**	**75**	S2/4
HH320	SZ IV	**197**	**73**	S2/4
HH320	SZ IV	**207**	**66**	SB
HH321	SZ IV	**199**	**66**	S2/4
HH321	SZ IV	**201**	**69**	SB
HH322	SZ IV	**098**	**37**	B3
HH322	SZ IV	**112**	**10**	L2/4
HH322	SZ IV	**190**	**71**	S2/4
HH322	SZ IV	**203**	**85**	SB
HH323	SZ IV	**111**	**05**	L2/4
HH323	SZ IV	**195**	**81**	S2/4
HH323	SZ IV	**205**	**74**	S2/4
HH324	SZ IV	**191**	**80**	S2/4
HH324	SZ IV	**230**	**50**	SB
HH325	SZ IV	**190**	**82**	S2/4
HH326	SZ III	**098**	**09**	B5
HH326	SZ III	**108**	**23**	B5
HH326	SZ III	**093**	**16**	L2/4
HH326	SZ III	**145**	**35**	S2/4
HH326	SZ III	**068**	**10**	S2/4
HH326	SZ III	**084**	**24**	S2/4
HH326	SZ III	**030**	**74**	S2/4
HH326	SZ III	**150**	**33**	S2/4
HH326	SZ III	**162**	**12**	S2/4
HH326	SZ III	**108**	**10**	S2/4
HH326	SZ III	**113**	**24**	S2/4
HH326	SZ III	**160**	**42**	S2/4
HH326	SZ III	**184**	**75**	S2/4
HH326	SZ III	**182**	**85**	S5
HH326	SZ III	**194**	**69**	S5
HH327	SZ III	**098**	**13**	B5
HH327	SZ III	**150**	**50**	S2/4
HH327	SZ III	**135**	**34**	S2/4
HH327	SZ III	**140**	**33**	S2/4
HH327	SZ III	**156**	**26**	S2/4
HH327	SZ III	**109**	**22**	S2/4
HH328	SZ III	**096**	**15**	B5
HH328	SZ III	**050**	**23**	S2/4
HH328	SZ III	**025**	**26**	S2/4
HH328	SZ III	**150**	**32**	S2/4
HH328	SZ III	**077**	**30**	S2/4
HH328	SZ III	**168**	**35**	S2/4
HH328	SZ III	**173**	**77**	S5
HH329	SZ IV	**186**	**52**	S2/4
HH329	SZ IV	**182**	**65**	S3
HH330	SZ III	**110**	**13**	L2/4
HH330	SZ III	**142**	**12**	S2/4
HH330	SZ III	**162**	**41**	S2/4
HH331	SZ III	**282**	**03**	L2/4
HH331	SZ III	**285**	**13**	L2/4
HH331	SZ III	**215**	**62**	S2/4
HH331	SZ III	**220**	**50**	S2/4
HH331	SZ III	**195**	**45**	S2/4
HH332	SZ III	**257**	**06**	L2/4
HH332	SZ III	**088**	**34**	L2/4
HH332	SZ III	**088**	**13**	L2/4
HH332	SZ III	**170**	**34**	S2/4
HH332	SZ III	**165**	**36**	S2/4
HH332	SZ III	**188**	**33**	S2/4
HH332	SZ III	**148**	**50**	S2/4
HH332	SZ III	**152**	**51**	S2/4
HH332	SZ III	**178**	**53**	S2/4
HH333	SZ III	**180**	**44**	S2/4
HH333	SZ III	**190**	**27**	S2/4
HH334	SZ III	**112**	**23**	L2/4
HH334	SZ II	**266**	**33**	L2/4
HH334	SZ II	**102**	**20**	L2/4
HH334	SZ III	**206**	**61**	S2/4
HH334	SZ III	**215**	**64**	S2/4
HH334	SZ II	**194**	**64**	S3
HH334	SZ II	**185**	**70**	S3
HH334	SZ II	**223**	**47**	S3
HH334	SZ II	**208**	**75**	S3
HH334	SZ II	**202**	**59**	S3
HH334	SZ II	**230**	**85**	SB
HH335	SZ II	**245**	**23**	L2/4
HH335	SZ II	**248**	**32**	L2/4
HH335	SZ II	**250**	**08**	L2/4
HH335	SZ II	**196**	**28**	S3
HH335	SZ II	**182**	**25**	S3
HH335	SZ II	**184**	**43**	S3
HH335	SZ II	**205**	**24**	S3
HH335	SZ II	**186**	**34**	S3
HH335	SZ II	**280**	**14**	SB
HH336	SZ II	**202**	**11**	S3
HH337	SZ II	**280**	**06**	L2/4
HH337	SZ II	**208**	**20**	S3
HH337	SZ II	**280**	**24**	S3
HH337	SZ II	**254**	**13**	S3
HH338	SZ II	**270**	**22**	L2/4
HH338	SZ II	**266**	**22**	S3
HH338	SZ II	**212**	**24**	S3
HH339	SZ II	**268**	**04**	L2/4
HH339	SZ II	**270**	**04**	S3
HH400	SZ II	**265**	**00**	L2/4
HH400	SZ II	**245**	**06**	L2/4
HH400	SZ II	**261**	**01**	L2/4
HH400	SZ II	**205**	**06**	S3
HH401	SZ II	**166**	**63**	BA
HH401	SZ II	**155**	**22**	BA
HH401	SZ II	**282**	**08**	L2/4
HH401	SZ II	**263**	**12**	S3
HH401	SZ II	**222**	**16**	S3
HH401	SZ II	**160**	**40**	S3
HH401	SZ II	**172**	**15**	S3
HH401	SZ II	**240**	**09**	S3
HH402	SZ II	**095**	**12**	B3
HH402	SZ II	**145**	**27**	S3
HH403	CO	**070**	**21**	S0
HH403	CO	**090**	**55**	S0
HH403	CO	**075**	**29**	S0
HH403	CO	**105**	**31**	S0
HH403	CO	**072**	**15**	S0
HH403	CO	**098**	**32**	S0
HH403	CO	**103**	**27**	S0
HH403	CO	**105**	**28**	S0
HH403	CO	**124**	**25**	S0
HH403	CO	**122**	**26**	S0
HH403	CO	**110**	**45**	S0
HH403	CO	**095**	**21**	S0
HH403	CO	**100**	**12**	S0
HH403	CO	**122**	**39**	S0
HH403	CO	**125**	**31**	S0
HH403	CO	**105**	**30**	S0
HH403	CO	**108**	**30**	S0
HH404	SZ II	**077**	**25**	B3
HH404	SZ II	**063**	**25**	S2
HH404	SZ II	**138**	**33**	S3
HH405	CO	**123**	**35**	S0
HH405	CO	**115**	**30**	S0
HH405	CO	**174**	**05**	S0
HH405	CO	**135**	**32**	S0
HH405	CO	**130**	**15**	S0
HH405	CO	**102**	**35**	S0
HH405	CO	**130**	**17**	S0

BA: basalt dike, **CO**: cover, **PE**: pegmatite dike, **SB**: shear band, **SZ I**: structural zone I, **SZ II**: structural zone II, **SZ III**: structural zone III, **SZ IV**: structural zone IV, **SZ V**: structural zone V, **SZ VI**: structural zone VI, **SZ VII**: structural zone VII, **TM**: Punta de li Tulchi metabasite, **TO**: Tanaunella orthogneiss

structural field data, NE-Sardinia, n: 3600 (approx.)

outcrop	structural zone/lithology	dipping-direction	dipping-angle	fabric
HH001	SZ I	**020**	**45**	B3

HH405	CO	**125**	**15**	S0
HH405	CO	**124**	**15**	S0
HH406	SZ II	**078**	**07**	B3
HH406	SZ II	**081**	**18**	L2/4
HH406	SZ II	**137**	**30**	S3
HH406	SZ II	**135**	**37**	S3
HH406B	CO	**120**	**26**	S0
HH406B	CO	**145**	**16**	S0
HH406B	CO	**133**	**17**	S0
HH406B	CO	**160**	**07**	S0
HH406B	CO	**102**	**26**	S0
HH406B	CO	**065**	**07**	S0
HH407	SZ II	**268**	**06**	L2/4
HH407	SZ II	**090**	**05**	L2/4
HH407	SZ II	**065**	**25**	L2/4
HH407	SZ II	**075**	**24**	S3
HH407	SZ II	**216**	**13**	S3
HH407	SZ II	**058**	**13**	S3
HH408	SZ II	**120**	**80**	BA
HH408	SZ II	**070**	**25**	L2/4
HH408	SZ II	**130**	**28**	S3
HH408	SZ II	**120**	**28**	S3
HH409	SZ II	**075**	**02**	B3
HH409	SZ II	**058**	**14**	L2/4
HH409	SZ II	**070**	**15**	L2/4
HH409	SZ II	**070**	**08**	S3
HH410	SZ II	**058**	**14**	L2/4
HH410	SZ II	**115**	**06**	S3
HH411	SZ II	**056**	**31**	B2
HH411	SZ II	**075**	**18**	L2/4
HH411	SZ II	**225**	**36**	S3
HH412	SZ II	**012**	**35**	S2
HH412	SZ II	**105**	**25**	S3
HH415	SZ II	**102**	**34**	B2
HH415	SZ II	**138**	**28**	S2
HH415	SZ II	**082**	**25**	S2
HH415	SZ II	**170**	**86**	S3
HH415B	SZ II	**135**	**30**	S2
HH415B	SZ II	**135**	**40**	S2
HH415B	SZ II	**080**	**28**	S2
HH416	SZ II	**070**	**01**	B3
HH416	CO	**134**	**60**	S0
HH416	CO	**130**	**40**	S0
HH416	CO	**150**	**25**	S0
HH416	CO	**130**	**25**	S0
HH416	CO	**136**	**27**	S0
HH416	CO	**134**	**25**	S0
HH416	CO	**136**	**46**	S0
HH416	CO	**120**	**55**	S0
HH416	CO	**136**	**50**	S0
HH416	CO	**116**	**20**	S0
HH416	CO	**117**	**23**	S0
HH416	CO	**146**	**19**	S0
HH416	SZ II	**348**	**74**	S3
HH416	SZ II	**359**	**79**	S3
HH416	SZ II	**330**	**76**	S3
HH417	SZ II	**085**	**15**	B3
HH417	SZ II	**078**	**28**	B3
HH417	SZ II	**165**	**58**	S3
HH417	SZ II	**165**	**80**	S3
HH418	SZ II	**078**	**32**	B3
HH418	SZ II	**159**	**62**	S3
HH419	SZ II	**055**	**13**	B3
HH419	SZ II	**332**	**86**	S3
HH420	SZ II	**071**	**27**	B3
HH420	SZ II	**125**	**65**	S2
HH420	SZ II	**162**	**85**	S3
HH421	SZ II	**070**	**20**	B3
HH421	SZ II	**061**	**26**	B3
HH421	SZ II	**149**	**74**	S3
HH422	SZ II	**110**	**23**	B2
HH422	SZ II	**070**	**06**	B2
HH422	SZ II	**070**	**24**	B3
HH422	SZ II	**085**	**05**	B3
HH422	SZ II	**105**	**29**	S2
HH422	SZ II	**090**	**24**	S2
HH422	SZ II	**025**	**87**	S3
HH423	SZ II	**353**	**04**	S2
HH423	SZ II	**270**	**01**	S2
HH424	SZ II	**277**	**01**	B2
HH424	SZ II	**276**	**06**	B3
HH424	SZ II	**355**	**32**	S2
HH424	SZ II	**002**	**65**	S3
HH425	SZ II	**270**	**22**	B2
HH425	SZ II	**266**	**24**	B2
HH425	SZ II	**078**	**14**	B3
HH425	SZ II	**235**	**20**	S2
HH425	SZ II	**273**	**22**	S2
HH425	SZ II	**295**	**27**	S2
HH425	SZ II	**165**	**80**	S3
HH426	SZ II	**170**	**12**	S3
HH427	SZ II	**090**	**26**	B2
HH427	SZ II	**110**	**20**	S2
HH427	SZ II	**143**	**35**	S3
HH427	SZ II	**140**	**37**	S3
HH428	SZ II	**080**	**24**	B3
HH428	SZ II	**078**	**28**	B3
HH428	SZ II	**064**	**25**	S2
HH428	SZ II	**086**	**26**	S2
HH428	SZ II	**111**	**33**	S3
HH429	SZ II	**073**	**33**	B3
HH429	SZ II	**080**	**15**	B3
HH429	SZ II	**080**	**04**	B3
HH429	SZ II	**165**	**75**	S2
HH429	SZ II	**162**	**89**	S2
HH429	SZ II	**088**	**07**	S2
HH429	SZ II	**154**	**63**	S3
HH430	SZ II	**174**	**75**	S2
HH430	SZ II	**077**	**32**	S2
HH431	SZ II	**070**	**04**	B3
HH431	SZ II	**141**	**64**	S2
HH431	SZ II	**125**	**17**	S2
HH431	SZ II	**153**	**42**	S3
HH432	SZ II	**076**	**01**	B3
HH432	SZ II	**161**	**83**	S2
HH432	SZ II	**158**	**75**	S2
HH433	SZ II	**077**	**07**	B5
HH433	SZ II	**153**	**39**	S2
HH433	SZ II	**163**	**45**	S2
HH433	SZ II	**347**	**24**	S5
HH434	SZ II	**200**	**30**	B3
HH434	SZ II	**278**	**73**	S2
HH434	SZ II	**278**	**65**	S2
HH434	SZ II	**117**	**75**	S3
HH435	SZ II	**210**	**23**	B3
HH435	SZ II	**284**	**50**	S2
HH435	SZ II	**290**	**75**	S2
HH435	SZ II	**204**	**25**	S2
HH435	SZ II	**295**	**43**	S3
HH436	SZ II	**045**	**09**	B3
HH436	SZ II	**041**	**12**	B3
HH436	SZ II	**233**	**27**	B3
HH436	SZ II	**302**	**58**	S2
HH436	SZ II	**232**	**28**	S2
HH436	SZ II	**302**	**77**	S3
HH436	SZ II	**305**	**80**	S3
HH437	SZ II	**270**	**12**	B3
HH437	SZ II	**349**	**89**	S3

BA: basalt dike, **CO**: cover, **PE**: pegmatite dike, **SB**: shear band, **SZ I**: structural zone I, **SZ II**: structural zone II, **SZ III**: structural zone III, **SZ IV**: structural zone IV, **SZ V**: structural zone V, **SZ VI**: structural zone VI, **SZ VII**: structural zone VII, **TM**: Punta de li Tulchi metabasite, **TO**: Tanaunella orthogneiss

structural field data, NE-Sardinia, n: 3600 (approx.)

outcrop	structural zone/lithology	dipping-direction	dipping-angle	fabric
HH001	SZ I	**020**	**45**	B3

HH437	SZ II	**004**	**89**	S3
HH437	SZ II	**172**	**75**	S3
HH438	SZ II	**090**	**04**	B3
HH438	SZ II	**188**	**60**	S3
HH439	SZ II	**081**	**13**	B3
HH439	SZ II	**015**	**40**	S2
HH439	SZ II	**160**	**50**	S2
HH439	SZ II	**356**	**61**	S2
HH439	SZ II	**195**	**72**	S3
HH440	SZ II	**076**	**15**	B3
HH440	SZ II	**005**	**77**	S2
HH440	SZ II	**002**	**67**	S2
HH440	SZ II	**198**	**69**	S2
HH440	SZ II	**198**	**65**	S2
HH440	SZ II	**166**	**19**	S2
HH440	SZ II	**162**	**57**	S3
HH440	SZ II	**166**	**75**	S3
HH441	SZ II	**239**	**15**	B3
HH441	SZ II	**346**	**23**	S2
HH441	SZ II	**162**	**65**	S2
HH441	SZ II	**160**	**50**	S3
HH441	SZ II	**160**	**47**	S3
HH441	SZ II	**010**	**05**	S5
HH442	SZ II	**158**	**56**	S2
HH442	SZ II	**146**	**47**	S2
HH442	SZ II	**068**	**09**	S2
HH442	SZ II	**133**	**40**	S3
HH443	SZ II	**086**	**02**	B3
HH443	SZ II	**171**	**50**	S2
HH443	SZ II	**153**	**67**	S2
HH444	SZ II	**087**	**17**	B3
HH444	SZ II	**058**	**07**	B5
HH444	SZ II	**166**	**38**	S2
HH444	SZ II	**150**	**55**	S2
HH444	SZ II	**170**	**62**	S3
HH444	SZ II	**345**	**20**	S5
HH445	SZ II	**145**	**61**	S2
HH445	SZ II	**145**	**74**	S2
HH446	CO	**122**	**37**	S0
HH446	CO	**122**	**31**	S0
HH446	CO	**130**	**26**	S0
HH446	CO	**116**	**24**	S0
HH446	CO	**125**	**35**	S0
HH446	CO	**118**	**36**	S0
HH446	CO	**095**	**30**	S0
HH446	CO	**116**	**42**	S0
HH446	CO	**132**	**27**	S0
HH446	CO	**130**	**18**	S0
HH446	CO	**170**	**16**	S0
HH446	CO	**120**	**18**	S0
HH446	CO	**118**	**33**	S0
HH446	CO	**121**	**27**	S0
HH447	SZ I	**205**	**15**	B3
HH447	SZ I	**201**	**16**	B3
HH447	SZ I	**206**	**19**	L2
HH447	SZ I	**140**	**45**	S2
HH447	SZ I	**264**	**26**	S2
HH447	SZ I	**130**	**50**	S2
HH447	SZ I	**145**	**25**	S3
HH447	SZ I	**144**	**15**	S3
HH448	SZ I	**213**	**19**	B3
HH448	SZ I	**204**	**20**	B3
HH448	SZ I	**140**	**53**	S2
HH448	SZ I	**287**	**65**	S2
HH448	SZ I	**145**	**35**	S3
M. Idda	CO	**114**	**60**	S0
M. Idda	CO	**120**	**37**	S0
M. Idda	CO	**096**	**57**	S0
M. Idda	CO	**112**	**32**	S0
M. Idda	CO	**098**	**30**	S0
M. Idda	CO	**164**	**05**	S0
M. Idda	CO	**140**	**32**	S0
M. Idda	CO	**140**	**20**	S0
M. Idda	CO	**096**	**54**	S0
M. Idda	CO	**108**	**57**	S0
M. Idda	CO	**101**	**26**	S0
M. Idda	CO	**133**	**30**	S0
M. Idda	CO	**115**	**57**	S0
M. Idda	CO	**115**	**40**	S0
M. Idda	CO	**103**	**34**	S0
M. Idda	CO	**108**	**38**	S0
M. Idda	CO	**100**	**36**	S0
M. Idda	CO	**080**	**61**	S0
M. Idda	CO	**106**	**46**	S0
M. Idda	CO	**100**	**36**	S0
M. Idda	CO	**107**	**36**	S0
M. Idda	CO	**115**	**33**	S0
M. Idda	CO	**111**	**47**	S0
M. Longu	CO	**233**	**12**	S0
M. Longu	CO	**252**	**20**	S0
M. Longu	CO	**253**	**04**	S0
M. Longu	CO	**256**	**06**	S0
M. Longu	CO	**102**	**14**	S0
M. Longu	CO	**070**	**13**	S0
M. Longu	CO	**150**	**07**	S0
M. Longu	CO	**128**	**03**	S0
M. Longu	CO	**015**	**02**	S0
M. Longu	CO	**090**	**07**	S0
M. Longu	CO	**120**	**21**	S0
M. Longu	CO	**106**	**27**	S0
M. Longu	CO	**115**	**16**	S0
M. Longu	CO	**121**	**13**	S0
M. Longu	CO	**132**	**27**	S0
M. Longu	CO	**142**	**10**	S0
M. Longu	CO	**184**	**20**	S0
M. Longu	CO	**168**	**12**	S0
M. Longu	CO	**165**	**20**	S0
M. Longu	CO	**188**	**13**	S0
M. Longu	CO	**078**	**12**	S0
M. Longu	CO	**184**	**11**	S0
M. Longu	CO	**146**	**20**	S0
M. Longu	CO	**140**	**05**	S0
M. Longu	CO	**220**	**06**	S0
M. Longu	CO	**108**	**06**	S0
Posada	CO	**030**	**45**	S0
Posada	CO	**020**	**24**	S0
Posada	CO	**360**	**27**	S0
Posada	CO	**003**	**36**	S0
Posada	CO	**017**	**31**	S0
Posada	CO	**010**	**26**	S0
Posada	CO	**070**	**05**	S0
Posada	CO	**030**	**15**	S0
Posada	CO	**020**	**31**	S0
Posada	CO	**040**	**24**	S0
Posada	CO	**100**	**10**	S0
Posada	CO	**110**	**24**	S0
Posada	CO	**112**	**25**	S0
Posada	CO	**080**	**24**	S0
Posada	CO	**168**	**05**	S0
Posada	CO	**042**	**15**	S0
Posada	CO	**113**	**12**	S0
Posada	CO	**146**	**25**	S0
Posada	CO	**075**	**10**	S0
Posada	CO	**109**	**15**	S0

BA: basalt dike, **CO**: cover, **PE**: pegmatite dike, **SB**: shear band, **SZ I**: structural zone I, **SZ II**: structural zone II, **SZ III**: structural zone III, **SZ IV**: structural zone IV, **SZ V**: structural zone V, **SZ VI**: structural zone VI, **SZ VII**: structural zone VII, **TM**: Punta de li Tulchi metabasite, **TO**: Tanaunella orthogneiss

Data from thin sections, n: 450 (approx.), NE-Sardinia

SAMPLE	ZONE	rock type	ROCK-FORMING MINERALS	FABRIC	THIN SECTION	ORIENTATION
HH001	Oz	ab-schist	qtz, ab, ms, bt, cc	F3	HH1,	297/71
HH001C	Oz	ab-schist	qtz, ab, ms, bt, chl, ep, grt	S2/3	HH1C, HH1C3	314/90
HH002	Oz	ab-schist	qtz, ab, ms, bt, chl, cc, ep, zrn	F3	HH2	128/68
HH002B	Oz	porphyroid	qtz, ab, ms, chl, bt, czo, ep, grt	S2/3	HH2B	322/63
HH002C	Oz	porphyroid	qtz, ab, ms, chl, bt	S2/3	HH2C	323/74
HH003	Oz	ab-schist	qtz, ab, ms, chl, bt, tur	S2	HH3	127/51
HH004	Oz	metabasite	qtz, tr, bt, ep, cc	F5	HH4	163/43
HH005	Oz	bt-gneiss	qtz, ab/olig, bt, chl	S4	HH5	296/45
HH005B	Oz	bt-gneiss	qtz, ab/olig, bt, chl	S4	HHB1, HH5B2	089/63
HH006	Sz	grt-schist	qtz, ab/olig, bt, chl, ms, grt, ep	S2/3/4	HH6	272/85
HH007A	Lo	orthogneiss	qtz, pl, kfs, bt, ms, chl	S2	HH7A	189/35
HH007B	Lo	orthogneiss	qtz, pl, kfs, bt, ms, chl	S2	HH7b	101/80
HH007C	Lo	orthogneiss	qtz, ms, fsp	S4	HH7C, HH7C3	192/28
HH008	Lo	orthogneiss	qtz, pl, kfs, bt, ms,	S2/4	HH8	141/30
HH009A	Lo	orthogneiss	qtz, pl, kfs, bt, ms, chl	S2	HH9A	022/74o
HH009B	Lo	orthogneiss	qtz, pl, kfs, bt, ms	F5	HH9B	022/71o
HH010A	Sz	grt-schist	qtz, ab/olig, ms, grt, chl	S2/4	HH10A	097/26
HH010b	Sz	grt-schist	qtz, ab/olig, ms, grt, tur, chl	S2/4	HH10B	154/62
HH011	Sz	grt-schist	qtz, ab/olig, ms, grt, chl	S2/4	HH11	140/18
HH012	Lo	orthogneiss	qtz, ms, fsp, tur, chl, ep	S2/4	HH12	198/52
HH013	Lo	orthogneiss	qtz, ms, pl, kfs, bt, chl, ap	S3/4	HH13, HH13B	204/43
HH014	Lo	orthogneiss	qtz, ms, pl, kfs, bt, chl	S3/4	HH14	317/70o
HH015	Sz	st-schist	st, grt, qtz, ms, bt, tur, chl, pl	S2/4	HH15	273/88
HH015B	Sz	quartzite	qtz, ms, bt, ap, chl, pl, ep	S2/4	HH15B	085/66o
HH016	Lo	orthogneiss	qtz, ms, pl, kfs	S2/4	HH16	167/62
HH017A	Lo	orthogneiss	qtz, ms, pl, kfs, bt	S2/4	HH17A, HH17A3	020/90
HH017B	Lo	orthogneiss	qtz, ms, pl, kfs, bt	S2/4	HH17B	295/71
HH018	Lo	orthogneiss	qtz, ms, pl, kfs, chl	S2/4	HH18	173/25
HH019	Lo	orthogneiss	qtz, ms, pl, kfs, bt	S2/4	HH19	182/85
HH019B	Lo	orthogneiss	qtz, ms, pl, kfs, bt	S2/4	HH19B1, HH19B2, HH19C3	141/28
HH019C	Sz	grt-schist	qtz, ab/olig, ms, grt, chl	S2/4	HH19C	120/51
HH021B	Sz	qtz-fsp-schist	qtz, pl, bt, ms, tur, chl, zrn	S2/4	HH21B	245/85o
HH022	Sz	st-ky-schist	qtz, ms, pl, st, ky, tur, bt, tur, ap, grt	S2/4	HH22	028/75
HH024	Pz	bt-schist	qtz, ms, pl, ap, bt, chl	S2/4	HH24	097/74
HH025A	Pz	metabasite	qtz, hbl, pl,czo	S2/4	HH25A	186/55
HH025C	Pz	grt-schist	qtz, ms, pl, chl, tur, grt	S2/4	HH25C	218/72
HH026	Pz	bt-schist	qtz, pl, ms, bt, tur	S2/4	HH26	140/57
HH027	Pz	sil-schist	qtz, pl, bt, sil, ms, chl, ep	S2/4	HH27	210/60
HH028	Pz	orthogneiss	qtz, kfs, grt, ms, chl	S2	HH28	120/81ü
HH028B	Pz	bt-schist	qtz, pl, bt, ms, chl, tur, ap	S2/4	HH28B	040/80
HH029A	Bz	bt-gneiss	qtz, pl, bt, ms, tur	F2	HH29A	305/84
HH029B	Bz	grt-gneiss	qtz, pl, bt, grt, ap, chl, zrn	S2/4	HH29B	297/80
HH029C	Bz	orthogneiss	qtz, kfs, pl, sil, bt, ms	S2/4	HH29C	263/87
HH029D	Bz	qtz-fsp-vein	qtz, pl, ap	F5	HH29D	263/87
HH030	Bz	bt-gneiss	qtz, fsp, bt, chl, ap, ms, zrn	S2/4	HH30	193/71
HH031A	Bz	bt-gneiss	qtz, fsp, bt, chl, cc, ms	S2/4	HH31A	331/68
HH031B	Bz	bt-gneiss	qtz, fsp, bt, chl, sil, ms	S2/4	HH31B	332/77
HH034	Bz	bt-gneiss	qtz, fsp, bt, chl, ap, ep	S2/4	HH34	197/63
HH035	Bz	bt-gneiss	qtz, fsp, ms, chl, bt, ap, ep	S2/4	HH35	196/26
HH036	Bz	orthogneiss	qtz, fsp, bt, ms, chl, sil	S2	HH36	167/50
HH037	Bz	orthogneiss	qtz, fsp, bt, ms, chl, sil	S2	HH37	168/44
HH038	Bz	orthogneiss	qtz, fsp, bt, ms, chl, sil	S2	HH38	172/46
HH039A	To	orthogneiss	qtz, fsp, bt, chl, ms, ep, ap	S2	HH39A	172/43
HH039B	To	orthogneiss	qtz, fsp, bt, chl, ep, ap, zrn	S2	HH39B1, HH39B2	062/12

symbols for rock-forming minerals after Kretz (1983) and Bucher & Frey (1994), **Bz**: Brunella zone, **Lo**: Lodè orthogneiss, **Oz**: Orune zone, **Pz** Posada zone, **Sz**: Siniscola zone, **Ta**: Punta de li Tulchi metabasite, **To**: Tanaunella orthogneiss

Data from thin sections, n: 450 (approx.), NE-Sardinia

SAMPLE	ZONE	rock type	ROCK-FORMING MINERALS	FABRIC	THIN SECTION	ORIENTATION
HH039C	To	orthogneiss	qtz, fsp, bt, chl	S2, S3	HH39C	236/11
HH039D	Bz	bt-gneiss	qtz, fsp, bt, chl, am, ep, ap	S2	HH39D	036/33
HH040A	Bz	bt-gneiss	qtz, fsp, bt, chl, ms, sil	S2/4	HH40A	072/35
HH040B	Bz	bt-gneiss	qtz, fsp, bt, chl, ms, sil	S2, F2	HH40B	101/72
HH040C	Bz	bt-gneiss	qtz, fsp, bt, chl, ms, sil	F5	HH40C	176/42
HH040D	Bz	bt-gneiss	qtz, fsp, bt, chl, ms, sil	F5	HH40D	327/75
HH040E	Bz	bt-gneiss	qtz, fsp, bt, chl, ms, sil	F5	HH40E	126/42
HH040F	Bz	bt-gneiss	qtz, fsp, bt, chl, ms	S2, F2	HH40F1, HH40F2	098/30
HH041A	Sz	cld-schist	qtz, ms, chl, grt, bt, cld, pl	S2, F2	HH41A	130/05
HH041B	Sz	grt-schist	qtz, ms, chl, grt, pl	S2	HH41B1, HH41B2	288/56
HH042A	Sz	grt-quartzite	qtz, ms, chl, grt, bt, ap, zrn	F2	HH42A	312/32
HH042B	Sz	ms-schist	qtz, ms, chl, bt, pl	S2	HH42B	030/23
HH042C	Sz	cld-schist	qtz, ms, chl, grt, cld, bt	S2	HH42C	158/22
HH042D	Sz	grt-schist	qtz, ms, chl, grt, ab, bt	F2	HH42D	278/48
HH042E	Sz	grt-schist	qtz, ms, chl, grt, pl, bt	S2, F2	HH42E	294/68
HH045A	Sz	grt-schist	qtz, ms, chl, grt, tur, bt	S2	HH45A	130/12
HH045B	Sz	grt-quartzite	qtz, ms, pl, grt	S2	HH45B	100/13
HH046A	Sz	grt-schist	qtz, ms, chl, grt, pl, bt	S2	HH46A	190/09
HH046B	Sz	grt-schist	qtz, pl, ms, chl, grt, bt	S2	HH46B	140/30
HH047	Sz	grt-schist	qtz, ms, chl, grt	S2	HH47	074/88
HH048A	Sz	grt-schist	qtz, ms, bt, chl, grt	S2	HH45A	079/10
HH048B	Sz	ms-schist	qtz, ms, pl	S2	HH48B	020/55
HH049	Lo	orthogneiss	qtz, kfs, pl, ms, bt, chl	S2	HH49	276/90
HH052	Lo	orthogneiss	qtz, kfs, pl, ms, bt	S2	HH52	121/20
HH053B	Sz	grt-schist	qtz, ms, pl, bt, grt, tur	S2	HH53B	043/40
HH055A	Sz	grt-schist	qtz, ms, chl, grt, bt, pl	S2	HH55A	208/20
HH055B	Sz	grt-schist	qtz, ms, chl, grt	S2	HH55B	160/23
HH057	Sz	grt-schist	qtz, pl, ms, chl, grt, bt, ap	S2	HH57	170/32
HH058	Lo	orthogneiss	qtz, kfs, pl, ms, bt	S2	HH58	171/34
HH058B	Lo	orthogneiss	qtz, kfs, pl, ms, bt	S2	HH58B	157/38
HH058C	Lo	orthogneiss	qtz, pl, ms	S2	HH58C	170/20
HH061	Bz	bt-gneiss	qtz, fsp, bt, ms, chl	S2/4	HH61	172/74
HH062A	Lo	orthogneiss	qtz, kfs, pl, ms, bt	S2	HH62A	053/17
HH062B	Lo	orthogneiss	qtz, fsp, ms	S4	HH62B	246/46
HH064	Pz	bt-gneiss	qtz, fsp, bt, grt, ms, tur, chl	S2/4	HH64	145/64
HH065A	Pz	bt-gneiss	qtz, fsp, bt, ms, chl	S2/4	HH65A	176/45
HH065B	Pz	pl-grt-nodule	pl, grt, bt, cc, ms, qtz,	S2/4	HH65B	280/60
HH065C	Pz	bt-gneiss	qtz, fsp, bt, st, chl, grt	S2/4	HH65C	190/33
HH065D	Pz	bt-gneiss	qtz, fsp, chl, ms	S2/4	HH68D	194/83
HH065E	Pz	ms-schist	qtz, fsp, ap, cc, ms	S2/4	HH68E	170/75
HH066	Pz	bt-gneiss	qtz, fsp, bt, ms, chl	S2/4	HH66	172/52
HH067A	Pz	mylonite	qtz, pl, ms, chl, tur, bt, ap	S4, F5	HH67A	088/47
HH067B	Pz	mylonite	qtz, pl, ms, py, cc, ap	S4, F5	HH67B1, HH67B2	150/55
HH067C	Pz	mylonite	qtz, pl, ms, grt, chl, tur, bt, cc	S4	HH67C	117/29
HH067D	Pz	mylonite	qtz, pl, ms, bt, cc, chl, grt	S4	HH67D	176/26
HH067E	Pz	metabasite	qtz, pl, hbl, cc, czo	S2	HH67E	282/46
HH067G	Pz	metabasite	qtz, pl, hbl, cc, czo	S2	HH67G	153/38
HH068A	Bz	bt-gneiss	qtz, bt, fsp, ms, sil, tur, ap	S2/4	HH68A	284/57
HH068B	Bz	bt-gneiss	qtz, bt, fsp, chl, ap	S2/4	HH68B	338/86o
HH068C	Bz	bt-gneiss	qtz, bt, ms, fsp, tur, sil	F5	HH68C	086/70
HH068D	Bz	bt-gneiss	qtz, bt, ms, fsp, tur	F2/3	HH68D1, HH68D2	277/32
HH068E	Bz	bt-gneiss	qtz, bt, ms, fsp, tur	F2/3	HH68E	200/64
HH070	Pz	sil-gneiss	qtz, bt, sil, ms, chl	S2/4	HH70	175/75
HH071A	Pz	pegmatite	qtz, bt, kfs, pl, sil, ms, chl, ap, tur	S2/4	HH71A	145/48
HH071B	Pz	pegmatite	qtz, bt, grt, chl, ap, tur	S2/4	HH71B	140/51
HH074	Pz	sil-gneiss	qtz, fsp, bt, ms, sil, bt	S2/4	HH74	196/16
HH075	Pz	sil-gneiss	qtz, fsp, bt, ms, sil	S2/4	HH75	195/75
HH076A	Pz	gr-schist	qtz, ms, fsp, gr	S2/4	HH76A	189/77o
HH076B	Pz	bt-gneiss	qtz, fsp, bt, ms, chl	S2/4	HH76B	180/65

symbols for rock-forming minerals after Kretz (1983) and Bucher & Frey (1994), **Bz**: Brunella zone, **Lo**: Lodè orthogneiss, **Oz**: Orune zone, **Pz** Posada zone, **Sz**: Siniscola zone, **Ta**: Punta de li Tulchi metabasite, **To**: Tanaunella orthogneiss

Data from thin sections, n: 450 (approx.), NE-Sardinia

SAMPLE	ZONE	rock type	ROCK-FORMING MINERALS	FABRIC	THIN SECTION	ORIENTATION
HH076C	Pz	bt-gneiss	qtz, fsp, bt, ms, chl, ep, ap	S2/4	HH76C	188/87
HH077A	Pz	bt-gneiss	qtz, fsp, bt, ms, hbl, grt, ap, chl	S2/4	HH77A	054/24
HH077B	Pz	bt-gneiss	qtz, fsp, bt, ms, chl, grt, ap	S2/4	HH77B	088/42
HH077C	Pz	bt-gneiss	qtz, fsp, bt, ms, tur, sil, chl	S2/4	HH77C	172/68
HH081	Pz	bt-schist	qtz, pl, bt, ms, chl, tur, ap	S2/4	HH81	202/83
HH083	Sz	bt-schist	qtz, pl, bt, ms, py, chl	S2/4	HH83	255/50
HH084A	Sz	bt-schist	qtz, pl, bt, ms, ap, grt	S2/4	HH84A1, HH84A2	128/29
HH084B	Sz	bt-schist	qtz, pl, bt, ms, grt, ap	S2/4	HH84B	101/31
HH085A	Sz	st-ky-schist	qtz, pl, bt, ms, grt, ky, st, tur	S2/4	HH85A	090/20
HH085B	Sz	bt-schist	qtz, pl, bt, ms	S2/4	HH85b	185/59
HH086	Sz	bt-schist	qtz, pl, bt, ms, grt, tur, st	S2/4	HH86	192/89
HH087A	Sz	bt-schist	qtz, pl, bt, ms, ap, chl	S2/4	HH87A	195/72
HH087B	Sz	bt-schist	qtz, pl, bt, ms, ap	S2/4	HH87B	110/85
HH088	Sz	ky-schist	qtz, pl, bt, ms, ky, grt, chl	S2/4	HH88	205/86
HH089	Sz	bt-schist	qtz, pl, bt, ms, chl, grt, ap	S2/4	HH89	078/65
HH090	Sz	st-schist	qtz, pl, bt, ms, grt, chl, ap, st, tur	S2/4	HH90	200/87o
HH091A	Sz	bt-schist	qtz, pl, bt, ms	S2/4	HH91A	218/45
HH091B	Sz	st-ky-schist	qtz, pl, bt, ms, st, ky, grt	S2/4	HH91B	225/86
HH092	Sz	st-ky-schist	qtz, pl, bt, ms, grt, ky, chl, st	S2/4	HH92	062/43
HH093A	Sz	metabasitic dike	qtz, pl, hbl, grt	S2/4	HH93A	068/15
HH093B	Sz	ky-schist	qtz, pl, bt, ms, grt, chl, ky	S2/4	HH93B	172/67
HH094	Sz	st-schist	qtz, pl, bt, ms, grt, st, chl	S2/4	HH94	048/35
HH095	Pz	bt-schist	qtz, pl, bt, ms, grt, tur, ap	S2/4	HH95	164/86o
HH097A	Pz	metabasite	qtz, pl, hbl, cpx, grt, cc, ttn	S2	HH97A1, HH97A2	094/40, 215/75o
HH097B	Pz	qtz-fsp-gneiss	qtz, fsp, bt, ms, chl, ap	S2	HH97B	080/35
HH097C	Pz	chl-schist	qtz, pl, bt, ms, chl, ap	S2/4	HH97C	090/73
HH099	Bz	metabasite	grt, cam, pl, chl, bt	S2	HH99	240/84
HH103	Bz	sil-gneiss	qtz, fsp, bt, ms, sil, chl	S2	HH103	155/53
HH104	To	orthogneiss	qtz, kfs, pl, bt, ms	S2	HH104	148/43
HH108A	Bz	bt-gneiss	qtz, fsp, bt, sil, ms, grt	S2, F2	HH108A	136/35
HH108A1	Bz	bt-gneiss	qtz, fsp, bt, sil, ms	S2	HH108A1	128/15
HH108B	Bz	bt-gneiss	qtz, fsp, bt, sil, ap, chl, ms, grt	F2	HH108B	080/36
HH108B1	Bz	bt-gneiss	qtz, fsp, bt, sil, ap, chl, ms	S2	HH108B1	120/24
HH108C	Bz	bt-gneiss	qtz, fsp, bt, ep, chl, ms	S2	HH108C	090/40
HH108D	Bz	bt-gneiss	qtz, fsp, bt, grt, ap, chl, ms	S2	HH108D	083/24
HH109A	Bz	bt-gneiss	qtz, fsp, bt	S2	HH109A	160/27
HH109C	Bz	bt-gneiss	qtz, fsp, bt, grt, sil, ap, ep	S2	HH109C	147/40
HH112	Bz	bt-gneiss	qtz, fsp, chl	S2	HH112	172/71
HH114A	Bz	bt-gneiss	qtz, kfs, pl, bt, sil, ms, grt	F2/3	HH114A	118/48
HH114B	Bz	bt-gneiss	qtz, fsp, bt, sil, ms, grt, chl	S2	HH114B	251/29
HH115A	Tm	metabasite	grt, hbl, pl, cpx, qtz, chl	S1	HH115A	329/73
HH115B	Tm	metabasite	hbl, pl,	S1	HH115B	246/24
HH115C	Tm	metabasite	hbl, pl, ap	S3	HH115C	350/74
HH117	Bz	bt-gneiss	qtz, kfs, pl, bt, grt, ms	S2	HH117	145/81
HH118A	Bz	orthogneiss	qtz, kfs, pl, bt, ms, chl	S2	HH118A	133/77
HH118B	Bz	orthogneiss	qtz, kfs, pl, bt	S2	HH118B	130/40
HH120	Bz	bt-gneiss	qtz, fsp, bt, ms, chl, ap	S2	HH120	092/05
HH121A	Bz	bt-gneiss	qtz, kfs, pl, bt, ms, chl, ap	S2	HH121A	302/43
HH121B	Bz	bt-gneiss	qtz, kfs, pl, bt, ms, chl, ap	F3	HH121B	183/68
HH121C	Bz	bt-gneiss	qtz, kfs, pl, bt, sil, ms, chl, ap	S2	HH121C	215/46
HH125A	Bz	alpine cataclasite	qtz, fsp, ms, chl, cc, sil		HH125A	170/29
HH125B	Bz	alpine cataclasite	qtz, fsp, cc, py, ms, ap		HH125B	093/25
HH125C	Bz	bt-gneiss	qtz, kfs, pl, bt, ms, chl, sil, py	S2	HH125C	050/81
HH125D	Bz	bt-gneiss	qtz, fsp, bt, ms, chl, ep, cc	S2	HH125D	144/35

symbols for rock-forming minerals after Kretz (1983) and Bucher & Frey (1994), **Bz**: Brunella zone, **Lo**: Lodè orthogneiss, **Oz**: Orune zone, **Pz** Posada zone, **Sz**: Siniscola zone, **Ta**: Punta de li Tulchi metabasite, **To**: Tanaunella orthogneiss

Data from thin sections, n: 450 (approx.), NE-Sardinia

SAMPLE	ZONE	rock type	ROCK-FORMING MINERALS	FABRIC	THIN SECTION	ORIENTATION
HH129	Bz	qtz-fsp-gneiss	qtz, kfs, pl, bt, sil, ms	S2	HH129	140/57
HH130	Bz	qtz-fsp-gneiss	qtz, kfs, pl, bt, grt, chl, sil, ms	S2	HH130	223/65
HH135	Sz	ms-schist	qtz, pl, ms, chl, bt	S2/4	HH135	246/85
HH135B	Sz	ms-schist	qtz, pl, ms, chl, tur, bt	S2/4	HH135B	182/38
HH136	Lo	qtz-fsp-schist	qtz, pl, ms, chl, tur	S2	HH136	178/35
HH137	Sz	ms-schist	qtz, ms, tur, bt	S2/4	HH137	170/42
HH138A	Oz	ab-schist	qtz, ab, ms, tur, chl, ep	F3	HH138A	136/59
HH138B	Oz	ab-schist	qtz, ab, ms, bt, chl, ap	S2, S3	HH138B	129/24
HH138C	Oz	ab-schist	qtz, ab, ms, bt, chl	S2	HH138C	091/18
HH138D	Oz	porphyric dike	qtz, fsp, ms		HH138D	117/72
HH138E	Oz	porphyric dike	qtz, fsp, ms		HH138E	232/78
HH141	Oz	ab-schist	qtz, ab, ms, bt, chl, tur	S0, S2, S3	HH141	084/10
HH142	Oz	porphyroid	qtz, ab, ms, bt, chl, czo, ep	S2	HH142	171/56
HH147A	Oz	quartzite	qtz, ms, pl	F3	HH147A	119/81
HH147B	Oz	quartzite	qtz, bt, chl, pl	S2	HH147B	065/35
HH151	Oz	ab-schist	qtz, pl, ms, bt, chl, tur, ap	S2	HH151	130/45
HH152A	Oz	ab-schist	qtz, pl, ms, bt, chl	F3	HH152A	132/40
HH152B	Oz	ab-schist	qtz, pl, ms, bt, chl, tur	F3	HH152B	032/76o
HH153	Sz	grt-schist	qtz, pl, ms, chl	S2/4	HH153	176/67
HH154A	Sz	ms-schist	qtz, pl, ms, chl, ep	F2	HH154A	249/84
HH154B	Sz	ms-schist	qtz, pl, ms, chl, bt, ep	F3	HH154B	126/44
HH155	Sz	qtz-fsp-schist	qtz, pl, ms, chl, ap	S2	HH155	006/81o
HH156	Sz	ms-schist	qtz, ab/olig, ms	S2	HH156	272/76
HH157A	Sz	grt-schist	qtz, ab/olig, ms, chl, tur, grt	S2/4, F2	HH157A	144/46
HH157B	Sz	grt-schist	qtz, ab/olig, ms, chl, tur, grt	S2/4, F2	HH157B	160/52o
HH159A	Sz	quartzitic schist	qtz, ab/olig, ms, chl, bt, tur	F3	HH159A	146/65
HH159B	Sz	ms-schist	qtz, pl, ms, chl, tur	S2/4	HH159B	257/70
HH160A	Lo	orthogneiss	qtz, pl, kfs, ms, bt	S2	HH160A	165/15
HH160B	Sz	grt-schist	qtz, ab/olig, ms, chl, bt, tur, grt	S2/4	HH160B	107/20
HH160C	Sz	grt-schist	qtz, ab/olig, ms, chl, bt, grt	S2/4	HH160C1	200/61
HH160D	Sz	grt-schist	qtz, ab/olig, ms, chl, bt, grt	S2/4, S2	HH160D	161/28
HH160E	Sz	grt-schist	qtz, ab/olig, ms, chl, bt, grt	S2/4	HH160E	122/61
HH162A	Sz	ms-schist	qtz, ab/olig, ms, bt, tur	S2/4	HH162A	127/45
HH162B	Sz	grt-schist	qtz, ab/olig, ms, bt, grt	S2/4	HH162B	145/42
HH165	Lo	orthogneiss	qtz, pl, kfs, chl, ms, bt	F5	HH165	111/35
HH166A	Lo	orthogneiss	qtz, pl, kfs, chl, ms, bt	S2/4	HH166A	200/75o
HH166B	Lo	orthogneiss	qtz, pl, kfs, chl, ms, bt, ap	F5	HH166B	068/57
HH167A	Sz	st-schist	qtz, st, bt, ms, pl, grt, chl, ap	S2/4	HH167	220/57
HH167B	Sz	ms-schist	qtz, ms, pl, grt, chl, ap	S2/4	HH167	272/63
HH168	Sz	st-ky-schist	qtz, st, ky, bt, ms, pl, grt, chl, ap	S2/4	HH168	020/80
HH168B	Sz	metabasitic dike	qtz, pl, chl, ap, grt, czo, ep, hbl, bt, ms, ttn	S2/4	HH168B1, HH168B2	097/68
HH168C	Sz	grt-gneiss	qtz, pl, grt, bt, chl, ms	F2	HH168C	099/48
HH168D	Sz	metabasitic dike	qtz, pl, chl, ap, grt, czo, ep, hbl, bt, ms, ttn	S2/4	HH168D1, HH168D2	116/80
HH169	Lo	orthogneiss	qtz, kfs, pl, chl, ap, ep, bt, ms	S2/4	HH169	175/51
HH170	Bz	bt-gneiss	qtz, fsp, grt, bt, chl, ms, ap	S2/4	HH170	180/24
HH174	Bz	bt-gneiss	qtz, fsp, tur, bt, chl, ms, ap	S2/4	HH174	190/78
HH175A	Bz	bt-gneiss	qtz, fsp, bt, chl, ms, sil	F5	HH175A1, HH175A2	208/85
HH175B	Bz	bt-gneiss	qtz, fsp, bt, chl, ms	F5	HH175B	190/30
HH183A	Bz	bt-gneiss	qtz, fsp, bt, chl, ms, grt	S2/4	HH183A1, HH183A2	205/39
HH183B	Bz	bt-gneiss	qtz, fsp, bt, sil, ms	F5	HH183B	309/14
HH184	Sz	grt-schist	qtz, ab/olig, bt, ms, tur, chl, grt	S2/4	HH184	138/37
HH185A	Sz	metabasite	qtz, pl, ak, chl, ep, bt, opaques	S2	HH185A	006/16

symbols for rock-forming minerals after Kretz (1983) and Bucher & Frey (1994), **Bz**: Brunella zone, **Lo**: Lodè orthogneiss, **Oz**: Orune zone, **Pz** Posada zone, **Sz**: Siniscola zone, **Ta**: Punta de li Tulchi metabasite, **To**: Tanaunella orthogneiss

Data from thin sections, n: 450 (approx.), NE-Sardinia

SAMPLE	ZONE	rock type	ROCK-FORMING MINERALS	FABRIC	THIN SECTION	ORIENTATION
HH185B	Sz	grt-schist	qtz, ab/olig, bt, ms, tur, chl, grt	S2/4	HH185B	027/78
HH185C	Sz	grt-schist	qtz, ab/olig, bt, ms, tur, chl, grt	S2/3	HH185C	027/78
HH186	Sz	grt-schist	qtz, ab/olig, bt, ms, tur, chl, grt, ap	F3	HH186	060/53
HH187	Sz	grt-schist	qtz, ab/olig, bt, ms, grt, chl	S2/4	HH187B	200/82
HH188	Sz	qtz-fsp-schist	qtz, tur, bt, ms, ap, ep	S2/4	HH188	188/56
HH190A	Sz	grt-schist	qtz, ab/olig, bt, ms, grt, chl	S2/4	HH190A	090/30
HH190B	Sz	grt-schist	qtz, ab/olig, bt, ms, grt, chl	S2/4	HH190B	115/28o
HH193	Lo	orthogneiss	qtz, kfs, pl, grt, chl, ap, ms	S2/4	HH193	182/06
HH194	Lo	ms-schist	qtz, pl, bt, ap, ms, tur	S2/4	HH194	148/73
HH196	Lo	ms-schist	qtz, bt, grt, chl, ap, ms	S2/4	HH196	210/32
HH203A	Sz	qtz-fsp-schist	qtz, pl, chl, bt, ms, tur, ep	S0, S2/4	HH203A	168/05
HH203B	Sz	qtz-fsp-schist	qtz, pl, chl, bt, ms, tur, ep, grt, ap	S2/4	HH203B	035/87
HH203C	Sz	qtz-fsp-schist	qtz, ms, chl, pl, ap	S2/4	HH203C1, HH203C2	206/17o
HH203D	Sz	grt-schist	qtz, ms, chl, pl, bt, ep, tur	S2/4	HH203D	164/50
HH203D1	Sz	qtz-fsp-schist	qtz, ms, chl, pl, ap	F3	HH203D1	226/21
HH203E	Sz	qtz-fsp-schist	qtz, ms, chl, pl, ap	S2/4	HH203E	002/68
HH203F	Sz	qtz-fsp-schist	qtz, ms, chl, pl, ap	S2/4	HH203F	349/55
HH203G	Sz	diorite	qtz, pl, bt		HH203G	156/68
HH204	Sz	grt-schist	qtz, pl, bt, ap, ms, chl, grt	S2/4	HH204	117/56
HH212A	Lo	orthogneiss	qtz, kfs, pl, bt, ms	F3	HH212A	188/81
HH212B	Lo	orthogneiss	qtz, kfs, pl, bt, ms	F3	HH212B	182/80o
HH213	Lo	orthogneiss	qtz, kfs, pl, bt, ms, ap	F3	HH213	255/47
HH213B	Lo	orthogneiss	qtz, kfs, pl, bt, ms	S2/3/4	HH213B1, HH213B2	194/78
HH213C	Lo	orthogneiss	qtz, kfs, pl, bt, ms	S2/3/4	HH213C1, HH213C2	212/53
HH213D	Lo	orthogneiss	qtz, kfs, pl, bt, ms	S2/3/4	HH213D	195/60
HH214	Sz	st-schist	qtz, bt, ms, st, chl, grt	S2/4	HH214	194/56
HH218A	Sz	st-schist	qtz, pl, ms, st, chl, grt	S2/4	HH218A1, HH218A2	175/87
HH218B	Lo	orthogneiss	qtz, kfs, pl, bt, ms	S2/3/4	HH218B1, HH218B2	083/73
HH222	Lo	orthogneiss	qtz, kfs, pl, bt, ms	S2/3/4	HH222	163/81
HH226	Lo	orthogneiss	qtz, kfs, pl, bt, ms	S2/3/4	HH226	078/47
HH227	Lo	orthogneiss	qtz, kfs, pl, bt, ms	S2/3/4	HH227A, HH227B	129/71
HH229	Lo	orthogneiss	qtz, kfs, pl, bt, ms	S2/3/4	HH229	197/85
HH230	Lo	orthogneiss	qtz, kfs, pl, bt, ms	S2	HH230	110/83
HH235	Lo	orthogneiss	qtz, kfs, pl, bt, ms, tur	S2/3/4	HH235	320/64o
HH236	Lo	orthogneiss	qtz, kfs, pl, bt, ms, tur	S2/4	HH236	032/47
HH237	Lo	orthogneiss	qtz, kfs, pl, bt, ms, chl	F3	HH237	030/79
HH243	Pz	cataclasite	st, qtz, fsp, chl, ms	S4	HH243	131/47o
HH244	Oz	ab-schist	qtz, ab, bt, ms	S2	HH244	058/26
HH247A	Oz	porphyroid	qtz, ab, bt, chl, ms, ep, czo	S2	HH247A	119/51
HH247B	Oz	porphyroid	qtz, ab, bt, chl, ms, ep, czo, tur	S2	HH247B1, HH247B2	120/42
HH247C	Oz	porphyroid	qtz, ab, bt, chl, ms, ep, czo, tur	S2	HH247C1, HH247C2, HH247C3	048/14
HH248	Oz	ab-schist	qtz, ab, bt, ms, ap	F3	HH248	066/41
HH249	Oz	ab-schist	qtz, ab, bt, ms	F3	HH249	146/27
HH254	Oz	ab-schist	qtz, ab, bt, ms, chl	F3	HH254	124/34
HH255	Oz	ab-schist	qtz, ab, bt, ms,	F3	HH255	113/32
HH257A	Oz	ab-schist	qtz, ab, bt, ms, cc	S2	HH257A	140/57
HH257B	Oz	ab-schist	qtz, ab, bt, ms, cc	S2/3	HH257B	117/74
HH258A	Oz	ab-schist	qtz, ab, bt, ms	S2	HH258A	138/54
HH258B	Oz	ab-schist	qtz, ab, bt, ms, tur	S2/S3	HH258B	151/68
HH259A	Oz	ab-schist	qtz, ab, bt, ms, tur	S2	HH259A	125/40
HH259B	Oz	ab-schist	qtz, ab/olig, bt, ms, tur	S2	HH259B	137/39
HH260A	Oz	bt-gneiss	qtz, ab/olig, bt, chl, ms, tur, ap	S4	HH260A	140/55

symbols for rock-forming minerals after Kretz (1983) and Bucher & Frey (1994), **Bz**: Brunella zone, **Lo**: Lodè orthogneiss, **Oz**: Orune zone, **Pz** Posada zone, **Sz**: Siniscola zone, **Ta**: Punta de li Tulchi metabasite, **To**: Tanaunella orthogneiss

Data from thin sections, n: 450 (approx.), NE-Sardinia

SAMPLE	ZONE	rock type	ROCK-FORMING MINERALS	FABRIC	THIN SECTION	ORIENTATION
HH260B	Oz	bt-gneiss	qtz, ab/olig, bt, ms, chl, tur, ap	S4	HH260B	137/39
HH264	Sz	ms-schist	qtz, ab, bt, ms, chl, ap	S2	HH264A, HH264B	249/83
HH265A	Sz	ms-schist	qtz, pl, bt, ms, chl, tur, ap	S2	HH265A	136/58
HH265B	Sz	grt-schist	qtz, ab/olig, bt, ms, chl, tur, ap	S2	HH265B	260/48
HH266A	Sz	ms-schist in contact to porphyric dike	qtz, pl, chl, ms	S2, S5	HH266A	276/90
HH266B	Sz	ms-schist in contact to porphyric dike	qtz, pl, chl, ms	S2, S5	HH266B	258/60
HH267	Sz	ms-schist	qtz, pl, chl, ms	S2, S3	HH267	177/58
HH268	Sz	grt-schist	qtz, pl, chl, ms, grt	S2/4	HH268	162/74o
HH270	Sz	st-schist	qtz, pl, chl, ms, grt, st	S2/4	HH270	188/34
HH271	Lo	ms-schist	qtz, ms, chl	S2/4	HH271	183/47
HH272	Lo	orthogneiss	qtz, kfs, pl, ms, chl, bt, grt	S2/4	HH272	194/34
HH273	Sz	grt-schist	qtz, pl, ms, chl, bt, grt	S2/4	HH273A, HH273B	176/24
HH274	Sz	grt-schist	qtz, pl, ms, chl, bt, ap, grt	S2/4	HH274	163/51
HH276	Lo	orthogneiss	qtz, kfs, pl, ms, chl, bt	S2/4	HH276A, HH276B	210/19
HH277	Sz	ms-schist	qtz, ms, chl, pl	F3	HH277A, HH277B	150/30
HH278	Lo	orthogneiss	qtz, kfs, pl, ms, chl, bt	S2/4	HH278A, HH278B	200/83
HH279A	Lo	orthogneiss	qtz, kfs, pl, ms, chl, bt	S2/4	HH279A	262/77
HH279B	Lo	orthogneiss	qtz, kfs, pl, ms	S2/4	HH279B	272/86
HH280	Lo	aplite	qtz, kfs, pl, ms	S2/4	HH280	183/67
HH283	Sz	bt-schist	qtz, pl, ms, bt, chl, ttn, grt, ap	S2/4	HH283A, HH283B	077/24
HH284	Sz	st-ky-schist	qtz, pl, ms, bt, grt, chl, st, ky, ttn	S2/4	HH284A, HH284B	008/75
HH285A	Sz	st-schist	qtz, pl, ms, bt, grt, chl, st	S2/3	HH285A1, HH285A2	007/81
HH285B	Sz	bt-schist	qtz, pl, ms, bt, grt, chl	S2/4	HH285B1, HH285B2	127/44
HH286	Sz	st-schist	qtz, pl, bt, grt, st	S3	HH286	205/70
HH287	Sz	st-schist	qtz, pl, bt, st, chl	S2/4	HH287A, HH287B	195/72
HH288	Pz	protomylonite	qtz, pl, bt, chl, ms	S4	HH288A, HH288B	200/53
HH288B	Pz	protomylonite	qtz, pl, bt, chl, ms, grt	S4	HH288B1, HH288B2	295/82
HH289	Pz	protomylonite	qtz, pl, bt, chl, ms	S4	HH289A, HH289B	205/58
HH290A	Pz	protomylonite	qtz, pl, bt, chl, ms, grt	S4	HH290A1, HH290A2	267/51
HH290B	Pz	protomylonite	qtz, pl, bt, chl, ms	S4	HH290B1, HH290B2	200/69o
HH290C	Pz	protomylonite	qtz, pl, bt, chl, ms, grt	S4	HH290C1, HH290C2	184/56
HH291	Pz	protomylonite	qtz, pl, bt, chl, ms	S4, F5	HH291A, HH291B	343/70
HH292	Pz	protomylonite	qtz, pl, bt, chl, ms	S4	HH292A, HH292B	196/82
HH293	Pz	protomylonite	qtz, pl, bt, chl, ms	S4	HH293	186/68
HH294A	Pz	metabasite	hbl, pl, ttn, chl	S2	HH294A1, HH294A2	179/70
HH294B	Pz	orthogneiss	qtz, pl, kfs, ms	S2	HH294B1, HH294B2	192/67
HH294C	Pz	bt-schist	qtz, pl, sil, bt, chl, ms	S4	HH294C	182/60
HH295	Pz	bt-schist	qtz, pl, ms, bt, chl	S4, F3	HH295A, HH295B	116/35
HH296	Pz	protomylonite	qtz, pl, ms, bt, chl	S4	HH296A, HH296B	328/20
HH297	Bz	bt-schist	qtz, pl, sil, bt, chl, ms	S2/4	HH297	230/74
HH298	Bz	bt-gneiss	qtz, pl, sil, bt, chl, ms	S2/4	HH298	180/83o
HH300	Bz	bt-gneiss	qtz, pl, sil, bt, chl, ms	F5	HH300	241/81
HH301	Bz	bt-gneiss	qtz, pl, bt, chl, ms	S2/4	HH301	258/13
HH303	Bz	bt-schist	qtz, pl, bt, grt, ttn, ap	S2/4	HH303A, HH303B	204/32
HH305A	Bz	pegmatite	qtz, kfs, pl, grt, tur		HH305A1, HH305A2	146/57
HH305B	Bz	bt-gneiss	qtz, pl, sil, bt, ms	S2/4	HH305B1, HH305B2	170/88
HH307A	Pz	orthogneiss	qtz, pl, kfs, bt, ms	S2/4	HH307A1, HH307A2	095/89
HH307B	Pz	orthogneiss	qtz, kfs, pl, bt, ms, chl, ak	S2/4	HH307B1, HH307B2	200/36
HH307C	Pz	cataclasite	qtz, ak, kfs, pl, ms, chl	S4	HH307C1, HH307C2	220/39
HH309A	Pz	metabasite	pl, hbl, grt, ep, chl, tr	S2/4	HH309A1, HH309A2	184/87
HH309B	Pz	metabasite	qtz, cc, pl, hbl, ep, czo, ttn	S2	HH309B1, HH309B2	178/76
HH310A	Pz	protomylonite	qtz, pl, chl, bt, ms, grt	S4	HH310A1, HH310A2	132/50
HH312	Sz	bt-schist	qtz, pl, chl, bt, ms	F3	HH312	270/85o
HH314	Sz	metabasitic dike	hbl, grt, pl, qtz	S2/4	HH314A, HH314B	118/43
HH317A	Sz	crd-gneiss	qtz, ms, crd, chl	F3	HH317A	330/56

symbols for rock-forming minerals after Kretz (1983) and Bucher & Frey (1994), **Bz**: Brunella zone, **Lo**: Lodè orthogneiss, **Oz**: Orune zone, **Pz** Posada zone, **Sz**: Siniscola zone, **Ta**: Punta de li Tulchi metabasite, **To**: Tanaunella orthogneiss

Data from thin sections, n: 450 (approx.), NE-Sardinia

SAMPLE	ZONE	rock type	ROCK-FORMING MINERALS	FABRIC	THIN SECTION	ORIENTATION
HH317B	Sz	and-crd-gneiss	qtz, ms, and, crd, chl	S2/4	HH317B1, HH317B2	095/53
HH327	Lo	orthogneiss	qtz, pl, kfs, bt, chl	F5	HH327	109/22
HH331	Lo	orthogneiss	qtz, pl, kfs, bt, chl	S2/4	HH331A, HH331B	196/32
HH334A	Sz	grt-schist	qtz, pl, bt, chl, ms, grt	S2/4	HH334A1, HH334A2	196/64
HH334B	Lo	orthogneiss	qtz, pl, kfs, ms, bt	S2/4	HH334B	211/61o
HH334C	Sz	grt-schist	qtz, pl, bt, chl, ms, grt	S2/4	HH334C1, HH334C2	160/75o
HH334D	Lo	orthogneiss	qtz, pl, kfs, ms	S2/4	HH334D1, HH334D2	214/74o
HH335A	Sz	grt-schist	qtz, pl, bt, ms, grt	S2/4	HH335A1, HH335A2	193/33
HH335B	Sz	grt-schist	qtz, pl, bt, chl, ms, grt	S2/4	HH335B1, HH335B2	182/28
HH335C	Sz	grt-schist	qtz, pl, bt, chl, ms	S2/4	HH335C1, HH335C2	181/26
HH402	Sz	grt-schist	qtz, ab/olig, bt, ms, grt	F3	HH402	162/34
HH404	Sz	grt-schist	qtz, ab/olig, bt, ms, grt	F3	HH404	122/27o
HH409A	Sz	grt-schist	qtz, ab/olig, bt, ms, grt, chl,	S2/4	HH409A	108/05
HH409B	Sz	grt-schist	qtz, ab/olig, bt, ms, grt, chl	S2/4	HH409B	116/36
HH410	Sz	grt-schist	qtz, ab/olig, bt, ms, grt, chl	S2/4	HH410	104/22
HH411A	Sz	ms-schist	qtz, pl, bt, ms, chl	F2	HH411A1, HH411A2	135/26
HH411B	Sz	grt-schist	qtz, ab/olig, bt, ms, grt, chl	S2/4	HH411B	112/29
HH415	Sz	grt-schist	qtz, ab/olig, bt, grt, chl	F2, S3	HH415	170/53
HH416	Sz	grt-schist	qtz, pl, grt, chl, ms, tur, bt	S2, S3	HH416A, HH416B	078/85
HH417	Sz	quartzitic schist	qtz, pl, ms, tur, ep		HH417	170/75o
HH422A	Sz	grt-schist	qtz, pl, ms, grt, bt	S2, S3	HH422A	155/29
HH422B	Sz	ms-schist	qtz, pl, ms, bt	S2, S3	HH422B	156/61
HH424A	Sz	grt-schist	qtz, pl, ms, grt, bt	S2, S3	HH424A	295/74
HH424B	Sz	grt-schist	qtz, pl, ms, grt, chl, bt	S2, S3	HH424B	005/85o
HH425	Sz	cld-schist	qtz, pl, ms, cld, grt, chl, bt	S1, F2	HH425	260/30
HH427	Sz	ms-schist	qtz, ab/olig, bt, ms, chl	S2/4	HH427	140/37
HH428	Sz	grt-schist	qtz, ab/olig, bt, ms, grt, chl	S2/4	HH428	250/62
HH429	Sz	grt-schist	qtz, ab/olig, bt, ms, grt, chl, tur	S2, S3	HH429	058/67
HH432	Sz	grt-schist	grt, chl, tur, pl, qtz, bt, ms	S2/3	HH432	170/79
HH436A	Sz	gr-schist	qtz, bt, ms, gr	F3	HH436A	126/90
HH436B	Sz	ms-schist	chl, tur, pl, qtz, bt, ms	F2, F3	HH436B1, HH436B2	131/79
HH442	Sz	grt-schist	grt, chl, tur, pl, qtz, bt, ms, tur	S2, S3	HH442	133/40

symbols for rock-forming minerals after Kretz (1983) and Bucher & Frey (1994), **Bz**: Brunella zone, **Lo**: Lodè orthogneiss, **Oz**: Orune zone, **Pz** Posada zone, **Sz**: Siniscola zone, **Ta**: Punta de li Tulchi metabasite, **To**: Tanaunella orthogneiss